3

THE EFFECT OF DRAWING STRAIN ON THE FATIGUE BEHAVIOUR OF STAINLESS AND CARBON STEEL WIRES

by

MIROSLAVA TOPIĆ

A thesis submitted to the Faculty of Engineering and Built
Environment
University of Cape Town in fulfilment of the degree of
Doctor of Philosophy

Centre for Materials Engineering
Department of Mechanical Engineering
University of Cape Town

September 2001

ACKNOWLEDGEMENTS

I would like to thank the following people who have assisted me during the course of this thesis:

Firstly, my supervisors Professor A. Ball and Professor C. Allen, who have assisted, advised and encouraged me from the beginning of this project to the very end. I would also like to thank my supervisor Associate Professor B. Tait, who has joined this research project due to the unfortunate and sudden death of Professor A. Ball. Associate Professor B. Tait has given me tremendous assistance and guidance towards the end of my thesis.

I wish to express my gratitude to "Haggie Rand" and "Columbus Joint Venture" for the project support.

Finally, I would like to thank the students and staff in "Centre for Materials Engineering" for their support and understanding.

Dedicated to Irena

ABSTRACT

The Comparative Effect of Drawing Strain on the Fatigue Behaviour of Stainless and Carbon Steel Wires

By: **Miroslava Topić**

A study has been made of the fatigue crack initiation and fatigue crack growth behaviour of three different steels in wire form, namely, an austenitic AISI 304 stainless steel, a corrosion resistant ferritic steel, 3CR12, and pearlitic high carbon steel.

The stainless steel wires were produced in the laboratory at a drawing speed of 50 mm min^{-1}, without intermediate annealing, whilst the high carbon pearlitic steel was manufactured commercially. Studies were made on stainless steel wires as a function of drawing strain between 0.09 and 0.585.
Fatigue testing was carried out on an ESH servo hydraulic testing machine on both notched and unnotched samples and the S-N curves were used to evaluate the fatigue properties of the steels. Tests were performed with sinusoidal loading and load ratios of $R=0.048$ and $R=0.22$ at a frequency of 2Hz.

The microstructural evolution during drawing was characterised by optical and transmission optical microscopy, and x-ray diffraction. Fatigue crack growth and fracture surfaces were studied using scanning electron microscopy.

In general, the fatigue limit was enhanced by increased drawing strain, but such strain also increased the subsequent crack propagation rates. The highest value of fatigue limit of 630 MPa was exhibited by the commercial pearlitic steel despite of its high notch sensitivity. Both shot peening of the steel wire surface

and reducing the surface roughness by manual polishing increased the fatigue limit between 40 and 25% respectively.
The fatigue limit of AISI 304 stainless steel wire was improved from 215 MPa to 650 MPa after drawing to 0.585 strain. This improvement is attributed to the deformation-induced phase transformation of (γ) austenite to α'-martensite. X-ray diffractometer traces show that the amount of strain-induced martensite varied from 8% in the wires drawn at low strain (0.09) to 36% in the wire samples drawn to 0.585 strain.

This study has established that approximately 20% of deformation-induced martensite, through drawing strain, is a critical amount which determines the subsequent fatigue response of this steel. If the amount of previously developed martensite is less than the critical amount of 20%, the martensite formed during the fatigue process will act beneficially by retarding fatigue cracking, raising the fatigue limit and resulting in a ductile fatigue fracture surface. However, in the presence of more than 20% of martensite, any martensite induced by cyclic strain will encourage more rapid crack initiation compared to a material containing less than 20% martensite which leads to more brittle fracture surface characteristics.

The fatigue limit of 3CR12 steel wire was also improved from 130 MPa to 310 MPa (maximum stress) after drawing to 0.68 strain. The experimental results indicate that the use of drawn 3CR12 ferritic steel for wire application under cyclic conditions is restricted to low stress levels. However, the application of heat treatment and the resultant development of a dual-phase microstructure, improved the fatigue limit to 470 MPa.

Based on the findings in this study, recommendations regarding material selection and drawing process optimisation for wire production to improve the fatigue performance of AISI 304 stainless steel is given.

NOTATION AND ABREVIATIONS

$\Delta\sigma$	The applied cyclic maximum principal stress range
σ_{max}	The maximum cyclic stress
σ_{min}	The minimum cyclic stress
σ_m	The mean tensile stress associated with $\Delta\sigma$
a_0	The initial depth of the fatigue crack which starts the failure process
ΔK_{th}	The appropriate threshold value of the Linear Elastic Fracture Mechanics cyclic stress intensity factor
N	The number of applied cycles associated with combination of $\Delta\sigma$, σ_m
LCF	Low cyclic fatigue
HCF	High cyclic fatigue
K_{cl}	Closure stress intensity factor
R	Load stress ratio, $R=\sigma_{min}/\sigma_{max}$
da/dN	Crack growth rate

f	The frequency of cyclic loading
LEFM	Linear Elastic Fracture Mechanics
FCGR	Fatigue crack growth rate
RICC	Roughness induced crack closure
PICC	Plasticity induced crack closure
TRIP	Transformation induced plasticity
b.c.c.	Body centred cubic
f.c.c.	Face centred cubic
UTS	Ultimate tensile stress
σ_Y	Yield stress
ε	Strain
SEM	Scanning electron microscope
TEM	Transmission electron microscope

CONTENTS

Page

ACKNOWLEDGEMENTS I

ABSTRACT ii

LIST OF NOTATION AND ABREVIATIONS iv

TABLE OF CONTENTS vii

CHAPTER 1 INTRODUCTION 1

CHAPTER 2 REVIEW OF METAL FATIGUE 4

2. Metal Fatigue 4

- 2.1. Introduction 4
- 2.2. Fatigue Crack Initiation 7
- 2.3. Fatigue Crack Propagation 8
- 2.4. Characterisation of Fatigue Behaviour 15
- 2.5. Fracture Mechanics Considerations 17
- 2.6. Factors Affecting Fatigue Crack Initiation and Propagation 21
  - 2.6.1. Microstructure 23
  - 2.6.2. Grain Size 24
  - 2.6.3. Stacking Fault Energy 27
  - 2.6.4. Material Strength 27
  - 2.6.5. Impurity Levels 30
  - 2.6.6. Surface Condition 32
  - 2.6.7. Load Ratio 34
  - 2.6.8. Crack Closure 37
  - *2.6.8.1. Roughness-Induced Crack Closure* 41

2.6.8.2. Phase-Transformation Induced Crack Closure 43
2.6.9. Environment 44
2.7. Deformation Mechanisms in FCC and BCC Metals 45
2.7.1. Deformation of Pearlite 46
2.7.2. Deformation of Austenite 49
2.8. Changes Caused by Fatigue Process 52

CHAPTER 3 MATERIALS AND EXPERIMENTAL PROCEDURE 55
3.1. Introduction 55
3.2. Materials 55
3.2.1. Specification 56
3.3. Wire Production 56
3.3.1. High Carbon Steel Wire 57
3.3.2. AISI-304-Austenitic Stainless Steel Wire 59
3.3.3. 3CR12-Ferritic Stainless Steel Wire 64
3.4. Experimental Testing Details 65
3.4.1. X-ray measurements on AISI 304 Stainless Steel 65
3.4.1.1. Notch Effect on Martensite Transformation 68
3.4.2. Mechanical Testing 69
3.4.2.1. Tensile Testing 69
3.4.2.2. Fatigue Testing 70
3.4.2.2.1. Fatigue Limit Data Acquisition 74
3.4.2.2.2. Fatigue Crack Growth Rate Data Acquisition 79
3.4.3. Microscopy 81
3.4.3.1. Quantitative Metallography 83
3.4.3.1.1. Grain Size 83
3.4.3.1.2. Interlamellar Spacing 84
3.4.4. Determination of the Residual Stresses 86

CHAPTER 4 RESULTS 87

4.1. High Carbon Steel Wire 87

4.1.1. Mechanical Properties 87
4.1.2. Microscopy 90
4.1.2.1. Surface Examination 90
4.1.2.2. Metallography 91
4.1.3. Fatigue Properties 96
4.1.3.1. Fatigue Limit of Smooth Wire Samples 96
4.1.3.2. Methods for Improving the Fatigue Limit 98
4.1.3.3. Fatigue Limit of Notched Wire Samples 100
4.1.4. Changes in High Carbon Steel Wire 102
4.1.4.1. Mechanical properties 102
4.1.5. Fractography 104
4.1.5.1. Static Tensile Fractography 104
4.1.5.2. Fatigue Fractography 105

4.2. AISI-304-Austenitic Stainless Steel Wire 113

4.2.1. Mechanical Properties 113
4.2.2. Microscopy 123
4.2.2.1. Surface Examination 123
4.2.2.2. Metallography 123
4.2.3. Fatigue Behaviour of AISI 304 Stainless Steel Wire 130
4.2.3.1. Fatigue Limit of Notched Wire Samples 130
4.2.3.2. Prediction of Smooth Fatigue Limit 133
4.2.3.3. Notch Effect on Martensite Transformation 141
4.2.3.3.1. Notch-Shape, Size, Producing Method 141
4.2.3.3.2. Notch Roughness Effect 145
4.2.3.3.3. Load Ratio Effect 146
4.2.3.4. Fatigue Crack Growth Rate 152
4.2.3.5. Influence of Yield Strength on Threshold Stress 156

4.2.3.5. Effect of Martensite Transformation on LCF 157
4.2.4. Changes caused by Fatigue Process 161
4.2.4.1. Mechanical Properties 161
4.2.4.2. Hardness Measurements 165
4.2.4.3. Microstructural Changes 166
4.2.5. Fractography 172
4.2.5.1. Static Tensile Fractography 172
4.2.5.2. Fatigue Fractography 173

4.3. 3CR12-Ferritic Stainless Steel Wire 185

4.3.1. Mechanical Properties 185
4.3.2. Microscopy 189
4.3.2.1. Surface Examination 189
4.3.2.2. Metallography 189
4.3.3. Fatigue Behaviour 195
4.3.3.1. Fatigue Limit of Notched Samples 195
4.3.4. Changes caused by the Fatigue Process 197
4.3.4.1. Mechanical Properties 197
4.3.4.2. Hardness Measurements 200
4.3.5. Fractography 201
4.3.5.1. Static Tensile Fractography 201
4.3.5.2. Fatigue Fractography 202

CHAPTER 5 DISCUSSION 209

5. Introduction 209
5.1. 304-Austenitic Stainless Steel Wire 210
5.1.1. Introduction 210
5.1.2. Mechanical properties 210
5.1.3. Fatigue Behaviour 212
5.1.4. Fatigue Fractography 218

5.1.5. Changes caused by Cyclic Strain 220
5.2. 3CR12 Corrosion Resistant Steel Wire 222
5.2.1. Introduction 222
5.2.2. Mechanical Behaviour 222
5.2.3. Fatigue Behaviour 223
5.2.4. Fatigue Fractography 224
5.2.5. Changes caused by Cyclic Strain 226
5.3. High Carbon Steel Wire 228
5.3.1. Introduction 228
5.3.2. Fatigue Behaviour 228
5.3.3. Fatigue Fractography 231
5.3.4. Changes caused by Cyclic Strain 232
5.4. Comparative Discussion 233

CHAPTER 6 CONCLUSIONS AND FUTURE WORK 255

6.1. Conclusions 255
6.2. Future Work 260

REFERENCES 262

CHAPTER 1

INTRODUCTION

A wire rope consists of many wires, usually steel, twisted together to make a complex structure combining axial strength and stiffness with flexibility in bending. The modern rope manufacturer offers a wide range of constructions, with different levels of helical complexity, and wires of different diameters in combinations, to achieve an acceptable performance in a wide range of applications, many of which are safety critical. In addition, a wire rope is designed so that it can withstand some individual wire breaks without loss of structural integrity.

In the great majority of applications, such wire rope is subjected to repeated bending and fluctuating tension. It is also subjected to high contact stresses and longitudinal sliding at points of contact with sheaves and winch drums. The magnitude and distribution of the stresses resulting from these forces determine the overall rope response, in terms of extension, and in certain circumstances, rotation. In the cases of a rope subjected to cyclic loading, stress levels at the critical position will also affect rope endurance. Of particular interest to rope designers is the fatigue behaviour of individual wires subjected to cyclic stresses.

Steel wire is in common use for ropes with strengths of up to 2500 MPa and correspondingly high fatigue strengths. The steel used for these wires is essentially plain carbon steel of carefully controlled composition and a carbon content generally close to the eutectoid. The 'patenting' process, of isothermal transformation and work hardening resulting from successive drawing, is largely responsible for achieving such high strengths without the expense of alloying and more complex heat treatments. The wires do, however, suffer from corrosion which can affect their behaviour in practice.

Stainless steels, particularly the austenitic types, offer a combination of very attractive engineering properties, namely, high strength, high toughness and high corrosion resistance compared to plain carbon steel wires [1]. Thus, the application of stainless steels in the production of wire ropes used in offshore mooring and floating production systems, is very attractive.

One 'stainless' steel, developed by Columbus Stainless Steel in South Africa under the name "3CR12", (which is an acronym for chromium containing corrosion resistant 12 wt% chromium steel) is of particular interest in this study since little is known about its fatigue performance. This steel has a dual phase structure in the normalised condition, consisting of a ferrite matrix and low carbon martensite islands. It also has a further advantage over austenitic stainless steels, such as AISI 304, in that it is a relatively low cost stainless steel.

The purpose of the present study was to compare the fatigue behaviour of these two types of stainless steel, AISI 304 and 3CR12 with that of high carbon pearlitic steel. The ultimate objective was to understand and quantify those characteristics of the stainless steels which enhance the fatigue behaviour of wires, thus leading to possibly greater utilisation of stainless steel in wire rope applications.

The specific aims of the present research were:

1. To investigate the effects of drawing strain on the microstructure, monotonic static and fatigue properties, of AISI 304 austenitic stainless steel and 3CR12 ferritic steel wires and to compare them with those of a high carbon pearlitic steel.

2. To attempt to understand the mechanisms of fatigue crack initiation and propagation in these different steels and the effects of surface characteristics, microstructure and strength on the fatigue limit.

3. To evaluate changes in the microstructure and mechanical properties of these steels as a result of cyclic strain.

In an attempt to meet these objectives a review of fatigue relevant to these materials, in wire form, is firstly considered in Chapter 2. Chapter 3 considers both materials and investigation techniques, including both mechanical tests and microstructural evaluation. Chapter 4 highlights the results of fatigue for each of the wire types, the implications and comparisons of which are presented in the Discussion, Chapter 5. The thesis is concluded with relevant conclusions and suggestions for future work, Chapter 6.

CHAPTER 2

LITERATURE REVIEW

2. Metal Fatigue

2.1. Introduction

A descriptive definition of fatigue is found in the report entitled *General Principles for Fatigue Testing of Metals,* which was published in 1964 by the International Organisation for Standardisation in Geneva [2]. In this report, fatigue is defined as a term which ***'applies to changes in properties which can occur in a metallic material due to the repeated application of stress or strains, although usually the term applies specially to those changes which lead to cracking or failure'.*** This description is also generally valid for the fatigue of nonmetallic materials [2].

Fatigue failures occur in many different forms. Mere fluctuations in externally applied stresses or strains result in *mechanical fatigue*. Cyclic loads acting in association with high temperatures cause *creep-fatigue*; when the temperature of the cyclically loaded component also fluctuates, *thermomechanical fatigue* (i.e. a combination of thermal and mechanical fatigue) is induced. Recurring loads imposed in the presence of a chemically aggressive or embrittling environment gives rise to *corrosion-fatigue*. The repeated application of loads, in conjunction with rolling contact between materials, produces *rolling contact fatigue*, while *fretting fatigue* occurs as a result of pulsating stresses along with small amplitude oscillatory relative motion and frictional sliding between surfaces. The majority of failures in machinery and structural components can often be attributed to one of the above fatigue processes.

Such failures generally take place under the influence of cyclic loads whose peak values are considerably smaller than the "safe" loads estimated on the basis of static fracture analysis.

Any final explanation of fatigue must be given in terms of the lattice defects that, according to solid-state theory, determine the processes of deformation and fracture. Fatigue deformation differs from other modes of deformation in causing these defects to behave in a special way. Unfortunately, the special behaviour cannot be predicted in sufficient detail by fatigue theory in its present state. It is still necessary to proceed by a combination of theory and experiment.

Essentially, fatigue is concerned with the cumulative effects of small strains occurring alternately in one direction and then in the reverse direction. Therefore, fatigue is simplified if the cycles are symmetrical about zero mean strain when the component is free from superimposed nondirectional strains. It is further simplified if the cycles are applied to material that is pure and undeformed and free from superimposed internal strains. The fatigue behaviour recommended for such material gives a standard for comparison. Complications due to unsymmetrical cycles, alloying elements, or for internal strains can be introduced singly, and their influence on the basic mechanism studied separately.

The damage caused by pure fatigue cycles may result from continued reversal of the elastic strain or the plastic strain which also, as damping experiments show, is always imposed by the cycle.

Elastic strain entails a reversible displacement of atoms from their normal lattice positions through distances no larger than about 1/1000 of the lattice spacing. Such small reversible movements are not likely to initiate any structural flaws. They could, however, start propagation of existing flaws, for example, by processes such as the Griffith mechanism, which transform elastic energy into the surface energy of growing cracks. These processes can come fully into play, however, only in the absence of plastic deformation, which provides simpler ways of transforming the elastic energy, for instance, by slip or twinning movements. Accordingly, we may expect elastic strain to play a part in the fatigue of brittle metals under all conditions and on the fatigue of ductile metals, under special conditions arising if the normal capacity of a ductile metal for plasticity were somehow suppressed or exhausted. Damage by the plastic component of the cycle, according to solid-state theory, may result not only from the intensifying of existing flaws but also from the starting of new ones. Since most metals of technical interest are capable of plastic flow, this component is likely to play the more fundamental part in practical fatigue.

The fatigue process can generally be characterised by two stages: Stage I, initiation, and Stage II, crack propagation, Fig.2.1 [3]. So called Stage I growth features microcracks which are oriented around 45° to the maximum principal stress.

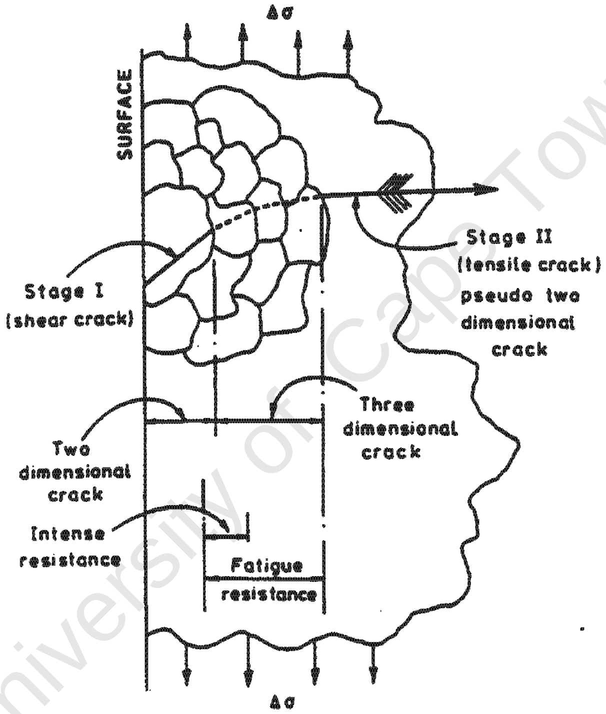

Fig.2.1. *Stages of fatigue crack propagation [3]*

During Stage II growth, the plane of the crack is normal to the direction of the maximum tensile stresses. The Stage I to Stage II transition is generally considered to result from the reduction in the ratio of shear to direct stress at the crack tip, as it moves from the weakly constrained surface crystals into the interior where slip may be inhibited.

2.2. Fatigue Crack Initiation

The origin of fatigue cracks in metals and alloys of high purity is often rationalised by mechanisms of the type first proposed by Wood [4]. The basic premise of Wood's postulate is that repeated cyclic straining of the material leads to different amounts of net slip on different glide planes. The irreversibility of shear displacements along the slip bands then results in the "roughening" of the surface of the material. This surface roughening is manifested as microscopic 'hills' and 'valleys' at sites where slip bands emerge at the free surface. The valleys and hills formed on the fatigued surface are commonly referred to as 'intrusions' and 'extrusions', respectively. The formation of an intrusion-extrusion pair during fatigue was identified by Forsyth and Stubbington [5] in Al-4.5 wt% Cu and by Cottrell and Hull [6] in copper.

For the nucleation of microcracks, a large number of models have been proposed [6,7,8,9]. According to the experimental results reviewed, it is clear that the proposed mechanisms may operate only in the nucleation sites, i.e. at the root of intrusions in the fatigue slip bands, in the vicinity of an inclusion, or near grain boundaries. The most widely accepted mechanism is that of fatigue slip band type nucleation, involving the formation of extrusions and intrusions, as stated by Klesnil and Lukas [10].

During the tensile ramp of a load cycle, dislocation slip occurs on a favourably orientated slip plane. On load relaxation, slip occurs on a parallel plane, since slip on the first plane is inhibited by strain hardening. These slip bands are often referred to as persistent slip bands (PSBs). The presence or creation of slip steps on the surface of a metal acts to localise or concentrate the stress and facilitate the formation of PSBs. The dislocation motion within the whole PSB is not fully reversible and leads to the formation of surface extrusions and intrusions, Fig.2.2.

There exists a great deal of documented evidence, which supports the formation of a unique surface topography as a consequence of cyclic stressing, that facilitates the nucleation of microcracks [4]. The model assumes that the formed intrusions act as stress raisers and promote further slip at the intrusions during subsequent cycles.

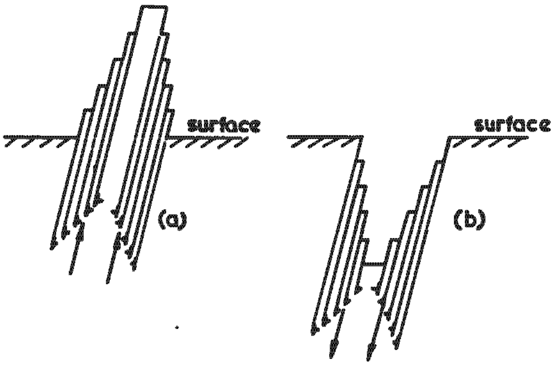

Fig.2.2. *Schematic representation of extrusions and intrusions formed at PSBs*

This leads to the formation of microcracks. In support of the model, it has been shown that microcracks are associated with sharp intrusions, and that they follow the primary slip plane [4]. Present models for the development of extrusions and intrusions are qualitative in that they do not account for dislocation impedance in polycrystalline materials. The emergence of extrusions and intrusions are dependent on the formation of slip bands, which are influenced by metallurgical defects. There is no clear-cut demarcation between nucleation and early-stage propagation since it is difficult to define the end of the nucleation stage. For practical purposes such a definition is often necessary.

A strong effect of environment on crack initiation was identified by Forsyth [7]. Experimental data show that the fatigue life of all materials tested in vacuum is considerably longer than the fatigue life in any other environment. A substantial part of the fatigue-life increase in vacuum is due to the inhibited crack initiation.

2.3. Fatigue Crack Propagation

The nucleation stage ends in the formation of surface microcracks. These microcracks lies along the active slip planes, i.e. along slip planes in which the shear stress has maximum values. By uniaxial loading, the maximum shear stress lies in planes orientated at 45° to the direction of applied stress.

As the number of slip systems in metals is relatively high, those which are active have orientations near to the maximum shear-stress planes, thus the planes of microcracks are always inclined approximately 45° to the vector of the applied stress. In the course of further cyclic loading, the microcracks grow and link together. A large majority of these microcracks stop propagating quite early and only some achieve a length greater than a few tens of microns. With increasing length, the growing cracks leave the original near the 45°-orientated slip planes and tend to propagate perpendicular to the stress axis. The transition of the crack plane from the active slip plane to a non-crystallographic plane perpendicular to the stress axis is often called the transition from Stage I (crystallographic propagation) to Stage II (non-crystallographic propagation). In Stage II of fatigue-crack propagation, only one crack usually propagates, all others stop well within Stage I. Both stages are shown schematically in Fig.2.1.

The crack length at which Stage I - Stage II transition occurs depends mainly on the material and the stress amplitude, but seldom exceeds a few tenths of a millimetre. In some high strength nickel-based alloys, the transition occurs for much longer cracks (of order of millimetres). Sometimes the transition does not take place at all and the whole propagation right through to fracture is Stage-I type [6]. Cheng and Laird proposed a theory for the Stage I-Stage II transition, based on the postulate that Stage II propagation occurs in a Stage I crack when work hardening at the tip of the crack in the primary persistent slip band raises the resolved shear stress locally acting on the secondary slip system to that required to initiate a PSB in that system [11]. This explains why and how the transition crack length depends on the orientation of cycled crystals. Generally, it holds that the lower the stress amplitude, the longer the transition crack length. A further factor strongly influencing the transition is the environment. It has been generally accepted that the environment plays a very important role in influencing the fatigue crack behaviour.

As the crack-propagation rate in Stage I is generally much lower than in Stage II, the number of loading cycles spent in Stage I propagation may be much higher than that spent in Stage II propagation. This is the case for unnotched specimens. The number of cycles necessary for Stage I propagation in sharply notched or precracked bodies becomes negligible and the whole fatigue-crack propagation is Stage II type. Crack propagation in Stage II ends by the fracture of the remaining cross-section. For thinner specimens the crack plane may change its orientation once more–from a plane whose normal is parallel to the stress axis, to the plane whose normal is at 45° to the stress axis, while the direction of the crack propagation remains perpendicular to the stress axis (double shear). These planes are not identical to the Stage-I- crack propagation planes. The explanation for this phenomenon probably lies in the transition from plane-strain to plane-stress conditions at the crack tip.

Stage I fatigue propagation along the slip bands is controlled by the shear component of the applied stress. Non-crystallographic propagation in Stage II is controlled by the normal component. Cracks nucleated at grain boundaries can propagate either along the grain boundaries or across the grains. Analogously, cracks nucleated in slip bands within the grains can propagate either across the grains (transcrystalline growth) or along the grain boundaries (intercrystalline growth). In engineering materials, the crack very often propagates by a combination of transcrystalline and intercrystalline growth. Beevers showed for Stage II cracks in steels, that the percentage of intercrystalline fracture depends on the crack growth rate [12]. For very slow crack growth rates (near-threshold region), the propagation is transcrystalline. For higher crack growth rates, the percentage of intercrystalline fracture increases with increasing crack rate and reaches a maximum (typically several tens of percent of intercrystalline fracture) and then decreases again. Thus the propagation is mostly transcrystalline for very low and very high crack growth rates and combined for medium crack growth rates.

These Stage II cracks will develop at cyclic stress levels above the fatigue limit and start at a depth of between 5 and 10 grains depending on the texture and strength of the material which is a function of grain size. Thus, in a large grained material with easy and numerous slip systems, Stage II cracks will rapidly develop and the criterion of a fatigue limit will become increasingly difficult, if not impossible.

A number of models have been proposed to explain Stage II cracking, one of which is the plastic blunting process model first suggested by Laird and Smith and subsequently modified by Laird and co-workers [13,14,15]. The model described in Fig.2.3., shows an initially sharp crack loaded in tension. Shear deformation is concentrated at the planes of maximum shear stress, which are at an angle of 60-70° to the crack plane (Fig.2.3.a). With increasing tensile stress, the crack tip becomes rounded, and 'ears' form in the apex of the rounded region (Fig.2.3.c). On compression, the rounded off crack comes to a sharp point by complete closure of the two crack surfaces. The deformation 'ears' close up and form the microcraks or troughs of the fractographic ripples, referred to as striations. The deformation produced at the crack tip during each tensile cycle results in the extension of the crack, and the resharpening of the crack tip on unloading ensures favourable conditions for continued crack growth.

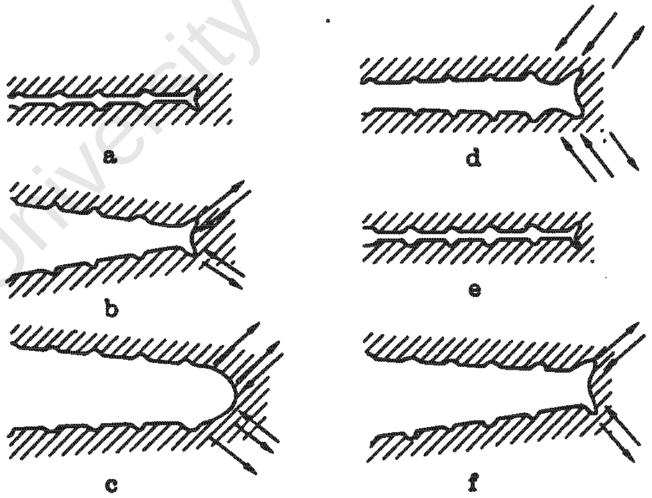

Fig.2.3. *Schematic of stage II crack propagation - after Laird [13]*

The reversed slip mechanism, involving the opening and closing of a crack with the formation of 'ears', provides a good explanation of the formation of striations. This model confirms the one-to-one relationship between the number of striations and the number of load cycles which has been observed by several workers. Although it is generally accepted that each striation is formed during one cycle, under complex loading conditions there may be 'dead' cycles during which the crack does not propagate [13].

Some of the first useful mechanistic information on fatigue crack growth was obtained from fracture surface examination. It was found very early, that many fracture surfaces formed under cycling loading showed periodic markings on both a macroscopic and microscopic scale. Microscale periodic markings are known as striations. One of the most popular topics in research on fatigue crack growth has been the development of descriptions of striation formation.

There are two interesting features of striations: their spacing and their shape and structure. There are two schools of thought on striation formation. Observations by early researchers showed that one striation formed on each loading cycle, and it was clear from experiments that one striation often evidenced an increment of crack growth and arrest. Examples of this work are highlighted in the investigations of Plumbridge and Pelloux [16,17]. However, more recent observations by numerous investigators have shown that one striation does not necessarily correspond to one cycle; it may require tens to thousands of cycles to obtain one striation, as stated by Davidson and Lankford [18]. Data of this type provide clear evidence that both groups of researchers were correct and that many of the differences found have been due to studying different part of the crack growth rates curve (Fig.2.5, p.20). Early works examined relatively large crack growth rates ($>10^{-6}$ m/cycle), where striation spacing approximately equals the crack growth rate. Later studies have emphasised lower growth rates where striation spacing is larger than the crack growth rate. Thus, the crack growth rate curve is divided into three parts.

Region I is defined as the range of ΔK below which striations do not form on every cycle, which usually corresponds to the non-linear region of near-threshold fatigue crack growth. (Historically, region II has been defined as the linear region, so there is some overlap between this and the definition of region I used here). The main focus in this thesis is region II, because most of the lifetime of a crack in a real structure is spent in this crack growth rate region.

Within region II, for materials which form striations, striation spacing (SS), can be related to the applied stress intensity factor by the relation:

$$SS \propto \Delta K^n \qquad \text{Eqn.1}$$

and it is generally found that $n > 2$.

In summary, it is apparent from recent measurements made for fatigue cracks growing in the near-threshold region, that striation spacing can exceed measured crack growth rates by orders of magnitude. This implies that crack advance is an intermittent process, and that many cycles may be required to extend the crack in this region. This same conclusion was reached by Miller in 1969 for steels and again by Broek in 1972 for crack growth through aluminium alloys tested in a vacuum, as stated by Davidson and Lankford [18,19].

The spacing of fatigue striations proved important evidence for understanding the fatigue crack growth process, not so much because the spacing necessarily reveals much about the process itself, but because striations constitute unambiguous, quantitative evidence of the average increment by which a fatigue crack advances.

The absence of fatigue striations does not mean that the basic mechanism by which cracks advance has been changed. It is not clear in many instances why fatigue striations do not form, but it is a subject which has attracted considerable investigation. Broek noted those continuous striations covering multiple grains requires the operation of many slip systems, easy cross slip, and preferably more than one crack propagation plane, as stated by Davidson and Lankford [18]. A lack of striations on a fatigue fracture surface may be due also to their having been obscured by crack closure induced rubbing of the fracture surfaces, as caused by mode II sliding.

Forsyth et al has identified two types of striations: ductile and brittle striations [20].

Ductile striations lie on irregular non-crystallographic plateaux or planes whilst brittle striations lie on crystallographic facets. Classic striations are not always observed on fracture surfaces, even though the reversed slip mechanism may be in operation. The morphology of striations differs widely and depends on symmetry and the number of available slip systems and the material strength level; striation formation is favoured in f.c.c. materials because cross slip is more difficult than in b.c.c. materials [21]. Since plastic deformation involves the generation and motion of dislocations, it is reasonable to expect that the dislocation behaviour at or near the crack tip influences the crack propagation behaviour. In f.c.c. metals, cross slip is thought to be important in the development and propagation of fatigue cracks. F.C.C. alloys of low stacking fault energies in which cross slip is difficult are more resistant to fatigue.

Striations must have a certain length otherwise they are not recognised as striations. The deformation possibilities should ensure similitude of deformation over a certain distance of the crack front, otherwise the ripple does not attain a regular appearance and a regular striation pattern would not be formed. In materials with limited deformation, possible striations may be ill-defined and be confined to a few favourably oriented grains, or may not develop at all.

The formation of regular striations requires:

i) many available slip systems and easy cross slip to accommodate the (usually curved) crack front and to facilitate continuity of the crack front through adjacent grains,

ii) preferably more than one possible crystallographic plane for crack growth.

If these requirements are met, the slip occurring during opening and closing of the crack can adjust to the conditions of the crack front, allowing well-developed striations to be formed.

If the above requirements are not fulfilled, slip will be irregular and fine periodic striations cannot develop.

Fatigue cracking may not always take place by the reversed slip mechanism. Cracking, especially in high strength steels, may occur by mechanisms of microcleavage, intergranular cracking or void coalescence. These alternative modes of crack propagation are thought to be environmentally controlled but may also be a function of microstructure and impurity element content [22].

2.4. Characterisation of Fatigue Behaviour

The Wöhler curve (also called the S-N curve) is often used for the evaluation of the base fatigue strength of materials, machine parts, and whole structures. It shows the relationship of the stress amplitude to the number of cycles to fracture, Fig.2.4.

The Wöhler curve or S-N curve can be determined experimentally for any type of loading and body, whatever its geometry. However, only one type of S-N curve can be considered to reflect material characteristics i.e. the case of homogeneous stress loading (push-pull loading) of smooth specimens. All other S-N curves, such as those obtained in cyclic bending or those obtained on notched bodies, reflect other factors as well as material properties.

Wöhler curves are most frequently determined from stress-amplitude-controlled tests. Alternatively, strain-controlled tests can be employed; the stress amplitude for construction of the S-N curves follows the simultaneous measurement of the cyclic stress-strain response.

The fatigue limit or endurance limit is usually understood as the stress limit at which material can be cycled either for an infinite or sufficiently high number of cycles without fracture. However, later investigators found that many materials did not exhibit an endurance limit response but rather continued to exhibit fracture, provided that the repetition of load was continued for a sufficiently large number of cycles. Thus, in general, under fatigue testing of smooth specimens, materials exhibit one of two types of responses. In mild steel or certain other steels, an endurance limit is observed below which the specimen appears to last indefinitely. Conversely, many materials do not exhibit a clear-cut endurance limit; the S-N curves continue to decrease as N increases. For these materials (e.g., most non-ferrous materials), it is customary to define the stress to cause failure in a given number of cycles as the endurance limit stress σ_s.

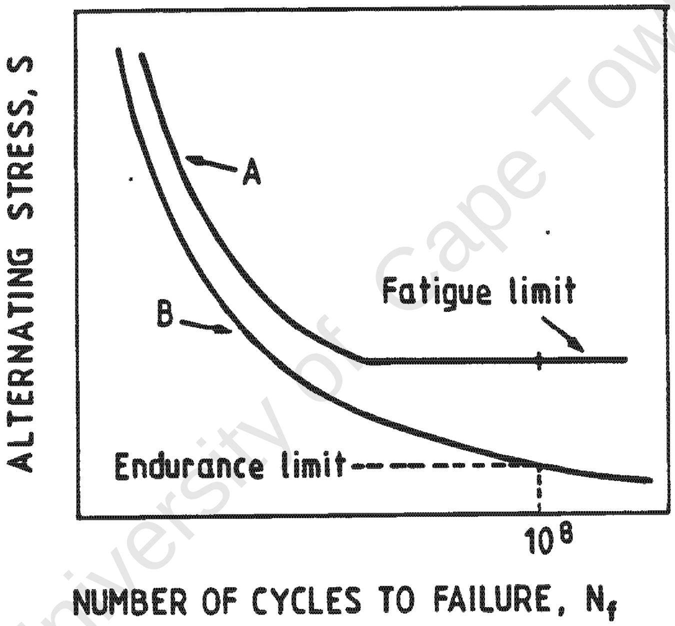

Fig.2.4. *S-N fatigue curves showing two types of behaviour. Type A is typical of alloys which strain age and type B, is typical of non-ageing alloys - after Knott [23]*

The endurance limit is an important material property for members subjected to fatigue loading, particularly as the number of cycles of loading approaches the number associated with σ_s. It should be noted that the other fatigue properties for a given material could be obtained from the S-N curve. For each value of N, there is a stress σ_{am}, the fatigue strength, where the subscript *am* denotes alternating maximum stress; a specimen subjected to completely reversed cycles of stress at σ_{am} will fracture after N cycles. Note that $\sigma_{am} = \sigma_S$ at the endurance limit.

Various factors are known to affect the fatigue strength. For example, the fatigue strength of material may be altered by such factors as frequency of cycling, cold working of the material, temperature, corrosion, residual stresses, surface finish and mean stress.

However, fatigue cracking in structural elements of large engineering components often originates from pre-existing manufacturing or fabrication defects, so that the major part, if not all, of the fatigue lifetime will be spent in propagating the crack.
The S-N information obtained for smooth specimens (where initiation may account for up to 90 % of the total fatigue life) is clearly not applicable under conditions of pre-existing flaws.
The application of linear elastic fracture mechanics and related small-scale crack tip plasticity, has provided the basis for describing the phenomenon of fatigue crack propagation.

2.5. Fracture Mechanics Considerations of Fatigue-Crack Propagation

The object of fatigue studies is ultimately to be able to quantify the rate of fatigue crack growth, and to be able to describe the conditions under which cracks arise, or at any rate grow. Traditional approaches to the quantification of fatigue have relied on the assumption that the nominal stress in the absence of the crack is sufficient to determine its behaviour.

A modern technique for analysing cracks, including crack growth rate, is to use fracture mechanics. Linear fracture mechanics postulates a dependence of the macroscopic crack behaviour on the local characteristics at the crack tip.

In the elastic solution, the stress and strain fields around the crack tip are fully described by the stress intensity factor, K. The local stress and strain fields are assumed to control the crack behaviour thus making the stress intensity factor the basis for describing the crack propagation behaviour. This means that the behaviour of a cracked body can be determined for arbitrary and for random geometries of externally applied forces.

The practical importance lies in the fact that results obtained from laboratory specimens can be related to the real engineering components of the same material, provided the relevant K calibration or geometrical factor is known.

In metals there is always a zone at the crack tip which undergoes plastic deformation. However, provided this region is small, the elastic solution may still give a good approximation of the behaviour of real cracks [22,23,24].

The stress intensity factor is given by:

$$K_I = Y \cdot \sigma \sqrt{\pi \cdot a} \qquad \text{Eqn.2}$$

Where Y = geometrical factor, σ = applied stress, a = crack length.

In fatigue mode, the cyclic stress intensity factor is described by the stress intensity factor range.

$$\Delta K = K_{max} - K_{min} \qquad \text{Eqn.3}$$

where K_{max} and K_{min} are the maximum and minimum and stress intensity factor respectively.

The characteristic dependence of the fatigue crack growth rate on the stress intensity factor range is represented schematically in Fig.2.5, where the fatigue crack growth rate (da/dN) is the crack length increment per load cycle.

For most engineering alloys, a plot of log da/dN against log ΔK exhibits a sigmoid variation, as shown in Fig.2.5. In this plot, three distinct regimes of crack growth can be identified: region I in which the average growth increment per cycle is smaller than a lattice spacing and is associated with the existence of a threshold stress intensity factor range ΔK_o. Below this threshold, cracks either remain dormant or grow at undetectable rates; above the threshold, there is a steep increase in da/dN with ΔK.

Region II, known as the Paris regime, exhibits a linear variation of log da/dN with log ΔK. Region III pertains to the range of high ΔK values where crack growth rates increase rapidly causing catastrophic failure.

Fatigue crack propagation in region I deals primarily with noncontinuum failure processes, where the increment of average crack extension is less than 10^{-6} mm/cycle. In this region, the stress intensity factor range approaches the fatigue crack growth threshold ΔK_o.

There have many attempts to describe the crack growth rate curve by 'crack growth laws', which usually are semi or wholly empirical formulae fitted to a set of data. The two most widely known are:

Paris equation [25] $$da/dN = C\,(\Delta K)^m \qquad \text{Eqn.4}$$

Forman equation [26] $$da/dN = C(\Delta K)^m/(1-R)\,K_c - \Delta K \qquad \text{Eqn.5}$$

where, C and m are materials constants, which may depend on material, microstructure, and environment; $R = \sigma_{min}/\sigma_{max}$ (load ratio);

K_c = material fracture toughness.

In these empirical relationships, ΔK is an independent variable and is computed on the basis of the continuum mechanics of a crack in a homogeneous medium using macroscopic information-crack length and applied stress.

da/dN is the dependent variable and represents the microscopic response of the material. Thus, the correlating parameters C and m describe the transfer of a macroscopic driving force to the microscopic response of the material.

In steels, this sigmoidal variation of growth rates with ΔK has been characterised in terms of different primary mechanisms of fracture.

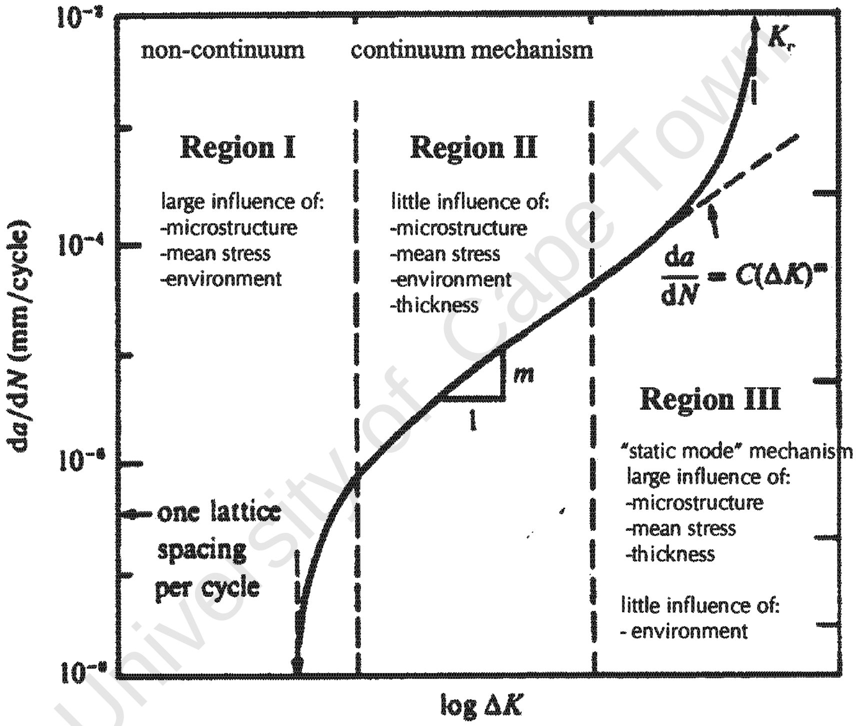

Fig.2.5. *Schematic illustration of the different regimes of stable crack propagation [22]*

At the midrange of growth rates (region II, where the Paris equation applies), fatigue failure generally is observed to occur by a transgranular ductile striation mechanism, and there is often little experimentally observed variation of growth rates with microstructure and mean stress [10,23,24,27]. At higher growth rates (region III), when K_{max} approaches K_{IC}, static fracture modes, such as cleavage, intergranular and fibrous fracture occur, in addition to striation growth, resulting in a marked sensitivity of propagation rates to both microstructure and mean stress [23,24,27].

At low (near-threshold) growth rates, region I, there is similarly a strong influence of microstructure and mean stress, although it is uncertain whether this can be directly related to a change in fracture mode [28,29,30]. However, at such near-threshold stress intensities, the scale of plasticity approaches the order of the microstructure size scales and measured propagation rates become less than an interatomic spacing per cycle, indicating that crack growth is not occurring uniformly over the entire crack front.

There is no unifying picture of how the environment may influence such fatigue crack propagation. The fatigue crack growth rate is influenced by several concurrent and mutually competitive mechanistic processes involving the microstructure, mechanical load variables and environment, as well as by crack closure effects. Therefore, it is not surprising to note that no single theory can successfully predict crack propagation rates for a wide variety of test conditions, even for a single alloy system, from fundamental principles, as stated by Ritchie [31].

2.6. Factors Influencing Fatigue Behaviour

The effects of various mechanical, microstructural and environmental factors on cyclic deformation as well as on crack initiation and growth in a vast spectrum of engineering materials have been the topics of considerable research in the past four decades.

Investigations of the effect of metallurgical variables on fatigue crack initiation have identified grain size, yield strength, impurity concentration, microstructure and stacking fault energy to be of major importance. The surface finish and load ratio R have been identified as mechanical factors which influence the fatigue behaviour [31,32,33]. Investigation of microstructural variables in fatigue crack initiation and propagation has long queried how these processes are related to each other.

Widespread observations indicate that nucleation usually occurs at the surface of a material, and both nucleation and propagation are a consequence of cyclic slip.

Initiation of fatigue cracks has been observed to occur along slip bands, at grain boundaries, at second-phase particles and at inclusion-second phase interfaces, depending upon which occurs most easily. During cyclic plastic deformation, dislocations that are formed can either emerge at the surface or pile up against obstacles, depending on the nature of the metal and the microstructure.

The mechanism of sufficient dislocations piling up at an obstacle to activate a dislocation avalanche, causing slip-band formation, inclusion cracking, or decohesion at a second phase-matrix interface, essentially depends on slip length. Smaller mean free slip paths, with corresponding reductions in the magnitude of the local plastic strain, reduce the stress for crack initiation and Region I growth and result in increased fatigue strengths. In the case of fully pearlitic steels, refining the lamellar spacing should reduce the pile-up stress, thereby increasing the applied stress that could cause a cementite plate to fail. This explanation showed that carbide lamellae are effective barriers to dislocation motion. This argument is additionally consistent with several theories of crack initiation in pearlite, which require the stress build-up at the ferrite-carbide interface to be large enough to cleave the carbide lamellae. Although colony and grain boundaries certainly obstruct dislocations, the finer spacing and difficulty to dislocation passage posed by the ferrite-cementite phase boundaries are thought to dominate.

Fatigue testing for basic research can be performed and usually has been under either constant stress amplitude or constant plastic strain amplitude. Most of the results from early literature were obtained from stress-controlled tests. It was previously explained by Baudry and Pineau that the mode of testing could affect the behaviour in cyclic deformation [34].

There is a possibility that the fracture behaviour under these modes might also be different. The differences in fracture mode have been observed and they can be attributed to the stress intensity variation at the crack tip. The stress intensity increases as the crack grows longer when the test is conducted in stress control and this causes the earlier onset of region II crack growth.

In plastic-strain controlled tests the stress intensity remains roughly constant with crack growth and there is therefore less inducement to change the growth mechanism. The results also indicate that there is no difference in the nucleation mechanism when the specimen is subjected to cycling under constant plastic strain or constant load.

2.6.1. Microstructure

Microstructure is now known to affect both the initiation and propagation of fatigue cracks. In a variety of metals and alloys, however, it has been shown that microstructural conditions resisting crack nucleation are not necessarily beneficial and in some cases are deleterious, to fatigue crack propagation resistance [30].

Very little information is available at present on the relative resistance to near-threshold fatigue-crack propagation of particular microstructures in metals, aside from data where particular structures have been compared at different strength levels.

The fully pearlitic eutectoid steel is of particular interest, because both strength and toughness increase with a reduction in pearlite lamellae spacing [35,36]. The pearlite spacing depends on the prior austenite grain size; smaller grains resulting in finer spacing.

The effect of microstructure on fatigue crack initiation of fully pearlitic steels was studied through independent variation of the prior austenite grain size, pearlite colony size, and the pearlite interlamellar spacing [35]. Increasing yield strength (controlled by decreasing the pearlite interlamellar spacing) was seen to increase the smooth and notched-bar crack initiation endurance limit. Grain and colony size variations, at constant strength, were seen to exhibit no effect on crack initiation.

Cyclic deformation behaviour in pearlitic eutectoid steel strongly depends on the interlamellar spacing with cyclic softening in fine pearlite, cyclic hardening in coarse pearlite and both cyclic softening and hardening depending on the strain amplitude in medium pearlite [35,36,37,38].

The austenite to martensite transformation in TRIP steels has been shown to play a beneficial role on the tensile strength, fracture toughness and fatigue-crack propagation properties [39,40,41]. The beneficial effect of the martensitic transformation on uniform elongation is due to the inhibition of necking by strain-hardening, while the toughness and fatigue-crack propagation properties are enhanced due to the adsorption of energy by the martensitic transformation occurring at the crack tip. However, the results indicate that the transformation does not play a similar beneficial role on the LCF properties; LCF properties were apparently superior in the absence of the martensitic transformation [42].

2.6.2. Grain size

The effect of grain size on fatigue life has been studied extensively [40,43]. In some systems, grain size has a negligible effect but in others the effect is significant. It is thought that in a number of materials the effect of grain size on fatigue behaviour depends on the ease of cross-slip [39].

When planar slip was present, fatigue life increased with decreasing grain size, but this effect was absent when wavy slip was observed. The development of a cellular substructure masked the effect of grain size. When no cellular substructure formed, the grain boundaries obstructed region I crack propagation [41]. As the effectiveness of this process decreased with increasing grain size, fatigue life was inversely related to the grain size.

Whereas refining grain size can be beneficial in raising the fatigue limit or endurance strength of (planar slip) materials, the effect of grain size on fatigue-crack propagation has been observed to be negligible, in most studies, at intermediate growth rates [43]. At low growth rates in room air, however, several workers have observed improved resistance at near-threshold crack propagation with coarser grain sizes. Furthermore, a marked increase in threshold values has been observed in a range of low-strength steels by increasing the ferrite grain size. In all of these studies, however, no attempt was made to control strength and the effect of coarsening the grain size may well have been masked by a concurrent decrease in strength, which is known to increase markedly the threshold in steels.

Comparisons at constant yield strength have been made in two high-strength steels, 300-M and Fe-Cr-C, where it was found that, in the cyclic softening 300-M, the prior austenite grain size decreased near-threshold growth rates by almost an order of magnitude yet left ΔK_{th} unchanged, whereas, in cyclic hardening Fe-Cr-C, similar coarsening of the structure increased near-threshold rates and reduced the threshold value. The variation of threshold values with grain size, for low- and high-strength steels, clearly shows the contrasting behavior between the two classes of steels.

Several explanations have been proposed to explain the grain-size effect, none of which is entirely satisfactory. It has been suggested, for example, that since near-threshold growth is 'microstructurally-sensitive', it may be confined to specific crystallographic planes so that in coarser structures, greater deviations of the crack path may occur from the plane perpendicular to maximum tensile stress.

Other authors have reasoned that, for high-strength steels, since plastic zones are often confined within a single grain during near-threshold growth, the probability that hydrogen atoms, generated by chemical reactions with the environment at the crack tip, can be swept into the grain boundaries by dislocation motion, is much smaller if the grain size is very large, as stated by Ritchie [44].

Effectively, this hypothesis states that by coarsening the grain size, the environmental contribution to near-threshold growth is reduced and this is consistent with an observed decrease in hydrogen-embrittlement susceptibility of high-strength steels as the grain size is increased. However, the conflicting results observed in Fe-Cr-C steel are not consistent with this explanation. A study of the influence of grain size (at constant strength) in inert environments is required before this effect can be resolved.

In some austenitic stainless steels martensite is formed during room temperature deformation, leading to reduced crack growth and rapid hardening [42-56]. In AISI 304 L stainless steel the peculiarities of fatigue hardening could be attributed to the microstructural changes introduced by martensite formation [46]. It was found that any martensite phase transformation that occurs during the fatigue process might act beneficially or deleteriously depending on the degree to which the austenitic steel has been previously strained. In steels with low prior strain, any transformation is beneficial but the opposite holds in highly strained austenite.

The effect of martensite formation on the room temperature LCF behavior of AISI 304 LN austenitic stainless steel specimens of two different grain sizes is considered by Chanani [42]. The differences in fatigue behavior were attributed to the dependence of martensite formation on grain size and strain amplitude.

It was concluded that crack initiation determines the fatigue life at low strain amplitudes. As cracks nucleate earlier in the coarse grained specimens, their LCF lifetimes are inferior compared with those of fine-grained specimens.

At high strain amplitudes, crack propagation determines the LCF life. More martensite forms at higher strain amplitudes and coarser grain sizes. Martensite formation is accomplished by a volume increase. When significant martensite formation is present, in a constant strain amplitude test, the compressive stress has to reach a higher value than the tensile component (in order to compensate for the volume increase). The compressive residual stresses introduced in this manner decrease the crack propagation rate [45,46]. This accounts for the increased fatigue life at high strain amplitudes in the specimens of coarse grain size because martensite formation increases with both strain amplitude and grain size.

At low strain amplitudes, on the other hand, since the amount of martensite formed was rather small, the beneficial effect of martensite formation on crack propagation was not significant and the conventional decrease in the LCF life with increasing grain size was present. Thus, the effect of martensite formed on the LCF life depended on the amount of transformation product, which was a function of strain amplitude, grain size, and whether crack initiation or propagation controlled the fatigue life at a given strain amplitude.

A comparative study considering the influence of grain size on the phase transformation during room temperature rolling of austenitic stainless steels has found that the amount of created α'martensite increases with the amount of deformation in AISI 304 as well as in AISI 316 [51]. Additionally, the α'-volume fraction was found to be grain-size insensitive in AISI 316 and grain-size sensitive in AISI 304; the smaller the grain size the more α'-martensite was detected.

2.6.3. Stacking Fault Energy

The dependence of fatigue life on grain size also varies depending on the deformation mode [57].

Grain size has its greatest effect on fatigue life in the low-stress, high-cycle regime in which Stage I cracking predominates. In high stacking fault energy materials (such as aluminium and copper) cell structures develop readily and these control the region I crack propagation. Thus, the dislocation cell structure masks the influence of grain size and the fatigue life at constant stress is insensitive to grain size.

However, in a low stacking fault energy material (such as alpha brass) the absence of a cell structure, because of planar slip, causes the grain boundaries to control the rate of cracking. In this case, fatigue life is proportional to (grain diameter)$^{-1/2}$.

2.6.4. Material Strength

Fatigue crack propagation has been generally found to be largely unaffected by yield strength. In fact, for steels, raising the strength by nearly an order of magnitude does not change crack-propagation rates over the midrange of growth rates by much more than a factor of two or three [44]. However, at near-threshold levels below 10^{-6} mm/cycle, a surprisingly large dependence of material strength has been observed on the value of the threshold ΔK_{th} and on subsequent growth rates. In low-strength ferritic-pearlitic steels with yield strengths less than 500 MN m^{-2}, for example, values of the threshold have been observed to decrease significantly with increasing strength. An even larger effect has been reported for high-and ultrahigh-strength martensitic steels (yield strengths between 1000 and 2000 $MNmm^{-2}$) with the exception that the controlling measure of strength was the cyclic, rather than the monotonic, yield stress [56,17]. Specifically, increasing the cyclic strength led to marked increases in near-threshold propagation rates, and a significant reduction in ΔK_{th}. Cyclic softening can thus be regarded as extremely beneficial in improving near-threshold fatigue-crack growth resistance in steels [56,17].

The effect of strength on near-threshold crack-propagation behaviour, is significantly less at high R values and not so evident in ferritic-pearlitic steels [17,53,57].

The latter probably results from the fact that data on the lower strength steels cover a relatively narrow range of strengths and is subjected to considerably more scatter. Furthermore, varying the strength in such steels generally involves variations in the ferrite grain size, which is also known to have a marked influence on near-threshold behaviour [2]. The dependence of near-threshold growth-rate behavior on material strength in steels has been rationalized, however, in terms of environmental arguments and notch sensitivity effects [17,5]. A comparison of growth rates in a single material, with varying strength, in vacuum is required to help resolve this issue.

An intriguing aspect of the strength effect in steels is the fact that whereas the fatigue-crack propagation threshold ΔK_{th} is decreased with increasing strength, the well known fatigue limit or endurance strength, is increased [56,58]. Both parameters represent limits for fatigue damage but the threshold ΔK_{th} must be regarded as the minimum stress intensity below which long macrocracks do not grow, whereas the fatigue limit is generally the minimum stress below which short macrocracks do not initiate (i.e. by coalescence of microcracks).

The variations of threshold ΔK_{th} with monotonic yield strength and ultimate tensile strength indicate a general trend of an inverse dependence of ΔK_{th} on material strength. As cyclic strength is increased, either because of high initial monotonic strength or by cyclic hardening, the threshold for fatigue-crack propagation is reduced. To summarize, the different steels having identical monotonic yield strength but different microstructure show widely differing values of ΔK_{th} [5]. The hardest structure showed the smallest threshold, due to cyclic hardening. On the other hand, the softest condition after cyclic softening has the largest threshold value.

Studies of the fatigue behaviour of metastable austenitic steels have shown interesting differences between the behaviour of high strength TRIP steels and that of lower-strength metastable austenites, identifying a marked contrast between the influence of the deformation-induced martensitic transformation under strain-control vs stress-control conditions [43,49,51,58-64]. Fatigue crack propagation studies (controlled ΔK) have indicated that the deformation-induced transformation retards crack propagation in the lower strength austenites, particularly at low ΔK, and also exerts a beneficial influence in high strength TRIP steels, though to a much lesser extent [50]. In smooth bar fatigue tests on lower strength austenites, the transformation was found to reduce fatigue life under conditions of controlled plastic strain amplitude [51]. Under controlled total strain amplitude, the transformation was found to be detrimental to low cycle fatigue life but it indicated that a small amount of transformation might be beneficial at high cycle limit [58]. Similarly, the low cycle fatigue properties of high-strength TRIP steels were found to be degraded by the deformation-induced transformation under controlled total strain amplitude conditions [58].

Under stress-control, however, the fatigue life of the lower strength metastable austenites is found to be greatly enhanced by the transformation; for smooth bar tests with a stress ratio of R=0, fatigue limits in excess of the yield strength have been reported [59]. This study was undertaken to extend the stress-control fatigue tests to the high-strength TRIP steels and determine whether the beneficial effect of the deformation-induced transformation persists to the high strength levels.

In addition, fatigue data generated under stress-control conditions may provide a more useful design criterion for many applications.

In one study, the TRIP steel samples of nominal composition: Fe-9Cr-8Ni-4Mo-2Mn-2Si-0.3C were prepared and the solution treated samples were strengthened by warm-extrusion through reductions of area of 40, 60, or 80% in the temperature range 400 to 850 °F [61,62]. The overall tensile properties of the extruded and tempered material were superior to those of warm rolled material. In this study, fatigue properties of both the as-extruded and the tempered material were examined to compare materials of different stability, thus allowing an assessment of the influence of the deformation-induced transformation.

In conclusion, although there are possible additional effects associated with tempering, the comparison of S-N curves of the as-extruded material and the less stable tempered material suggests that the deformation-induced martensitic transformation does increase the fatigue strength of TRIP steels in smooth bar tests under stress-control conditions, in accordance with observations on lower strength metastable austenites.

2.6.5. Impurity Levels

It is well known that the presence of geometrical discontinuities, such as nonmetallic inclusions and corrosion pits, can have a deleterious effect on the fatigue and fracture resistance of a material. The crack nucleation characteristics of inclusions play an important role in influencing fatigue failure, and it has been reported that surface inclusions are more harmful than subsurface ones [65]. The number, size, and type of inclusion have been found to be of importance in determining their effects on subsequent fatigue behavior. It has been shown that the orientation of the inclusions with respect to the orientation of the stress field and the relative deformability of inclusions with respect to that of the matrix, owing to the mismatch of physical, thermal, mechanical and chemical properties, are also important. Crack nucleation at inclusion sites is also believed by some investigators to be operated by interfacial debonding mechanisms [65].

Corrosion environments can enhance fatigue damage by affecting crack initiation and propagation. The crack nucleation process is often facilitated by pitting that can lead to cracking and corrosion pits frequently are observed to form at the sites previously occupied by inclusions. Materials that show a fatigue limit when tested in air, will have their fatigue limit reduced or even removed when a corrosive environment is introduced. The effect of non-metallic inclusion content on near-threshold fatigue behavior has been examined in a medium-strength pearlitic rail steel [66]. Here it was found that whilst decreasing the volume fraction of inclusions (sulfide stringers and oxide-type) led to marked increases in the fatigue or endurance limit, no systematic effect was observed on the value of the threshold stress intensity factor.

Generally, inclusions can affect fatigue properties in two ways. First, because of the different deformabilities of the inclusion and matrix, those inclusions with low deformability can introduce microcracks at the matrix-inclusion interface during hot or cold working of the metal. These microcracks, which already are present in the material from the beginning of the service may cause direct propagation of cracks leading to failure and as a result, eliminate the initial stage of crack nucleation. Secondly, if the microcrack does not exist prior to fatigue loading, inclusions still can affect the fatigue resistance strongly, mainly by facilitating the crack initiation phase.

As summarized by Kiessling, for an inclusion to be a potential source for fatigue failure, two main criteria must be fulfilled; the inclusion should have a critical size, depending on the depth below the steel surface, and the inclusion should have a low deformability, related to its expansion coefficient taken at the actual temperature during fatigue [66].

For steels, dangerous inclusions include single-phase alumina (Al_2O_3), spinels, and calcium-aluminates greater than 10 μm in size. The MnS types appeared to be the least harmful.

2.6.6. Surface Conditions

It is well established practically that the fatigue process is very sensitive to surface state. Fatigue life is strongly influenced by surface finish and surface treatment [2]. The reason why fatigue is a surface-sensitive process lies in the fact that fatigue cracks usually nucleate from free surfaces of cyclically loaded metals.

The nucleation, as well as the whole fatigue process, is controlled by the cyclic-plastic deformation. Therefore, it can be expected that cracks nucleate at positions where the cyclic-plastic deformation is higher than average, in another words, in places of plastic-strain concentration. Besides macroscopic sources of stress concentration on the surface, there are also microscopic stress concentrators, which are effective even under conditions of ideal uniaxial loading. The stress level at the surface is sensitive to surface topography. The surface is never ideally smooth. For example, very fine grinding produces grooves with depth of the order of tenths of a micron, which locally can increase the stress by tens of percent. Fortunately, the surface finish often produces a thin plastically deformed surface layer with compressive residual stress, which may balance or even compensate for the detrimental effect of microscopic stress concentration on the resulting life.

A further type of microscopic stress concentration is the surface step produced by a dislocation leaving the metal during plastic deformation, so that the cycle itself can produce localized stress concentrations at the surface. Second-phase particles, such as inclusions and precipitates, having elastic properties different from the matrix, generally also serve as stress concentrators.

From all the facts presented, it could be stated that at the surface of cyclically loaded metal there is a higher stress than in the interior and therefore, also a higher plastic strain. This explains why fatigue cracks nucleate from the surface, on the basis of applied stress alone.

The surface finish of a component will depend upon its method of production. In the case of wire drawing, important factors that influence surface quality are the surface roughness of the initial bar, surface coating process, and drawing parameters themselves. Therefore, surface conditions become an extremely important factor influencing the fatigue strength. The effect of surface finish on fatigue life is quite clear; the fatigue life decreases as the surface roughness increases. The reduction in fatigue life is related to the development of more microcracks and microvoids as the surface roughness increases. Because the condition of the surface can have a profound effect on fatigue strength, attempts have been made to increase the fatigue strength by suitable surface treatments.

Fatigue life depends very strongly on the state of the surface layer. As this is of great practical importance; there are a number of technological methods for fatigue-life improvement.

Residual stresses arising from fabrication or surface and heat treatments, when superimposed with the applied fatigue loads, alter the mean level of the fatigue cycle and the fatigue life for crack nucleation. In general, residual stresses affect the fatigue behaviour of materials in the same way as the static mechanical stresses superimposed on cyclic stress amplitude. Therefore, residual stresses are favourable if compressive and detrimental if tensile; this is especially true for high strength materials. The beneficial effect of residual stresses introduced by surface treatments becomes less significant at larger applied stresses because large amplitudes of the pulsating stress easily 'relax' the residual stress, particularly in softer materials.

Shot peening is widely used to improve the fatigue life of many engineering structural parts. In the shot peening process, a stream of small, hard spheres (typically 0,1 to 1mm in diameter) is shot at a surface which is to be treated. Depending of the diameter of the shots, the velocity of their impingement on the surface and the duration of the process, the maximum compressive residual stress generated by the localised plastic deformation of the surface layer can reach about one-half the yield strength of the material [67]. As the shot-peened surface layer has a compressive mean stress, it acts to enhance significantly the total fatigue life by reducing the damaging effect of the tensile portion of fully reversed cyclic loads.

After shot peening, obvious changes occur on the surface layer: i) changes in microstructure (subgrain formation, crystal distortion and increasing dislocation density); ii) plastic deformation causes the surface to become slightly dimpled, so that surface roughness is increased, iii) plastic working on the surface means that strain hardening occurs, resulting in a change in surface hardness and an increase in the yield strength of material, iv) elastic-plastic relaxation of near surface layers as the shot rebounds induces residual compressive stresses.

The major benefit of shot-peening in improving fatigue and fretting fatigue strength is undoubtedly the residual compressive stresses generated in the surface which retards the propagation of fatigue cracks.

2.6.7. Influence of Load Ratio R

In fatigue studies, the effect of mean stress is often expressed in terms of the stress or load ratio $R = K_{min} / K_{max}$. Whereas little influence of R can be seen for the midrange of growth rates, near-threshold propagation is generally extremely sensitive to the load ratio [68,69,70,71]. If the load is positive, experiments have shown that the required stress intensity factor range for growth decreases with increasing positive R values.

Several authors have proposed empirical equations to describe the dependence of the threshold value on R. It is generally recognised that a phenomenon of major influence in this issue is the decrease in the contribution of crack closure as the positive load ratio increases.

On the other hand, if the load ratio is negative, it has been observed that the required stress intensity factor range for growth (threshold stress intensity range) decreases as R becomes more negative, and after a certain point, it remains constant. In fact, the common analytical practice has been to exclude the compression segments since it seems reasonable to believe that no contribution to crack growth developed during a compressive excursion. Thus, in the case of a negative load ratio R, the stress intensity factor range is effectively equal to the maximum positive stress intensity factor. This is based on the assumption that a crack would be closed in compression and only the tensile portion of the loading cycle can attribute to crack growth.

However, a common conclusion from a number of experimental programs during the past several years, has been that the use of the foregoing assumption of neglecting the compressive segment may lead to non-conservative predictions.

Since much of the observed near-threshold behaviour can be attributed to the closure phenomenon, many studies have been performed in an attempt to understand the effect of surface roughness on fatigue crack growth. The closure obstruction effect of a plastic wake is generated as the crack advances.

In a fundamental paper, Forsyth suggested that the topography of a fracture surface near the crack tip, as well as the extremely applied loads, was important to an understanding of crack advance [7].

Modelling surface features, e.g. asperities which act as obstructions to closure leads to a partitioning of the crack tip state into two components, i.e. a component caused by external forces which may be classified as global, and one resulting from asperity contact forces which may be termed local. Since there are a variety of local contact force types that can be developed, different crack type states are possible.

Experiments show that the influence of R on the crack growth rate is greater near the threshold [68]. The experimental results show that, for the pearlite steel, the crack propagation rate at $\Delta K = 5$ MP $m^{-1/2}$ is two orders of magnitude greater for R=0.8 than for R=0.1. Although qualitatively this phenomenon has been widely explained, the efforts to give a quantitative explanation from a theoretical model have not been successful, due to the large influence of microstructural factors.

Actually, these factors may produce an increment of crack closure by increasing the roughness of the crack surface, or provide different preferential orientation for the advance of the crack front leading to crack branching. The influence of these microstructural factors is thus very important and not easily quantified. In pearlitic steels, the two main characteristics are the austenitic grain size and the interlamellar spacing of the pearlite. Large austenitic grain sizes, as well as high pearlite interlamellar distance, produce rougher crack surfaces increasing the crack closure effect and diminishing the effective force available to produce the crack propagation. Among the empirical expressions proposed by Mausonave and Bailon, the simplest relation that gives a good fit to experimental results has been the linear relationship [71]:

$$\Delta K_{th} = \Delta K_{tho} - A \cdot R \qquad \text{Eqn.6}$$

where, ΔK_{tho} is the threshold stress intensity factor at load ratio R=0.

The value of parameter A has to be a function of the mechanical properties and the microstructure of the steel. Since the yield stress is a function of the pearlitic interlamellar spacing (in pearlitic steels), it can be assumed that the A value will decrease for stronger steels giving rise to a weaker influence of R on the threshold value.

As outlined above, ΔK_{th} depends on the mechanical and microstructural properties of the steel. In pearlitic steels, there exists a simple relationship between them, because the higher the yield strength, the lower the pearlite interlamellar distance. Therefore, it seems possible to estimate ΔK_{th} from σ_y, and this possibility would be very interesting since the yield strength determination is quite simple. The influence of σ_y on ΔK_{th} is less important for higher values. The explanation might be as follows; the two main effects promoting the crack closure are the plasticity induced closure near the crack tip and the surface roughness closure; since for high R values the crack is always open and the CTOD values are greater than the crack rugosities, the only effect on the crack closure is the plasticity induced and thus the influence of R is much smaller. The influence of the load ratio on the fatigue crack growth rate in 304 stainless steels, shows that as the load ratio R increases, for a given ΔK, the fatigue crack growth rate curves shifts sharply to the left for the unstable alloys. An increase in the fatigue crack growth rate with load ratio is a common phenomenon, but the effect is usually small. The results showed that in all cases, the fatigue crack growth rate increases with R but by an amount that is significantly greater under conditions where the austenite is relatively unstable [69]. These results suggest that the martensitic transformation exaggerates the load-ratio effect.

The abnormally large R-ratio effect in metastable austenitic steels is surprising since the extent of the martensitic transformation increases with R at given ΔK.

The results suggest that the reduction in the crack growth rate due to the transformation depends on the load ratio; that is, high tensile mean stress lessens and even eliminates the effect of the transformation.

2.6.8. Crack Closure

The mechanism of fatigue crack closure, particularly at very low stress intensities approaching the threshold stress intensity range ΔK_{th} below which cracks remain dormant or grow at experimentally undetectable rates, has been studied extensively [7,6,69,71-75].

Crack closure, as first popularised by Elber, was considered to arise from the fact that during fatigue crack growth, material is plastically strained at the crack tip, and due to the restraint of surrounding elastic material on this localised residual stretched zone, some closure of the crack surfaces occurs above the minimum load of the fatigue cycle [76]. This concept which is termed *plasticity-induced crack closure*, has proved to be extremely effective in explaining many aspects of fatigue crack propagation behaviour, including the influence of load ratio, and the role of variable amplitude loading. Since the crack cannot propagate while it is physically closed, the stress intensity range experienced at the crack tip is reduced from the nominally applied value ($\Delta K = K_{max} - K_{min}$) to some effective value ($\Delta K_{eff} = K_{max} - K_{cl}$), where K_{cl} is the stress intensity to close the crack. Note that K_{cl} is bigger than K_{min}, so ΔK_{eff} is less than ΔK. Such *plasticity-induced closure*, however, is most prevalent under essentially plane stress conditions; yet recent studies on fatigue crack propagation at ultralow growth rates ($da/dN < 10^{-6}$ mm per cycle), approaching the threshold for fatigue crack growth (ΔK_{th}), have clearly shown that very significant closure effects can also occur in plane strain [7,8,68,71-81].

Two mechanisms have been proposed to account for such closure in plane strain, based on the role of crack surface corrosion deposits and fracture surface roughness or morphology, Fig.2.6. The first of these mechanisms, the so called *oxide-induced crack closure*, arises from the fact that when oxide deposits, formed on freshly exposed surfaces at the crack tip in moist environments, reach a thickness comparable to crack tip opening displacements, the crack can become effectively wedged-closed at stress intensities below K_{min}. This concept proved to be particularly effective in explaining certain aspects of the role of the environment in influencing near-threshold, fatigue crack growth. The second mechanism, termed *roughness-induced crack closure*, arises in situations where the size-scale of the fracture roughness is comparable to crack tip opening displacements and where significant Mode II displacements exist, e.g., at near-threshold levels [71]. As shown in Fig.2.6, closure can again be promoted since the crack can become wedged-closed at discrete contact points along crack faces.

It is evident that crack closure is a phenomenon whose influence on fatigue crack growth rates is strongly dictated by microstructural and environmental factors, and mechanical loading parameters. However, there are certain basic characteristics and trends, which are common to various types of crack closure and to a wide variety of materials [2].

(1) Crack closure is generally more dominant at lower ΔK levels and at lower R ratios because of the smaller minimum crack opening displacements of the fatigue cycle. For plasticity-induced or transformation-induced crack closure, the possibility of enhanced crack closure may also increase as a result of the larger crack wake stretch or transformed zone size at higher ΔK levels and R ratios. However, this increased propensity for closure may be offset by the larger minimum crack opening displacements.

(2) There is a characteristic size scale associated with each closure process, such as the height of the residual plastic crack wake stretch for plasticity-induced crack closure, the thickness of the fracture surface oxide layer for oxide-induced crack closure, the height of the fracture surface asperities for the crack closure due to roughness and the height of the transformation zone for the closure arising from phase changes. When the size of these characteristic closure dimensions becomes comparable to the crack opening displacement, premature crack face contact has a marked effect on the rate of fatigue crack growth.

(3) As a fatigue crack emerges from a free surface or a stress concentration, the extent of crack closure generally increases with an increase in the crack length up to a certain saturation crack length, beyond which closure is normally crack length independent.

(4) Closure is produced by mechanisms which are operative both at the tip of fatigue crack, such as plastic deformation or phase transformations, as well as phenomena which occur in the wake of the fatigue crack tip, such as fracture surface oxidation.

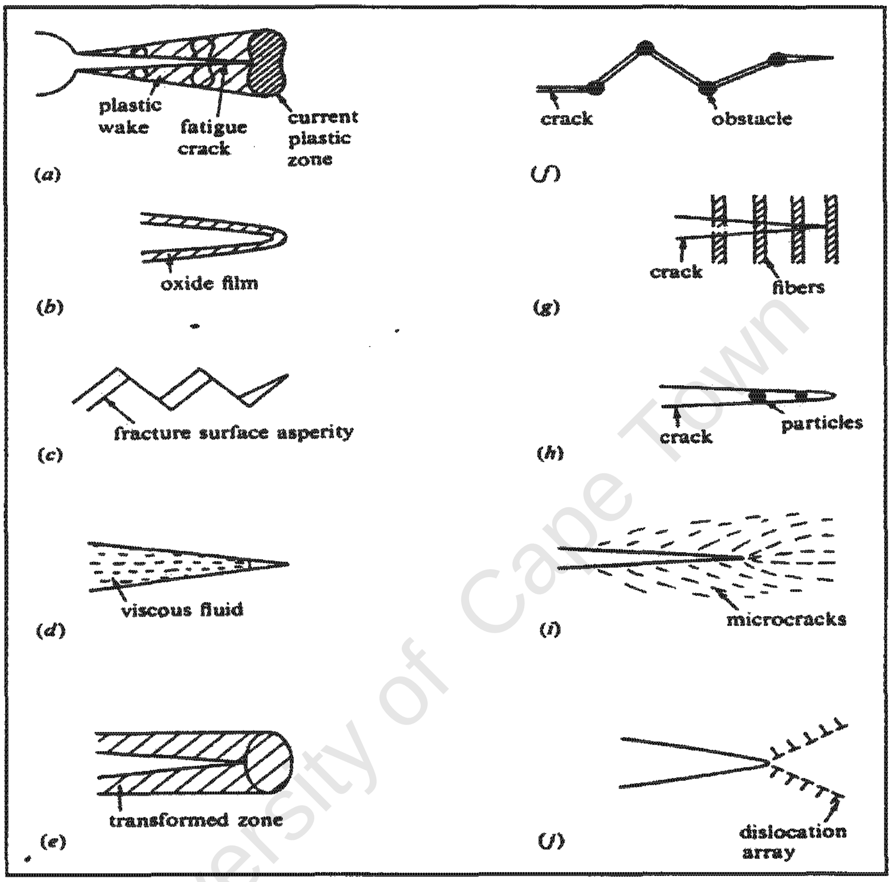

Fig.2.6. *Schematic illustration of mechanisms of fatigue crack-closure*

after Suresh [2]

***a)** plasticity crack closure, **b)** oxide-induce crack closure, **c)** roughness-induced crack closure, **d)** fluid-induced crack closure, **e)** transformation-induced crack closure, **f)** crack deflection, **g)** crack-bridging by fibres, **h)** crack-bridging by particles, **I)** crack-shielding by microcracks, **j)** crack-shielding by dislocations*

For the former two crack tip processes, inelastic deformation should remain confined to a small region in the vicinity of the crack tip; if the entire specimen deforms plastically or undergoes martensitic transformation, closure will not play a significant role during crack growth.

Greater attention is paid to two types of fatigue crack closure, roughness induced crack closure and phase transformation induced crack closure. The reason for this is that RICC and TRIP are the most prevalent mechanisms in fully pearlitic and 304-stainless steel, respectively.

2.6.8.1. Roughness-Induced Crack Closure

Roughness-induced crack closure has come to be recognised as one of the mechanisms by which certain microstructural effects on fatigue crack growth can be rationalised. This phenomenon provides an explanation for many apparently anomalous effects of microstructure on fatigue crack growth, especially in the near-threshold regime.

It was first noted by Purushothaman and Tien [79] and Walker and Beevers [73] that discrete points of contact between fracture surface asperities could cause enhanced levels of crack closure. Halliday and Beevers [78] and Ritchie and Suresh [77] also utilised this mechanism to explain microstructural effects on near-threshold fatigue crack growth. A quantitative model for crack face contact due to mode II displacements and fracture surface roughness was proposed by Minakawa and Mc Evily [82,83]. A comprehensive investigation of roughness-induced crack closure was conducted by Gray, Williams and Thompson on well characterised, fully eutectoid steels [84].

Experimental observations in a wide range of ductile materials reveal that crack propagation, in the near-threshold fatigue regime, occurs by means of a single slip mechanism. At low ΔK levels, where the maximum plastic zone size, on average, is typically smaller than a characteristic microstructural dimension such as a grain size, a crystallographic fracture process is promoted. The region I growth mechanism leads to a highly serrated or faceted fracture morphology and an elevation in the crack closure stress. It is also known that permanent plastic deformation ahead of the crack tip, as well as the possibility of slip irreversibility during unloading from the peak stress, cause mismatch between the fracture surface asperities. The tortuous crack path promoted by the crystallographic growth mechanisms, in conjunction with the occurrence of mixed-mode sliding of crack faces and the mismatch between the crack face asperities, immediately provides a mechanism for enhanced crack closure. The maximum crack opening displacement at threshold (for low R ratios) for most metallic materials is of the order of a fraction of a micrometer. These processes, occurring in a fatigue cycle as proposed by Minakawa and McEvily is schematically illustrated in Fig.2.7 [82].

Roughness-induced crack closure is promoted by: i) low stress intensity factor levels where plastic zone dimensions at the crack tip are typically smaller than an average grain dimension, ii) small crack tip opening displacements (at low ΔK levels and low R ratios) which are of a size scale comparable to the average height of the fracture surface asperities, iii) microstructures consisting of coarser grains and shearable and coherent precipitates which generally engender highly planar, crystallographic slip, iv) periodic deflections in crack path induced by grain boundaries, second phase particles, composite reinforcements or abrupt load changes, and v) enhanced slip irreversibility, especially due to slip step oxidation in moist environments. The most dramatic effects of roughness-induced crack closure are often observed whenever microstructurally induced crack deflections generate premature contact between fatigue fracture surfaces.

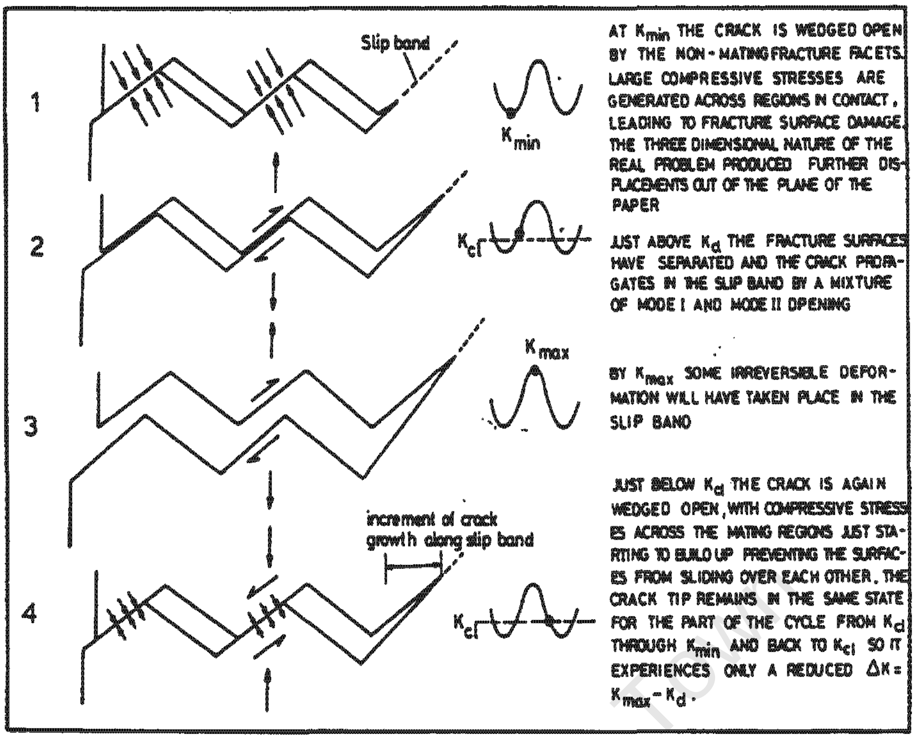

Fig.2.7. *The development of roughness induced crack closure during crack growth in planar slip materials [82]*

2.6.8.2. Phase Transformation-Induced Crack Closure

It has long been recognised that phase transformations at the tip of a fatigue crack can lead to a retardation in crack growth rates (e.g., Pineau, [48]; Hornbogen, [53]). This phenomenon is commonly referred to as the TRIP (Transformation-Induced Plasticity) effect in metals [64].

The TRIP effect is characterised by phase changes at the tip of a crack leading to a net increase in the volume of transforming region. As the enlarged material in the transformed zone is left behind the advancing fatigue crack tip, a net reduction in the crack opening displacement ensues. With reference to fatigue crack closure, crack tip phase transformation is analogous to crack tip plasticity in the sense that compressive residual stresses are induced within the non-linear zone during cyclic tension. Furthermore, in both cases, the residual displacements left in the wake of the extending fatigue crack act to close the crack prematurely at a far-field stress.

Pineau and Pelloux [48] and Hornbogen [53] studied fatigue crack growth in metastable austenitic stainless steels and showed that strain-induced martensitc transformation generally resulted in reduced crack growth rates at low to mid-ΔK levels. The crack propagation rates increased in the following sequence of microstructural variations: metastable austenite→ stable austenite →martensite of the same composition. As in the case of plasticity-induced closure, the constraint of the surrounding elastic material on the deformed region at the crack tip is necessary to promote transformation-induced closure since the transformation of the entire specimen would not result in appreciable crack face contact.

2.6.9. Environment

Exposure to aggressive environments generally decreases the resistance of a material to fatigue crack initiation; aqueous environments have been shown to incur the most severe effect. Possible mechanisms of crack initiation in aqueous environment include; i) assistance with the formation of persistent slip bands, ii) the formation of pits by localised dissolution, iii) destruction of thin, protective oxide films which may result in electrochemical activity, iv) the reduction of surface energy by the adsorption of an aggressive ionic species [2].

The extent of the influence that an environment has on the fatigue crack initiation behaviour of metal is dependent on the complex interaction between mechanical, chemical and metallurgical factors.

Whereas it is generally accepted that the nature of the environment plays a prominent role in influencing intermediate growth-rate fatigue crack propagation behaviour, opinion is still somewhat divided with respect to the influence of the environment at near-threshold rates. Thus, although the extent of data is still somewhat limited, there is good evidence in the literature to support the hypothesis that near-threshold fatigue crack propagation is environmentally sensitive.

2.7. Deformation Mechanisms in BCC and FCC Materials

Work hardening is an important strengthening process in steel, particularly in obtaining high strength levels in rod and wire, both in plain carbon and alloy steel. In general, bcc metals deform by slip, as do fcc metals with medium to high values of stacking fault energy. In metals with low values of stacking fault energy such as austenitic stainless steels, the dislocations dissociate to form stacking faults and twinning is the preferred mode of deformation. The tendency to deform by twinning is increased if the deformation temperature is lowered or the strain rate increased.

The chromium-nickel austenitic steels have stacking faults energies in the range of 5-60 m J m^{-2} and it would be expected that the highest nickel alloys would show the lowest work hardening as nickel is one of the elements that raises the stacking fault energy of austenite. However, the largest effect on work hardening rates is undoubtedly the transformation to martensite, i.e. decreasing stability of austenite.

The correlation between microstructure and its influence on strain hardening in eutectoid steels has been studied. The results show a unique relation between microstructure and strain hardening [86]. Since some mechanical properties, such as the ultimate tensile stress and strain, are determined by strain hardening, they are thus also dependent on microstructure.

In general, fcc metals exhibit higher work hardening rates than bcc metals because of the more stable dislocation interactions possible in the fcc structures. A material with a low stacking fault energy will have a high work hardening rate.

2.7.1. Deformation of Pearlite

The structure and properties of drawn pearlite were investigated and discussed by Embury and Fisher [85]. They noted that the principal effect of drawing was to produce a highly elongated microstructure, in which the spacing of the cementite lamellae decreased continuously as drawing strain increased. The pearlite lamellar structure of high-carbon steels used for drawing is a composite structure comprising ferrite and cementite phases.

Although some proportion of cementite, which is considered to be undeformable, is present, a wire consisting of pearlite lamellar structure can be drawn to an extremely small diameter [86]. Many studies have also been connected with fracture and the plastic deformation mechanism of cementite during wire drawing.

Many reports have been published about the flow stress of pearlite steel. Embury et al. considered that the interlamellar spacing is equivalent to the crystal grain size and the strength of pearlitic steel depends on the interlamellar spacing [85]. They reported that the yield stress σ_y is proportional to exp ($\varepsilon/4$) by combining the Hall-Petch equation and the interlamellar spacing decrease by wire drawing. Here ε is the amount of strain.

The deformation was apparently homogeneous, i.e. the interlamellar spacing (S) was reduced in proportion with the wire diameter D, so that

$$S / S_0 = D / D_0 \qquad \text{Eqn.7}$$

where S_0 is the interlamellar spacing at the initial wire diameter D_0. This relationship gives rise to an exponential relation between S and the drawing strain, ε:

$$1 / S = 1 / S_0 \cdot \exp(\varepsilon / 2) \qquad \text{Eqn.8}$$

The 0,2% proof stress of the material was found to be a linear function of $S^{-0,5}$, giving rise to an exponential relationship between proof stress and wire drawing strain:

$$\sigma = \sigma_0 + k/\sqrt{2S_0}\exp(\varepsilon/4) \qquad \text{Eqn.9}$$

where S_0 is the initial pearlite interlamellar spacing.

In order for pearlite to work harden as it does, lamellar cementite must be ductile [85]. Nondeforming, hard particles do not bring about exponential strain hardening in carbon steels or other materials. It has been shown that there is an effect of thickness of the cementite plates on their deformability. However, the nature of this evidence so far precludes any quantitative description of the magnitude of the size effect. However, there is no evidence for gross plastic deformation of cementite plates thicker than 0,1µm, and there is no evidence for extensive, brittle fragmentation of cementite plates thinner than 0,01µm. Another feature is that most of the evidence for plasticity of cementite in fine pearlite was obtained from drawn or swaged wires, while most of the evidence for brittleness of cementite in coarse pearlites was obtained from tension or compression specimens.

Cementite lamellae in heavily deformed pearlite are quite fine, ranging in probable thickness from 0,06µm down to less than 0,001µm. They probably exhibit the familiar 'whisker' type of strength-size effect, but this has to be verified.

There is abundant evidence that the cementite constituent in pearlite is capable of extensive plastic deformation and Langford has argued that an important strengthening effect is the propagation of slip through the cementite lamellae [87]. Langford derived an expression for the strength of pearlite on the basis that flow occurs when the shear strength of cementite is overcome by dislocation pile-up in the ferrite constituent, giving strengthening with a linear relation between flow stress and $S^{-0,5}$, with an extra component proportional to S^{-1}, due to dislocation multiplication within the ferrite lamellae.

Evidence has been given for the brittle behaviour of cementite and Langford has argued that there is an important size effect in the deformation characteristics of cementite, with brittle behaviour common in coarse lamellae (app.0,1μm) and fully plastic behaviour in lamellae which are thin enough (<0,01μm). It is also likely that ductile behaviour is promoted in conditions of high hydrostatic stress during deformation, but reduced by high strain rate processing [87].

It has been noted that the strain hardening of steels is a function of the mode of deformation, in that quite different results are obtained by deformation to equal strains by wire drawing or by pure torsion. Sevillano attributed this to possible non-independence of subgrain formation and texture development [88]. Texture formation does play an important role in the deformation process in wire drawing, and one consequence of the <110> texture in wire of bcc metals is the evolution of a 'swirly' microstructure of curled grains, which has been explained as arising from plane strain elongation of individual grains. 'Swirly' transverse microstructures have been observed in drawn wire, implying a similar plane-strain deformation mode in this material [85].

However, theoretical calculations of the variation of the interlamellar spacing with strain assuming plane strain conditions, show that the spacing does not decrease as rapidly as expected in this mode of deformation. Langford initially attempted to resolve this apparent paradox between microstructural evidence for local plane strain elongation and macroscopically homogeneous deformation by assuming extensive fragmentation of the cementite lamellae [87]. This opinion was revised in a later, more detailed study, in which differing modes of deformation were considered which apply to pearlite colonies in varying orientations to the plane of strain, in which it was shown how local inhomogeneous deformation (interlamellar 'deck of cards' slip) could give rise to the exponential relationship between interlamellar spacing and drawing strain, which had been attributed by Embury and Fisher to completely homogeneous deformation [85].

It should be noted that, in this connection, metalforming operations such as wire drawing do not in fact consist of homogeneous deformation, and that 'redundant work' in the deformation is often associated with macroscopic regions on inhomogeneous deformation in the deforming zone. The distribution of this redundant deformation is dependent upon parameters of the forming process, and deformation by methods with high deformation such as extrusion may promote highly inhomogeneous local deformation, such as the extensive lamellar fragmentation.

2.7.2 Deformation of Austenite

The transformation from austenite to martensite in ferrous systems can be accomplished by heat treatment or deformation of austenite. Two different types of martensite can be obtained by these methods. The heat treatment produces body-centred tetragonal martensite, while deformation can result in a martensite that can have either body-centred cubic (bcc) or hexagonal close-packed crystal (hcp) structures, known as α' and ε martensites, respectively.

The deformation-induced martensite may be classified under two categories: stress assisted or strain induced. Maxwell et al, have indicated that the stress-assisted martensite is formed during the deformation when the stress levels simply provide for the reduction in driving force required for transformation from austenite to martensite [86]. The type of martensite formed by stress-assisted deformation involves the spontaneous nucleation and growth in a plate form, usually in a manner similar to that obtained by thermal quenching of austenite [86,89,90]. However, strain-induced martensite is a direct consequence of the plastic-deformation and can be morphologically different from stress-assisted or thermally produced martensites. The production of lath-type martensite by strain-induced processes appears to be quite common in ferrous systems. The literature also presents a point of view that the formation of ε martensite could be a prerequisite to α' formation.

However, the formation of α' has been quite conclusively shown to be independent of ε martensite by several authors, as stated by Otte [91].

The strain-induced martensite α' forms by the plastic deformation of the parent austenite, where a proper defect structure is created and acts as an embryo for the transformation product. The potential nucleation sites for these embryos may include deformation twins, stacking faults, and the hcp martensites [86,92].

The appearance of an hcp structure in the transformation from austenite to martensite of Fe-Ni-Cr alloys was reported by Breedis and Robertson, Binder, Otte [91,93,94]. Bilby and Christian have summarised that the hcp phase may be associated with stacking faults in the parent austenite and that these stacking faults may be the nucleation sites for the martensitic transformation [95]. Venables conducted a study on a thin film of deformed 18/8 stainless steels and inferred that a possible sequence in the transformation could be from fcc (γ) to hcp (ε) and finally to bcc (α') crystal structures [96]. Bastein and Dedieu studied the austenite to martensite transformation in low-carbon 18/8 stainless steels and noted that while simple cooling of the steel to very low temperatures produces very little α', the plastic deformation at temperatures slightly higher or lower than room temperature produces a considerable amount of α' [97]. Lagneborg concluded that the martensite produced during the deformation of 18/8 steels at room temperature occurred in the shape of thin needles in contact with a <111> habit plane and that the intersection between the ε sheets constituted a preferred nucleation site for martensite [98].

Lecroisey and Pineau and Venables established that the shear band intersections could be very effective sites for strain-induced martensite nucleation in 304 SS [89,99,100]. Olsen and Cohen and Olsen and Azrin did the pioneering work in this field of deformation-induced martensite [101-103]. Hecker et al. have studied the effect of different strain states (uniaxial and biaxial) and strain rates on α' formation in 304 SS [104].

They observed that at low strains, α′ formed more readily than at high strain rates (10^{-3}/s). However, at true strains higher than 0.25, they noted that the situation was just the reverse and attributed this phenomenon to adiabatic heating, which inhibits α′ formation at high strain rates.

Murr et al. have observed the regular (lath) morphology for low strains and blocky morphology at high strains is a result of the coalescence of α′ embryos [105]. Lecroisey and Pineau have noted the morphology of α′ as being only lath type [89]. They did not observe any plate-type martensite even at low temperatures.

Brooks et al have conducted an in situ study on the formation of α′ in three different SS, 16 % Cr-14 % Ni, 16 % Cr- 12 % Ni, and 18 % Cr-10 % Ni, and proposed that the martensite always nucleates from suitable dislocation configurations, which are generated by the stress associated with the transformation, and the presence of pre-existing embryos is not required for martensitic nucleation as the heterogeneities can be provided by dislocations formed prior to the transformation [90].

Murr et al. have also explained the growth phenomenon of α′ embryos [105]. They proposed from their transmission electron microscopy observations that at low strain levels for a particular stress state, the α′ formation is restricted to small intersection volumes and with increasing strain, the α′ product appeared to grow. In uniaxial tension tests, the growth looked similar to long laths and in the case of biaxial tension, it was an irregular and blocky α′product.

They concluded from these observations that α′ laths grow by the formation of many embryos at intersections spaced closely along a shear band. They have also observed the evidence of α′ martensite growing out of (111) planes, some in specific crystallographic directions and others at random. They believe that the regular, blocky polyhedral were being formed by the coalescence of individual embryos.

Varma et al. have recently studied the effect of grain size on the α' formation in 304 and 316 SS during tensile testing and rolling at room temperature [106]. It was found that the amount of α' formed in 304 SS increased with the increase in true strains for both modes of deformation, but considerably larger amounts were formed in rolling compared to those formed in tension for similar true strains. It has been shown that α' formation is grain size dependent in 304 SS. The α' formation was also observed in 316 SS in rolling, but it was not detected during the tensile deformation. The grain size dependence on α' formation was also confirmed in 316 SS during rolling. It must, however, be noted that a larger volume fraction of α' formed in 304 SS during rolling than in 316 SS for similar true rolling strains.

2.8. Changes caused by the Fatigue Process

Cyclic loading of metals and alloys leads to changes in their structure. These changes manifest themselves by changes in measurable mechanical, electrical, magnetic and other properties. Experimental results show that these changes are typically of a saturating character. At the beginning of cycling the changes are very marked, their intensity decreases with the increasing number of cycles and after a relatively small number of cycles (in comparison with the total number of cycles to fracture), the measured quantity usually reaches its saturated value.

Of all the changes mentioned, those in the mechanical properties are most important. A great amount of experimental data has shown that the fatigue hardening/softening curves almost always have a saturation character. The experimental data obtained on the fatigue hardening/softening process under different conditions is numerous. This makes it possible to summarise the most important facts from the point of view of the type of material [4]:

1. Fatigue hardening, is typical for annealed metals. On the other hand, fatigue softening is typical for materials hardened by one of the known methods:

deformation hardening, martensitic-transformation hardening, solid-solution hardening, precipitation hardening, and dispersion hardening. Fatigue softening may or may not occur; this depends on the stability of the prior hardening and on the conditions of cycling. From a practical point of view, fatigue softening is usually considered undesirable.

2. The most important parameter determining the number of cycles spent in the hardening/softening process, i.e. saturation, is cross slip. From the point of view of cross slip, it is possible to divide all metals roughly into two groups: wavy-slip materials (carbon steels) and planar-slip materials (austenitic stainless steels).

If the nature of the complicated slip processes in metals is taken in account, the conclusion is that wavy slip is conditioned by a frequent and therefore easy cross slip, while planar slip is associated with a rare and difficult cross slip. The cross-slip difficulty is given by more parameters, which are not well known.

The interpretation of cross-slip difficulty in single-phase fcc metals is relatively easy. The cross-slip difficulty can be directly related to the stacking-fault energy. The higher stacking fault energy, the more frequent the cross slip and the more markedly wavy the slip on the primary slip planes. Generally, the number of cycles spent in hardening / softening is lower in the case of wavy-slip materials, than in the case of planar-slip materials [4].

3. Extensive low-cycle fatigue data enabled the formulation of an empirical rule, predicting, on the basis of the conventional tensile diagram, whether the material will cyclically soften or harden. If the ratio of the tensile strength to the yield stress (or proof stress) is higher than 1.4 the material will harden under cyclic loading. If this ratio is lower than 1.2 the material will soften. For the values of the ratio between 1.2 and 1.4 the material should be more or less cyclically stable. This rule is based on low-cycle data and should therefore be used only for low-cycle, high-amplitude cycling.

4. Some materials exhibit more complicated behaviour under cyclic loading, namely superposition of fatigue hardening and softening.

The processes mentioned above are conditioned by cyclic plastic deformation. Plastic deformation is generally produced by the motion of dislocations. Fatigue hardening/softening and the stress-strain response in saturation are therefore determined by the motion of dislocations, their mutual interactions, and interactions with other types of lattice defects. The dislocation motion is further influenced by precipitates, foreign particles, grain boundaries, etc. The dislocation substructure and density undergo changes during cycling loading.
Dislocation structures in cold worked metals depend primarily on three factors: i) the degree of deformation, ii) the cross-slip difficulty and iii) the temperature of cold working. If very low and very high temperatures of cold working are excluded, then there are two principal types of dislocation structure after monotonic deformation: cell structure for easy cross-slip materials and more or less homogeneous planar-array distribution for difficult cross-slip materials. The cell structure formed during cold working differs from the fatigue dislocation structure mainly in the width of the cell wall; the fatigue cell structure exhibits sharper cell walls.

Of greater importance are phase transformations during cycling. Generally, martensite is considered to be detrimental to fatigue life. This is true without exception for the quenched carbon steels. On the other hand, the cyclic deformation-induced martensitic transformation in high strength TRIP steels and in lower-strength metastable austenites may be both beneficial and detrimental as a function of the mode of test control (stress-and strain controlled tests) and of the amplitude [107].

This aspect, amongst other, is investigated in more detail through the fatigue of the three materials mentioned including particularly AISI 304 stainless steel. The materials and experimental techniques for this are presented in the next chapter.

CHAPTER 3

MATERIALS AND EXPERIMENTAL PROCEDURE

3.1. Introduction

In this chapter the materials used, the drawing processes they were subjected to, the various mechanical tests and microstructural characterisations are discussed. Tests were carried out to determine the static tensile properties and fatigue behaviour of three types of steel in terms of different drawing strains.

3.2. Materials

The alloys investigated during this study included a *high carbon steel*, an *AISI 304-austenitic stainless steel*, and a *ferritic steel* (3CR12); the compositions of which are shown in Table 3.1.

High Carbon Steel Wire is a well-established material, which has been used for many years in the manufacture of cables and mine ropes. The wire is essentially plain carbon steel with a carbon content generally close to the eutectoid composition of 0.8wt% carbon. It is one of the strongest materials produced commercially.

304-Austenitic Stainless Steel offers a combination of good engineering properties, namely, high ductility and toughness even at high temperature, and especially high corrosion resistance. These desirable properties make austenitic stainless steel wire particularly attractive for rope application.

3CR12-Ferritic-Corrision Resistant Steel is an acronym for chromium containing corrosion resistant 12%-chromium steel. 3CR12 was developed in the late 1970's from AISI 409 ferritic steel and produced by Columbus Stainless in South Africa. 3CR12 stainless steel belongs to the ferritic group of stainless steels, with excellent corrosion resistance in many environments and possesses considerable economic advantage over austenitic stainless steels.

3.2.1. Specification

Table 3.1. Chemical compositions of the steels used in this investigation (wt%)

Material	C	Si	S	P	Mn	Cu	Co	Ti	Mo	Cr	Ni	N	Fe
Carbon steel	0,82	0,4	0,02	0,01	0,65								rem.
304 rods	0,021	0.846	0,09	0,015	1,78					18,65	8,15		rem.
304 wire	0,021	0,56	0,092	0,019	1,70					18,80	8,92		rem.
3CR12	0,02	0,28	0,004	0,021	1,22	0,09	0,01	0,54	0,01	11,33	0,64	0,013	rem.

3.3. Wire Production

The principles involved in the drawing of bars, rod, or wire are basically similar and involve pulling metal through a die by means of a tensile force applied to the exit side of the die to cause a reduction in the metal diameter.

Most of plastic flow is caused by compression forces which arise from the reaction of the metal with the die. A cross section through a conical drawing die is shown in Fig.3.1.

The entrance of the die is shaped so that the wire entering the die will also draw lubricant through the die. The shape of the bell causes the hydrostatic pressure to increase and promote the flow of lubricant into the die. The approach angle region, Fig.3.1. is the section of the die where the actual reduction in diameter occurs. The half die angle α is an important process parameter. The bearing region does not cause reduction but it does produce a frictional drag on the wire. The chief function of the bearing region is to permit the conical approach surface to be refinished (to remove surface damage due to die wear) without changing the dimensions of the die exit. The back relief allows the metal to expand slightly as the wire leaves the die. Most drawing dies are manufactured from cemented carbide or industrial diamond (for fine wires). The die nib is encased for protection in a thick steel casing.

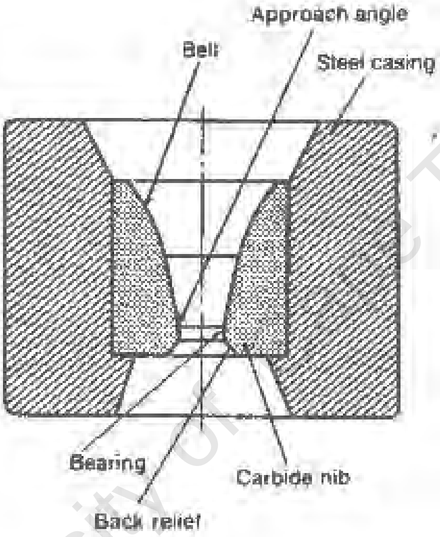

Fig.3.1. Schematic drawing of drawing die

3.3.1. High Carbon Steel Wire

The carbon steel wire used in this study was produced by the Haggie Rand Company. The process of wire production is given below.

Hot rolled high carbon steel rods are heat treated before they are cold worked by drawing to a degree necessary for the development of sufficiently high tensile strength.

In the patenting method used by Haggie Rand, the steel is heated to a high temperature in a furnace at 1050-1100° C and cooled in a lead bath held at 550° C to form a fine pearlitic structure as indicated in Fig.3.2.

The patented rods of 8mm diameter, produced in this way, have a UTS of approximately 1300 MPa.

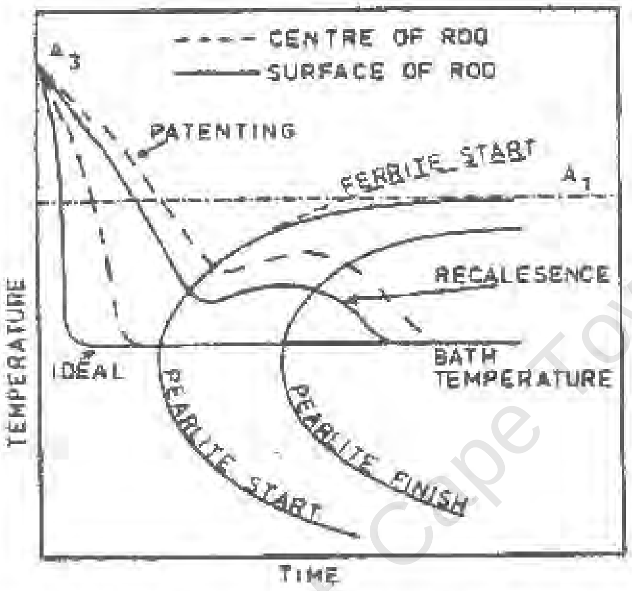

Fig.3.2. *Time-Temperature-Transformation diagram for eutectoid steel [108]*

The patented rods are then cold drawn in nine passes to achieve a diameter of 3.15 mm. The rods are coated in borax and phosphate prior to drawing to aid soap lubricant pick up at the die entry point.

The wire obtained by this patenting and cold drawn process achieves an overall reduction of 84.5%, i.e. from a diameter of 8.0 mm to 3.15 mm and true strain of 1.86. The true strain is determined using the following equation [109]

$$\varepsilon = 2 \cdot \ln\left(\frac{d_0}{d}\right) \qquad \text{Eqn.3.1.}$$

where d_0 is the diameter before drawing and d is the final diameter.

The Table 3.2. shows the drawing reduction schedule. During the drawing process, on a nine hole drawing machine, direct water cooling of all drawing blocks was used. One direct water cooler is positioned at the final die exit and blasts a spray of water directly on the wire surface. The water-cooling removes excess heat which can affect the properties of the wire.

Heat generation is a major concern in drawing operations and in plastic deformation processes since friction can generate wire temperatures of several hundred degrees Celsius. Typical temperatures of the wire at the die exit are about 150°C.

These cooling precautions are taken because of the susceptibility of high carbon steel wire to strain ageing. Fine pearlite drawn to high strains is more susceptible to ageing which is considered to be virtually eliminated using the direct water cooling method.

Table 3.2. Drawing Schedule for Carbon Wire obtained from Haggie Rand Co.

Block Number	1	2	3	4	5	6	7	8	9
Wire dia. [mm]	6,9	6,1	5,4	4,9	4,4	4,0	3,7	3,4	3,15
Wire Red.Area [%]	23,9	22,0	20,5	19,2	18,1	17,1	16,3	15,6	14,9
Wire O/A Red. Area [%]	23,9	40,7	52,8	61,9	68,8	74,1	78,4	81,7	84,5
True Strain	0,27	0,24	0,23	0,21	0,20	0,18	0,17	0,17	0,16
O/A True Strain	0,27	0,52	0,75	0,96	1,16	1,3	1,5	1,7	1,86
Die angle 13 [deg]	1,6	1,8	1,9	2,1	2,2	2,4	2,5	2,6	2,8
Wire UTS [MPa]	1407	1505	1595	1679	1757	1831	1901	1968	2031
Wire speed [m/s]	0,6	0,7	0,9	1,2	1,4	1,8	2,1	2,5	3,0
Practical power [kW]	16,7	16,7	16,7	16,7	16,7	16,7	16,7	16,7	16,7

3.3.2. 304-Austenitic Stainless Steel Wire

Stainless steel rods having different initial diameters were used to produce wire with different strains. The rods were initially annealed at 1050 °C for 15 minutes and afterwards water cooled, in order to eliminate the previous rolling history.

Suitable equipment for wire drawing was not available in the experimental laboratory and consequently a tensile machine together with drawing dies and a die holder, designed and manufactured in the workshop, was used for the process. A schematic drawing of a "ZWICK"-tensile machine with drawing accessories is shown in Fig.3.3. Tungsten carbide dies, (WC inserts supported by a steel casing) produced by "Sandvik" were used in the drawing process. The procedure for single drawing (one pass per sample) involved placing a die into the steel seat and fitting this unit into the cross-head of the tensile machine. The cross-head was then moved as close as possible to the jaw of the machine into which was clamped the end of the wire which had been reduced in size allowing it to pass through the die. The cross-head of the tensile machine was then moved vertically downwards to draw the wire through the die in a uniform and continuous manner.

The lubricated samples, having different initial diameters, were repeatedly drawn without intermediate annealing to the fixed final diameter of 3.55 mm. The exceptional ability of 304-austenitc stainless steel to work harden resulted in the constant breakage of wire due to the reduced end or shank not being able to sustain the great increase of strength of the material during the drawing process. These problems, during the multiple drawing process, were solved by cutting off the previous shank end and machining a new one from the already hardened material, for each single drawing pass undertaken. It should be also noted that the successful drawing of wire requires very careful selection of process parameters. All the wires were ultimately of the same diameter (3.55 mm) and the different drawing strains were achieved by starting with different initial diameters (achieved by drawing) and annealing. The wire drawing procedure used in laboratory conditions is shown in Table 3.3. An example of multiple drawing to achieve 0.585 strain performed in laboratory conditions is schematically presented in Fig.3.4.

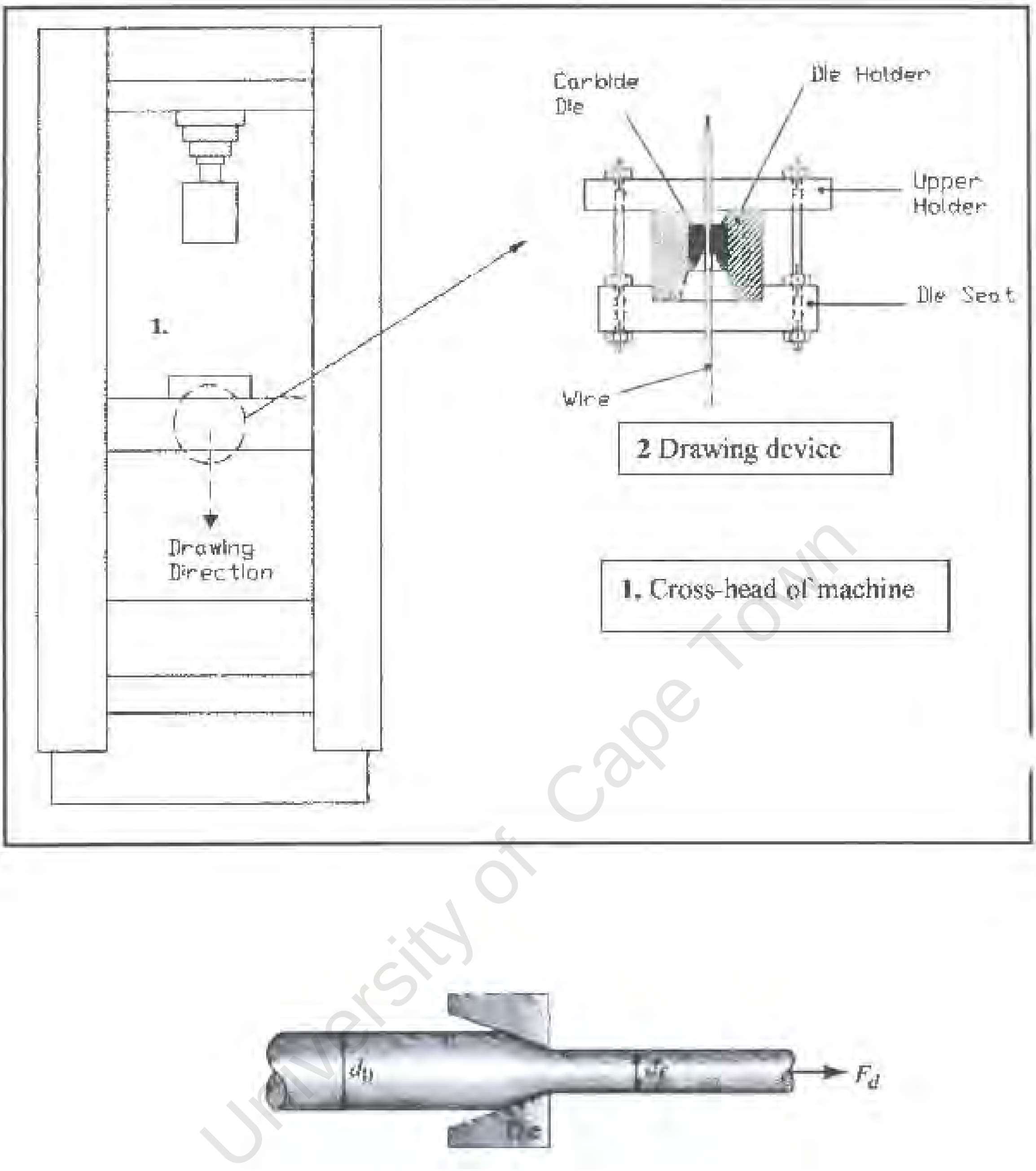

Fig.3.3. *Schematic of the ZWICK-tensile testing machine and drawing device with a closer view of the wire-drawing process*

In wire drawing and other deformation processes, a large proportion of the total work done is converted into heat due to friction effects at the interface or within the deforming material. The determination of the operating speed for a wire drawing operation is probably one of the most important but also one of the most complex tasks. The speed at which a particular machine can produce good quality products is limited by surface and structural damage. In this particular case, it was found by experimentation, that a speed of 50 mm/min resulted in the absence of any major surface structural damage. To reduce friction between the drawing die and the wire and thus reduce wear and the pulling force on the die itself, whilst giving the wire the necessary structural and aesthetic characteristics, vaseline was used as a lubricant.

When the function of drawing is merely to reduce the size of the wire, a thick film of lubricant is beneficial, with low friction and large heat capacity, so that drawing may be done in the least number of passes. Reductions of more than 25% per pass were found difficult to achieve under laboratory conditions since they resulted in the breakdown of lubrication and the deterioration of the wire surface finish.

Table 3.3. Drawing procedure for AISI 304 stainless steel wire drawn in the laboratory

Initial Bar Diameter mm	Die dia mm	Pass 1	Pass 2	Pass 3	Final Dia. mm	Drawing strain	Reduction Area %
3.72	3.55	3.55			3.55	0.09	8.93
4	3.55	3.55			3.55	0.238	21.25
4.28	4.15-3.95-3.55	4.15	3.95	3.55	3.55	0.37	34.39
4.6	4.15-3.95-3.55	4.15	3.95	3.55	3.55	0.52	47.39
4.76	4.15-3.95-3.55	4.15	3.95	3.55	3.55	0.58	52.6

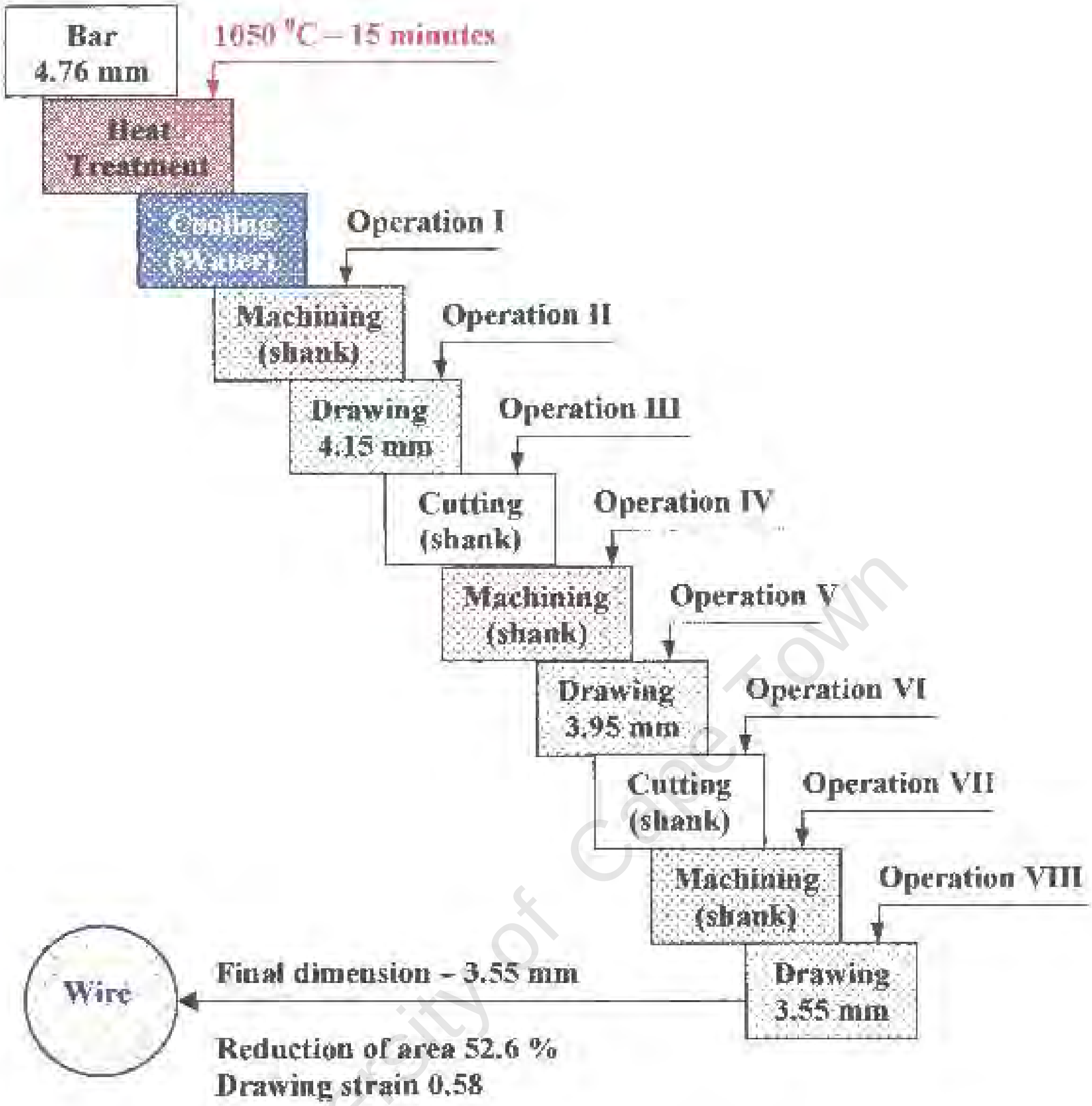

Fig.3.4. *Schematic of multiple drawing performed in the laboratory conditions for achieving 0.585 strain in AISI 304 stainless steel wire*

The wire obtained by cold drawing under laboratory conditions achieved an overall reduction between 8 to 53% and a true strain ranging from 0.09 to 0.585.

3.3.3. 3CR12-Ferritic Steel Wire

Reinforcing 3CR12 steel rebars were used as the initial starting material for the production of wire. The rebars were supplied in the hot rolled condition, having a diameter of 18mm. Extensive machining was performed on these bars in order to reduce the initial diameter to 5mm.

In order to eliminate the previous hot rolling history and to obtain a microstructure more suitable for drawing, the bars were annealed at 760 °C for 30 minutes and air cooled. The 3CR12 annealed bars had a UTS of 442 MPa and were drawn on the same equipment, using the same drawing speed and lubricant, as for the AISI 304-stainless steel.

The final wire produced through a combination of machining, annealing and drawing processes is shown in Fig.3.5. It was intended to manufacture wire samples with the same overall reduction as the 304-stainless steel wires. However, the application of high drawing strains was limited by wire-surface damage and the restrictive drawability of this type of steel. The production life of drawing dies was reduced by almost 80% compared to those dies used in the wire drawing of AISI 304 stainless steel.

Fig.3.5. *3CR12 wire- 3.5mm dia obtained from 3CR12 rebar-18mm diameter*
1.- reinforcing 3CR12 steel bar; 2.- drawn 3CR12 wire; 3.- drawing die

3.4. Experimental Testing Details

3.4.1. X-Ray Measurements on AISI 304 Stainless Steel

The complex morphology of deformation-induced martensite does not allow for easy measurement of its volume fraction by light microscopy. Martensite laths occur in sheaves or elongated clusters and are too small to be resolved individually. As a result, optical microscopy indicates greater amounts of strain-induced martensite than actually exists. X-ray diffraction is potentially the most accurate method for the quantitative detection of martensite.

The X-ray intensity diffracted from each crystal phase is proportional to the volume fracture of that phase present. X-ray diffraction results in a trace of reflected intensity against 2θ (where θ is the Bragg angle). The Bragg angle is related to the interplanar spacing of the crystal by Bragg's law [110].

$$n\lambda = 2\, d \sin\theta \qquad \text{Eqn.3.2.}$$

where: $n = 1,2,3\ldots$

λ = X-ray wavelength

d = interplanar spacing

θ = angle between the atomic plane and the X-ray beam

The X-ray intensity (measured from the heights on the X-ray plot) of each phase is not proportional to the integrated peak area (which is proportional to the phase volume fraction). The volume fraction of each phase is therefore calculated using the area under the peak, rather than the peak height.

For microstructures consisting essentially of austenite and martensite, the ratio of the volume fraction of austenite (V_γ) and martensite ($V_{\alpha'}$) can be written as :

$$V_\gamma / V_{\alpha'} = I_\gamma^{hkl} R_{\alpha'}^{hkl} / I_{\alpha'}^{hkl} R_\gamma^{hkl} = S \qquad \text{Eqn.3.3}$$

I_{hkl} is the integrated intensity of a particular *hkl* reflection in a phase while R_{hkl} is a factor depending on the specimen crystal structure, the reflecting set of planes and θ; S (V_γ/V_α) is the ratio of the volume fraction of austenite (V_γ) and martensite (V_α).

If $V_\gamma + V_{\alpha'} \approx 1$ (provided that the volume contributed by carbides and /or nitrides is very small) then:

$$V_{\alpha'} = 1 / [1+S] \text{ and } V_\gamma = S / [1+S] \qquad \text{Eqn.3.4.}$$

Diffraction line broadening usually occurs and the intensity of an X-ray at a particular Bragg angle follows a Gaussian distribution. Two integrated areas under the peak are thus obtained which are then averaged to give the integrated intensity (I_{hkl}) corrected for the background.

R_{hkl} can be calculated from basic principles and a list of these values are given in Table 3.4. These R-factors, together with the I_{hkl} values for each reflection were then substituted into Eqn.3.2. to obtain S, which was then used in Eqn.3.3. to obtain the martensite volume fraction.

A computer interfaced Philips x-ray diffractometer was used to collect x-ray data using a copper tube, which generates x-rays with a wavelength of 1,54 Å. X-rays were collected over a 2-theta range of 62° to 93° at an increment of 0.01°, and the x-rays of each increment were collected for 2 s. The voltage was set at 40 kV and the current at 25 mA. The tested intensities of peaks were (220) and (311) for austenite and the (211) and (200) reflections for α'-martensite.

However, the error margin of the x-ray technique is approximately ±2% [127].

Table 3.4. Bragg angles and R-factors of (γ), (α′) peaks used for CuK$_\alpha$ radiation [111].

Peak	**Bragg Angle**		**R$_{hkl}$**
	θ	2θ	
$200_{\alpha'}$	32.5	65	32
$211_{\alpha'}$	41.2	82.4	61
$310_{\alpha'}$	58.0	116.0	19
200_{γ}	25.4	50.8	82
220_{γ}	37.3	74.6	44
311_{γ}	45.5	91.0	51

Specimen Preparation

In order to obtain a bigger scanning area, approximately six longitudinal samples (approximate length 25mm) were mounted side by side in resin and ground to the mid-point of the wire diameter. The samples were further polished using a STRUERS automatic polisher to a 0.25 μm finish. The mounted samples were then electro-polished, in a solution with the composition given below, at 20 V for up to 60 seconds at room temperature.

25 g chromic acid
133 ml acetic acid
7 ml distilled water

Electropolishing was performed in order to eliminate any possible martensite transformation occurring during polishing.

A similar method was also used to investigate the martensite transformation that occurred during the fatigue process. Longitudinal samples, approximately 25 mm in length, were removed from the fractured ends of the wires, mounted in resin and polished as previously. Care was taken to ensure that the sections were normal to the notch in order to observe the fatigue crack path through the structure.

3.4.1.1. Notch Effect on Martensite Transformation

The changes produced by the introduction of a notch have important consequences in the fatigue process. For example, the presence of a notch will affect the martensite phase transformation in the AISI 304 stainless steel wire samples. In order to investigate the effect of shape and size of notch on the martensite transformation, fatigue tests were performed on both V-shaped and U-shaped notched wire samples, as shown in Fig.3.6. The notches were made using fine files having different profiles or a cutting wheel. Notch-sizes were 300 and 800 microns in depth. In order to achieve the consistency, the depths were measured by digital vernier. It should be mentioned, however, that the error margin of cutting by hand is approximately ±5%. Such variation in notch depths effects the values of K_t and it will be addressed later, p.136.

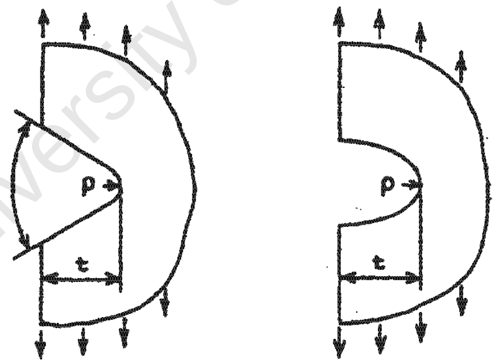

Fig.3.6. *Schematic of V-shaped and U-shaped notch*

The amount of martensite induced by V and U notches having different sizes was determined using x-ray diffraction in the same way as previously described.

3.4.2. Mechanical Testing

3.4.2.1. Tensile Testing

Tensile properties were determined using a ZWICK universal testing machine with a 200 kN load cell. The wire specimens had a gauge length of 320 mm and were investigated in the annealed condition and also drawn to different strains. Similarly, the fatigued wire samples were also tested to determine whether changes in mechanical properties had occurred during the fatigue process.

All tensile tests were performed at room temperature and at a strain rate of 10^{-3} per second.

Wire samples were wrapped in brass foil of 0.3mm thickness in order to avoid the breakage in the grips. Nevertheless, despite these precautions, samples often broke in the gripped portion which was most significant during the testing of AISI 304 stainless steel wires. All samples which broke in this manner were discarded.

Engineering stress-strain curves were constructed from the load-elongation measurements, while the true stress-true strain was derived using the well-known tensile curve equations

$$\varepsilon_t = \ln(1+\varepsilon_n) \quad \text{Eqn.3.3.} \qquad \sigma_t = \sigma_n(1+\varepsilon_n) \quad \text{Eqn.3.4.}$$

where ε_t and σ_t are the true strain and true stress respectively and ε_n and σ_n are the engineering strain and engineering stress respectively.

The work hardening rate curve was obtained using linear regression, equation eqn.3.5.

$$\frac{\sum\varepsilon\cdot\sigma - n\cdot\sum\varepsilon'\cdot\sigma'}{\sum\varepsilon^{2}-\sum\varepsilon'^{2}} \qquad \text{Eqn.3.5.}$$

One hundred points were regressed to obtain the instantaneous gradient which when plotted for all the points against strain gives *$d\sigma/d\varepsilon$* which represents the work hardening rate of the tensile curve.

The maximum uniform elongation (ε_u) was determined from the yield strain up to the point of instability which represents the case where the work hardening rate is equal to the true stress (i.e. $d\sigma/d\varepsilon = \sigma_t$).

3.4.2.2. Fatigue Testing

Fatigue tests were carried out in accordance with the ASTM standard E647-78T using a 50 kN servo-hydraulic ESH universal testing machine under load control and a frequency of 2 Hz (120 cycles per minute) at ambient temperature [112].

Nomenclature and Definitions

Maximum stress = $\sigma_m + \sigma_a$

Minimum stress = $\sigma_m - \sigma_a$

Range of alternating stress, or difference between the maximum and minimum stresses = $2\sigma_a$

Stress ratio, R = $\sigma_{min}/\sigma_{max}$ = Minimum stress / Maximum stress, schematically presented in Fig.3.7.

The carbon steel wire was investigated in (i) as the received condition, after it had been drawn to 1.86 strain by Haggie Rand, and also after the surface was polished (ii) and shot peened (iii). Fatigue behaviour investigations of AISI 304 and 3CR12 steel wires were undertaken on wires in the annealed condition and drawn to different strains.

Additionally, commercially supplied AISI 304 stainless steel wires, with a completely unknown drawing history were tested under similar fatigue conditions. The purpose of this was to compare the fatigue behaviour of commercially supplied wire having a higher nickel content and monotonic mechanical properties to those obtained during drawing in the laboratory.

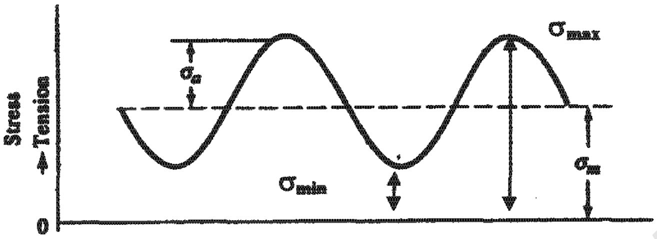

Fig.3.7. *Schematic of the nomenclature for the stress parameters which affect fatigue limit of materials*

Both the fatigue limit and the fatigue crack growth rate tests were performed on the ESH testing machine shown in Fig.3.8.(a,b).

The materials exhibited significant variation in strength. For example, high carbon steel wire had a strength of 1982 MPa and highly drawn AISI 304 stainless steel wire 1346 MPa. However, AISI 304 stainless steel wire and 3CR12 steel wire, both drawn to 0.09 strain had strengths of 752 MPa and 516 MPa respectively. For this reason the materials could not be subjected to identical fatigue conditions. An attempt was made to fatigue test the high carbon and highly drawn AISI 304 stainless steel (0.58, 0.52, 0.37 drawing strain) comparably i.e. at constant mean stress of 550 MPa and amplitude 500 MPa or 350 MPa. This gave σ_{max} and σ_{min} stresses of 1050 MPa and 50 MPa, and 900 and 200 MPa respectively. Similarly the lower strength materials, i.e. AISI 304 drawn to (0.09, 0.238 and annealed) as well as 3CR12, were also tested at a constant mean stress of 120 MPa and amplitude of 100 MPa and 80 MPa, on the one hand, and 200 MPa and 40 MPa on the other. Thus, in order to compare the fatigue behaviour of different types of steel wires, similar cyclic parameters were kept throughout the experimental procedure.

Gripping Techniques

To ensure that fracture of these samples did not occur in the gripped portion of the wire, it was essential to establish a suitable test procedure. Due to the inherent physical characteristics of individual machines, it was not practical to use a universal gripping procedure that was suitable for all testing machines. Therefore, different methods of gripping described in A7.3.2. to A7.3.8. according to ASTM standard A370 were employed within this work.

One of methods used was tinning, in which the portions of the wire to be gripped were cleaned, fluxed and coated by multiple dips in a molten tin alloy. The tinning method was found to be the most suitable in the fatigue testing of high carbon pearlitic steel wire.

The application of the tinning method was found not to be appropriate for the coating of stainless steel wires and it was replaced by another alternative method. In this method, brass foil, having a thickness of 0.3 mm, was placed between the grips and the wire to minimise the notching effect of the teeth into the wire.

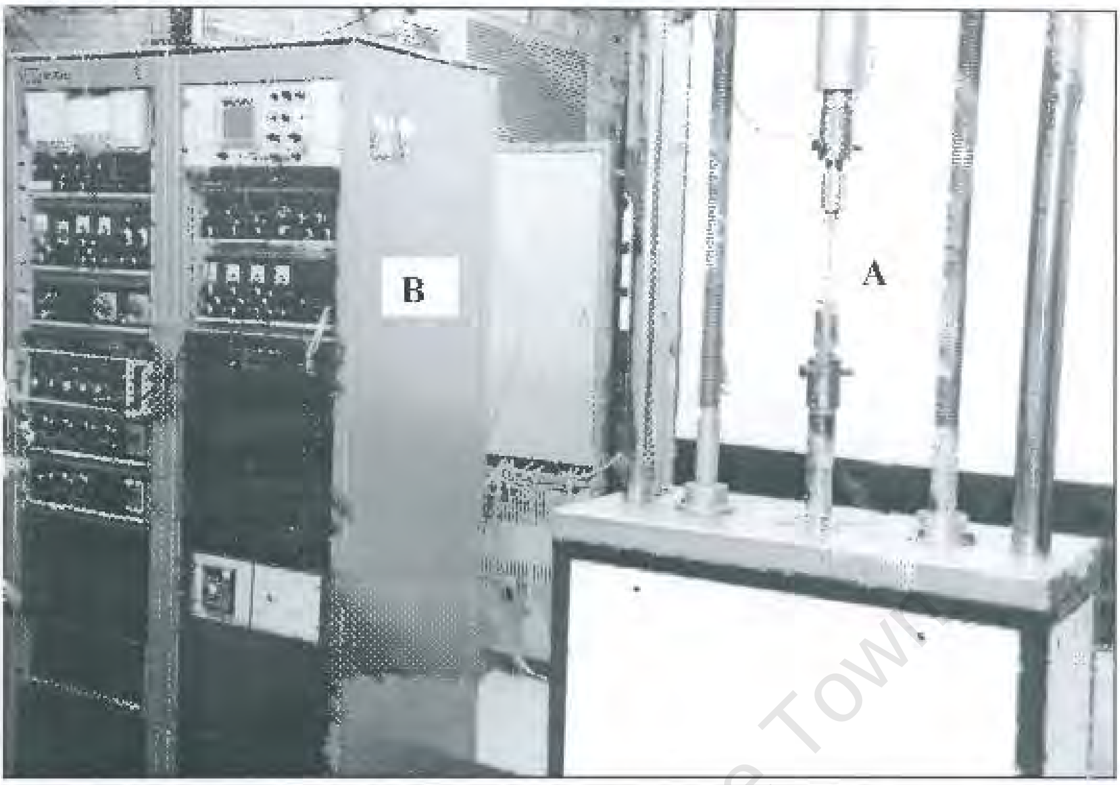

Fig.3.8.(a) *The FSH servo-hydraulic universal testing machine; A – wire sample; B – UTM control panel*

Fig.3.8.(b) *Closer view of notched wire sample tested under the fatigue conditions*

3.4.2.2.1. Fatigue Limit – Data Acquisition

The basic method of presenting engineering fatigue data is by means of the S-N curve, a plot of maximum stress S against the number of cycles to failure N. A log scale is normally used for the maximum stress, S or sometimes amplitude. The S-N relationship is determined for a specified value of σ_{mean} (mean stress).

The usual procedure for determining an S-N curve is to test the first specimen at a high stress where failure is expected in a fairly short number of cycles, e.g. at about two-thirds the static tensile strength of material. The test stress is decreased for each succeeding specimen until one or two specimens do not fail in the specified numbers of cycles, which is usually at least 10^7. The highest stress at which a nonfailure is obtained is taken as the fatigue limit. An indication of the S-N curve behaviour is obtainable with a minimum of about ten specimens but, for reliable trends, this number needs to be increased by an order of magnitude. It has been found that there is a usually considerable amount of scatter in the results.

As stated earlier, the fatigue limit was determined on high carbon steel wire in the "as-received" condition, and also after being polished and shot peened. In order to determine the fatigue limit of the polished steel wire, the samples were polished longitudinally using successive grades of SiC-paper having numbers of 80, 180, 220, 320, 600, 800, 1000, and 1200. They were finally longitudinally polished with 1μm diamond paste to an R_a value of 0.3 microns. After polishing, the samples were degreased in acetone.

Another set of high carbon steel wire samples was subjected to shot peening, to induce compressive stresses into the material. The process of shot peening was performed using silica carbide balls in a compressed air steam. The shot peening procedure was done commercially and sets of wire samples were shot peened under the same conditions with the same intensity. The shot peening was undertaken merely to show its benefit to fatigue life of wires and it was difficult to control coverage, intensity, nozzle rate and consequently Almen index.

The tensile fatigue testing of smooth stainless steel wire samples, both AISI 304 and 3CR12, was found to be impossible to perform. The reason for this difficulty was that fatigue cracks always initiated in the grip region despite the use of foil as documented previously. This particular difficulty necessitated the use of a different option; i.e. calculation and prediction of the smooth fatigue limit based on the fatigue limit of notched samples.

The fatigue limit of a notched specimen is lower than the fatigue limit of an unnotched specimen. The ratio of the fatigue limit of an unnotched specimen to that of a notched one, having the same cross-sectional area, is called the fatigue notch factor, K_f [113]

$$K_f = \textit{unnotched sample fatigue limit / notched sample fatigue limit} \qquad \text{Eqn.3.6.}$$

The degree of agreement between theoretical predictions of elastic stress concentration and actual effects is often measured by the so-called notch sensitivity index, q, defined as:

$$q = \frac{K_f - 1}{K_t - 1} \qquad \text{Eqn.3.7.}$$

This equation shows that if $q=0$, then $K_f=1$ as the material has no sensitivity to notches. If $q=1$, then $K_f=K_t$ and the material is fully notch sensitive.

K_t is the theoretical stress concentration factor, the subscript 't' indicates that the stress concentration value is a theoretical calculation based only on the geometry of the component and discontinuity.

However, several formulae have been suggested for the calculation of the K_f factor. K_f calculated from the well known Peterson equation for ferrous alloys is given by:

Peterson [113] equation $$K_f \approx 1 + \frac{(K_t - 1)}{\{1 + (\frac{A_n}{\rho})\}}$$ Eqn.3.8.

where A_n is a constant whose value depends on the strength and ductility of a material (A_n=0.25 mm for annealed steels and A_n=0.025 mm for steels of very high strength) and ρ is the notch-root radius.

Neuber postulated that the strength depends on the average stress acting over an elementary cubic block within the material, taking account of the stress distribution near the point of maximum stress in the notch. The empirical solution is given by Neuber's equation, as stated by Forest [114]

Neuber's equation $$K_f = 1 + \frac{K_t - 1}{1 + \frac{\pi}{\pi - \omega} \cdot \sqrt{\frac{A}{R}}}$$ Eqn.3.9.

where A = a material constant having dimensions of length, and representing half the width of the elementary block;

R = root radius of notch;

ω = included angle of notch in radians, for notches in the form of V grooves.

The determination of stress concentration factors mathematically is a very difficult problem. Values of the stress concentration factors for a wide range of notches were obtained mathematically by Neuber and Peterson [113,114]. From their results it is possible to estimate the stress concentration factor, K_t, for most grooves and notches with sufficient accuracy for most practical purposes.

In addition, the stress concentration factors are also provided in a graphical form on the basis of the formulae so that they can be used easily in design or research. Predictions of the smooth fatigue limit are based on the theoretical stress concentration factor, K_t which has been adopted from Neuber's calculation, having a value of $K_t = 3$, whilst the K_f has been calculated using eqn.3.9.

Bending Fatigue Limit

In order to classify the influence of a notch on the fatigue behaviour of steels used in this study, a determination of the smooth fatigue limit was an absolute necessity. Consequently, bending tests were also performed which overcame the gripping problem outlined previously. Samples were tested in a three-point bending rig, as shown in Fig.3.9.(a,b). Smooth wire samples having a total length of 60 mm were also subjected to similar fatigue conditions.

S-N curves obtained for the smooth samples subjected to bending fatigue were generated using the same procedure as previously described. These curves, together with S-N curves for notched wire samples fatigued under axial loading conditions, were used to estimate the influence of a notch or/and an influence of the microstructure on the fatigue limit.

These results were helpful in comparing the influence of notches in material which does not undergo phase transformations, and to estimate the influence of notches and microstructure respectively in the material which does transform during fatigue.

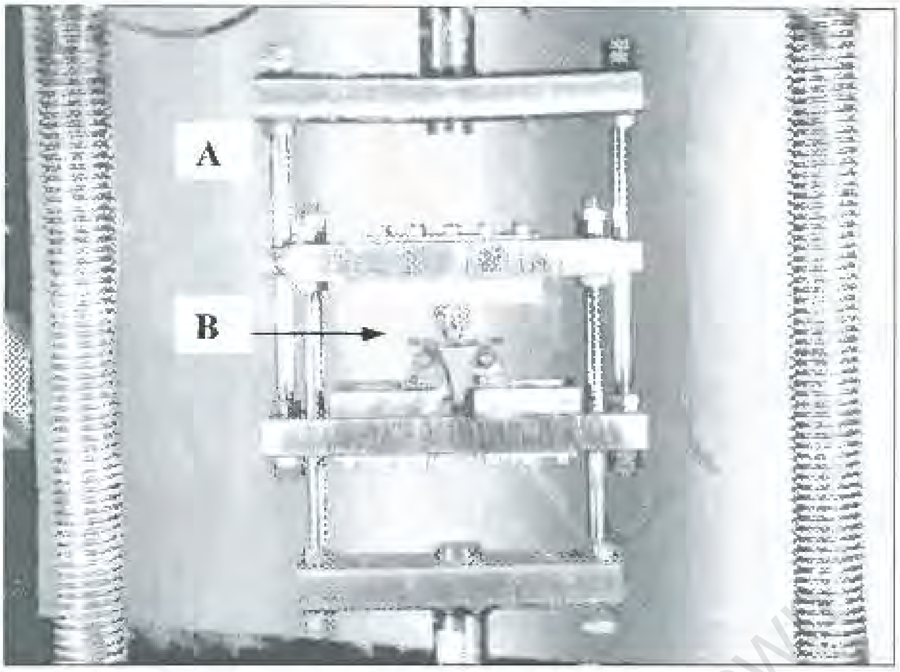

Fig.3.9.(a) Setting of three-point bending rig in ESH - testing machine; A - three-point bending rig; B - wire sample

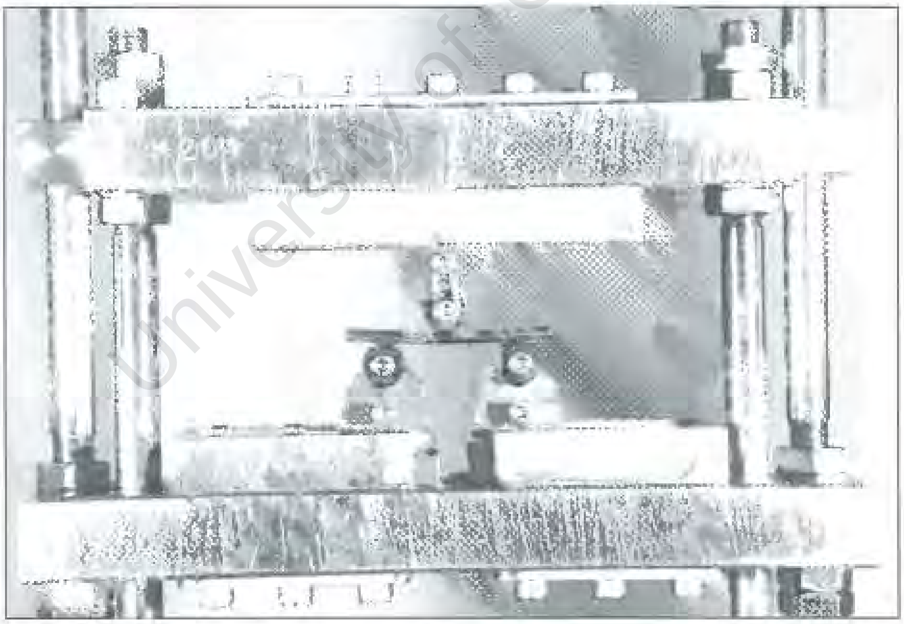

Fig.3.9.(b) *Closer view of smooth wire sample tested under bending fatigue conditions*

3.4.2.2.2. Fatigue Crack Growth Rate – Data Acquisition

The detection and measurement of cracks lengths, particularly in the early stages of a specimen's life, was found to be difficult because of the uncertainty of knowing (i) where and when the fatigue crack initiated, and (ii) whether the detected crack was the dominant one leading to final fracture. Due to the small diameter of the steel wires and its circular shape, the usual techniques employed to determine the crack growth rate were found difficult to apply in order to obtain the threshold stress intensity factor range which necessitates a high accuracy in crack length measurements.

As a consequence, the crack growth rate was measured using the following method [70]. The samples were initially notched perpendicularly to the drawing direction by means of file, to a depth of about 300 microns. After fatigue testing at a given stress level, the specimens were broken in tension and the crack increment was measured in a scanning electron microscope after different numbers of cycles. The effect of notch stress concentration, together with the relatively high level of cyclic stress, meant that the fatigue crack initiated almost immediately. It's because of this rapid crack initiation that this estimate of fatigue crack growth rate is reasonable [70]. This method is schematically presented in Fig.3.10.

Example:

Sample 1. – Notch + Fatigue at N = 1000 cycles + Break + Crack measurement in SEM ($a_1 = 40\ \mu m$)

Sample 2. – Notch + Fatigue at N = 2000 cycles + Break + Crack measurement in SEM ($a_2 = 55\ \mu m$; crack increment $\Delta a = 15\ \mu m$), etc.

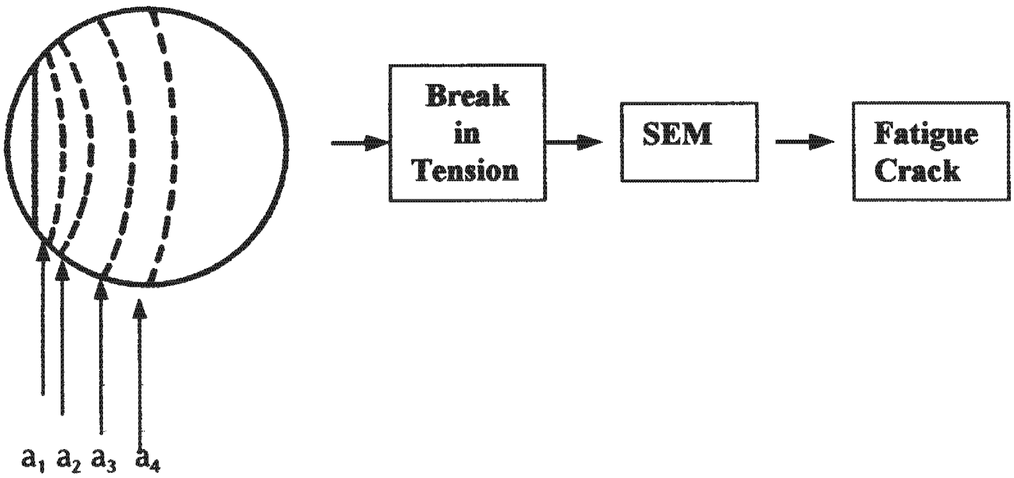

Fig.3.10. *Fatigue propagation stages and measuring method*

These experimental results of crack growth rates have been used in the determination of the stress intensity factor ΔK for different values of the stress ratio. From the values Δσ and a, the stress intensity factor range ΔK was determined by the expression eqn.21.

$$\Delta K = Y \cdot \Delta\sigma \cdot \sqrt{\pi \cdot a} \qquad \text{Eqn.3.10.}$$

valid for a/D values greater than 0.15, the parameter Y [70] being

$$Y = (0.473 - 3.286\,(a/D) + 14.797\,(a/D)^2\,)^{1/2}\,((a/D) - (a/D)^2\,)^{-1/4} \qquad \text{Eqn.3.11.}$$

where D is the diameter of the wire.

In order to obtain reliable values of ΔK_{th} the following system for different values of the load ratio, R, was used. For both R=0.048 and R=0.2, notches were created using a file and the maximum stress was progressively decreased for each stress block until ΔK was small enough.

In all tests, the crack propagated at least 20 μm in the last loading block. The crack propagation was measured as described previously, by breaking under monotonic loading and measuring in a scanning electron microscope.

In summary, although the proposed technique used for the monitoring the fatigue crack growth is not considered to be the most reliable method, it is the most 'convenient' in terms of specimen size, inexpensive but also time consuming.

With this system an accuracy of ±3 μm in the measurement of Δa (crack increment) was achieved. Sufficient confidence was gained in this method to continue its use.

3.4.3. Microscopy

The general investigation of microstructure both in the longitudinal and cross-section was performed using optical microscopy, while the fatigue crack growth rates and fracture modes were investigated using scanning electron microscopy.

Dislocation structures and the measurement of very fine microstructural parameters, such as interlamellar spacing and deformation twinning required the use of a transmission electron microscope.

Light Optical Microscopy

The wire samples were sectioned in both the longitudinal and transverse sections. The specimens were then mounted in resin and polished using a STRUERS automatic polisher to a 0.25 μm finish.

In order to reveal the microstructures of different types of steel wires, the following solutions were used:

High Carbon Steel

4 g Picric acid
100 ml Methyl alcohol

AISI 304 Stainless Steel

Solution A:

25 ml Nitric acid
75 ml Hydrochloric acid

or, solution B, to observe the martensite phase

Solution B:

10 g Cupric sulphate
50 ml Hydrochloric acid
50 ml Methanol

3CR12 Steel

25 ml Hydrochloric acid
2 g $NH_4F.\ HF$
1 g $K_2S_2O_5$

Light microscopy was carried out using a REICHERT Me3A light microscope. The images obtained from this microscope showed the general microstructure of different types of steel. In the case of annealed AISI 304 stainless steel the morphology and distribution of α'-martensite phase transformed during the drawing and subsequent fatigue process was observed.

Scanning Electron Microscopy

A CAMBRIDGE STEREOSCAN 200X scanning electron microscope was used for the analyses of the fatigue cracks and to characterise the fatigue fracture modes.

Transmission Electron Microscopy

TEM observations were made of cross-sections of as-drawn wires and after they were subjected to the fatigue process.

The specimens were sectioned and mechanically ground to a thickness of about 70-90μm. The disks were further thinned electrochemically to perforation, using a STRUERS TENUPOL jet electropolisher with the following polishing solutions:

High carbon steel-	*10% perchloric acid, 90% acetic acid at -15℃*
AISI 304 Stainless steel-	*5% perchloric acid, in ethanol at -10℃*
3CR12 steel-	*5% perchloric acid, in ethanol at -15℃*

Samples were polished at 20 V, using an appropriate flow rate setting of 5 on the instrument.

The specimens were examined in a high voltage transmission electron microscope, a Joel 2000 CX operating at 220 kV.

3.4.3.1. Quantitative Metallography

Quantitative analyses of the microstructures developed during drawing included measurements of the prior austenite grain size in all types of steel and the pearlite colony and interlamellar spacing in the high carbon steel.

3.4.3.1.1. Grain Size

Estimates of the prior austenite grain size were determined for the carbon steel in the following way. The method involved intentionally decarburising a specimen during austenitisation at a temperature above 1000°C for approximately 30 minutes; just long enough to return the carbon to the austenite solid solution, and then allowing it to cool slowly in the furnace.

During slow cooling, the ferrite deposits at the grain boundaries of the prior austenite, thus revealing, in the final structure, the size of the original austenite grains.

The determination of the grain size in AISI 304 austenitic stainless steel also involved heat treatment at 1050° C and rapid cooling in water. This resulted in a microstructure which was fully austenitic with recrystalised equiaxed grains.

The 3CR12 steel was annealed at 780° C for the period of 30 minutes; long enough to dissolve the martensite islands, followed by air-cooling.
The random intercept method, ASTM E-112 was used to determine the grain size in all types of steel [115].

3.4.3.1.2. Experimental Measurement of Interlamellar Spacing

Measurements of the interlamellar spacing of pearlite in carbon steels have been commonly employed in the development of structure-property correlations for pearlitic steels [116]. Interlamellar spacing can be related to the heat treatment and drawing conditions and determines the mechanical properties such as the tensile strength, hardness and toughness.

The measurements are complicated by the spacing variations within a given pearlite colony, those between different colonies and those produced by the metallographic sectioning plane with respect to the orientation of the lamellae. When the sectioning plane is perpendicular to the lamellae, the true interlamellar spacing of the colony can be determined. As the sectioning plane becomes less perpendicular and approaches an orientation parallel to the lamellae, the apparent spacing and the apparent carbide thickness increases dramatically.

The measure of fineness of the lamellar structure or the true interlamellar spacing, is defined as the perpendicular distance across two consecutive lamellae, i.e. ferrite and cementite, Fig.3.11.

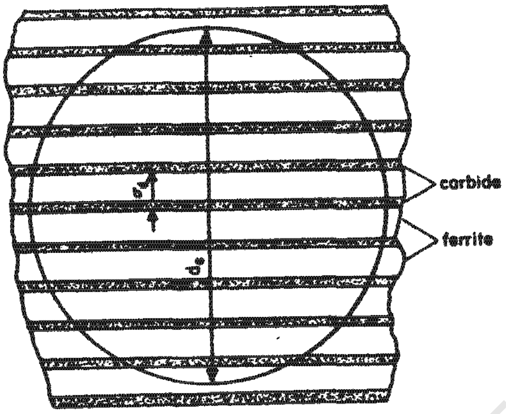

Fig.3.11. *Schematic illustrating a pearlite colony intersected by a circular test grid*

The interlamellar spacing of the pearlitic steel wire used in this study was measured using transmission electron microscopy. Thin foils were prepared from cross sectional areas and examined in the transmission electron microscope. Colonies in which the lamellae appeared to be perpendicular to the foil surface were photographed and then used to measure the interlamellar spacing at three locations within each colony. The average of such measurements was 45nm.

3.4.4. Determination of the Residual Stresses in Carbon Steel Wire

The distribution of the axial component of the residual stress in the cross-section of wires was estimated using Heyn's method, which consists of successive measurements of the change in the diameter and gauge length (~60 mm) of the wires, caused by material removal, layer by layer [117]. The removal of the wire surface was performed by immersing in 10% nitric acid. After every five minutes, the samples were ultrasonically washed in alcohol and the diameter measured.

The measurements of wire dimensions were performed using an electronic micrometer. The average thickness of the material removal each time was approximately 10 μm. The stress in a layer was calculated using the following equation:

$$\sigma = E \cdot \frac{D_n^2 \cdot (l_n - l_0) - D_{n-1}^2 \cdot (l_{n-1} - l_0)}{(D_{n-1}^2 - D_n^2) \cdot l_0} \qquad \text{Eqn.3.12.}$$

where σ = average residual stress in the axial direction within the n-th layer, E = elastic constant (2.06×10^5 MPa), l_0 = gauge length prior to removal, l_n = gauge length after removal of the n-th layer, l_{n-1} = gauge length after removal of the n-1th layer, D_n = wire diameter after removal of the n-th layer, D_{n-1} = wire diameter after removal of the n-1th layer, respectively.

The residual stresses were calculated using the same method in both the as received and shot peened condition. It was found that the dimensional measurements of wire samples after being immersed in nitric acid significantly vary from one to another. The use of a digital vernier did not give enough accuracy and the major problem was in measurement of length.

For instance, an error in length measurement of 20 μm gives a value of residual stress which is approximately five times higher. This problem is addressed in more detail on p.101.

CHAPTER 4

RESULTS

The experimental results are presented in the following order:

(i) Static mechanical properties
(ii) Characterisation of the microstructures
(iii) Fatigue behaviour
(iv) Characterisation of changes caused by the fatigue process
(v) Fractography

The intention in this chapter is to present mainly experimental observations and data, and to continue with a comprehensive discussion in Chapter 5. However, in order to present the results as clearly as possible, it has been necessary in certain situations to include some discussion.

4.1. High Carbon Steel Wire

4.1.1. Mechanical Properties of High Carbon Steel Wire

According to the data obtained by other authors, the effect of drawing strain on the mechanical properties of this type of steel are essentially dependent on the interlamellar spacing [37,118]. The minimum interlamellar spacing is controlled primarily by the transformation temperature but the effect of other processing variables, such as the austenitizing temperature, are also critical in the patenting process for steel wire and rods.

The tensile properties of high carbon steel, drawn to 1.86 strain as supplied by Haggie Rand Co, have been investigated in order to ascertain the influence of this particular drawing strain, on the yield strength, ultimate tensile strength, elongation to failure and fatigue performance.

The results of tensile testing are shown in Fig.4.1. and Table 4.1. together with hardness measurements and grain size. Both Fig.4.1. and Table 4.1., illustrate the high strength properties of drawn pearlitic steel wire with an ultimate tensile strength of 1982 MPa and a yield strength of 1546 MPa. It can be also noted from Table 4.1. that the steel possesses a small elongation to failure (3%) and the loss of ductility results from the substantial amount of plastic deformation that this steel has received during manufacture.

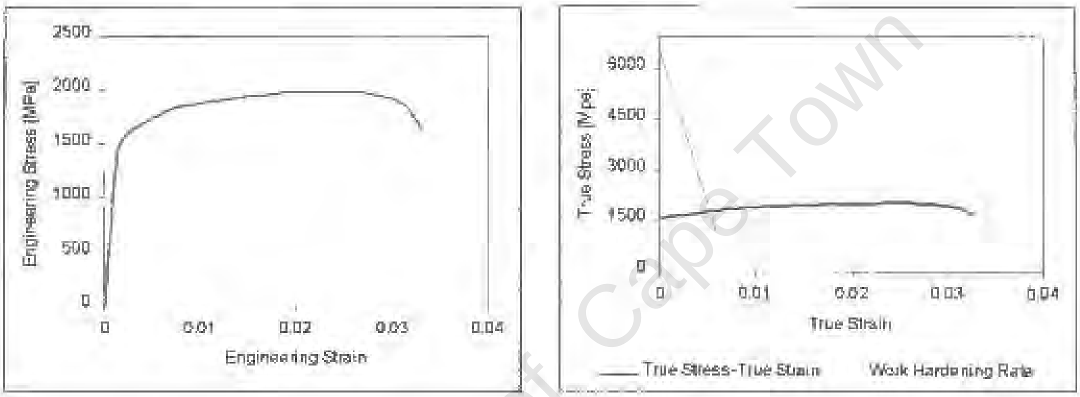

a)

b)

Fig.4.1. (a,b) *Tensile results of high carbon steel wire drawn to 1.86 strain*

a) engineering stress-strain curve, and b) true stress-strain curve

Table 4.1. Mechanical Properties of Pearlitic Steel Wire Drawn to 1.8 Strain

Ultimate Tensile Strength	**Yield Strength**	**Total Elongation to Failure**	**Reduction of Area**	**Grain Size**	**Hardness Vickers**
[MPa]	[MPa]	[%]	[%]	µm	HV25
1982	1546	3.4	31	30	465

The true stress-true strain curve of the drawn pearlitic steel wire together with the work hardening rate curve is shown in Fig.4.1.(b). These curves reveal important information such as the strain at which necking begins and the uniform plastic elongation to failure.

Results obtained for heavily drawn pearlitic wire (strain 1.86) show a negative work hardening rate and the work hardening rate curve intercepts the flow curve at a low strain of 0.5%. The reason for such behaviour is due to the very high plastic deformation applied during the drawing of wire, effectively exhausting the extremely high ability of this steel to work harden further.

The hardness measurements taken across the section thickness of drawn pearlitic wire are presented in Fig.4.2.

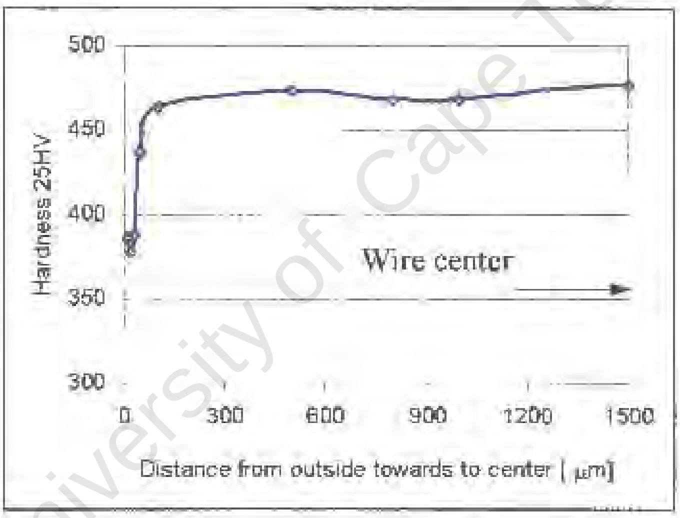

Fig.4.2. *Microhardness measurements in high carbon steel wire drawn to 1.86 strain*

The hardness measurement curve shows the variation of hardness from 388 HV25 measured at approximately 25 μm below the surface to 470 HV25 in the wire bulk. This variation is due to the decarburisation developed during the patenting process.

4.1.2. Microscopy in High Carbon Steel Wire

4.1.2.1. Surface Examination

Since surface defects can lead to premature failure during fatigue testing and affect results, a careful examination was carried out on the surface of the wire using both optical and scanning electron microscopy. Figures 4.3.(a,b) are typical of the many different types of surface defects, such as mechanical scratches, drawing marks, cavities and corrosion pits, which exist on these wires. Some cavities appear to be deep and wide, between 20-50 µm, and contain substances that are non-conductive and become electrically charged by the electron beam in the scanning electron microscope.

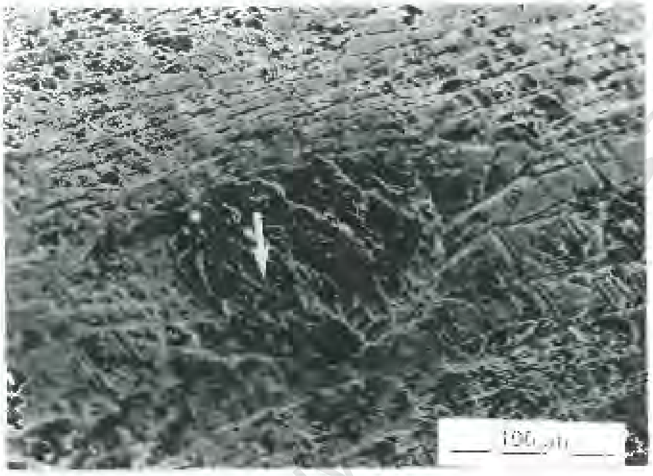

Fig.4.3.(a) *SEM micrograph of drawn carbon wire, showing surface markings aligned in the drawing direction and a piece of metal re-drawn into the wire.*

Fig.4.3.(b) *Corrosion pits filled with a Zn-P deposit observed on the wire surface.*

Sample condition: Pearlitic carbon steel wire drawn to 1.86 strain in cross-section

An X-ray microanalysis of these included substances showed evidence for the presence of zinc and phosphorous. It is considered that the zinc-phosphorous deposit originates from the coating applied prior to the wire drawing process.

An average value of surface roughness, measured in the longitudinal direction was $R_a = 1,6$ µm. This was achieved using a Taylor Hobson profilometer and was the average of ten readings. Roughness measurements in the transverse direction were very difficult to record and considered to be inaccurate due to the small diameter of the wire and the very deep grooves left after the drawing process.

4.1.2.2. Metallography of High Carbon Steel Wire

Extensive metallographic analyses performed on the wire samples showed the presence of decarburisation. The depth of decarburisation was approximately 25 µm which is approximately 0.8% of the diameter of the wire. Decarburisation is known to affect fatigue life detrimentally since it influences crack initiation by changing the fatigue strength and residual stresses of the surface metal.

It is well known that the presence of geometrical discontinuities, such as non-metallic inclusions and corrosion pits, can also have a deleterious effect on the fatigue and fracture resistance [34]. The number, size, location and type of inclusions have been found to be of importance in determining their effects on subsequent fatigue behaviour. The orientation of inclusions with respect to the orientation of the stress field and the relative deformability of inclusions with respect to that of the matrix also greatly affect the crack nucleation behaviour.
The deleterious effect of inclusions on the fatigue resistance of materials is related conventionally to the localised stress/strain concentration at the boundary of the inclusions and matrix, owing to the mismatch of physical, thermal, mechanical and chemical properties.

The interaction between geometric discontinues and cyclic loading results in plasticity localisation and thus facilitates crack development. Similarly, enhancement of localised dissolution, resulting from plasticity localisation, contributes to corrosion pit development at non-metallic inclusion sites, thus promoting early crack development when a corrosive environment is present.

Two main kinds of inclusions were detected in this work: heavily elongated sulphide-type inclusions distributed along the longitudinal direction of the specimen, and a smaller population of angular-shaped inclusions that were identified as calcium-aluminate.

Figure 4.4. shows a calcium-aluminate inclusion, which occupies the space in the matrix between the highly deformed cementite lamellae.

Fig.4.4. *Scanning electron micrograph of angular calcium- aluminate inclusion imbedded between cementite lamellae, creating a massive crack.*

Conditions: Longitudinal section of high carbon steel wire drawn to 1.86 strain

Etchant: 2.5% Nital

The bulk of the cold drawn steel wire had a fully pearlitic microstructure. Figures 4.5.-4.6. show the microstructures of the drawn wire in both the longitudinal and transverse cross-sections respectively.

Figure 4.5. shows the microstructure of a longitudinally sectioned wire sample, which consists of very fine lamellar pearlite; the colony nodules are clearly seen in the transverse sectioned sample, Fig.4.6.

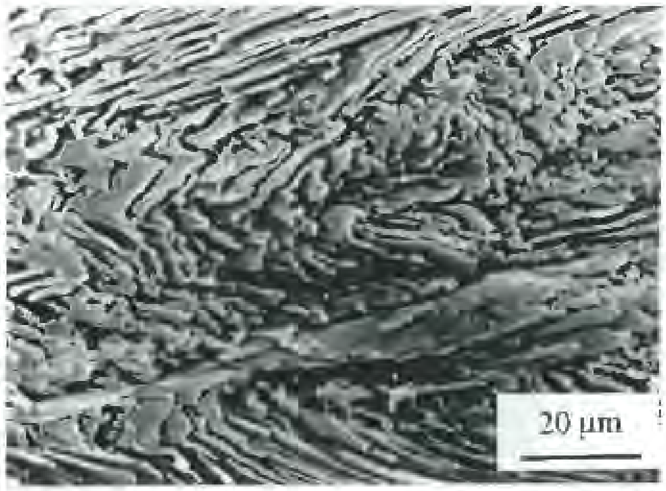

Fig.4.5. *Scanning electron micrograph taken in the longitudinal section, showing an aligned cementite lamellae.*

Etchant: 2.5% Nital
Wire drawn to 1.86 strain

Each pearlite nodule is composed of colonies within which the lamellae are essentially parallel, but differ in orientation from the lamellae in adjacent colonies. Repeated sectioning studies have shown that pearlite is essentially a branched structure so that each pearlite colony consists of two interwoven crystals, one of ferrite and the other of cementite. The apparently wide range of interlamellar spacing visible in Fig.4.6. reflects the range of interlamellar angles at which the pearlite colonies are intersected by the plane of sectioning.

A curly grain structure is observed in the transverse cross-section of heavily drawn wire, in which convolution and interlocking of neighbouring grains can be observed. The final grain shape is quite variable and reflects the unusual degree of nonuniformity of plastic strain from grain to grain. The wavy nature of the grains in heavily drawn bcc metals has been explained with reference to the wire texture [119]. As a result, the change in grain shape occurs only in one transverse dimension, becoming ribbon-like and these curl around one another in order to maintain compatibility with neighbouring grains.

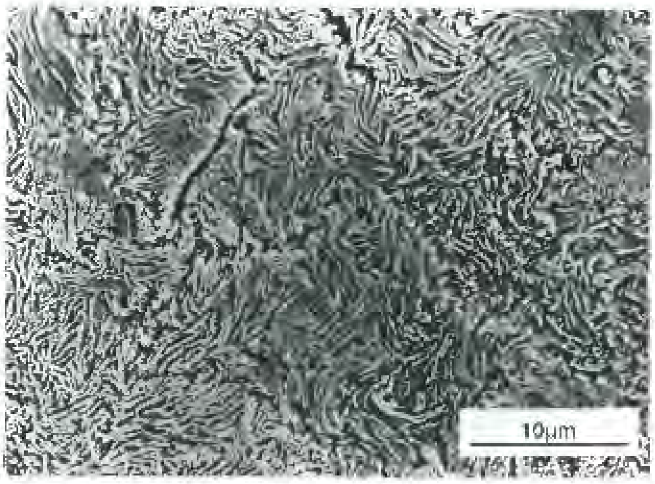

Fig.4.6. *SEM of fully pearlitic microstructure in a transverse cross section. Note: the pearlite colonies, the pearlite nodules and the interlamellar spacing.*

Etchant: 2.5% Nital
Drawing strain 1.86

The schematic description of the curly structure in cold drawn carbon wire is given in Fig.4.7.

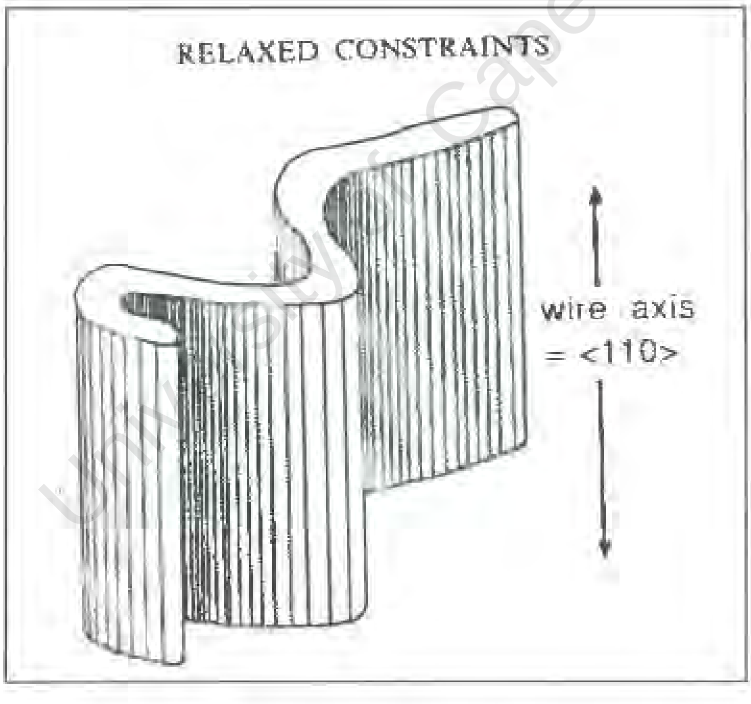

Fig.4.7. *The shapes of grains in a drawn bcc metals can be described as ribbons aligned and folded parallel to the wire axis [119]*

All these microstructural parameters, the size of the primitive grains, the pearlite nodule size and interlamellar spacing were measured. In order to determine the grain size, the samples were heated up to 1100^0 C for approximately 30 minutes and cooled in the air. The ferrite phase outlined the former austenite grains and the primitive grain size was measured at approximately 30 µm. The pearlite nodule size was determined on the polished cross-section of the wire using the linear intercept method, described in Chapter 3, p.84. It was found that the nodules were between 10 and 15 µm in diameter. This data was taken as the average of approximately 25 measurements.

An optical examination of deformed pearlite is limited due to the low resolution of the optical microscope and it was found necessary to employ electron microscopy and particularly transmission electron microscopy. The interlamellar spacing and the thickness of the cementite lamellae were determined from transmission electron micrographs using the random intercept method, which is fully described in Chapter 3, p.84.

A transmission electron image shows the width and distribution of the cementite lamellae, Fig.4.8.

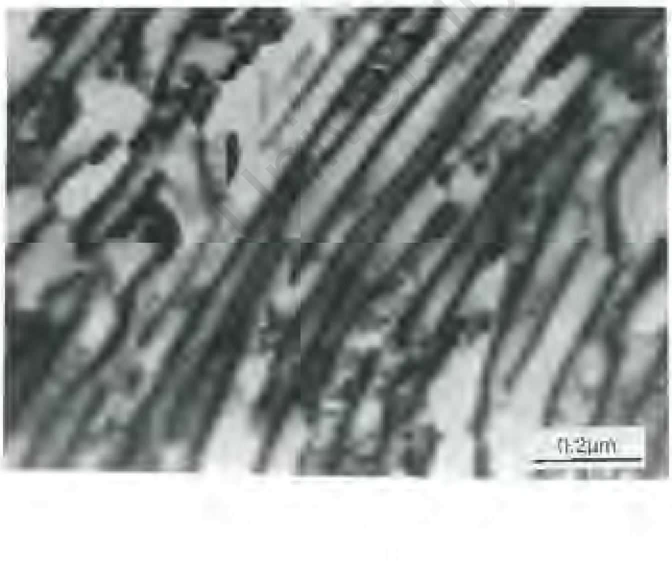

Fig.4.8. *Transmission electron micrograph of transverse section of drawn carbon steel wire, showing the distribution of interlamellar spacing with strain of 1,86*

The results show that the cementite lamellae are very fine, ranging in thickness from 60 nm to less than 100 nm. The interlamellar distance is approximately 45 nm, indicating the extremely fine microstructure developed by the drawing process at a strain of 1.86.

One of the most obvious characteristics of the highly deformed pearlite structure, observed by transmission electron microscopy, is the blurring of the ferrite-cementite interface.

4.1.3. Fatigue Properties of High Carbon Steel Wire

The fatigue behaviour considering in particular the fatigue limit and fatigue crack growth rate of the pearlitic steel has been studied using both smooth and pre-notched samples, and the results of this study are presented in this section.

4.1.3.1. Fatigue Limit of Smooth Wire Samples

The study of the fatigue limit involves considerable and careful experimental work since data based upon the Wöhler, (S-N) curve is not directly applicable due to the high scatter of empirical results without the support of statistical models. The reason for such a high scatter is due mainly to the defects of ranging size found in the surface of steel, which act as stress concentrations leading to crack initiation at variable cyclic stresses.

The results of the S-N tests shown in Fig.4.9.(a) and Table 4.2. indicate that the fatigue limit (the stress level at which fatigue tests continue indefinitely or simply 'run out') for the pearlitic steel wire investigated in this study, occurs at a stress amplitude of approximately 250 MPa, for a mean stress of 550 MPa (i.e. cyclic stress was between 300-800 MPa). In maximum stress terms the fatigue limit for the as drawn material was therefore 800 MPa, Fig.4.9.(a).

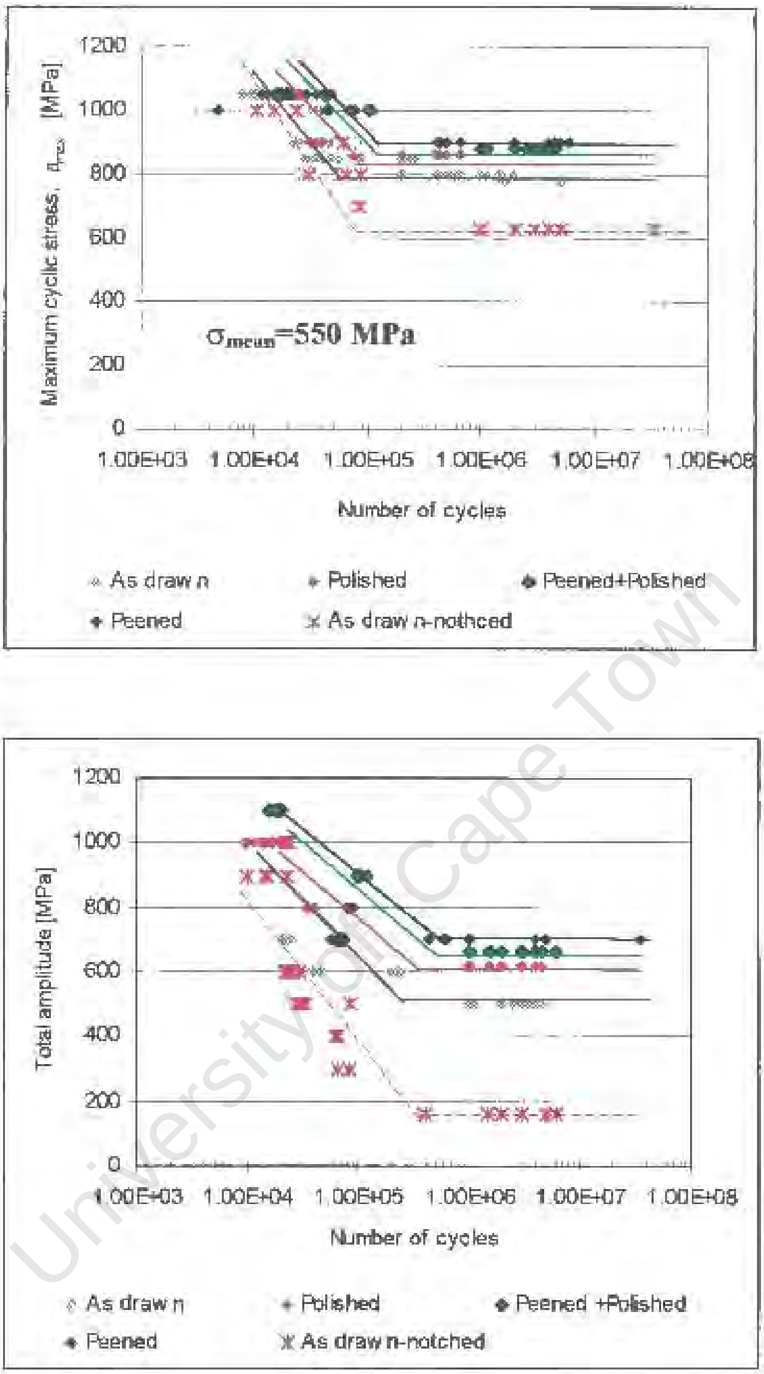

Fig.4.9. *S-N curves for pearlitic carbon steel wire (drawn, polished and shot peened) are presented in terms of maximum stress* ***(a)*** *and cyclic amplitude* ***(b)***

Note: Notch of 300 μm depth, V-shaped, made by fine file

Table 4.2. Fatigue Limit of High Carbon Steel Wire

	Smooth Fatigue Limit MPa		Notched Fatigue Limit MPa	
	Maximum Stress	**Amplitude**	**Maximum Stress**	**Amplitude**
As Received	800	250	630	80
Shot Peened	900	350		
Shot Peened-Polished	880	330		
Polished	860	310		

The fatigue limit for the as drawn pearlitic microstructure of 800 MPa is approximately 50% of the static yield strength. The value of the difference between the yield stress and fatigue limit ($\sigma_t - \sigma_L$) can be used to characterise the resistance to crack initiation [120]. Thus, if the value of fatigue limit is higher, the smaller difference ($\sigma_t - \sigma_l$), indicates a higher relative resistance to crack initiation in the steel.

4.1.3.2. Polishing and Shot Peening of High Carbon Steel Wire

Since the fatigue limit of cold drawn eutectic wires is highly dependent on the presence of surface defects, the fatigue limit is expected to improve if the surface is polished to eliminate surface imperfections. The roughness of the wire surface after being polished was reduced from $R_a = 1.6$ to $R_a = 0.3$ μm and showed a significantly higher resistance to crack initiation. The polishing process did not result in a significant change in diameter.

The fatigue limit of the polished carbon steel wire was found to be 310 MPa (stress amplitude) which is an improvement of approximately 24% compared to the original wire samples, Fig.4.9. In maximum stress terms, the fatigue limit was 860 MPa compared to 800 MPa for the as drawn material, Fig.4.9.(a).

The effect of shot peening of the wire surface, on the fatigue behaviour was also examined. The results showed that the fatigue lives for peened samples are greater than those for unpeened specimens. Shot peening was expected to influence the initiation and propagation of cracking since work hardening of the surface layer should increase the resistance to the development of crack tip plasticity. Shot peening increased the surface hardness to 525 HV from a bulk hardness of 460 HV (the hardness of the distorted layer is approximately 10% above that of the unpeened material) at a depth of approximately 50 μm, as shown in Fig.4.10.

The inherent compressive residual stress was expected to lower the effective stress intensity and therefore, the resistance to crack initiation should increase. The combined action of these two effects was expected to result in an increase in the maximum stress necessary for crack initiation. Experimental results show that this was indeed the case and that the amplitude fatigue limit of peened wire samples was increased to 350 MPa (stress amplitude) which is about 40% higher compared to the unpeened carbon steel wire of 250 MPa, Fig.4.9.(b). In maximum stress terms the fatigue limit of peened specimens increased from 800 MPa to 900 MPa, Fig.4.9.(a).

An attempt was made to separate the three effects of shot peening (residual stress, work hardening, and surface roughening). The samples were longitudinally polished after shot peening, using 0.25 μm diamond paste to remove the sharp asperities of the peened surface layer.

Unfortunately, the subsequent tests did not confirm an increase of fatigue strength, which indicated that perhaps some of the compressive residual stress from the shot peening layer had possibly been removed during the polishing process. This was borne out by subsequent microhardness testing. Further examination of the shot peened wires were consequently discontinued.

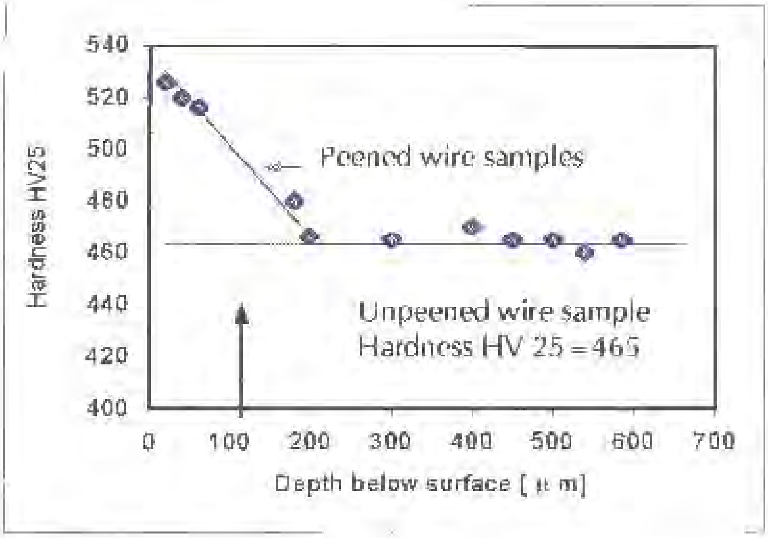

Fig.4.10. *The variation in hardness, caused by shot peening of carbon steel wire*

4.1.3.3. Fatigue limit of Notched Wire Samples

The fatigue limit of high carbon steel wire was also investigated on the pre-notched samples. A notch of approximately 300 μm depth, having a V-shape was induced using a file.

The experimental results show a very low fatigue limit of approximately 160 MPa (total amplitude), Fig.4.9.(b) or maximum stress fatigue limit of 630 MPa, Fig.4.9.(a) which illustrates the significant effect of the stress concentration on the notch and relatively speaking reduced the influence of microstructure on fatigue behaviour. This result illustrates that the microstructure does not control the crack initiation but rather that the stress concentration of the notch itself is the primary controlling factor on the fatigue process and shows the inadequacy of using notched specimens to study microstructural effects on crack initiation. However, the notched samples are further used in this study in order to correlate fatigue behaviour of high carbon steel, AISI 304 stainless steel and 3CR12 steel in terms of notch effect.. The fatigue limit data for the notched wire samples is also presented in Fig.4.9.

Residual Stress Distribution in the Pearlitic Steel Wire

Measurements of residual stresses in the peened surface layers were measured using Heyn's method as reported by Katagiri [117], as described in Section 3.6., p.86.

The distribution of the axial component of the residual stresses in the cross-section of wires is obtained from successive measurements of the change in the diameter and gauge length of the wires, caused by removal, layer by layer, of the surface of the wire, as explained in Chapter 3, p.86.

The residual stresses in the axial direction at the surface, extrapolated from the stress distribution profiles, as a function of a drawing strain, are shown in Fig.4.11. and Table 4.3.

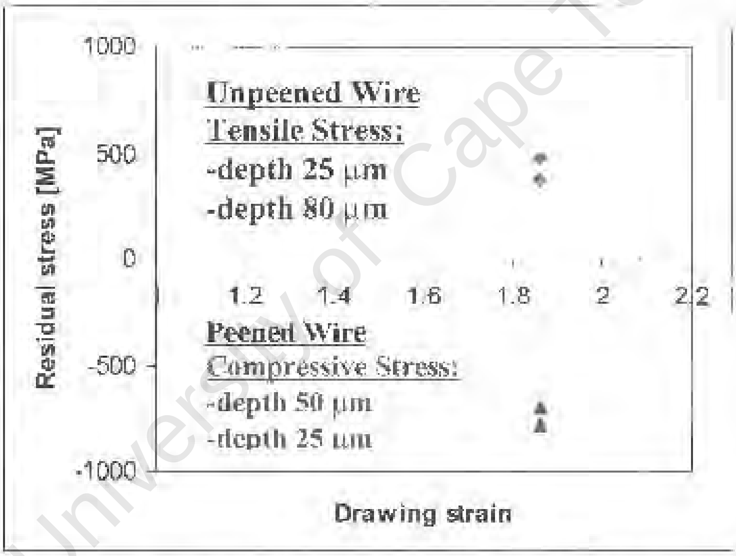

Fig.4.11. *Residual stresses in the drawn carbon wire as a function of drawing strain (wire used in this study was drawn to 1.86 strain)*

High residual tensile stresses reside in the surface layers since severe plastic deformation has occurred during the drawing process. It was calculated, using Eqn.3.12., that the residual axial tensile stresses at the wire surface reaches

480 MPa at approximately 25 μm beneath the immediate surface. The tensile stress decreases to 380 MPa at a depth of 80 μm below the surface.

High compressive residual stresses in the direction of the wire axis are induced in the surface region from the shot peening treatments. The compressive stresses reach a level of 780 MPa at a depth of 25 μm below the surface and then gradually decrease to 700 MPa at a depth of 50 μm.

Table 4.3. Example of Material Removal in High Carbon Steel Wire

	5 min	**10 min**	**15 min**	**20 min**	**25 min**	**30 min**	**35 min**
Length-mm	58.80	58.79	58.77	58.73	58.72	58.68	58.68
Diameter-mm	3.14	3.10	3.07	3.06	3.04	3.00	2.98

Table 4.3. shows an example of six measurements taken on the wire sample. There appears to be a trend of decreasing in length and diameter of wire sample after etching which is less than 10 μm. Error in the measurement of length is similar to this change and consequently the effect of residual stresses was not taken into further consideration.

4.1.4. Changes in High Carbon Steel Wire Induced by Fatigue

4.1.4.1. Mechanical Properties

Stress-strain curves are presented for drawn carbon steel wire and after being subjected to fatigue, at a load ratio of R=0.048 for a period of 1,000,000 cycles, Fig.4.12. The tensile curves show a slight decrease in the strength properties after the carbon steel wire samples were subjected to fatigue and the cyclic yield strength appears to be less sensitive to cyclic softening than the ultimate tensile strength.

The ultimate tensile strength and yield strength decrease by approximately 6% and 3% respectively indicating a softening caused by the fatigue process. Due to the very small extent of softening, clear differences in hardness values were not observed. This data was obtained from the results of testing approximately ten samples subjected to cyclic strain at a particular load ratio and duration of test.

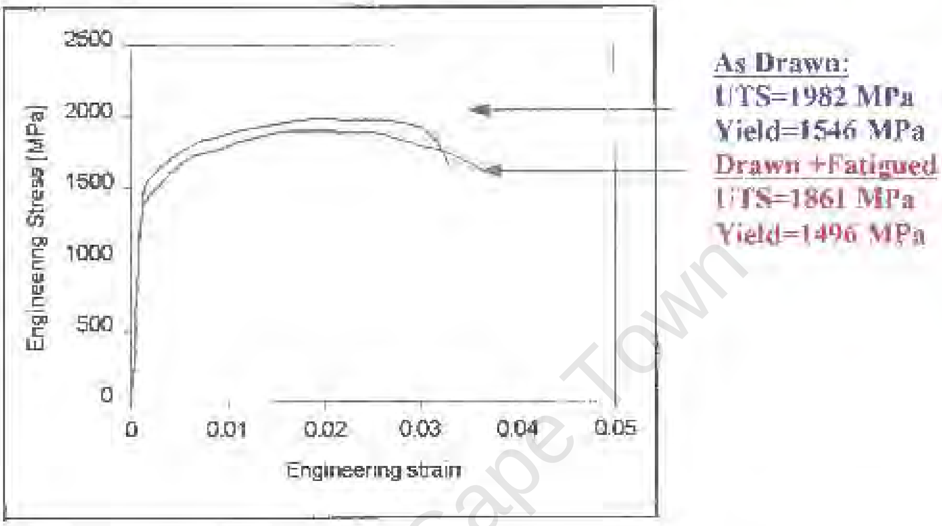

Fig.4.12. *Tensile test results of high carbon steel wire in as-received condition and after fatigue at a load ratio of R=0.048 and N=1,000,000 cycles*

Attempts to investigate the changes caused by cyclic strain, by observing the microstructure using transmission electron microscope, were not successful and significant changes in the dislocation density were not observed. The possible reason is that the very small interlamellar spacing obtained during drawing resulted in blurring in the contact area between the cementite lamellae and ferrite matrix. Thus, any further slight increase of dislocation density was not readily observed.

Nevertheless, it is believed that the fine interlamellar pearlite underwent cyclic softening probably due to an increase in dislocation mobility.

4.1.5. Fractography of High Carbon Steel Wire

The fracture surfaces were studied using both scanning and light optical microscopes in order to relate the effect of drawing and cyclic strains on the failure mode. The differences between the static and fatigue fracture modes of high carbon steel wire were observed and are presented in this section.

4.1.5.1. Static Tensile Fractography

The static tensile fracture surface was investigated and compared to the fatigue fracture surfaces using both pre-notched and smooth wire samples.

The static tensile fracture surface observed on the pre-notched wires was characterised by many radial ridges. The general topography was found to be very rough and it appears that ductile separation is the main fracture mode, as shown in Fig.4.13.

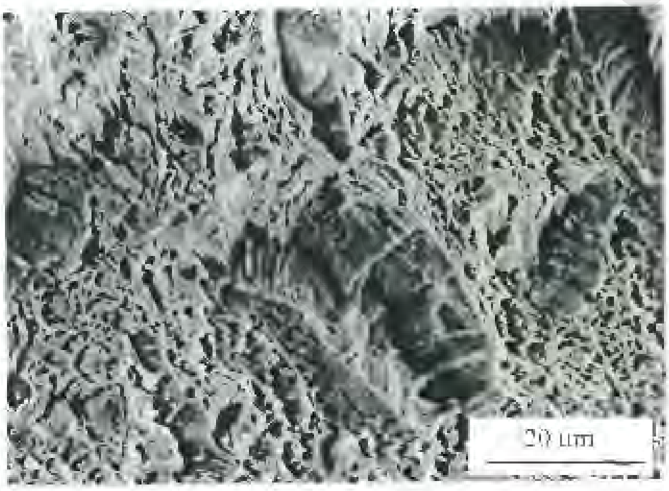

Fig.4.13. *SEM micrograph of the static tensile fracture surface of the high carbon pearlitic steel wire, showing ridges and ductile separations.*

<u>Conditions:</u>
Wire sample drawn to 1.86 strain,
tensile test performed at a strain rate of 0.001 s^{-1}

4.1.5.2. *Fatigue Fractography of High Carbon Steel Wire*

During the fractographic examination of highly drawn and fatigued carbon wire, a number of fracture modes were identified, namely: mode A-ductile transgranular cracking, mode B-tearing topography and mode C-intergranular separation.

A comparison also was made of the cracking obtained from fractography and from subsurface longitudinal sections. Fractographic observations emphasize the behaviour of the fatal crack(s), while subsurface sections reveal the non-fatal cracks which were often numerous. Once a crack nucleates, it grows and carries most of the strain in strain control, or load in load control, and retards the growth and nucleation of small cracks in stress shadows. The later transgranular cracks will therefore initiate and propagate slowly.

Other important conclusions were also derived from such analysis. It was found for example that the fatigue fractures initiated in all cases at a surface flaw. These flaw depths were generally between 50 and 80 microns.

The general macroscopic fracture appearance is presented in Fig.4.14. The cracks always initiated at the specimen surface in unnotched specimens and propagated radially from the grain of initiation into the specimen interior. As the cracks increased in size beyond the first prior austenite grain, they typically began to change orientation, gradually becoming perpendicular to the applied stress, as seen in Fig.4.15.

Many cracks in fact stopped growing during this transition period, and only one crack (per specimen) completed the transition to Region II and eventually caused failure.

Fracture surfaces, initiated by a notch, revealed that the mode of propagation did not fit any of the usual categories.

There was, however, evidence that extensive plastic flow accompanied crack extension. This is called 'ductile tearing' or TTS or 'Hill and Valley' fracture surface [70] with a coarse ridge structure running parallel to the macroscopic growth direction, Fig.4.16.(a,b).

Fig.4.14. *Surface defect from which a ductile fatigue crack propagated.*
Fatigue crack initiated at a surface flaw having a depth of approximately 40 microns Arrow indicates direction of the crack propagation.
Note the splitting and final fast fracture.

Sample condition: wire drawn to 1.86 strain

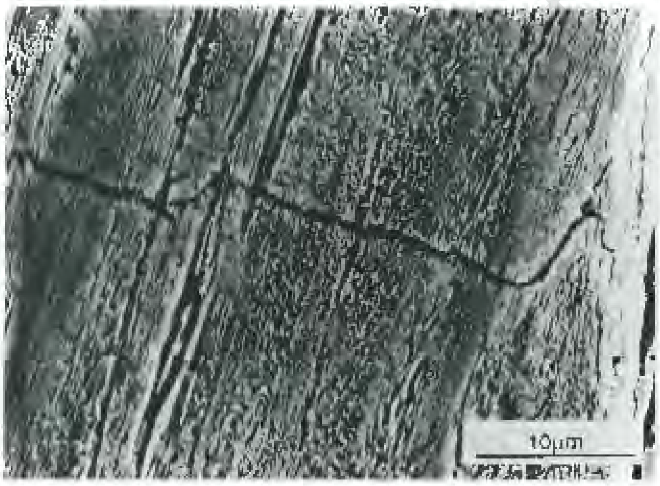

Fig.4.15. *Fatigue crack initiation and propagation in fully pearlitic steel wire drawn to 1.86 strain - fatigue crack started from the surface*

↑

Direction of applied stress

↓

Fig.4.16.(a) *SEM micrograph of irregular torn-topography fracture typically observed in high carbon steel wire, starting at a notch*

Fatigue fracture mode: tearing topography-mode - B

Sample condition:-notched wire drawn to 1.86 strain

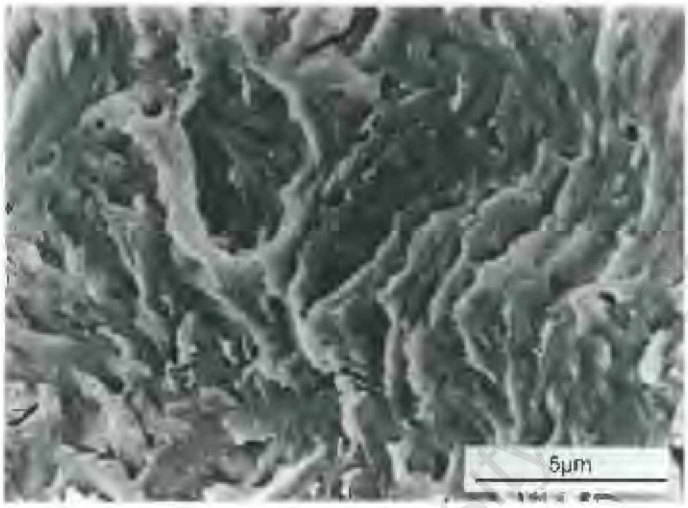

Fig.4.16.(b) *SEM micrograph illustrates 'ductile' microplastic tearing, as the second stage of main crack. Fatigue fracture surface resembles ill-defined fatigue striations typical of fully pearlitic steel.*

Fracture mode: Mode –B tearing topography

A detailed examination of the main cracks and branch cracks showed that three fracture modes could be associated with the surface observations and the microstructure through which the crack passes.

1. The crack tends to propagate through the pearlite colonies at approximately right angles to the lamellae. A detailed examination of the crack profile across the lamellar pearlite revealed that individual or groups of cementite lamellae protrude from the fracture surface.

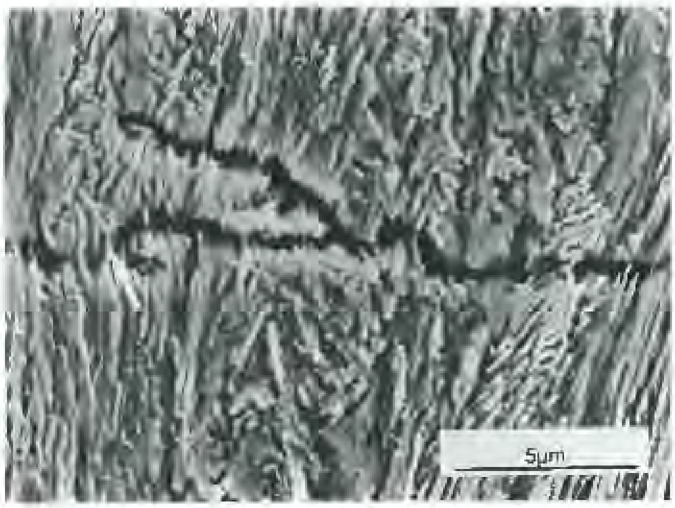

Fig.4.17. *Scanning electron micrograph of the fatigue crack propagating in the longitudinal direction illustrates the microcombination of brittle cementite lamellae and plastically deformed ferrite matrix.*
Arrow indicates plastically deformed ferrite.

Conditions: fatigued pearlitic steel wire drawn to 1.8 strain

Branch cracks also show this type of feature as well as cases of lamellae spanning a crack, which appears to progress ahead in the ferrite.
On the basis of these observations it is considered that crack propagation through pearlite colonies occurs preferentially by a mechanism of void formation in the interlamellar ferrite ahead of the cracks, followed by tearing of the remaining ferrite and brittle failure of the cementite, Fig.4.17.

2. Less commonly, the crack grew parallel to the pearlite lamellae in a step-wise fashion, as shown in Fig.4.18. This type of cracking was observed as part of a main crack or in isolation, ahead of branch cracks and adjacent to the main crack. This appeared to be a form of damage occurring at the crack tip that may subsequently be incorporated into the main crack. This type of cracking possibly results from the residual stresses induced during the drawing process.

A relatively high frequency of branch cracking was observed, which was often associated with low growth rates.

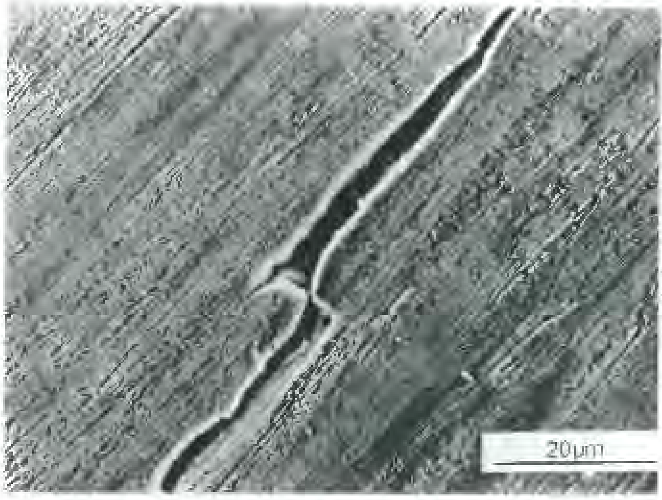

Fig.4.18. *Etched profile of fatigue cracking along the pearlite lamellae. This type of cracking was observed as a part of the main crack.*
Conditions:Longitudinal section of pearlitic steel wire subjected to the fatigue process.

3. A relatively small amount of intergranular fracture was observed at pearlite colony boundaries and along cementite-ferrite boundaries.

The nature of fatigue crack initiation and propagation in pearlitic steels and some typical propagation modes are shown in Figs.4.19.-4.21.

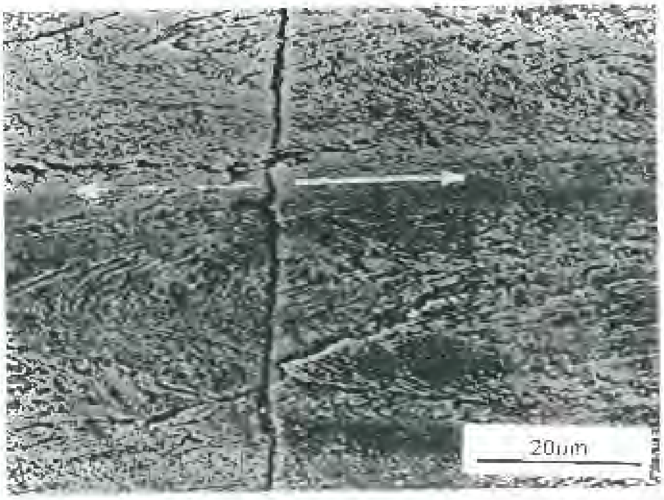

Fig.4.19. *SEM micrograph of the crack path across a pearlite colony. Micrograph is taken in the longitudinal section of cold drawn pearlitic wire (drawing strain 1.86)*
Etchant:2.5 % Nital
Arrow indicates the direction of applied stress

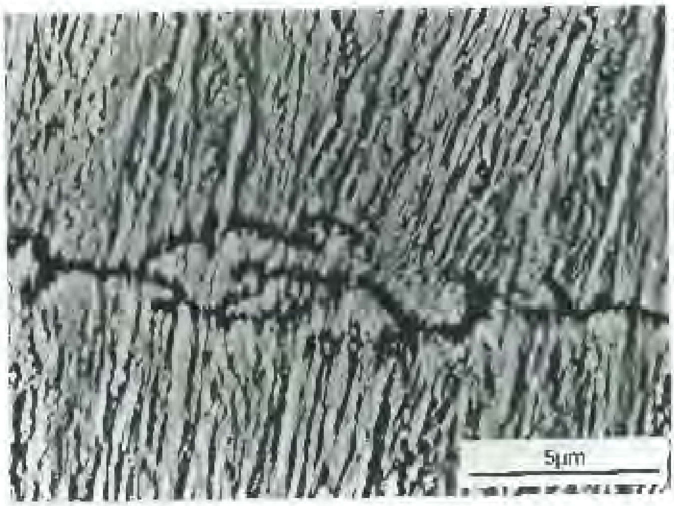

Fig.4.20. *Scanning electron micrograph showing typical zig-zag path of the fatigue crack observed in cold drawn pearlitic wire.*

Etchant: 2.5% Nital

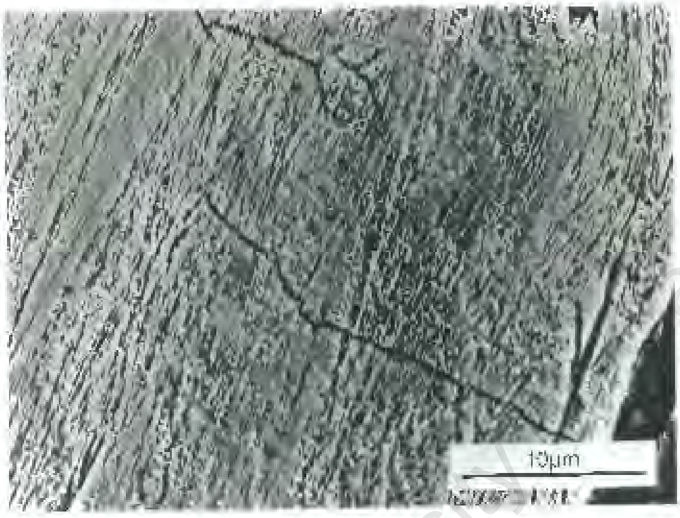

Fig.4.21. *SEM micrograph taken in the longitudinal section of the wire, showing the appearance of typical secondary cracks.*

Conditions: high carbon steel wire, drawn to 1.86 strain, subjected to fatigue.
Etchant: 2.5 % Nital

The scanning electron micrographs in Fig.4.22.(a,b) show the difference in roughness observed on the fracture surface.

The fracture modes, which have been observed in the 'Haggie Rand' –wires, parallel those results obtained by Cooke and Beevers [69].

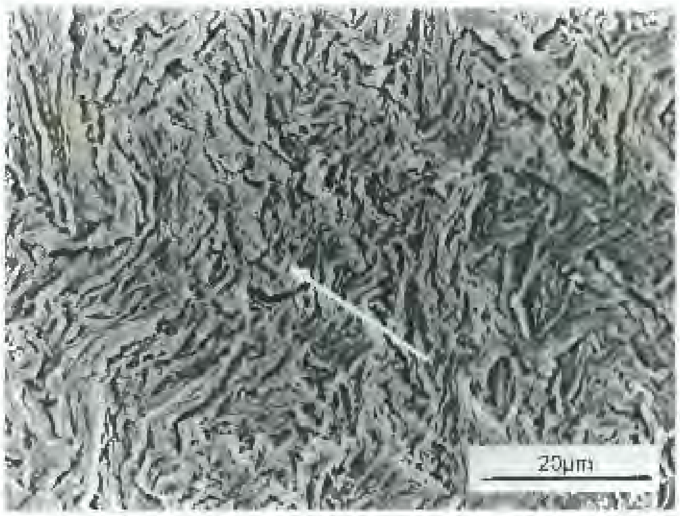

Fig.4.22.(a) *SEM micrograph showing the fatigue fracture surface close to the notch*

Load ratio R = 0.048

Fracture mode:
Transgranular ductile mode A

Arrow indicates the direction of crack propagation.

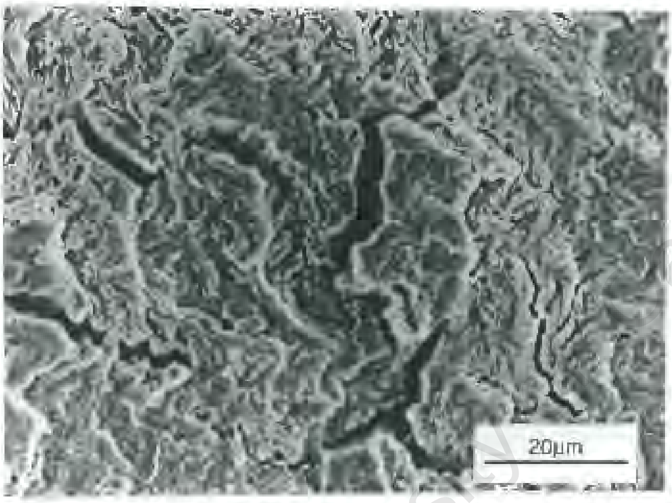

Fig.4.22.(b) *The fatigue fracture surface observed far from the notch*

Load ratio R=0.048

Fracture mode:
Transgranular ductile mode-A, and intergranular separation mode –C

The fracture surface and resulting profile suggest that crack extension occurs by microstructural damage in the form of interlamellar cracks followed by tearing across the damaged region.

Summary:

The results obtained from this research indicate that the extremely high strength of carbon steel wires achieved by cold drawing may be negated in cyclic conditions if the wire surface contains significant defects. It has been found that the high strength associated with a very fine pearlite microstructure makes carbon wires very sensitive to stress concentrators.

In order to overcome the surface quality problem, either polishing or shot peening methods should be employed. Polishing significantly improved the fatigue limit by approximately 25%. However, the shot peening method was more efficient, improving the fatigue limit by approximately 40%.

4.2. 304-Austenitic Stainless Steel Wire

4.2.1. Mechanical Properties

The tensile properties of AISI 304 stainless steel wire drawn to five different strains have been investigated in order to determine the influence of work hardening and/or strain-induced martensite, on the yield strength, ultimate tensile strength and elongation to failure. Further, the results of the tensile tests have been compared to those obtained from wires subjected to cycling strain in order to identify any changes in mechanical behaviour which are a consequence of the fatigue process.

The results of the tensile tests are shown in Fig.4.23. The data for all of the drawing strains is shown on the same set of axes for purposes of comparison. Table 4.4. lists each of the properties that were calculated from the tensile data, together with the results of Vickers hardness and the volume percentage of strain-induced martensite obtained by x-ray diffraction analysis. Figures 4.24.-4.25. show the XRD traces of wires drawn to 0.09 and 0.585 strain respectively, while the relationship between the drawing strain and the amount of martensite phase developed during the drawing is shown in Fig.4.26.

Figure 4.23. shows that the ultimate tensile strength, yield strength and hardness are all increased by increasing drawing strain. The ultimate tensile strength approximately doubled from 642 MPa to 1346 MPa whilst the yield strength increased from 267 MPa to 1137 MPa as the strain increased from zero to 0.585. It can be also noted from Table 4.4. that the elongation and reduction of area values decreased as the yield and tensile strengths increased. Figure 4.23. shows that wire drawn to a strain of 0.58 has the greatest yield strength and ultimate tensile strength, but the smallest elongation to failure.

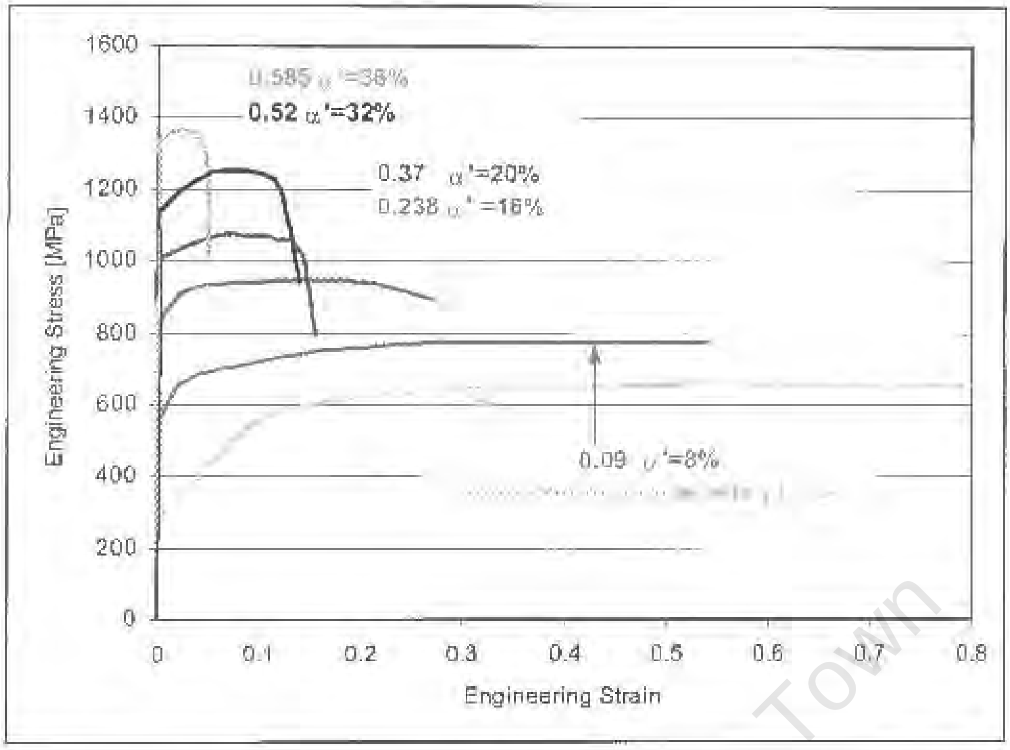

Fig.4.23. Tensile test results of AISI 304 stainless steel wires drawn to different strains between 0.09 to 0.585

Table 4.4. List of tensile properties and hardness of AISI 304-steel wires

Drawing Strain (ε)	Strain-Induced Martensite [%]	Yield Strength [MPa]	Ultimate Tensile Strength [MPa]	Total Elongation to Failure [%]	Hardness (Vickers) 25 HV
Annealed	0	267	642	79	180
0.09	8	480	752	54	192
0.238	16	810	941	28	310
0.37	20	995	1060	17	360
0.52	32	1100	1247	14	410
0.585	36	1137	1346	5	440
2.5 mm*	10	1260	1550	16	465
3 mm*		1300	1590	16	460

*Commercially supplied wires (2.5 and 3mm dia – estimated strain 0.6)

The loss of ductility measured by elongation to failure corresponds to the formation of a large amount of strain-induced martensite of 36%. Wire samples drawn to a low strain of 0.09 have the lowest volume fraction of the strain-induced martensite, 8%, and as a consequence a greater elongation to failure (54%).

The tensile test results also indicate that the formation of strain-induced martensite during drawing decreases the capacity for plastic work significantly. Plastic elongation to failure decreases from 75% in the annealed condition of AISI 304 stainless steel to approximately 4% in highly drawn wire (0.585 strain). Table 4.4. also shows that the commercially supplied wires of 2.5 and 3mm diameter have higher mechanical properties, compared to those drawn in laboratory conditions. Ultimate tensile strengths were approximately 200 MPa greater and yield strengths between 100 and 150 MPa larger.

The volume fracture of the α'-martensite phase was found by x-ray diffraction analysis to be 8% in the specimens drawn to a low strain of 0.09 and 36% in the specimens drawn to 0.585 strain, as shown in Figs.4.24.-2.25. No ε martensite was detected by x-ray diffraction analysis.

Figure 4.26. shows the relationship between the drawing strain, the amount of transformed martensite and its influence on yield strength. It was shown that the volume fracture of martensite formed is directly related to the square of the drawing strain.

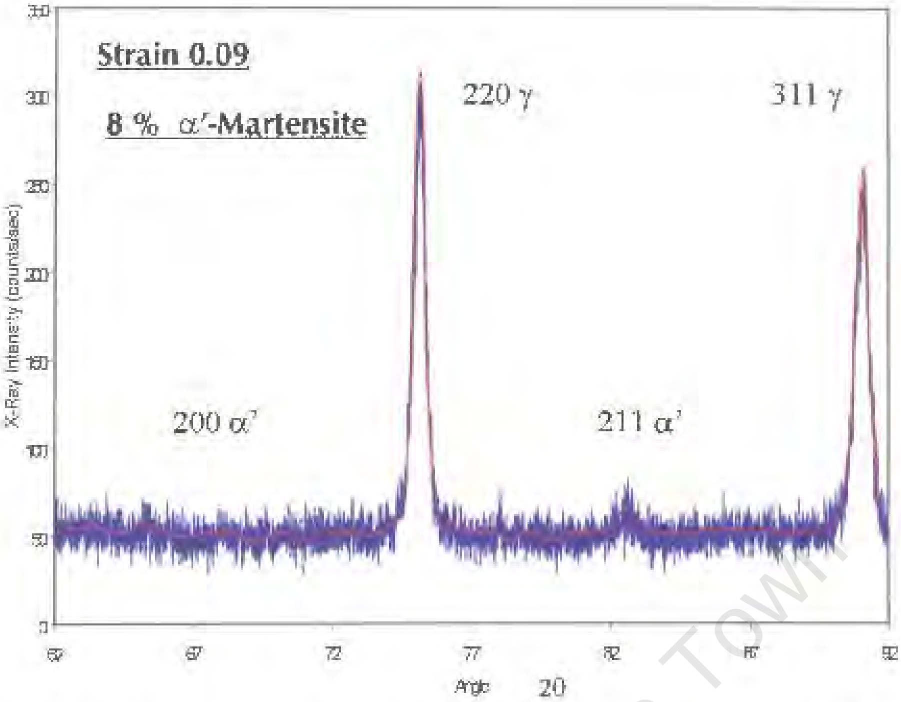

Fig.4.24. *XRD trace for AISI 304-stainless steel wire drawn to 0.09 strain*

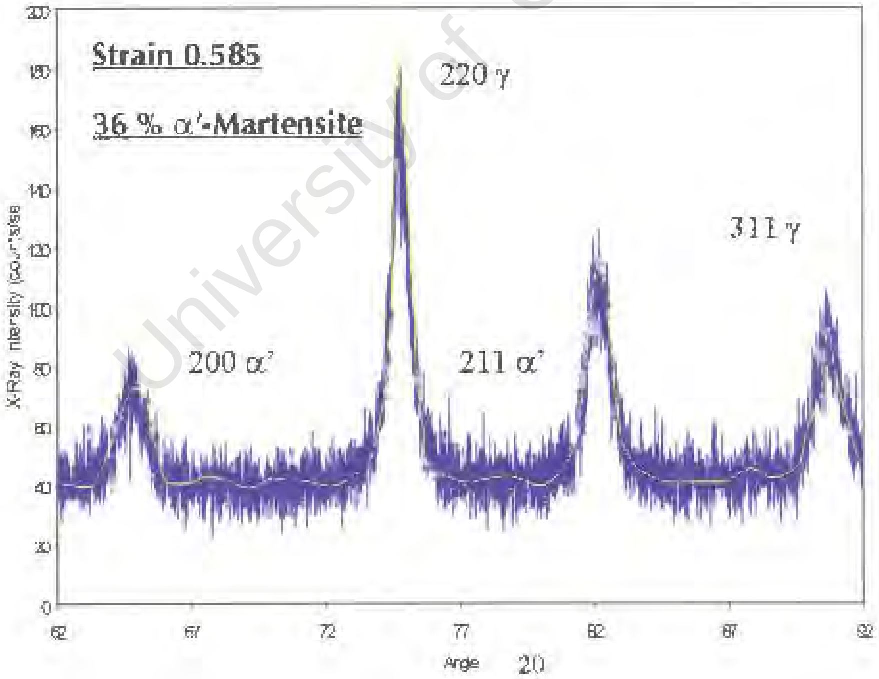

Fig.4.25. *XRD traces for AISI 304-stainless steel wire drawn to 0.585 strain*

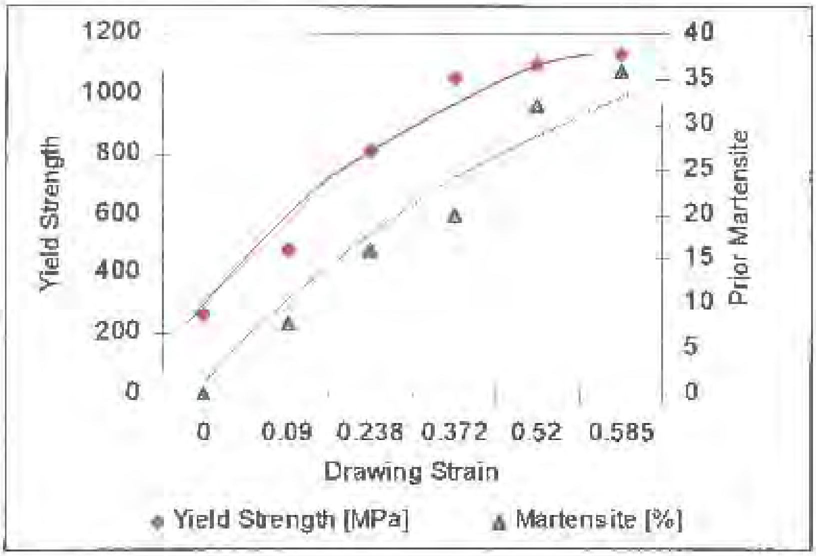

***Fig.4.26.** Influence of prior α'-martensite on yield strength of drawn AISI 304 stainless steel wire*

The results obtained for commercially supplied wires showed that they contained approximately 10% of strain-induced martensite. The small amount of strain-induced martensite in commercial samples indicates either a difference in the drawing process parameters and/or a difference in chemical composition between the two steels employed in this work.

In general, the composition of metastable austenitic stainless steels should be balanced to produce an M_d temperature (temperature at which martensite transformation caused by plastic deformation takes place) above room temperature, which results in austenite remaining stable during plastic deformation at room temperature.

The chemical composition of this steel showed that the percentage of nickel was higher than that found in the steel used for drawing in the laboratory (Table 3.1., at p.56). This would result in a higher M_d temperature and lower values of strain-induced martensite.

It can be noted from Table 4.4. that the hardness increases from 180 HV25 to 440 HV25 and follows a similar trend to strength increases. Hardness measurements taken across the section thickness of wires examined in this study are presented in Fig.4.27.

Wires produced in the laboratory showed no significant variation in hardness across the section, with the exception of the highly drawn wires. The highest variation in hardness was observed in wire samples drawn to 0.585 strain and the hardness measurement curve revealed three distinct regions. Significant variation in hardness was observed to occur in the immediate sub surface region of approximately 250 µm, where the hardness varied between 397 HV25 to 446 HV25.

This region was followed by a second region where the hardness measurements become approximately constant at 440 HV25, after which the hardness decreased to approximately 410 HV25 at a depth of 900 microns. The hardness measurement curve for wire drawn to 0.37 strain followed a similar trend, showing an initial variation in hardness of approximately 50 HV25 to a depth of 150 µm below the surface.

The variation in hardness is probably due to the non-uniform strain distribution and thus the amount of strain-induced martensite developed during the drawing process. The hardness gradient observed, particularly in the highly drawn wire, corresponds to the position of a 'central dumbbell' pattern, Fig.4.27., where the arrow indicates the direction of the hardness measurements.

A variation in hardness was also observed across the section of both the 2.5 and 3mm diameter commercially drawn wire. The lowest hardness was found to occur some hundreds of microns below the surface in the 3mm diameter wire (approx. 360 HV25) and it was associated with the presence of extremely large grains of 130 µm diameter. This suggests that some recrystallisation of the cold worked structure occurred during drawing through excessive frictional surface heating. The hardness measurements in the 2.5mm wire samples show significantly less variation across the section, although there was a gradual increase in hardness from the surface (430 HV25), for approximately 300 μm, after which the hardness remained constant at 460 HV25.

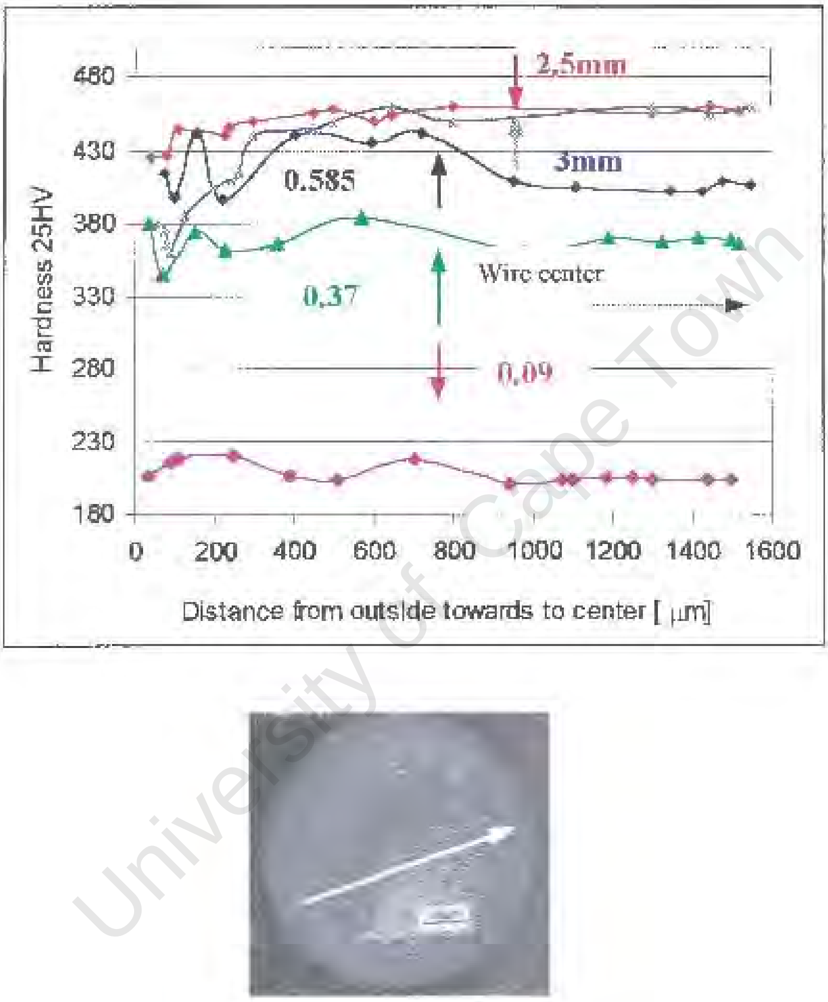

Fig.4.27. *Microhardness measurements in AISI 304 stainless steel wires*

Note: Arrow indicates the direction of hardness measurements

True Stress-True Strain Tensile Behaviour

The true stress-true strain curves of the drawn wires are shown in Fig.4.28.(a-d). In addition, the work hardening rate for each of these curves has also been plotted.

Important parameters such as the strain at the onset of martensite transformation, uniform elongation and the strain that defines the onset of necking during tensile deformation can be roughly predicted from these curves.

The onset of necking during deformation can be predicted from the intersection point of the flow curves and work hardening rate curves. The strain or stress that defines the onset of necking during tensile deformation is an important parameter, which describes the ability of a material to withstand plastic deformation.

The work hardening rate curves intercept the flow curves at approximately 50% strain for the annealed condition and at 35% strain in lightly drawn AISI 304 stainless steel wires (drawing strain 0.09), Fig.4.28.(a,b) indicating the great ability of this material to be plastically deformed.

If the work hardening curve intercepts the flow curve at low strain, this is a clear indication that the larger amount of martensite in drawn material causes early necking and thus a restricted ability for further plastic deformation.

The work hardening rate behaviour is closely related to martensite formation during deformation and it has been ascertained that the onset of positive work hardening occurs as a consequence of martensite formation [121].

Positive work hardening was observed in annealed and lightly drawn wires, whilst the work hardening was negative in the highly drawn wires (drawing strain greater than 0.37). Thus, it appears that strain-induced martensite, already present in drawn wires, delays the onset of martensite transformation during the tensile deformation process.

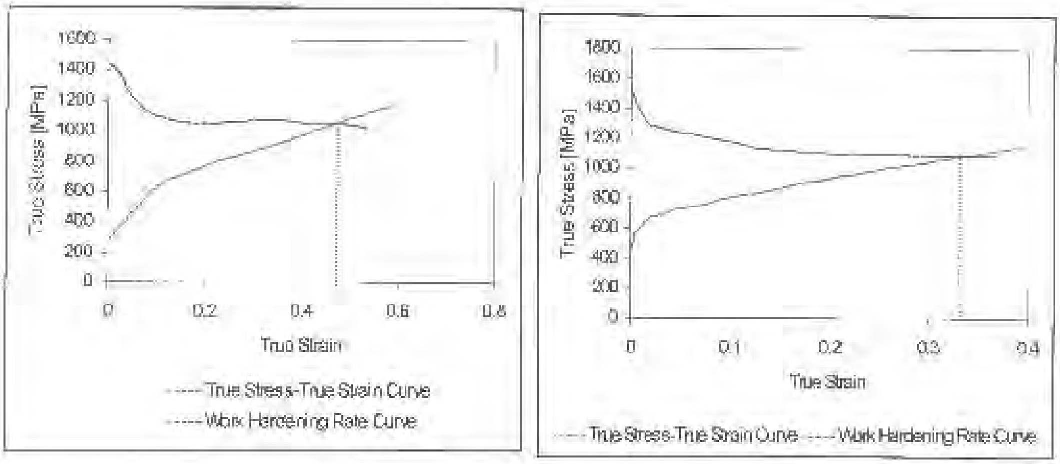

a) Annealed AISI 304 stainless steel wire, having austenitic structure

b) Drawn AISI 304 wire (strain 0.09) with approximately 8% of α′-martensite

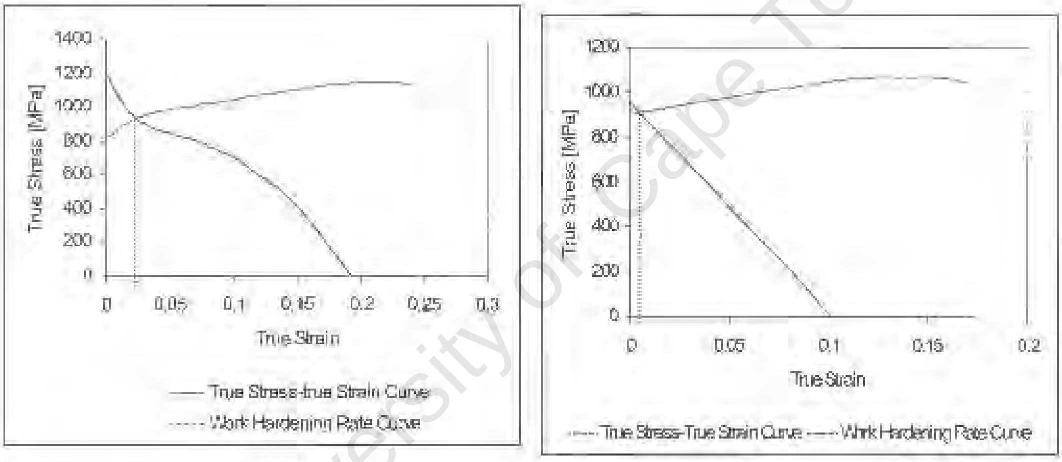

c) AISI 304 stainless steel wire drawn to 0.238 strain; having approximately 16% of strain-induced martensite

d) Drawn AISI 304 stainless steel wire (0.37 strain) with approximately 20% of α′-martensite phase

Fig.4.28. (a-d) True Stress-True Strain and Work Hardening Graphs for annealed and drawn AISI 304 stainless steel wires

Note: True stress-true strain and work hardening curves are not presented for highly drawn wires (0.52 and 0.585 strain). The negative work hardening rate and necking almost at the yield point were observed in both cases.

However, the work hardening rate curve shows that the lightly drawn AISI 304 stainless steel is less susceptible to this phase transformation, compared to annealed condition due to the level of martensite induced by the drawing process (8%), Fig.4.28.(b). In these lightly drawn wires (0.09 drawing strain), the work hardening rate remains constant over a large variation in strain, indicating a large uniform elongation to failure due to the beneficial effect of martensite transformation.

In wires drawn to 0.238 strain, Fig.4.28.(c), necking occurs at approximately 2% of strain resulting from the amount of martensite formed during the drawing process (approximately 16%). Results obtained for highly drawn wires, containing between 20% and 36% of strain-induced martensite, showed extremely low or no uniform elongation at all and necking started almost immediately after the yield strength was reached. Thus, high amounts of strain-induced martensite formed during the drawing process results in early necking and low uniform elongation in highly drawn wires.

In conclusion, the strain-induced martensite from the drawing process influences the ultimate tensile strength, the yield strength, the onset of further martensite transformation, the uniform elongation to failure and the necking point. It would appear that an amount of strain-induced martensite of approximately 20% is critical in determining the tensile deformation behaviour. In lightly drawn AISI 304 stainless steel wires, having up to approximately 20% of strain-induced martensite, the martensite formed during the tensile deformation is beneficial in allowing the material to withstand significant plastic deformation. Conversely, amounts of more than 20% of strain-induced martensite lowers uniform elongation and causes early necking during tensile deformation.

4.2.2. Microscopy of AISI 304 Stainless Steel Wire

4.2.2.1. Surface Examination

An examination of the wire surfaces revealed a much superior surface finish compared to the carbon steel wire. No mechanical defects or corrosion pits were observed unlike the carbon steel wires. The surface roughness was measured in the longitudinal direction of wire samples and varied between $R_a = 0.6–0.7$ µm for all wires drawn to different strains.

4.2.2.2. Metallography

The microstructure was examined both in the annealed condition and also in the samples drawn to different strains together with the commercially supplied wire samples. Figure 4.29. shows that the microstructure of an annealed wire is fully recrystallised, and consists of equiaxed austenitic grains. The optical micrograph shows that the grains are relatively small with an average size of 20 µm determined using the standard linear intercept method, Chapter 3, p.84.

Fig.4.29. *SEM micrograph of AISI 304 steel after annealing for 10 minutes at 1050° C and water cooling, showing the equiaxed grains of austenite and annealing twins.*

Etchant:
(HNO_3+HCl+methanol)

The drawn wire samples were prepared for optical microscopy by sectioning both parallel and transverse to the drawing direction. Following mechanical and electropolishing, the samples were chemically etched using a solution containing $HNO_3 + HCl$ + methanol.

Figure 4.30. shows the typical microstructure of wires produced in laboratory conditions. The micrograph taken in the transversal cross section reveals a characteristic feature of a 'central dumbbell'. It was noted that the distribution of martensite/strain is not uniform and according to visual observation, more martensite is formed around the circumference and in the 'central dumbbell' of the wire samples.

Fig.4.30. *General appearance of AISI 304 stainless steel wire produced in the laboratory.*

Note: ***'Central Dumbbell'*** *shape in the transverse cross-section of drawn wire*

Etchant:
($HNO_3 + HCl$+methanol)

Observation of the microstructure of commercially supplied wire showed that more martensite/strain is formed in the middle of cross-section and only partially around the circumference.

The reason for the different distribution of martensite/strain formed in the wires produced in the laboratory compared to the locally supplied wire is probably due to the nature of the manufacturing process. The process of drawing wire on a multiblock wire drawing machine consists of two stages of deformation, i.e. a process of drawing through a die and coiling of the drawn wire on a block (or capstan) of a drawing machine. The second stage of the process, i.e. coiling the wire on the block gives additional deformation after drawing and results in a change of stresses in the wire created during drawing, by coiling and unloading at the end of the wire drawing process. In general, it has been found that during the process of wire drawing on a multi-block machine, non-uniformity in the distribution of stresses over the cross-section of the wire decreases gradually in successive passes. This is due to a decrease in an interaction related to the change of curvature during coiling of the wire on the block [122].

A drum or capstan was not used in the laboratory conditions, i.e. the wire was kept straight during the drawing process. Other factors, such as drawing speed, also have an influence on the drawing process and consequently the strain distribution across the wire cross section.

Figures 4.31-4.32(a,b) show typical microstructures of stainless steel wires drawn to different strains, both in transverse sections. Deformation markings in the form of slip traces, deformation twins, and probably α'-martensite phase can be seen in these figures. The effect of increased deformation is also apparent.

The strain markings appear similar to strain-induced martensite and partially obscure the α'-martensite phase structure. The formation of martensite in metastable austenitic steels is well documented although differentiation between strain-induced martensite and bands of twins remains difficult.

Fig.4.31. *Transverse direction of lightly drawn AISI 304 stainless steel wire*

Conditions:
Drawing strain-0.09
Etchant:
HNO_3*+HCl+methanol*

Fig.4.32.(a)*Optical micrograph of the middle area of wire. The strain marks are more significant in the central area of highly drawn wire.*

Conditions:
Drawing strain 0.585
Etchant:
HNO_3*+HCl+methanol*

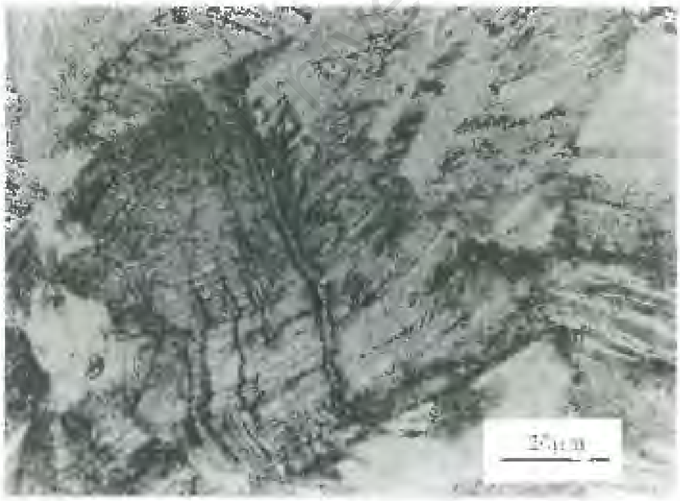

Fig.4.32.(b)*Optical micrograph of the surface layer of AISI 304 stainless steel wire produced in laboratory conditions. Microstructure consists of austenite and strain-induced martensite.*

Conditions:
Drawing strain 0.585
Etchant:
HNO_3*+HCl+methanol*

Figure 4.33. is a micrograph taken in the longitudinal direction of highly drawn wire (0.58 strain). The microstructure consists of fine particles or laths that occur in elongated clusters.

The individual particles or laths of the strain-induced martensite were too small to be clearly resolved by light microscopy. Consequently, light micrographs give the impression of considerably greater volume percentages of strain-induced martensite than actually exist.

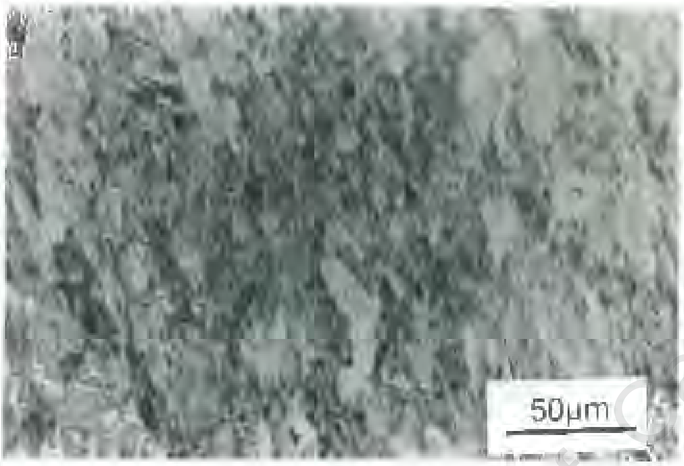

Fig.4.33.*Optical micrograph of AISI 304 stainless steel wire drawn to a strain of 0.585 showing the highly deformed microstructure in the longitudinal section.*

Etchant:
NHO_3+HCl and methanol

Transmission electron microscopy studies show that any deformation greater than 0.3 strain leads to the formation of twins and their density increases with increasing degrees of deformation. At a deformation of $\varepsilon = 0.37$, the critical stress for twinning is exceeded only in some grains. With increasing deformation the critical stress of twinning is achieved in more and more grains and there is a considerable rise in twin density.

In order to observe the effect of cold drawing on the dislocation microstructures, and the morphology of strain-induced martensite, thin foil specimens for TEM observation were prepared by the jet-polishing method, as outlined previously.

The evolution of the dislocation structure developed during the drawing process is shown in Figs.4.34.-4.36.

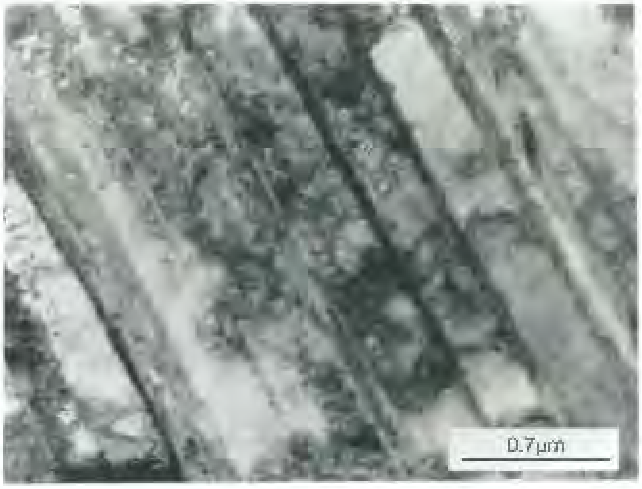

Fig.4.34. *TEM micrograph of AISI 304 stainless steel wire drawn to 0.238 strain showing the high density of dislocations in the walls.*
Width of dislocation walls is approximately 315 nm.

Produced in the laboratory

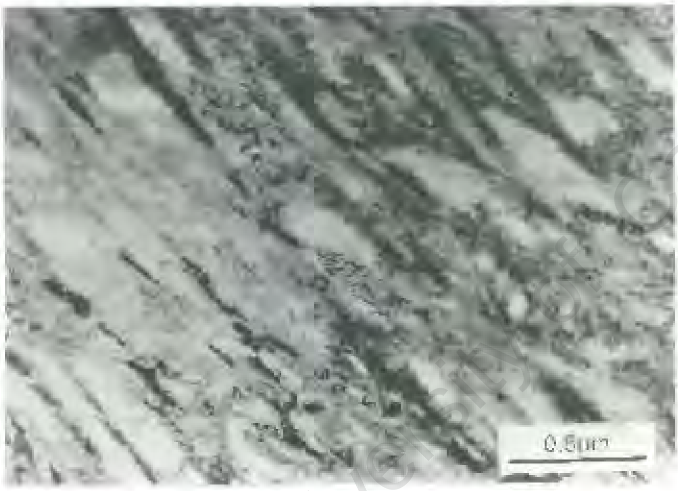

Fig.4.35. *TEM of dislocation structure observed in the drawn AISI 304 steel wire. Drawing strain $\varepsilon=0.585$.*
The width of a dislocation *wall is 166 nm.*

Produced in the laboratory

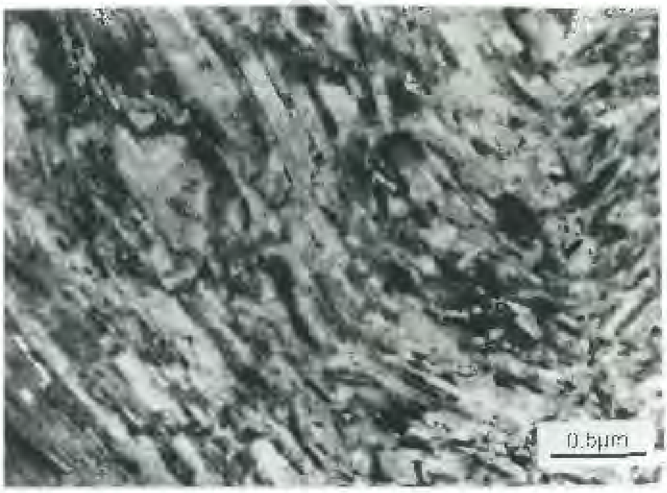

Fig.4.36. *TEM micrograph of microstructure observed in commercially supplied wire (AISI 304 steel, 2.5 mm) Width of the walls are much smaller compared to those in wire produced in the laboratory.*

Commercially supplied (estimated strain - 0.6)

Deformation twins are generally lenticular (lenses shaped). In fcc and bcc metals twins are very narrow and in fact usually look like parallel lines. Twinning may feature a multiple character analogous to planar glide.

Additionally, second order twinning occurs at the most heavy deformations, i.e. structures having already been twinned undergo another, second twinning shear. These twinned structures are generally of a very fine character. The micrographs in Figs.4.37.-4.38. show the microstructure of supplied wire, showing lens-shaped deformation twins and blocky type of twins.

This investigation of dislocation structures showed a significantly lower frequency of deformation twining in the laboratory produced wires, even in highly drawn wires.

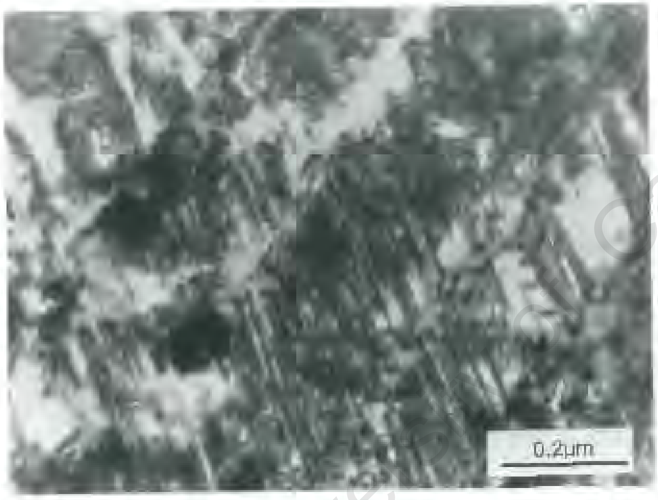

Fig.4.37. *TEM micrograph of AISI 304 commercial wire, showing the high frequency of needle shaped deformation twins.*

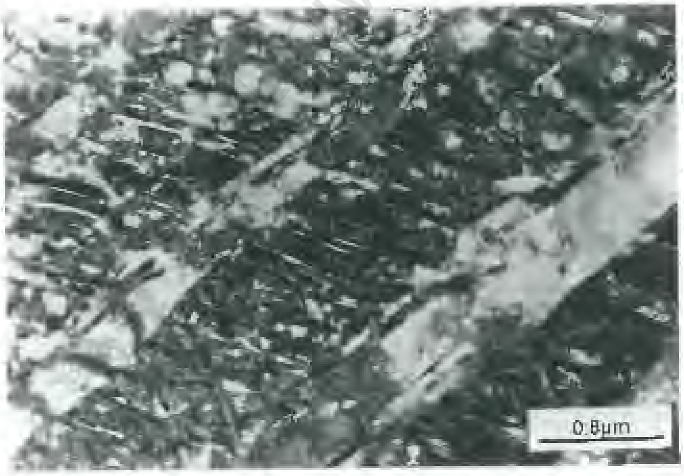

Fig.4.38. *TEM micrograph of microstructure observed in commercial AISI 304 steel wire, drawn to unknown strain (estimated strain 0.6)*
<u>Note:</u> blocky twins

The twins are extremely fine, with thicknesses in the range of 0.5-3 nm. The high frequency of deformation twins and the appearance of blocky twins indicate that high strain was applied during the drawing process of commercially supplied wire. It is deduced from the results of mechanical testing, microstructure and dislocation structure, that the commercial wires have been drawn to a strain in excess of 0.6 to 0.65.

An investigation of wire samples produced in the laboratory showed that deformation twins (needle type) started to appear at a drawing strain of 0.37. The blocky type of deformation twins was only observed in laboratory produced wire drawn to strain higher than 0.37. They were also much larger compare to those found in commercial wire.

4.2.3. Fatigue Behaviour of AISI 304 Stainless Steel Wire

The characterisation of the fatigue behaviour of AISI 304 stainless steels involved a study of the fatigue limit and the fatigue-crack propagation properties. These results have been related to the changes in mechanical properties and microstructural evolution caused by the fatigue process.

4.2.3.1. Fatigue Limit of Notched Wire Samples

The fatigue limit is usually understood as the stress limit, at which the material can be cycled either for an infinite or sufficiently high number of cycles without fracture. The fatigue strength was measured on pre-notched samples at 10^7 cycles under stress controlled conditions. Pre-notched wire samples were used in this study due to the difficulties with the gripping system in conducting axial tensile fatigue tests. However, it is important to ensure notch consistency. Having a consistent shape and size of notch allows stress concentration factors (SCF) to be calculated and thus the ability to predict the fatigue limit of smooth wire samples.

Figure 4.39. shows the micrographs of wires having a nominal notch depth of 300 μm, which have been sectioned and polished in the longitudinal direction.

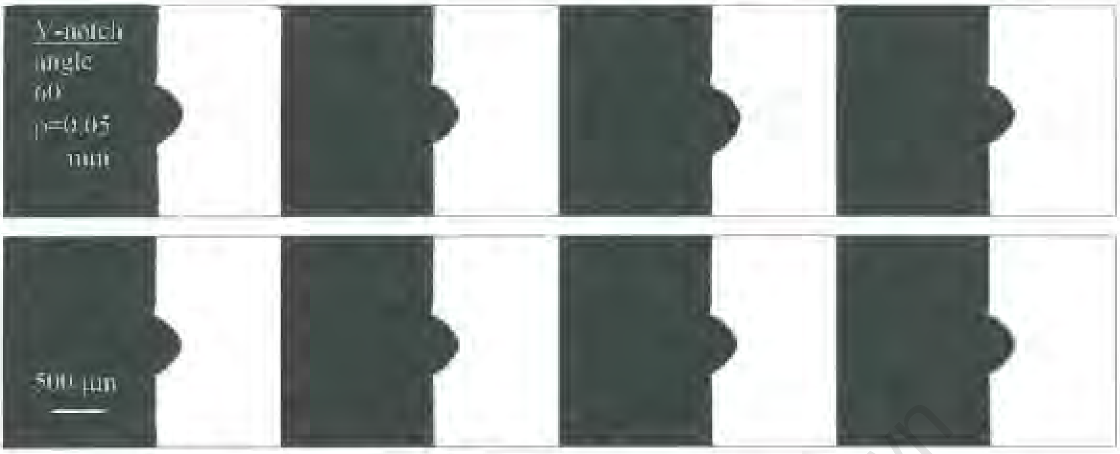

Fig.4.39. Profile of notches measured in the longitudinal wire section

Table 4.5. Notch Depth Measurements

Notch 300 μm	1	2	3	4	5	6	7	8	9	10
Measured Depth μm	288.5	293.3	301	292	311.3	302	307	290.5	305	315.6

The measured depths of the notches obtained from micrographs shown in Fig.4.39. are listed in Table 4.5. The results show an error of 4% in depth which gives sufficient confidence for the use of this method. Accordingly, a prediction of the fatigue limit of smooth samples can be based on the stress concentration factor calculation using Peterson's curves [113].

Notched fatigue limit data, Fig.4.40., indicate that drawing strain improves the fatigue limit over the entire life range examined. Tests performed on annealed wires show fatigue limit of 215 MPa; the fatigue limit of wire drawn to a low strain of 0.09 is improved almost 50% and approximately 95% after 0.238 strain. These results indicate the beneficial influence of the deformation-induced transformation of austenite to martensite on the fatigue strength in low strength austenites. The fatigue limit of wires drawn to higher strains, between 0.238 and 0.585, increased from 420 MPa to 630 MPa respectively.

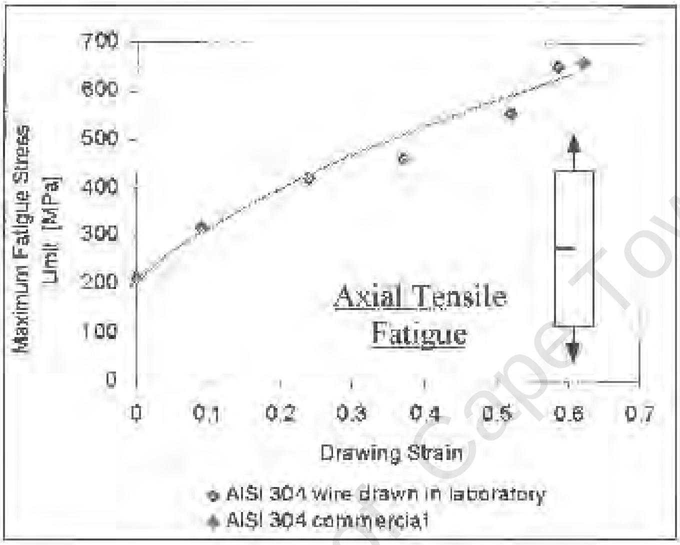

Fig.4.40. Influence of drawing strain on fatigue limit of pre-notched AISI 304 stainless steel wires, tested in axial tensile fatigue conditions

Commercially supplied wire showed a better performance, having a fatigue limit of 650 MPa. A higher fatigue limit is thought to be associated with the influence of the higher yield strength due to its' different chemical composition (higher nickel content) and probably due to a higher drawing strain employed during its' manufacture.

4.2.3.2. Prediction of Smooth Fatigue Limit

The fatigue limit of un-notched wires has been calculated on the basis of the notched fatigue limit obtained experimentally (axial tensile fatigue tests) and also on calculations using values of stress concentration factors. There are however, two problems to be solved in connection with stress concentrations. The first is the ability to determine the theoretical stress concentration factor, K_t and the second is to determine the strength reduction factor, K_f. Factors K_t are often presented in graphical form for a wide range of notches. From these curves it is possible to estimate the factor K_t for most grooves and notches with sufficient accuracy for most practical purposes.

The investigation performed in this study involved a V-shape notch with an angle of 60^0 and $\rho=0.05$ mm radius at the root of the notch and notch depth $t=0.3$ mm. The K_t factor was determined using Peterson's curve for this particular case as shown in Fig.4.41.

As shown in the graphical presentation, the values of the theoretical stress concentration factor, K_t are highly dependent on the notch geometry such as depth, angle at the root and the specimen size.

The fatigue strength of smooth and pre-notched AISI 304 stainless steel wires were compared by means of the strength reduction factor (s.r.f.) which was calculated according to the equation given in Table 4.6. This factor is also influenced by the angle at the root of the notch and by the strength parameter of the material (A). The assumed values of A as a material constant are $A=0.25$ mm for annealed steel and $A=0.025$ mm for high strength steels.

The values of both the theoretical stress concentration factor and the strength reduction factor for AISI 304 stainless steel wire used in this study are presented in Table 4.6.

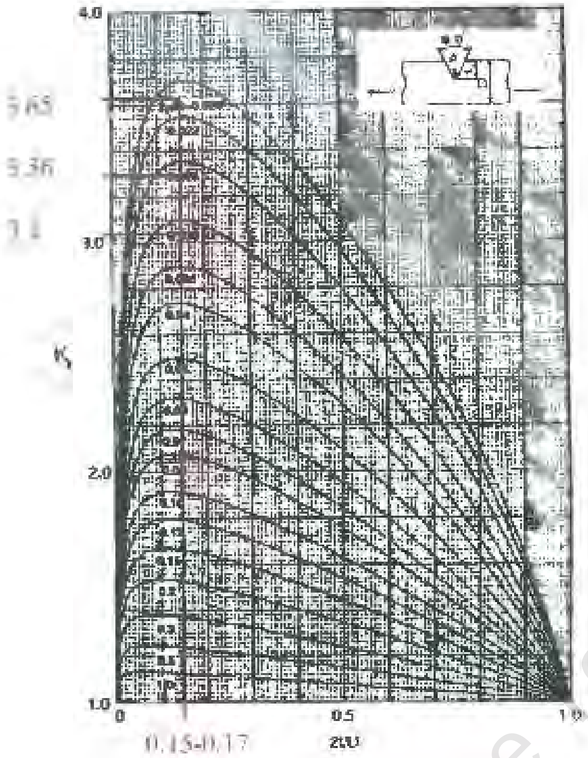

Fig.4.41. *K_t theoretical factor of V-shaped notched bar under pure tension [113]*

Table 4.6. Stress Concentration Factors (SCF) for AISI 304 Stainless Steel Wire

AISI 304 Wire	**Peterson's equation** $K_f \approx 1 + \frac{(K_t - 1)}{\{1 + (\frac{A_n}{\rho})\}}$ **Method A**	**Peterson's Curves** **K_t**	**Neuber's Values** 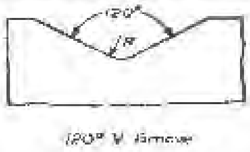 **Method B**
Annealed	1.39	3.36	1.71
0.09	1.44	3.65	1.71
0.238	1.36	3.2	1.71
0.37	<u>1.36</u> / 2.46	3.2	1.71
0.52	<u>1.36</u> / 2.46	3.2	1.71
0.58	<u>1.36</u> / 2.46	3.2	1.71

<u>Method A</u>: V-shaped notch, angle of notch 60^0, based on theoretical stress concentration factor (Peterson curve for the single notched bar under pure tension and Eqn.3.8.)

<u>Method B:</u> accepted $K_f = 1.71$, for V-shaped notch, angle 120^0, based on Neuber's findings. In both methods - notch depth 0.3 mm, root diameter of notch 0.05 mm and 10^6 number of cycles.

<u>Note:</u> Underlined values shown in Table 4.6. are obtained using a material constant $A = 0.25$mm (for annealed steel) for all wires, having a different strength, while the higher values are obtained using an adequate value for A, since the wires drawn to strain higher than 0.37 can be classified as high strength wires.

With reference to the graphical determination of the K_t factor, it should be mentioned that the shape of a notch made manually by a 60^0 V-shape file does not correspond completely to conditions given by the Peterson graph (60^0 V-shape notch). The polished longitudinal sections of the notched wire samples, Fig.4.39. show that the angle at the notch was approximately 112^0.

In order to be able to predict the smooth fatigue limit as closely as possible to the real fatigue limit, the stress concentration factor K_t should be determined accurately. Therefore, another method based on Neuber's calculation for a 120^0 V-shape notch was used for comparative purposes [114].

Neuber postulated the relationship given by Eqn.3.9. (Experimental Procedure, p.76) which takes into account the size effect by incorporating a critical dimension of the notch and the root radius. In Neuber's formula the effect of flank angle is assessed twice, first by a dependency of the value of the theoretical factor on the flank angle, and secondly by the term $\pi/\pi\text{-}\omega$. The values of $K_t = 3$ and $K_f = 1.71$ and a typical value of Neuber's material constant of $A = 0.09$ mm for a steel having the strength of approximately 690 MPa, were adopted in method B.

The smooth fatigue limit predicted by the two methods are given in Table 4.7.

Table 4.7. Fatigue Limit of Predicted Smooth AISI 304 Wire

Drawing	**Predicted-Smooth Fatigue Limit [MPa]**	
Strain	**Method A**	**Method B**
Annealed	299	367.65
0.09	461	547.2
0.238	571/1033.2	718.2
0.37	626/1131.6	860.13
0.52	684/1360.4	860.13
0.58	857/1599	1077.3

Note: Underlined values are obtained using a material constant A=0.25mm (for annealed steel) for all wires, having a different strength, while the higher values are obtained using an adequate value for A, since the wires drawn to strain higher than 0.37 can be classified as high strength wires.

In order to summarise the work performed on the fatigue limits obtained using different methods to predict these values, the following points need to be understood. It is important therefore to consider the possible sources of errors arising from errors in angle (ω) and notch root (R) measurements determined from enlarged micrograph. Simple mathematical calculations show that an angular deviation of 2 deg leads to an error in the K_t value of approximately 3%, whilst a similar error in the R measurement leads to an error in the K_t value which is more significant, approximately 10%.

Since the K_t value directly influences the fatigue notch factor K_f, the predicted fatigue limit values are also affected. In the worse case scenario, an approximate 10% error in the fatigue notch factor effectively influences the fatigue limit by approximately 5% which is considered to be within an acceptable experimental error. Further, these calculations show that the general trend mentioned previously is not significantly changed due to any small errors made in notch geometry measurement.

Secondly, the materials constants "A" values are not strictly correct from the strengths of drawn wires used in this work. However, these values were used due to lack of information presented in the literature and are not considered to have an influence on the trends in behaviour recorded.

In order to estimate the elastic-plastic notch tip stress, the finite element analysis can be used as accurate and sophisticated tool rather than empirical formulas. However, the effect of a notch on the fatigue response of three different alloys was one of objectives of this study and the main attention was to show how notch sensitivities vary from steel to steel and with strength level. Thus, the empirical formula (Eqn.3.9.) was used in a general predictive sense instead of the finite element analysis. It's use would not have changed the trends in behaviour being examined and further requires a degree of sophistication not required in this work.

In order to emphasize the limitation of models predicting behaviour, the notch sensitivity indexes for AISI 304 stainless steel wires are presented in the following table (Table 4.8.).

According to the values of the notch sensitivity index, (q) it appears that both annealed, and wires drawn to different strains, are similarly sensitive to a notch and the material would therefore be expected to be relatively insensitive to notches of large sizes. Experimental results show that the notch sensitivity index does not increase with increase in tensile strength, and thus wire drawn to different strains, despite having significantly different tensile strength properties, have an approximately equal sensitivity index.

This conclusion and the influence of size, shape and roughness of notches are shown, examined and discussed in a later section (Section 4.2.3.3.,p.141).

Table 4.8. Notch Sensitivity Index for AISI 304 Stainless Steel Wire

Drawing Strain ε	Stress Concentrat. Factor K_t Method A	Strength Reduction Factor K_f Method A	Notch Sensitivity Index $q = \frac{K_f - 1}{K_t - 1}$
Ann.	3.6	1.39	0.15
0.09	3.65	1,44	0.166
0.238	3.2	1.36	0.163
0.37	3.2	1.36	0.163
0.52	3.2	1.36	0.163
0.58	3.2	1.36	0.163

Three-Point Bending Fatigue – Smooth Wire Specimens

The experimentally obtained data for the smooth fatigue limit of annealed and drawn AISI 304 stainless steel wires are presented in Fig.4.42 and Table 4.9.

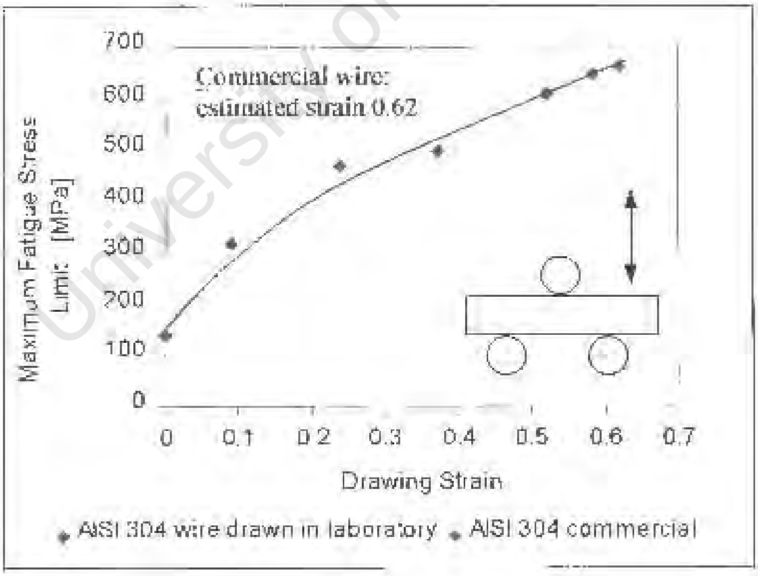

Fig.4.42. Fatigue limit data of smooth AISI 304 stainless steel wires as a function of drawing strain, tested in three-point bending fatigue

The experimental results show that as in the case of the notched fatigue limit, the smooth fatigue limit also increases with the drawing strain. More important observations reveal that the fatigue limit of smooth and annealed wires is lower than that of notched samples. The fatigue limit for smooth specimens was 140 MPa while for the notched samples the fatigue limit was found to be 215 MPa. Conversely, the notched fatigue limit was always lower for drawn stainless steel wires compared to the un-notched specimens. It was also observed that the fatigue limits are almost equal for smooth and notched wire drawn to a low strain of 0.09.

Table 4.9. Summary of the Fatigue Limit of AISI 304 Stainless Steel Wires

Drawing Strain	**Notched Fatigue Limit-MPa** -Experimental Data-	**Smooth Fatigue Limit-MPa** -Experimental Data-
Annealed	215	140
0.09	320	320
0.238	420	471
0.37	460	498
0.52	503	610
0.58	630	650

The higher notched fatigue limit phenomenon can be explained by two competing factors, such as the stress concentration factor and the austenite to martensite transformation. The stress concentration factor (SCF) of the notch leads to a lower fatigue limit and at the same time the notches induce martensite transformation, which raises the fatigue limit. The relevant fatigue limit depends on relative influence of these two competitors. The effect of different factors that influence the austenite to martensite transformation at a notch tip are shown in following section which concerns the notch and phase transformation interactions. Typical S-N curves for annealed and wire specimens drawn to 0.37 and 0.585 strain are shown in Figs.4.43-4.44.

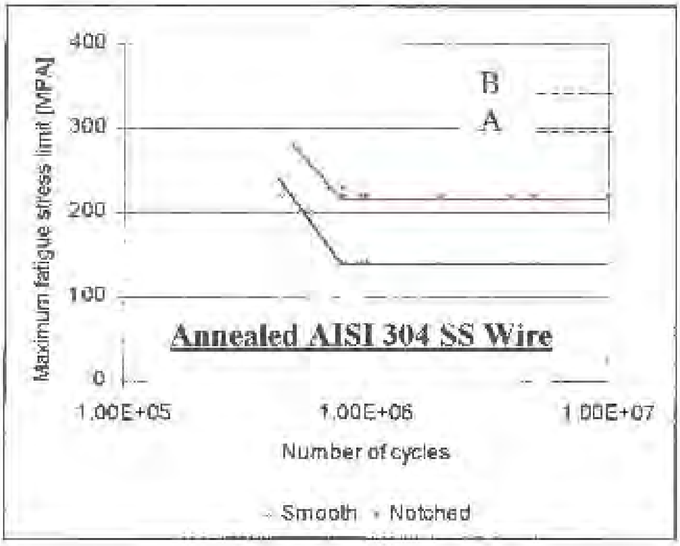

Predicted Smooth Data
Method B:368 MPa
Method A: 299 MPa

Experimental Data
Notched: 215 MPa
Smooth: 140 MPa

Fig.4.43. *Comparative presentation of smooth, and notched fatigue limit for annealed AISI 304 stainless steel wire* *(experimental data)* *and* *predicted-smooth by method A and method B*

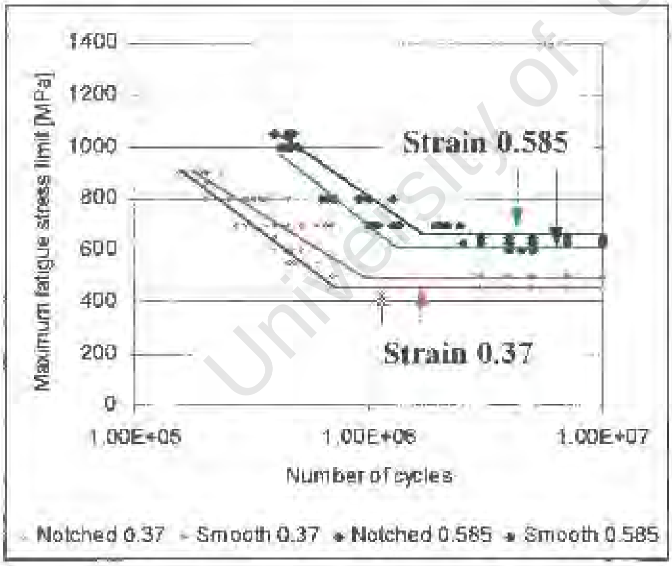

Strain: 0.37

Predicted Smooth Data
Method A: 626 MPa
Method B: 860 MPa
Experimental Data
Smooth: 498 MPa
Notched: 460 MPa

Strain 0.585

Predicted Smooth Data
Method A: 857 MPa
Method B: 1077 MPa
Experimental Data
Smooth: 650 MPa

Fig.4.44. *S-N curves for AISI 304 stainless steel wire drawn to 0.37 and 0.585 strain, obtained experimentally in bending fatigue conditions*
Note: the predicted fatigue limit values (method A and B) are given separately

4.2.3.3. Notch Effect on Martensite Transformation

4.2.3.3.1. Notch - Shape, Size, and Production Method

In order to understand the influence of notches on the fatigue behaviour of AISI 304 stainless steel, a series of experiments were conducted on samples in which contrasting notches of different size, shape and forming methods were introduced. Both V and U shaped notches were introduced by using a file and a cutting wheel to depths of 300 and 800 μm. It was estimated from X-ray measurements that approximately 3% of martensite was introduced into the surface of the specimen through these different processes. Following notching, each specimen was subjected to fatigue at a mean stress of 120 MPa and 120,000 fatigue cycles before being broken and the amount of strain induced martensite measured using X-ray diffraction. This technique allowed an estimate of the flaw severity on subsequent strain induced martensite formation.

It was found that the shape of the notch has a significant influence on the amount of deformation-induced martensite following partial fatigue. A V-shape notch induced a larger amount of deformation-induced martensite of approximately 36% while approximately 28% of the α′-martensite phase was found in samples having a U-shape notch, Figs.4.45-4.46. Furthermore, the size of the induced notch also affects martensite formation significantly. A higher amount of the martensite phase was found in the partially fatigued samples having a bigger notch, as shown in Figs.4.47 and 4.48. Surprisingly, approximately 28% of the martensite phase formed during the fatigue of wire having a small U-notch (300 μm) made a by file, Fig.4.46., whilst only 15% of martensite formed in the sample having the same shape and size with a similar notch induced by a cutting wheel, Fig.4.47.

Such an analysis shows that the presence of a notch in metastable AISI 304 stainless steel wire has a critical role in determining the rate of martensite formation during fatigue. Furthermore, it was found that the phase transformation was highly localised in the notch volume regardless of shape and notch size.

Consequently, the rest of the material contained lower amounts of the martensite phase compared to similar unnotched samples which had been fatigued. Figure 4.49. shows that approximately 11% of deformation-induced martensite was formed in the smooth wire samples fatigued under the same conditions as the notched samples. However, the X-ray diffraction technique was not sensitive enough to determine the precise amount of martensite formed during the fatigue process in the bulk material of prenotched wire samples which was very small and within the error margin of the X-ray diffraction technique which is approximately ± 4%.

It should be mentioned, however, that these results are for partially fatigued samples. In specimens which have been fatigued normally, the amount of martensite found in the vicinity of the fractured surface was found in all cases to be in the region of 40%.

In conclusion, it appears that the total amount of deformation-induced martensite that forms during the fatigue process in smooth or pre-notched wire specimens is approximately equivalent, although the dangers of the notch-like surface defect should be recognised, i.e. the pre-notched samples accumulate a greater percentage of martensite at the notch, while having a relatively low percentage martensite in the bulk material.

The average martensite percentage in a notched sample is roughly equivalent to the percentage of martensite phase in an unnotched wire sample.

Notch-Shape Effect

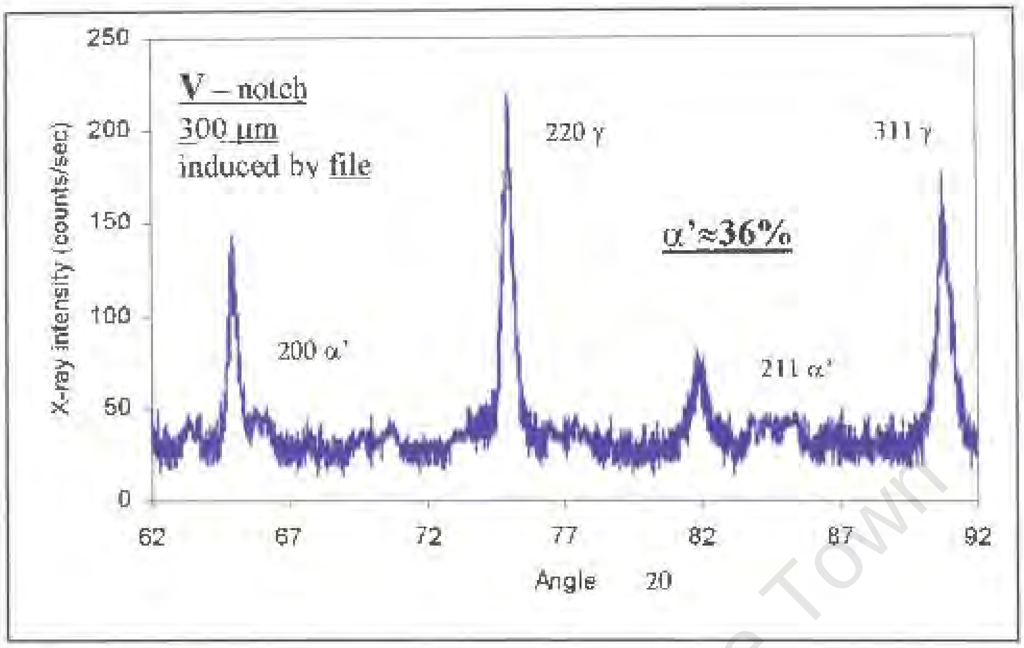

Fig.4.45. XRD traces for **V-notched AISI 304 steel wire** subjected to fatigue

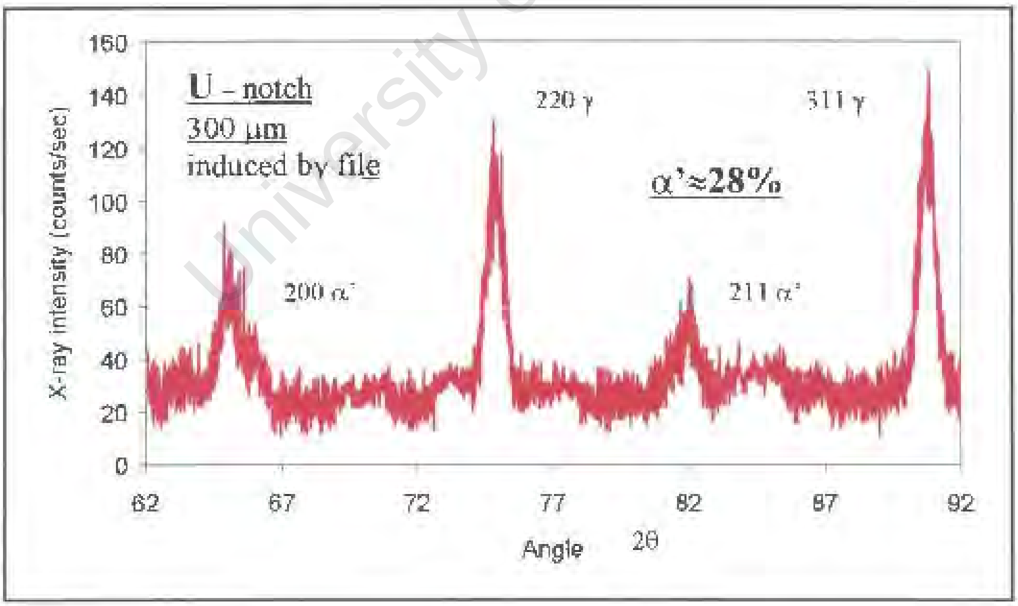

Fig.4.46. XRD traces for **U-notched AISI 304 steel wire** subjected to fatigue

Notch-Production Effect

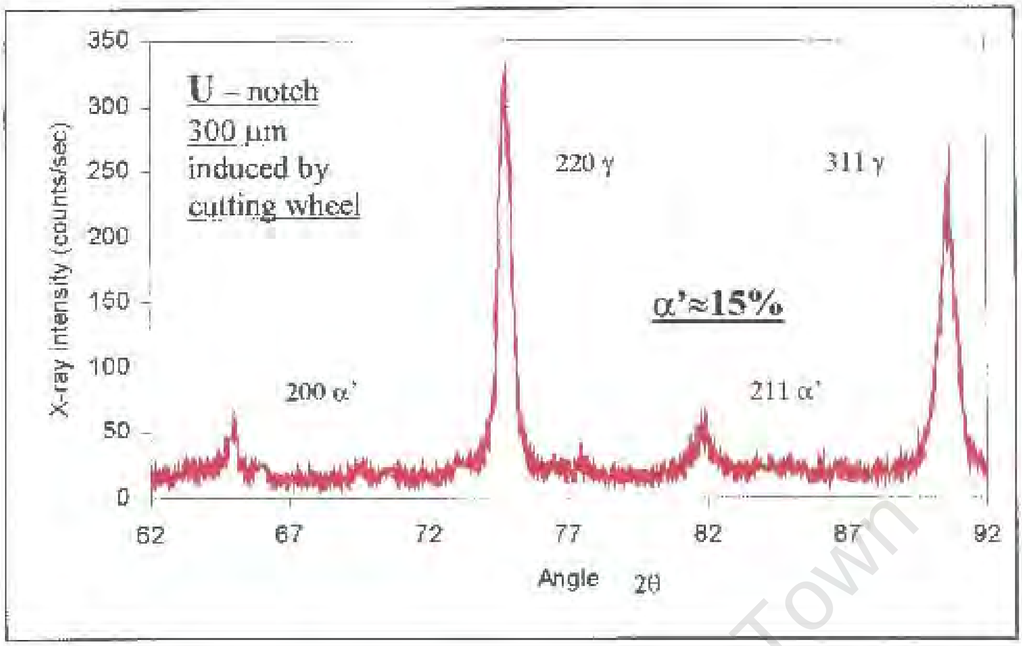

Fig.4.47. XRD traces for ***U-notched AISI 304 steel wire*** subjected to fatigue

Notch-Size Effect

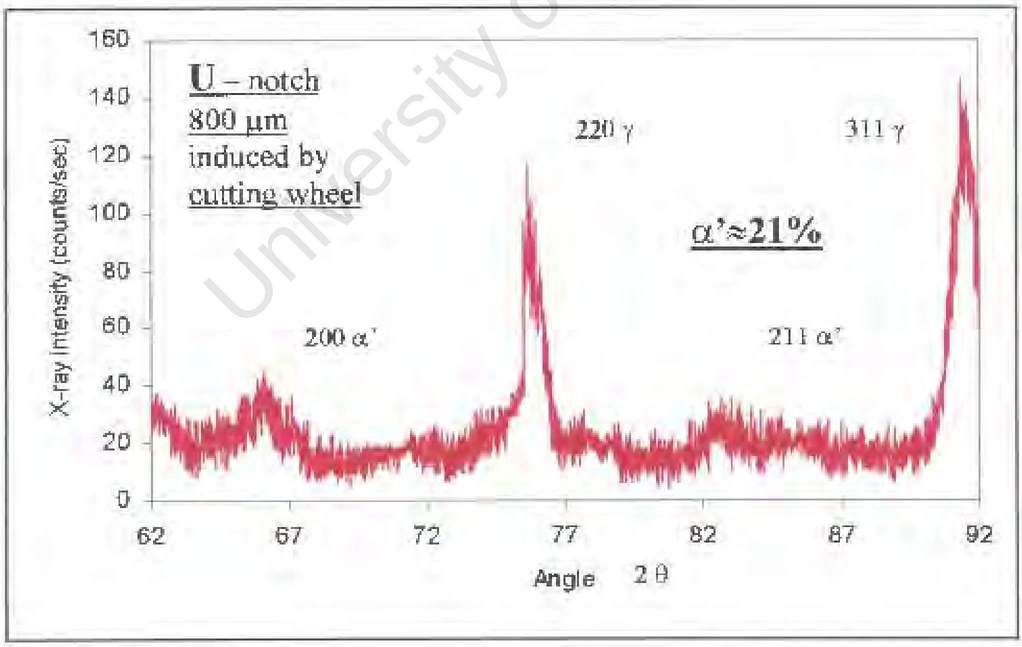

Fig.4.48. XRD traces for ***U-notched AISI 304 steel wire*** subjected to fatigue

Smooth Wire Sample

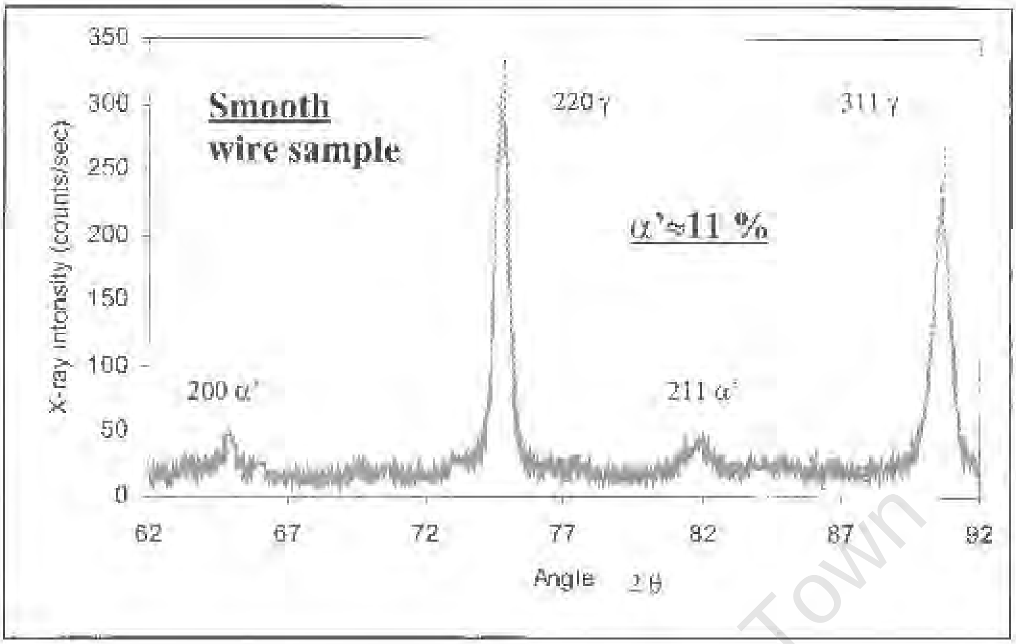

Fig.4.49. *XRD traces for* ***smooth AISI 304 steel wire*** *subjected to fatigue*

4.2.3.3.2. Notch-Roughness and Martensite Transformation

It is well known that the surface roughness influences fatigue crack initiation and the fatigue limit of materials. Consequently, a correlation between the notch roughness and the amount of the phase transformation that occurs at the notch tip and the fatigue limit was explored using annealed and notched steel wire.

The notches were polished using fine silica carbide paper of 1200 grit and by electropolishing. Fatigue testing performed under similar conditions as for the unpolished-notched samples showed, however, no significant influence on the fatigue limit.

Thus, the shape, size and production method influences the fatigue behaviour of AISI 304 stainless steel wire by "localising" the martensite phase at the tip and by enhancing work-hardening of annealed stainless steel.

Generally, the sharper and deeper notches induce larger amount of deformation-induced martensite phase.

4.2.3.3.3. Load Ratio and Martensite Transformation

In order to clarify the influence of the martensite transformation associated with a notch, the influence of the load ratio R was also investigated at different and constant load ratios.

It should be mentioned that these experiments were performed on the annealed material with an initial single-phase microstructure compared to the mixture of austenite and α'-martensite phases, which are present in drawn wires. The results of the austenite to martensite transformation presented in this section were obtained from the vicinity of the notch.

Experimental results showed that the maximum applied cyclic stress has the predominant influence on the phase transformation and that approximately 11% and 4% of α'-martensite phase was induced by peak fatigue stresses of 228 and 200 MPa respectively, both measured at the same number of cycles (N = 120,000), as presented in the following section 4.2.4., p.161 which concern the changes caused by fatigue.

The results show that the higher stress levels σ_{max}, and $\Delta\sigma$ do indeed affect the amount of phase transformation that occurs at the notch, as shown schematically in Fig.4.50.

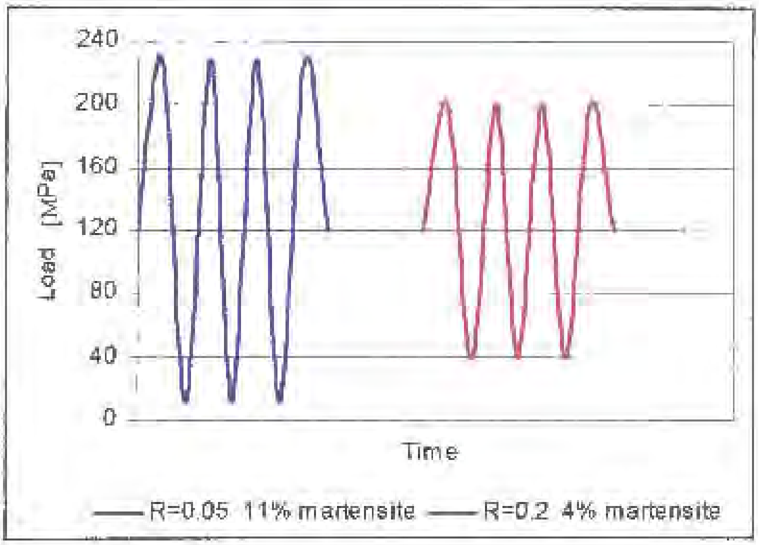

Fig.4.50. *Load ratio R=0.05 vs load ratio R=0.2, schematic presentation*

<u>Case 1. R=0.05</u> σ_a *= 108 MPa,* *<u>Case 2. R=0.2</u>* σ_a *= 80 MPa;*
σ_{mean} *= 120MPa, N = 120,000 cycles for both cases*

The amount of the martensite phase developed at a notch was also determined at a constant load ratio R=0.2, but at different numbers of fatigue cycles, Figs.4.51-4.53. X-ray diffraction analysis (as described in Section 3.3.) revealed that approximately between 4%, to 20% of α'-martensite phase was developed during fatigue cycling at 120,000 and 1.000,000 cycles respectively. The error in reading the amount of martensite was typically ±4%. Therefore, the results indicate that the martensite transformation in the fatigue process is time, or number of cycles, dependent and thus, significantly influences the fatigue behaviour of AISI 304 stainless steel.

Effect of Number of Cycles at Load Ratio R = 0.2

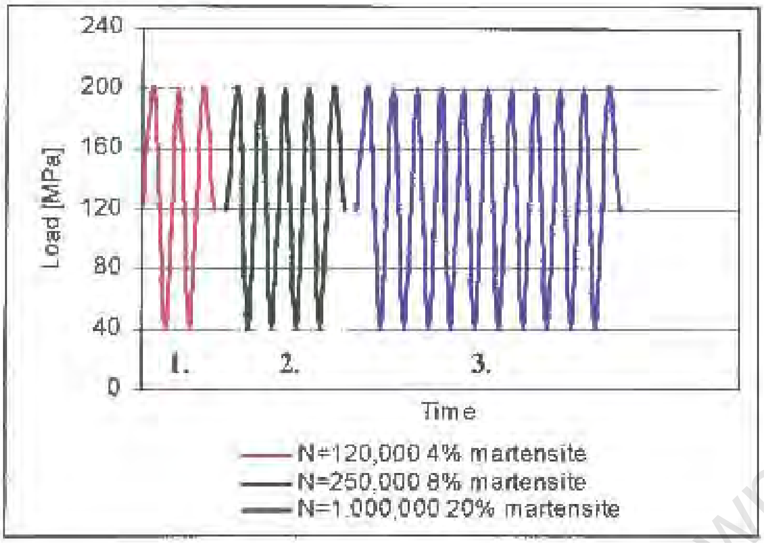

Fig.4.51. *Influence of number of cycles at a load ratio R=0.2, schematic presentation (Note: $\Delta\sigma$, σ_{max}, σ_{min} were all constant in this test. Only the number of cycles were different for cases 1,2,3)*

Fatigue conditions: R=0.2, σ_{mean}=120 MPa, σ_a=80 MPa

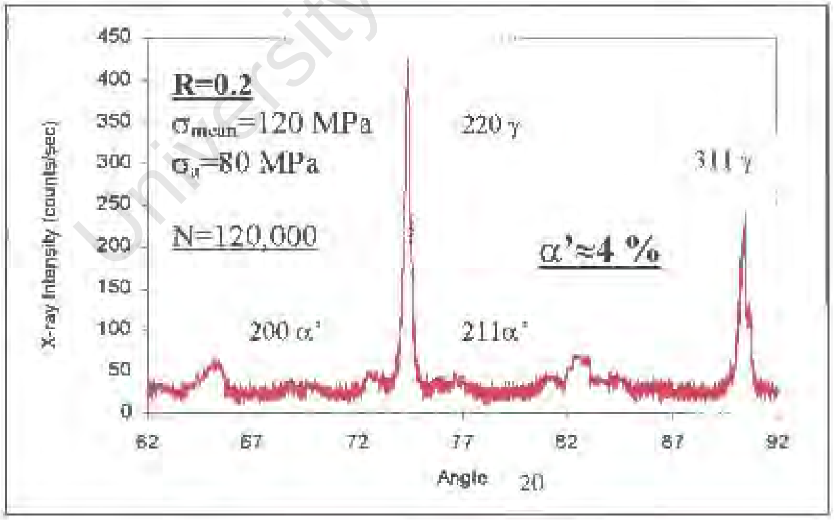

Fig.4.52. *Influence of 120,000 cycles on the amount of the α'-martensite phase*

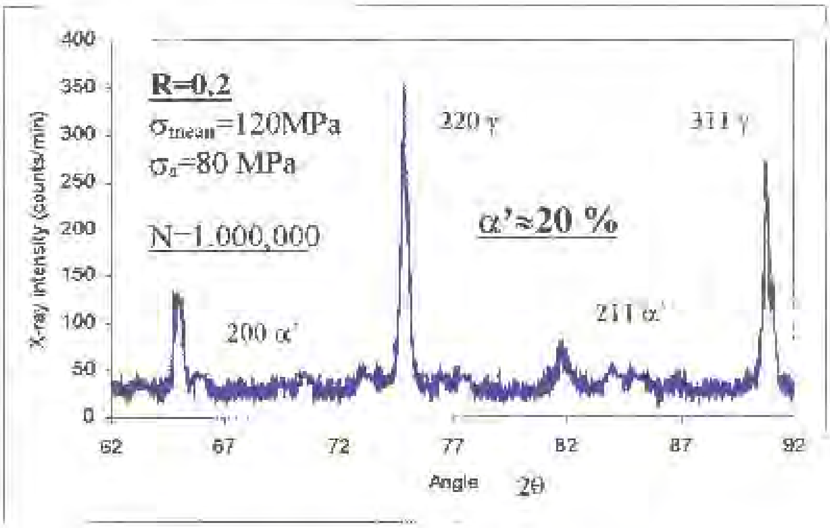

Fig.4.53. *Influence of the number of cycles (N=1,000,000) on the amount of the α′-martensite phase transformed in notched AISI 304 stainless steel wire*

Note that the amount of austenite is indicated by the 220 γ and 311 γ lines, whereas, the amount of martensite is indicated by the 200 α′ and 211 α′ lines. It is clear that the percentage of martensite in Fig.4.53. is greater than in Fig.4.52. if one compares the relevant peaks.

The effect of changing the maximum load, σ_{max}, the minimum load, σ_{min} and the load amplitude, $\Delta\sigma$=const. was also investigated. The following figures, Figs.4.54.-4.56. show the results obtained for annealed AISI 304 stainless steel wire subjected to cyclic strain for the same period of time (1,000,000 cycles).

Effect of Constant Maximum and Minimum Load

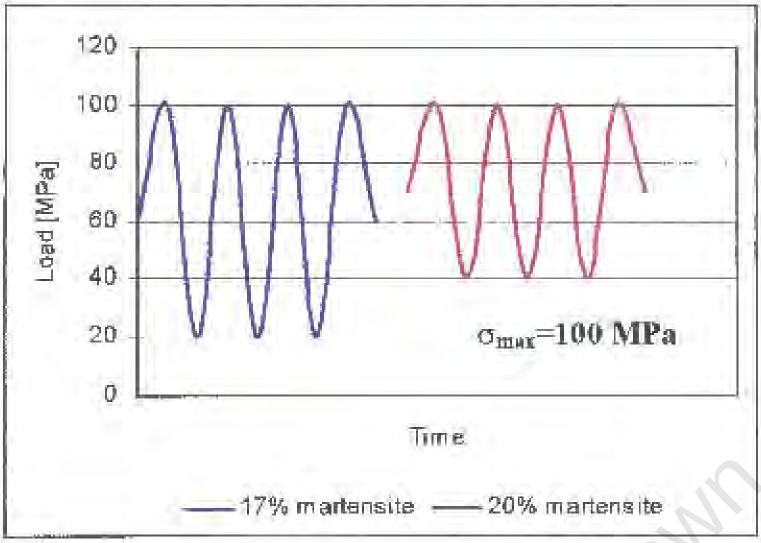

Fig.4.54. *Schematic of influence of the maximum load, σ_{max} = 100 MPa, on martensite formation*

<u>Case 1.</u> σ_{mean} = 70 MPa, σ_a = 30 MPa; <u>Case 2.</u> σ_{mean} = 60 MPa, σ_a = 40 MPa

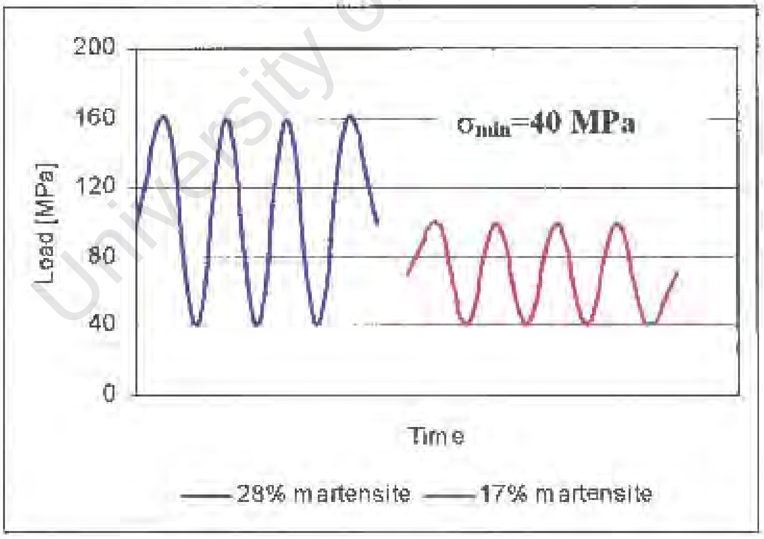

Fig.4.55. *Schematic of influence of minimum load, σ_{min} = 40 MPa*

Case 1. σ_{mean} = 100 MPa, σ_a = 60 MPa; <u>Case 2.</u> σ_{mean} = 70 MPa, σ_a = 30 MPa

Effect of the Constant Alternating Load

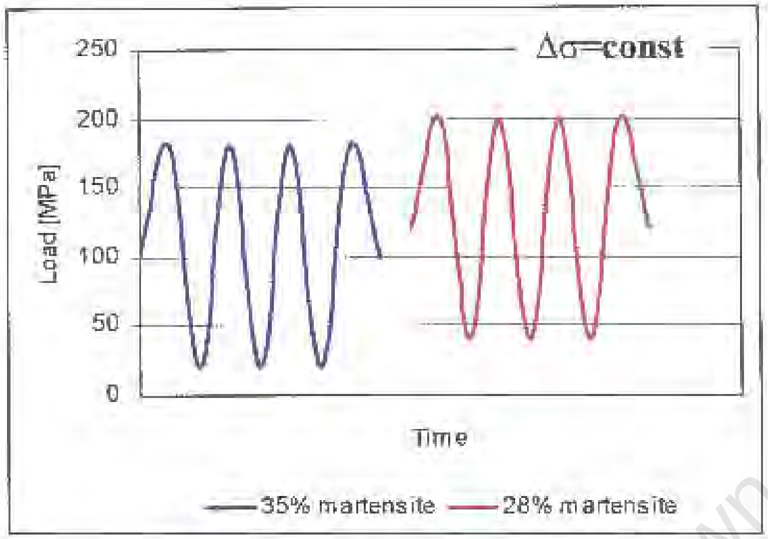

Fig.4.56. *Influence of the constant load, $\Delta\sigma$ on the amount of α'-martensite phase formed, (schematically presented)*

Case 1. $\sigma_{mean} = 100$ *MPa,* $\sigma_a = 80$ *MPa; Case 2.* $\sigma_{mean} = 120$ *MPa,* $\sigma_a = 80$ *MPa*

According to the experimental data presented in Figs.4.50-4.56., the following conclusions can be drawn. Firstly, it is apparent that a higher amount of the α'-martensite phase was dependent principally on the maximum stress level, σ_{max}; secondly on the cyclic amplitude, $\Delta\sigma$, and thirdly on number of cycles. These results suggested that crack initiation from a notch is strongly dependent on the microstructure present at the notch tip which is itself dependent on the amount of martensite. Higher amounts of martensite delay crack initiation and thus the austenite to martensite transformation which occurs at the notch acts beneficially in extending fatigue lives.

This is borne out in Fig.4.50. where it appears that at the same mean stress, the higher peak stress or higher amplitude induces more martensite phase. Fatigue tests results showed that the amplitude of $\sigma_a = 108$ MPa induces approximately 11% of martensite phase while the smaller amplitude of 80 MPa induces only 4% of α'-martensite phase, Fig.4.50.

From Fig.4.51. it is clear that an increased number of cycles under constant cyclic fatigue load conditions leads to more martensite transformation.

For constant cyclic peak stress but variable amplitude, Fig.4.54., the amount of martensite is effectively the same (17% and 20%).
Fig.4.55. concerning fatigue tests at the same minimum stress also indicate that the higher the maximum stress (160 MPa) the greater the martensite transformation (28% vs 17%) compared to maximum stress of 100 MPa.

This high stress increase in martensite transformation trend is further borne out in Fig.4.56. However, also appears to be a positive additional effect due to minimal stress level. This should be the basis for further study (see Chapter 6, p.260).

4.2.3.4. Fatigue Crack Growth Rate

An important parameter, the crack growth rate, has been determined using the experimental procedure outlined earlier. The experiments were performed at two values of load ratio, R=0.048 and R=0.2, i.e. at mean stress of 550 MPa, maximum stress of 1050 and 900 MPa and minimum stress of 50 and 200 MPa.

Figures 4.57.-4.58. show the influence of two load ratios on the crack growth rate in terms of drawing strain.

The experimental results show that the cyclic stress levels have a significant influence on both crack initiation and crack growth rates, Figs.4.57.-4.58. The influence of the load levels on the fatigue crack growth rate show that as the load ratio, R, increases from 0.048 to 0.22 the fatigue crack growth rate curve shifts to the left, i.e. to a lower level of stress intensity factor. This increase in the fatigue crack growth rate with the load ratio is a common phenomenon. Although these curves should not be regarded as rigorously derived Paris equation data, since the specimens are so small, they are nevertheless consistent with accepted Paris behaviour. For example, the Paris equation for the blue line (0.238 strain) in Fig.4.57. is approximately

$$\frac{da}{dN} = 1.83 \cdot 10^{-11} \cdot \Delta K^{2.62}$$

where da/dN is in m/cycle and ΔK in MPa $m^{1/2}$, which is of the right order for such steel.

The fatigue crack growth rate is presented as a function of drawing strain at the particular value of cyclic stress intensity factor, $\Delta K = 30$ MPa $m^{1/2}$, Fig.4.59. An increase of the fatigue crack growth rate with increasing drawing strain was observed for the wire samples drawn to different strains. The highest crack growth rate of $6.47\ 10^{-4}$ mm/cycle was observed for wires drawn to 0.585 strain measured at a load ratio of $R = 0.22$. The highest crack growth rate in wires drawn to 0.585 strain is a consequence of the large amount of α'-martensite phase transformed during drawing. The austenite to martensite transformation induced by cyclic strain promoted a rapid crack growth.

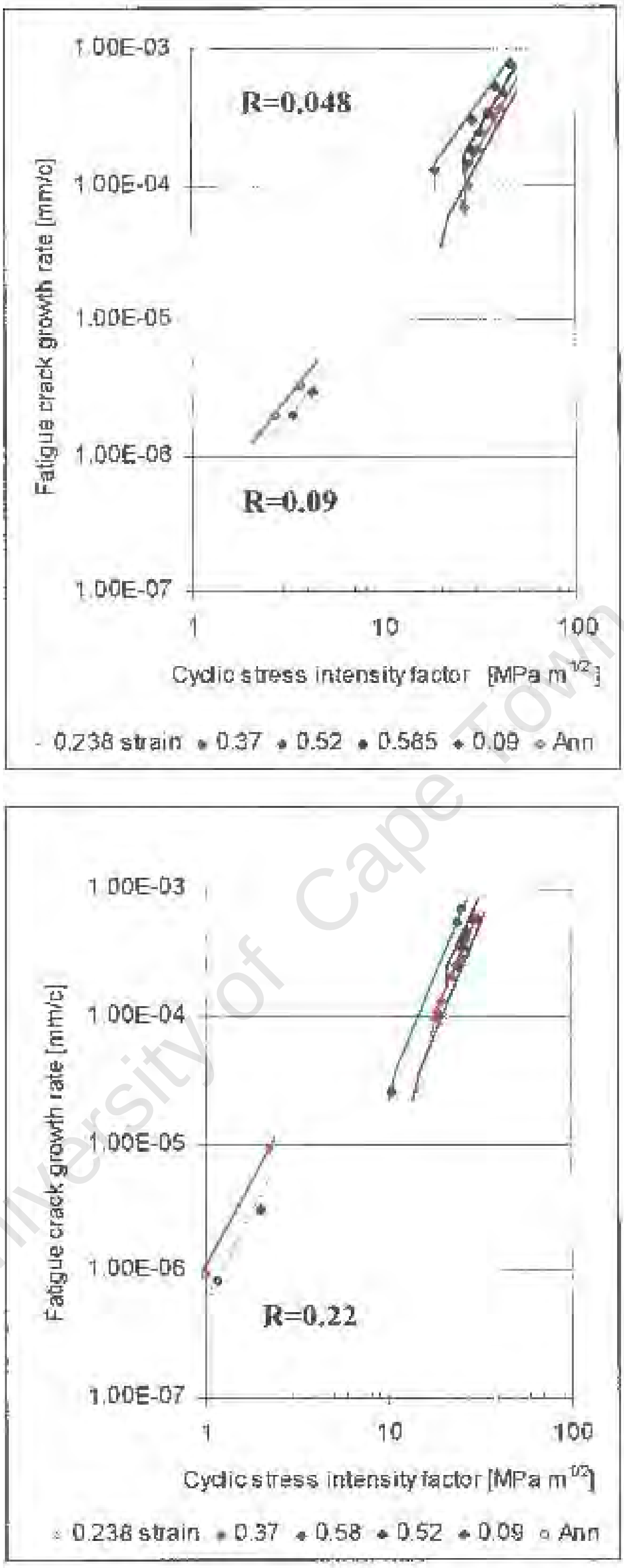

Figs.4.57-4.58. *Influence of drawing strain on fatigue crack growth rate of AISI 304 stainless steel wire, at load ratios of R=0.048 and R=0.22*

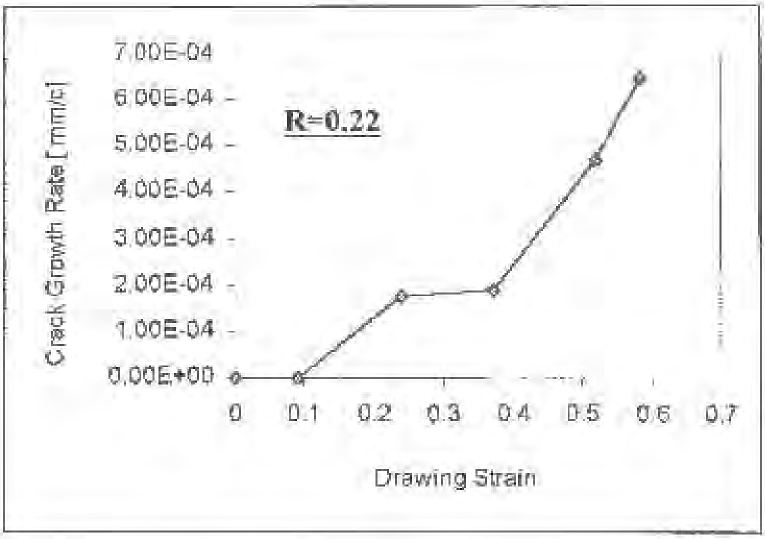

Fig.4.59. *Influence of drawing strain on the crack growth rate in drawn AISI 304 stainless steel wires, at* $\Delta K = 30$ *MPa* $m^{1/2}$ *and load ratio* $R = 0.22$

In general, the results suggest that the fatigue crack growth is influenced by the amount of strain-induced martensite and any reduction or increase in the crack growth rate, due to martensite transformation, depends on the load ratio.

The influence of load ratio on the threshold stress intensity factor, ΔK_{th} as a function of yield strength is presented in the following section 4.2.3.5. The fatigue crack growth rate has also been investigated in terms of the fracture mode. Fractured surfaces and the typical fracture modes are presented in section 4.2.5.

4.2.3.5. Influence of Yield Strength on the Threshold Stress Intensity Factor for metastable AISI 304 Stainless Steel Wires

The variation of the threshold stress intensity factor ΔK_{th} (investigated on pre-notched wire samples) with monotonic and cyclic yield strengths, which are plotted on Fig.78, indicate a general trend of the dependence of ΔK_{th} on material strength.

Cyclic hardening is attributed to the transformation-induced hardening of retained austenite to martensite during cyclic strain. As the cyclic strength is increased, either because of the high initial monotonic strength or by cyclic hardening, the threshold for fatigue crack propagation is increased. Experimental results indicate that this trend of increasing threshold stress intensity factor with increasing strength exists for metastable austenitic stainless steels.

The minimum value of threshold stress intensity of 1.1 MPa $m^{1/2}$ has been observed for annealed wire at a load ratio R=0.22, while the maximum value of threshold, $\Delta K_{th}=15$ MPa $m^{1/2}$ is obtained for wires which have been drawn in the laboratory, to a strain of 0.52. There was no measurable fatigue crack growth rate below 15 MP $m^{1/2}$, although this is too high to be regarded as a conventional 'threshold value'.

The wire samples drawn to a strain $\varepsilon=0.585$ (highest achievable strain under the laboratory conditions) and having 36% of strain-induced martensite showed a decrease of threshold stress intensity values to $\Delta K_{th}=9$ MPa $m^{1/2}$, at a load ratio of R=0.22. In spite of a high ultimate tensile strength of 1130 MPa, an amount of 36% of martensite formed during the fatigue process acted deleteriously.

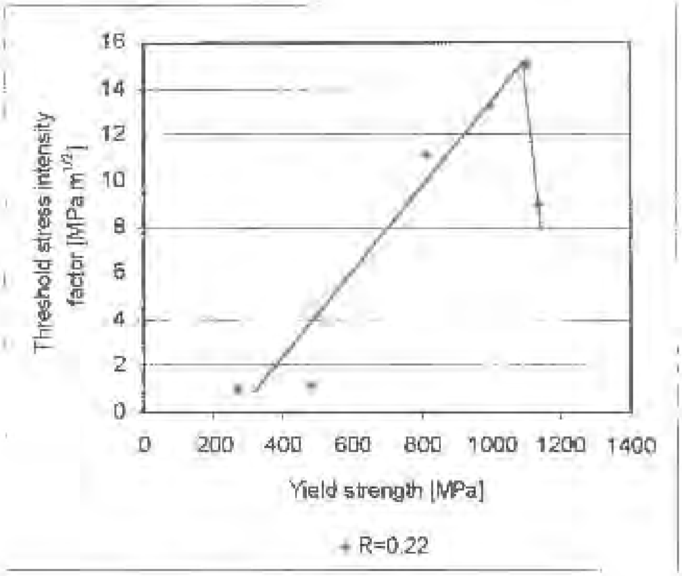

Fig.4.60. *Influence of the yield strength on the threshold stress intensity factor for AISI 304 stainless steel wires*

4.2.3.6. Effect of Martensite Transformation on Low Cycle Fatigue (LCF) of AISI 304 Stainless Steel Wires

It has been shown that the austenite to martensite transformation in metastable AISI 304 stainless steel investigated in this study has been shown to play a beneficial role on the tensile monotonic properties and the high cycle fatigue limit. However, the results of this study also show that the transformation does not always play a beneficial role on the fatigue properties.

In order to illustrate this effect during low cycle fatigue conditions, the crack advance with the number of cycles and also the total number of cycles leading to final failure were investigated on notched wire samples drawn to different strains and in the annealed condition.

Figures 4.60. and 4.61. show the differences in the fatigue crack advance at load ratios of R=0.048 and R=0.22. Higher stresses cause faster crack propagation, although it depends on the static mechanical properties obtained after different drawing strains.

In both cases, the fatigue crack increment is significantly higher in the wire samples having high strength. It was also observed that the highest fatigue crack advance was shown by specimens drawn to the highest strain in the laboratory. Commercially supplied AISI 304 stainless steel wire showed a similar behaviour to the wire sample drawn to 0.52 strain.

Figure 4.62. together with Table 4.10. show the effect of amount of α'-martensite phase on the number of cycles leading to failure for wires drawn to different strains for a load of R=0.22. A similar peak at approximately 20% martensite for load ratios of 0.048 and 0.09, were also indicated.

The numbers of cycles leading to fatigue failure increases with the amount of deformation-induced martensite phase, up to approximately 20%, which indicates the beneficial role of the phase transformation on the lifetime of the low strength austenites.

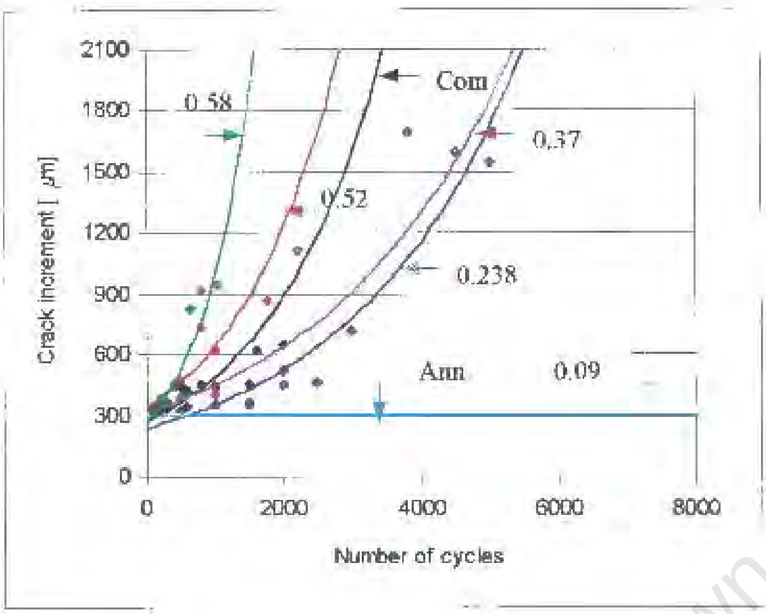

Fig.4.60. *Fatigue crack advance with number of cycles at load ratio R=0.048*

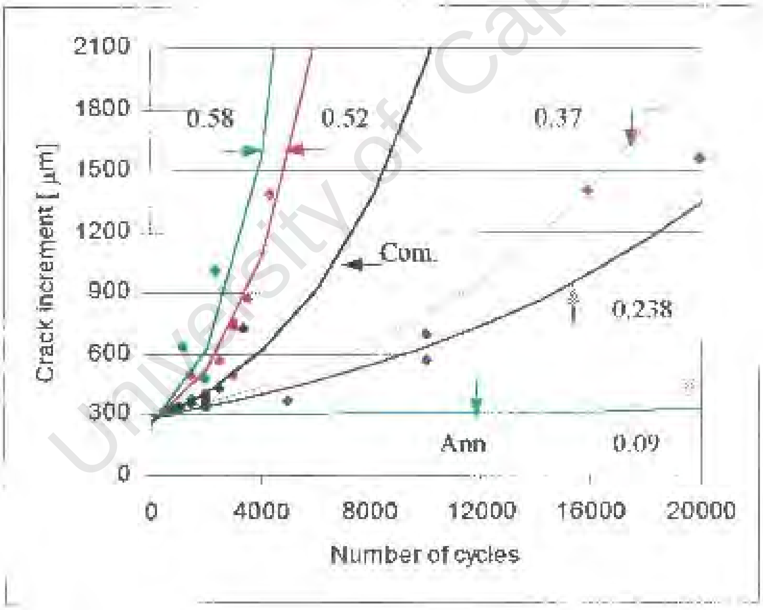

Fig.4.61. *Fatigue crack advance vs number of cycles at load ratio R=0.22*

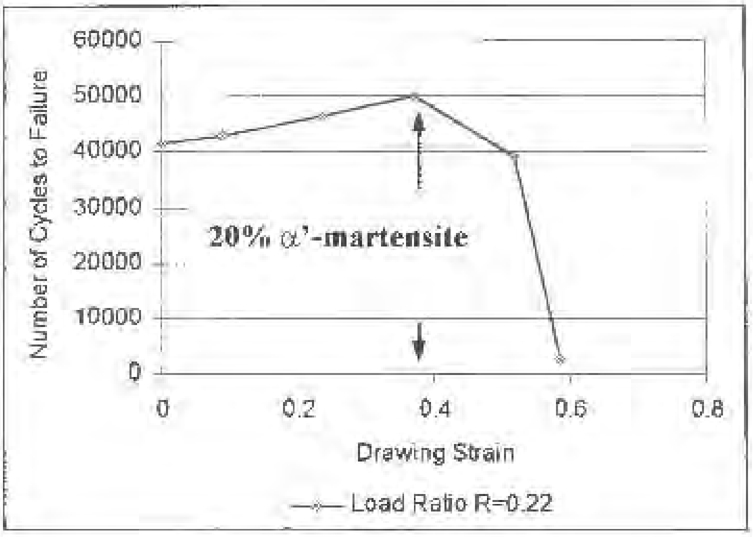

Fig.4.62. *Influence of amount of α'-martensite phase on the number of cycles to failure in drawn AISI 304 stainless steel wires, at load ratio R=0.22*

Table 4.10. Number of Cycles to Failure as a Function of Drawing Strain

Drawing Strain	Yield Strength MPa	Amount of Martensite %	Number of Cycles to Failure R=0.2
0	267	0	41,560
0.09	480	8	43,000
0.238	810	16	46,655
0.37	995	20	50,000
0.52	1100	32	39,150
0.585	1137	36	2,347

However, in the high strength AISI 304 stainless steel wires, having more than 20% of α'-martensite phase, the number of cycles to cause fatigue failure is drastically decreased. A large amount of martensite changes the properties of the steel by promoting brittle behaviour, and it is also possible that the deformation-induced martensite gave rise to more crack initiation sites. Further, as shown previously, a notch strongly influences the phase transformation. This is particularly important with regard to the drawing process itself since a high strain can also create many plastic flaws which act as stress concentrators.

4.2.4. Changes in AISI 304 Stainless Steel Wire

The changes in static tensile properties, hardness and microstructure caused by cyclic strain are presented in this section.

4.2.4.1. Mechanical Properties

To assess the influence of cyclic strain on the changes in mechanical properties, tensile tests were performed on the smooth annealed wires after they were subjected to fatigue, which are shown in Fig.4.64. and Table 4.11.

The results show that the monotonic mechanical properties, such as the ultimate tensile strength and yield strength were increased as a consequence of fatigue, and the improvements depend on the duration of the fatigue process and load ratio, R. The ultimate tensile strength was increased from 668 MPa in the annealed condition to 688 MPa, or approximately 3%, after being subjected to fatigue at a load ratio of R = 0.22 for 120,000 cycles.
The same fatigue conditions increased the yield strength from 278 MPa to 318 MPa, by approximately 14%.
Tensile tests conducted on the wire samples, which were subjected to fatigue under the same load force ratio, R = 0.22, for double the number of cycles (250,000), showed an increase in both the ultimate tensile strength and the yield strength. The ultimate tensile strength was improved by approximately 6%, whilst the yield strength was increased by 26%.
Comparing the results obtained by fatiguing at two different load ratios, R = 0.048 and R = 0.22, and at the same number of cycles N = 120,000, it was noticed that both the ultimate tensile strength and yield strength were increased more significantly at the lower load ratio R = 0.048. The ultimate tensile strength was improved approximately 11%, whilst the yield strength increased approximately 23%.

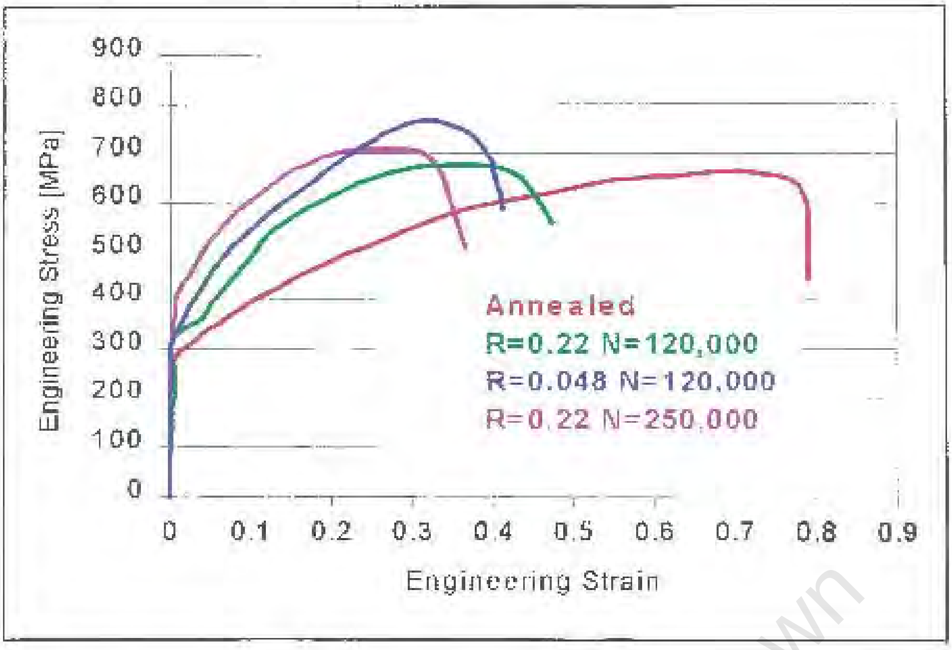

Fig.4.64. *Tensile tests results of annealed AISI 304 stainless steel wire subjected to different fatigue conditions (load ratios and number of cycles)*

Table 4.11. Changes in Mechanical Properties caused by the Fatigue Process

Conditions: AISI 304-Stainless Steel Wire	Yield Strength [MPa]		Ultimate Tensile Strength [MPa]		Total Elongation to Failure [%]	
Annealed	278		668		79	
Annealed + Fatigued R=0.048 N=120,000	342	+23%	740	+11%	42	↓
Annealed + Fatigued R=0.22 N=120,000	318	+14%	688	+2%	47	↓
Annealed + Fatigued R=0.22 N=250,000	350	+26%	708	+6%	36	↓

The total elongation to failure was found to decrease in all cases.

An increase in the yield strength and the ultimate tensile strength was not observed in heavily drawn wires in which the amount of strain-induced martensite already exceeded 20%.

Tensile graphs for annealed specimens as well as those fatigued at different load ratios and number of cycles are presented in Fig.4.65.(a,b,c). In addition, the amounts of α'-martensite phase developed during fatigue at particular load ratios and duration of fatiguing are given for each condition.

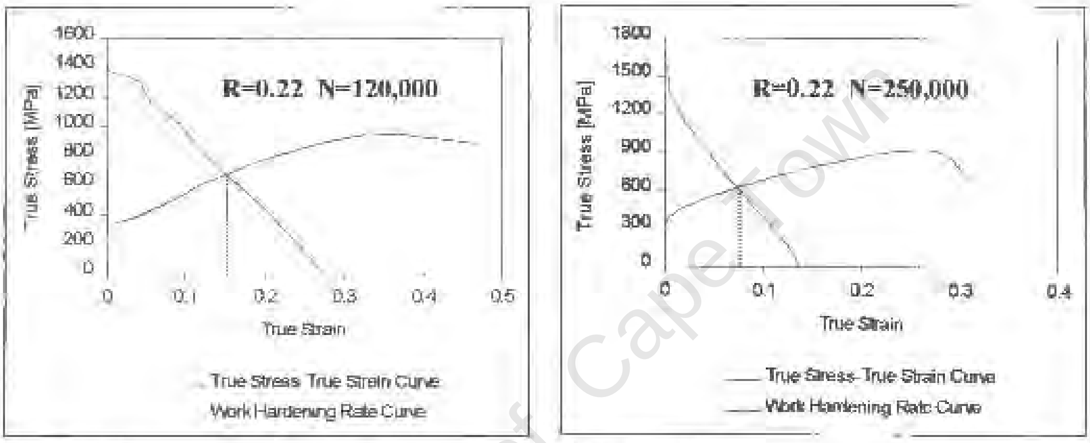

a) *α'=4%* ***b)*** *α'=8%*

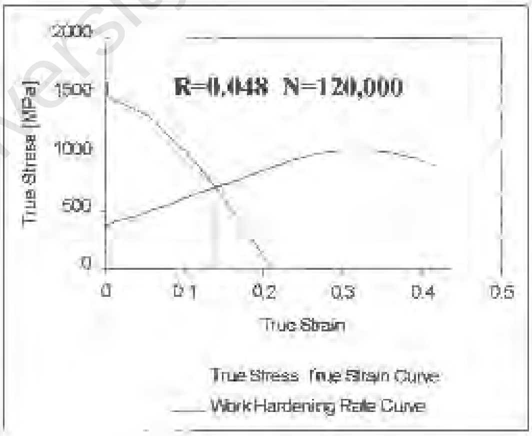

c) *α'=11%*

Fig.4.65.(a,b,c) *True Stress-True Strain and Work Hardening Rate Graphs for annealed and fatigued AISI 304 stainless steel wire, together with α'-martensite phase formed during fatigue*

Necking occurs at 15% strain corresponding to a small amount of strain-induced martensite (4%) in the annealed AISI 304 stainless steel wire subjected to cyclic strain at load ratio of R=0.22 and 120,000 cycles, Fig.4.65.(a). A longer period of fatigue N=250,000, produced a larger amount of martensite (approximately 8%), decreased uniform elongation and necking occurred at approximately 8% strain, Fig.4.65.(b).

The influence of the load ratio on the cyclic tensile properties and the amount of martensite phase can be also seen by comparing the graphs in Figs.4.65.(a,b,c). The load ratio R=0.048 is considered beneficial in terms of improving the tensile properties, compared to those observed at a load ratio R=0.22, for the same number of cycles, Fig.4.65.(a,c). An improvement of the yield strength is enhanced by higher amounts of martensite (approximately 11%) formed during fatigue at R=0.048 load ratio, compared to only 4% of martensite formed at R=0.22 for the same number of cycles.

In conclusion, an improvement of the mechanical properties of AISI 304 stainless steel wire by fatigue is time dependent; the longer fatigue process improves the mechanical properties more significantly. Experimental results show that the yield strength is more significantly affected by fatigue than the ultimate tensile strength.

4.2.4.2. Hardness Measurements

Hardness is another an important characteristic which can be influenced by cyclic strain. Figure 4.66. and Table 4.12. and show the changes in hardness caused by subsequent fatigue. The hardness was measured on annealed samples and on wire drawn to different strains, before and after the fatigue process.

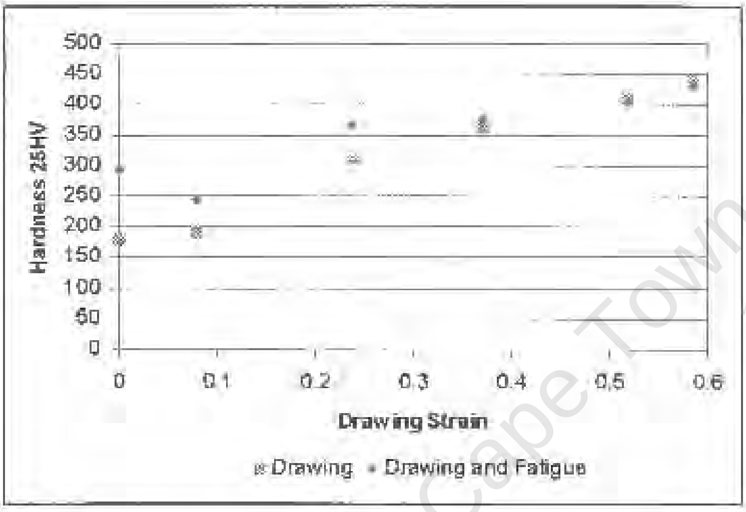

Fig.4.66. Hardness test measurements of AISI 304 stainless steel wire in the drawn condition and after the fatigue process

Table 4.12. List of hardness measurements of AISI 304-stainless steel wire, before and after the fatigue process

	Hardness HV 25 Drawn Condition	Fatigue Conditions	Hardness HV 25 After Fatigue
Annealed	180	R=0.048 N=120.000 cycles	295
Strain 0.09	192	R=0.048 Cycled to failure	245
Strain 0.238	310	R=0.048 Cycled to failure	366
Strain 0.37	360	R=0.048 Cycled to failure	370
Strain 0.52	410	R=0.048 Cycled to failure	No changes
Strain 0.585	440	R=0.048 Cycled to failure	No changes
2.5 mm	465	R=0.048 Cycled to failure	No changes

Fatigue cycling significantly hardened both the annealed and lightly drawn wire samples. The biggest increase was observed in annealed wires where the hardness increased from 180HV25 to 295HV25. Cyclic hardening is attributed to the transformation-induced hardening of retained austenite to martensite during cyclic straining.

Highly drawn laboratory wire samples did not appear to harden during fatigue and commercially supplied wires showed a similar behaviour.

4.2.4.3. Microstructural Changes

The effect of stress on the formation and propagation of slip traces, annealed and notched samples were examined metallographically following fatigue in both the longitudinal and transverse sections.

Figures 4.67.(a,b) show the microstructural changes in the transverse cross-section, in a position (a) very close to the notch and (b) far away from the notch, which indicate the rate of slip line propagation.

Fig.4.67.a) *Optical micrograph of annealed AISI 304 stainless steel wire subjected to the fatigue process.*

<u>Conditions:</u> $\sigma_m = 90$ *MPa*
amplitude $\sigma_a = 80$ *MPa*
N = 120,000 cycles
Position: <u>close to the notch</u>

Etchant:
$HNO_3 + HCl +$ *methanol*

A micrograph taken close to the notch, Fig.4.67.(a) shows a higher rate of slip line formation and propagation. More slip lines and bands are distinct and are present in numerous crystallites. It was observed that the number and extent of the slip traces also increase with increasing number of cycles.

Fig.4.67.b) *Optical micrograph taken at the fracture surface, <u>far from the notch</u>, showing deformation markings in the form of slip traces, and deformation twins.*

<u>Conditions:</u>
Annealed AISI 304 stainless steel wire
Mean stress $\sigma_m = 90$ MPa
Amplitude $\sigma_a = 80$ MPa
$N = 120{,}000$ cycles

In order to observe any possible changes around the fatigue crack, a longitudinal section was polished and the observed microstructure is shown in Fig.4.68.

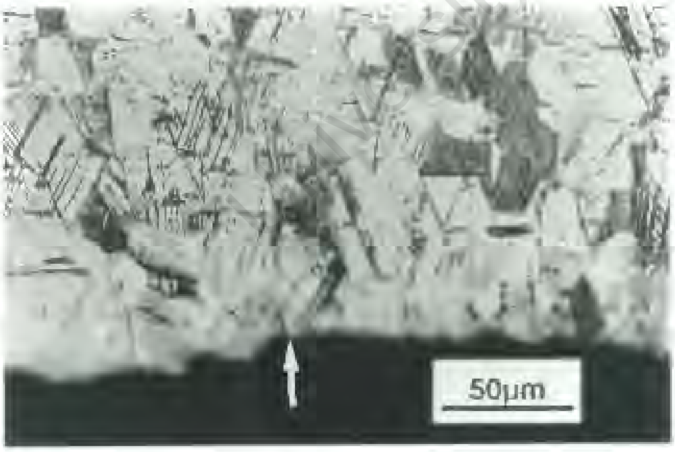

Fig.4.68.*Optical micrograph of longitudinal section.*
<u>Note</u>: fractured surface is on the bottom of the micrograph
Microstructure contains elongated grains, deformation twins and slip traces.

Etchant:
HNO_3+HCl+methanol

Figure 4.69. shows a short fatigue crack initiated at the notch. It appears that the crack started at the grain boundary and propagated intergranularly.

__Fig.4.69.__ A short fatigue crack started from the notch. Note well resolved slip lines in the elongated grains.

Conditions: Annealed AISI 304 stainless steel wire
Etchant: as in Fig.4.66.

It is very difficult to observe deformation-induced α'-martensite using the optical microscope because the deformation markings present appear similar to the martensite phase created by drawing and they partially obscure the α'-martensite phase structure.

In order to quantify the amount of phase transformation associated with crack advance, ten fracture surfaces were mounted in the transverse cross section, and electropolished for observation using X-ray diffraction technique.

The attempt failed to reveal changes in α'-martensite formation and possible reasons for this may be: a) the volume fracture of martensite phase formed around the crack is small and possibly polished away during the sample preparation, or b) the resolution of X-ray radiation is not accurate enough to resolve a very small variation in the volume fraction of a particular phase.

X-ray diffraction analysis performed on the longitudinally sectioned wire samples, as described in Chapter 3, p.65, successfully determined the amount of the α'-martensite phase developed in cyclic conditions.

Subsequently, in order to determine the amount of martensite phase at the notch tip in highly drawn wire samples, thin foils were prepared for transmission electron microscopy. Foils were taken from notched commercially supplied wire samples, which were subjected to fatigue, 500 μm below the fracture surface.

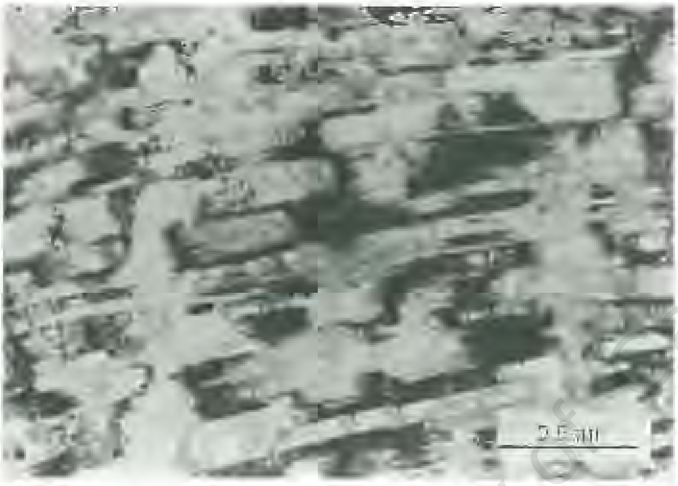

Fig.4.70. *TEM micrograph of AISI 304 stainless steel wire taken in the transverse cross section, as close as possible to the fractured surface. Substructure consists of high dislocation density, forming dislocation cells. Width of dislocation walls is approximately 27nm.* *<u>Conditions</u>: highly drawn wire subjected to fatigue at* $\sigma_{mean} = 550$ *MPa,* $\sigma_a = 450$ *MPa* *N = 2,000 cycles*

Figure 4.70. shows the dislocation structure in the immediate vicinity of the fracture surface. The high density of dislocations and the tendency to the development of a rough cell structure is apparent even in the low stacking fault energy material. According to the substructure developed in the vicinity of the fracture surface, dislocation wall thicknesses of approximately 27nm were found and thus the amount of martensite formed around the fatigue crack can be estimated at 36%.

Importantly, the notch induces a significant amount of the α'-phase, in spite of a very stable microstructure shown in the smooth samples which were also subjected to cyclic strain. The stable microstructure of commercial wire samples has been explained by the higher nickel quantity and carefully selected drawing parameters, compared to those formed in the laboratory conditions.

Influence of Applied Stress on Twinning

The influence of twinning on the work hardening behaviour has also been studied under cyclic conditions.

In the tensile deformation of fcc polycrystals, twinning starts at a critical plastic strain which corresponds to the existence of a critical resolved shear stress for twinning. The shear stress for twinning (τ_T) was calculated from the tensile stress (σ_T) using Taylor's theory, i.e., $\sigma_T = 3.06\ \tau_T$ [123].

It can be assumed that twinning is induced at the same critical stress under cyclic and monotonic conditions. According to this assumption, and applying Taylor's theory, twins were identified in the annealed and fatigued samples at a strain range between 28% and 32%. The range of applied stress in which twins were identified was between 620 and 644 [MPa]. It has also been noted that the identification of twinning on the stress-strain curves was a very rare case. Figure 4.71. shows twinning on the fractured surface of the annealed wire subjected to fatigue.

Fig.4.71. *Fractured surface of annealed and fatigued wire, showing microcracks and twins.*
Fatigue conditions:
Load ratio R=0.2
Number of cycles:N=566,000

However, considering the cyclic stress-strain curves, differences appear with the monotonic behaviour, where twinning has not been identified.

It is believed that the stress required for the formation of deformation twins is controlled mainly by the value of stacking fault energy of material. It has also been suggested in literature that another microstructural parameter influencing deformation twinning is the grain size [47]. In order to establish the conditions and their role on the initiation of deformation twinning under fatigue conditions, it is necessary to extend investigations to include a number of other parameters which has not been done in the present work.

4.2.5. Fractography of AISI 304 Stainless Steel Wire

Fractographic studies performed on the AISI 304 stainless steel wire involved an investigation of both static tensile and fatigue fracture surfaces. In both cases the examination was performed on the pre-notched wire samples drawn to different drawing strains.

4.2.5.1. Static Tensile Fractography

The static tensile fracture surfaces investigated on the AISI 304 stainless steel wires drawn to different strains, ranging from 0.09 to 0.585 strain, are generally the same. Namely, it appears that the ductile transgranular mode is the fracture mode of drawn AISI 304 stainless steel wires.

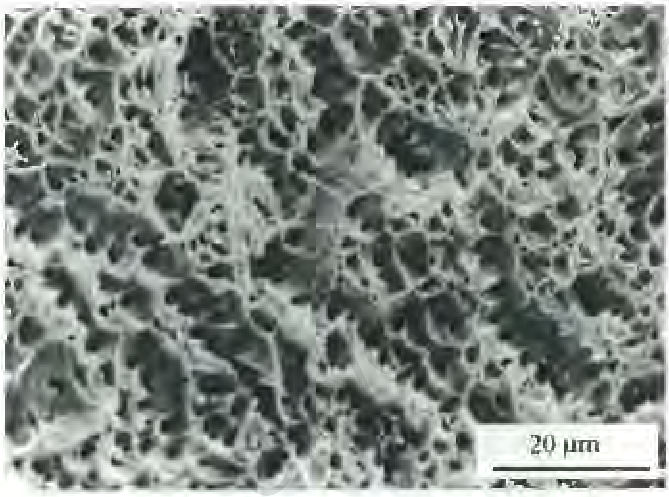

Fig.4.72. *Typical scanning electron micrograph of the static tensile fracture surfaces observed in the AISI 304 stainless steel wire, drawn to different strains.*

Conditions:
Tensile test performed at strain rate 0.001 s^{-1}

Figure 4.72. shows the general topography of the AISI 304 stainless steel wires drawn between 0.09 to 0.585 strain. The fracture surfaces are characterised by microvoid coalescence.

4.2.5.2. *Fatigue Fractography of AISI 304 Stainless Steel Wire*

Smooth Wire Samples

The fracture surfaces of smooth and pre-notched samples have been examined together with the influence of drawing strain on the fatigue mode. A typical fracture surface of smooth samples shows that the transgranular fracture mode is a dominant feature immediately after cracking has been initiated. Figures 4.73. and 4.74. show two types of crack initiation sites at surface flaws and twin boundaries respectively. Experimental results showed that only in a very small number of samples had the fatigue crack initiated at twin boundaries.

Fig.4.73. *Intergranular mode of crack initiation at a surface flaw, having a size of 30μm The arrow indicates surface flaw developed during the fatigue process.*

Fig.4.74. *SEM micrograph of a crack initiation in the smooth AISI 304 stainless steel wire. Micrograph shows dark, shiny faces; arrow indicates twin boundary*

Pre-Notched Wire Samples

A typical fracture surface of pre-notched sample shows that the transgranular fracture mode is a dominant fracture immediately after cracking has been initiated. Figure 4.75. shows the fracture started from a notch.

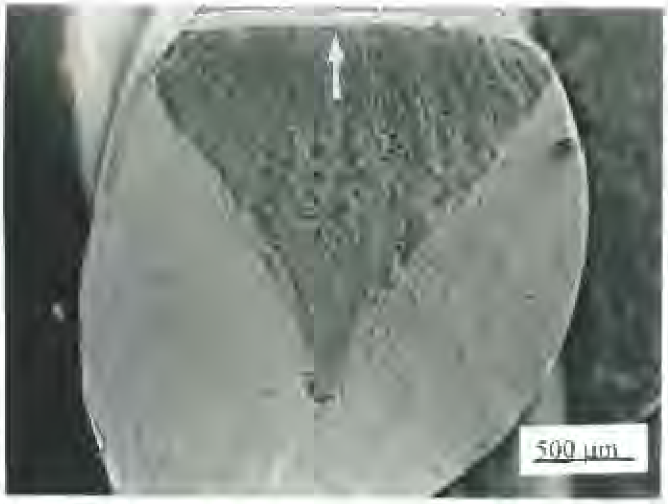

Fig.4.75. *Scanning electron micrograph showing a typical fatigue fracture surface of AISI 304 stainless steel wire, started from a notch.*
Note: Arrow indicates the notch position

The application of linear elastic fracture mechanics has provided the basis for describing the phenomenon of fatigue crack propagation. The crack growth rate per cycle (da/dN) is primarily controlled by the alternating stress intensity (ΔK) and this sigmoidal variation can be characterised in terms of different primary fracture mechanisms, Fig.4.76.

In the slow fatigue crack growth region below the threshold stress, the fatigue crack growth is sensitive to microstructure and load ratio and the formation of crystallographic facets was noted. This mode of fatigue-crack growth manifests itself as planar transgranular or intergranular facets. In AISI 304 stainless steels the facets are transgranular. An example of the facets is shown in Figs.4.77.-4.79. The fracture morphology showed a flat, ductile transgranular mode with isolated segments of intergranular separation. Close to the threshold stress value the proportion of intergranular facets is small, which increases to a maximum and then gradually diminishes at high stress intensities to zero. Significant numbers of these intergranular facets were observed in lightly drawn samples. The development of the facets was associated with the change from microstructurally insensitive to microstructurally sensitive crack growth and a transition from mode B to A, Fig.4.77.

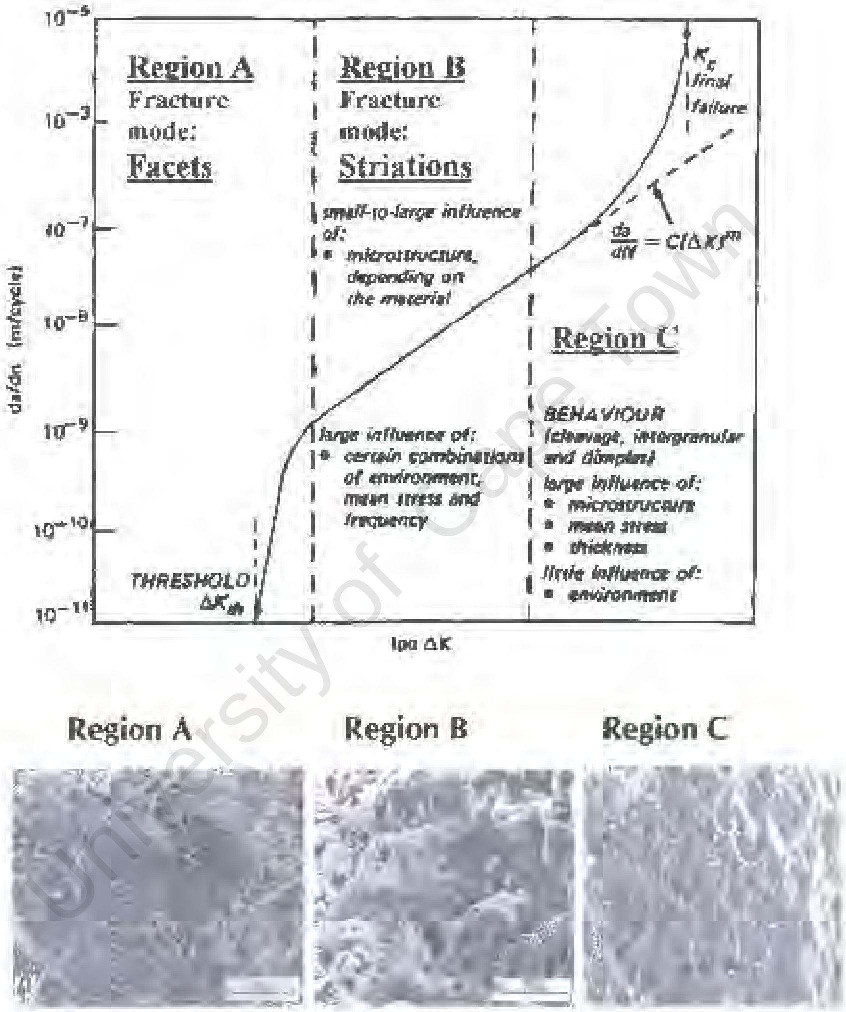

Region A

Region B

Region C

Fig.4.76. Primary fracture mechanisms in AISI 304 stainless steel wires associated with the sigmoidal variation of fatigue crack propagation (da/dN) with alternating stress intensity (ΔK)

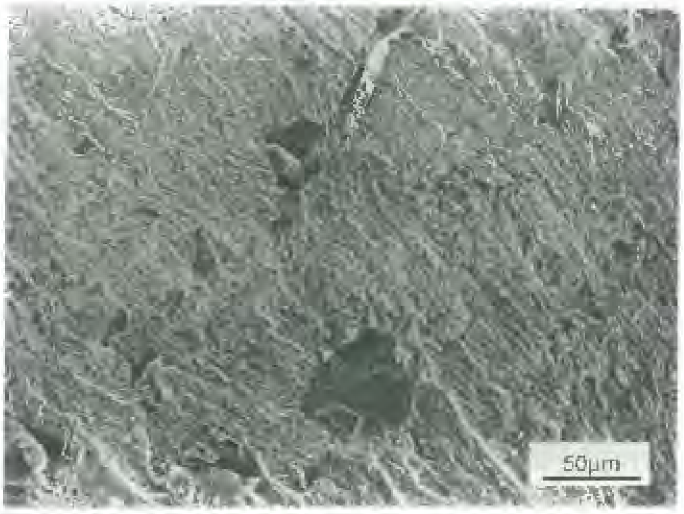

Fig.4.77. *General view of the fracture surface observed in an annealed wire sample, close to the threshold stress value.*

SEM micrograph shows ductile transgranular mode with areas of intergranular separation

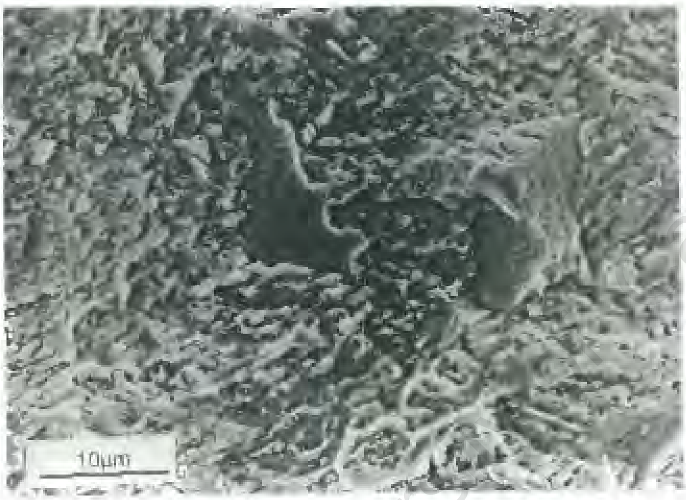

Fig.4.78. *Cleavage-like growth of fatigue cracks through a grain, observed in the near-threshold region in lightly drawn wire.*
-drawing strain - 0.09.

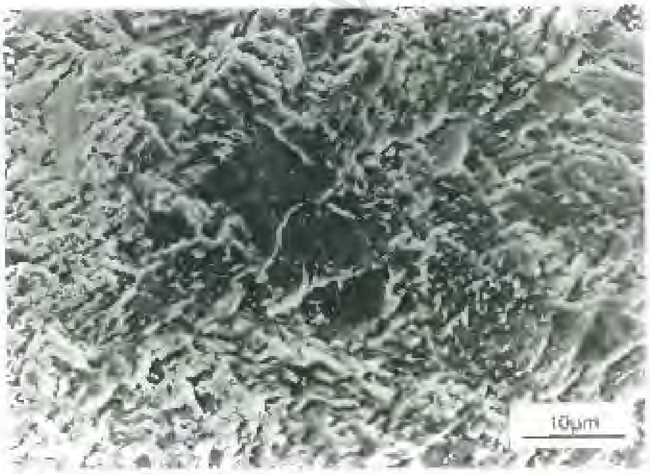

Fig.4.79. *SEM micrograph of lightly drawn wire AISI 304 stainless steel wire (drawing strain - 0.238),*
showing 'quasi-cleavages' typical in lightly drawn wires.

The separation at the crack front of material which did not show facets involved a ductile tearing process. The facets that form as a result of continued load cycling did not have the same appearance as "cleavage" facets in the true sense because they exhibited slow, progressive failure rather than brittle separation. Figures 4.78. and 4.79. show a scanning electron micrograph of a fracture surface taken from wire samples drawn to 0.09 and 0.238 strain respectively. In lightly drawn wires, intergranular separation is observed in both low and high fatigue crack growth rate regions.

The presence of such "cleavages" were not observed in the highly deformed wire samples. A transgranular ductile mode was observed in both low and high crack growth rate regions. Figure 4.80. shows the typical fracture surface of highly drawn wire samples.

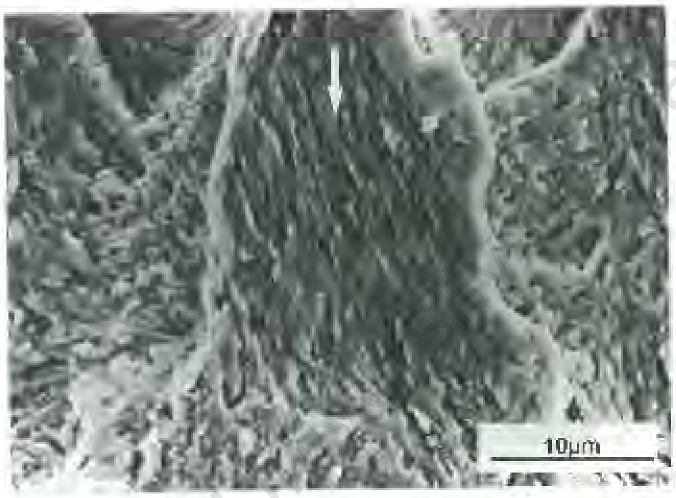

Fig.4.80. *Transgranular ductile fracture mode observed in the highly drawn AISI 304 steel -strain-0.585*
Fatigue conditions:
Mean stress: $\sigma_m = 550$ *MPa*
Amplitude: $\sigma_a = 500$ *MPa*
Failure at N=2,000 cycles

Arrow indicates the crack started from notch.

An analysis of the fractured surfaces of highly drawn wires produced in laboratory conditions, and commercially supplied wire (2.5mm) show a similar ductile fracture mode. The fracture surface of a 3mm diameter wire showed a similar transgranular mode and partially intergranular fatigue crack propagation. The intergranular mode of failure was observed only in the surface layer, involving a volume of large grains, Fig.4.81.

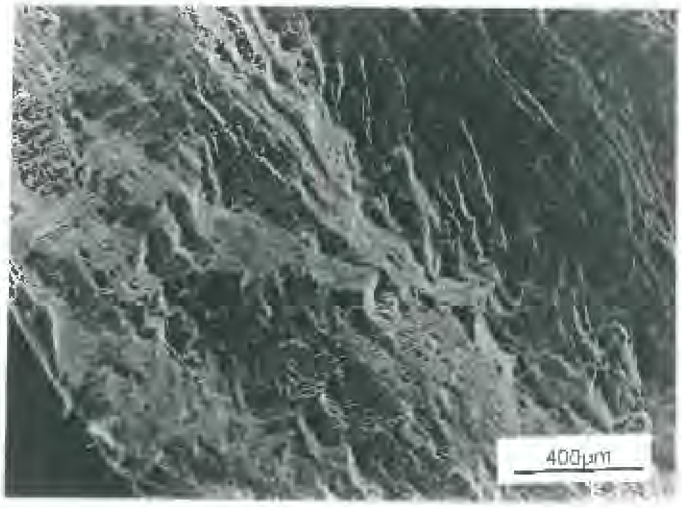

Fig.4.81. *SEM micrograph of AISI 304-commercial wire of 3 mm diameter, showing the transition from intergranular mode to transgranular mode. Note: intergranular mode is associated with large grains*

For the mid-range of growth rates (Regime B), failure generally occured in steels by a transgranular ductile striation mechanism. Fatigue striations have been observed on fractured surfaces, especially those fractured at high amplitude fatigue cycles, Fig.4.82.

The matrix of austenitic stainless steel is ductile, but the presence of hard and brittle carbides cause void formation because they are unable to accommodate the large plastic strains imposed by the more ductile matrix. Void formation is caused either by breakage of the hard and brittle particles and separation of the broken parts, or by separation at the particle-matrix interface.

Fig.4.82. *SEM micrograph of fractured surface in highly drawn AISI 304 steel wire (drawing strain 0.52), showing well developed striations.*
Fatigue conditions:
Mean stress: 550 MPa
Amplitude: 500 MPa

Figures 4.83.-4.84. shows the fracture surface of heavily drawn wire after being fatigued at a cyclic amplitude of 500 MPa. Figure 4.83. shows the different striation spacing across the fracture surface as a consequence of fatigue crack propagation, while Fig.4.84. shows a typical striation shape.

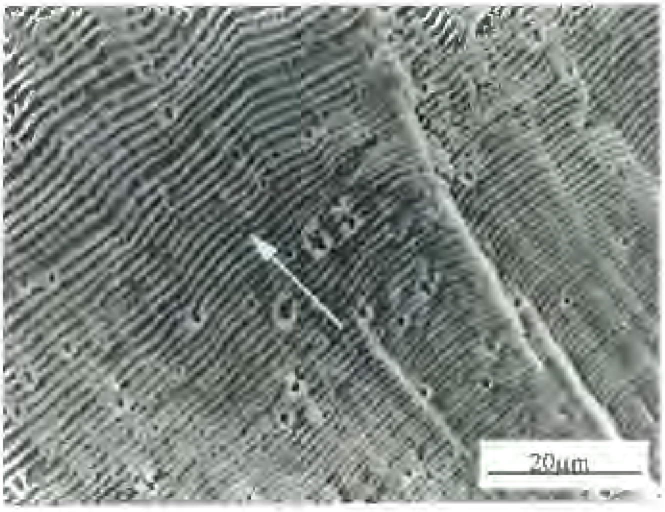

Fig.4.83. *SEM micrograph of a fractured surface under fatigue conditions, showing different striation spacing, as seen at different positions on fractured surface*

Macroscopic examination of the fracture surfaces showed that the initial region of fatigue crack initiation and propagation had a smooth appearance, whilst striations were easily observed with the scanning electron microscope when the crack propagated deeper into the specimen.

Figures 4.85. and 4.86. show the fracture surfaces appearance after the fatigue test was stopped and the specimen fractured after 100 and 1000 cycles respectively.

Three distinct regions are visible on the fracture surface:

a) the region which did not contain dimples represents an area in which martensite transformation occurred during fatigue testing,
b) the region which does contain dimples shows the further crack advance during fatigue process,
c) the final ductile fracture.

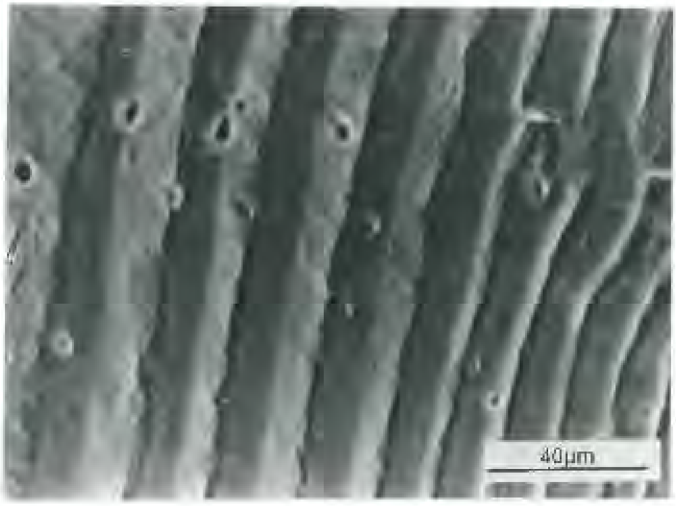

Fig.4.84.*SEM micrograph taken close to the final fracture. High magnification shows the typical 'A' striation's shape.*
Fatigue conditions:
Mean stress: 550 MPa
Amplitude: 450 MPa

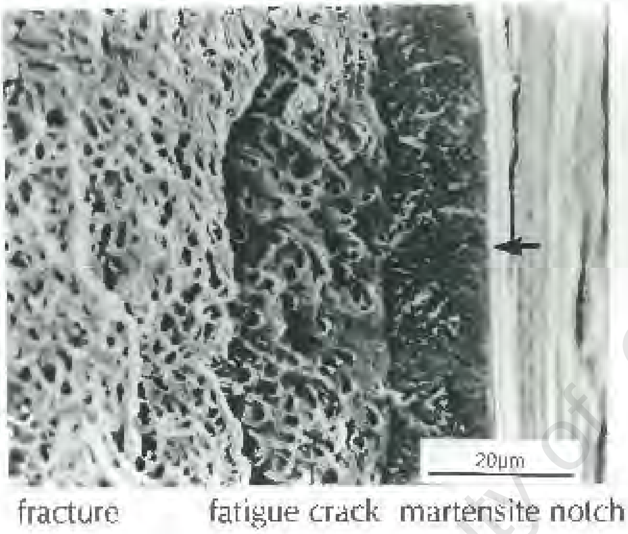

Fig.4.85.*SEM of fractured wire; fracture started at notch. Fatigue test were stopped at N = 100 cycles.*
Fatigue conditions:
Mean stress: 550 MPa
Amplitude: 500 MPa

Arrow indicates the martensite transformation started at notch

Fig.4.86. *Micrograph taken at same mean stress 550 MPa and amplitude of 500 MPa, test stopped at N = 1000 cycles Micrograph shows significant advance of martensite transformation during the longer period of time.*

Martensite formed during the fatigue process is observable on the fracture surface in a shape of "butterfly-martensite", which occurs in pairs, joined at one end, as shown in Fig.4.87. "Butterfly-martensite" was also documented previously by Maxwell et al [86].

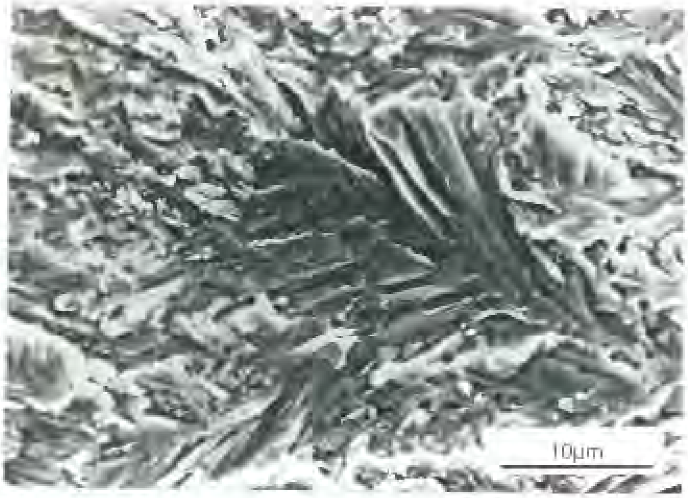

Fig.4.87.*"Butterfly martensite" observed on the fractured surface of AISI 304 stainless steel wire drawn to 0.37 strain*

The advance of martensite transformation during fatigue together with crack length is graphically presented in Fig.4.88. These measurements were obtained from experiments performed on commercially supplied wire, at a load ratio R=0.048. The results indicate that the martensite transformation occurs in front of the crack tip.

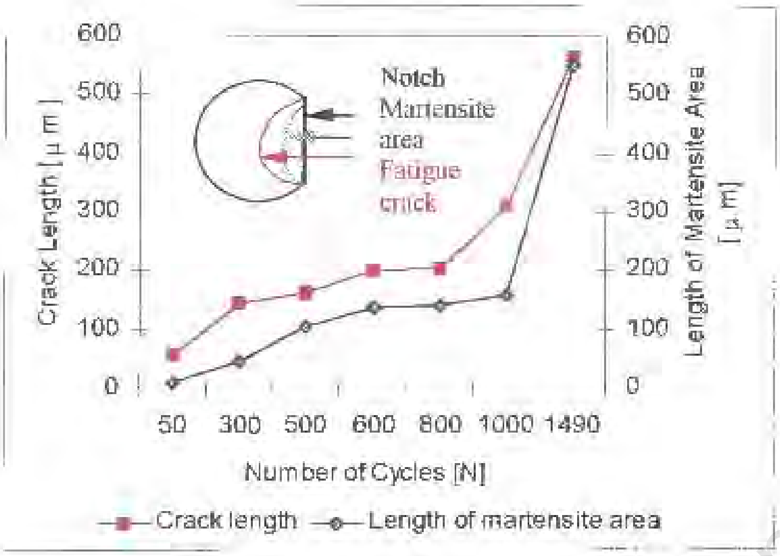

Fig.4.88. *Influence of number of cycles on length of martensite transformed area*

In conclusion, the investigations performed on the pre-notched samples revealed different fracture modes, depending on the drawing strain. Several mechanisms were observed during the fatigue crack growth. A ductile transgranular mechanism with segments of intergranular separation operate at low growth rates, ductile striation mechanisms occurs in the mid-regime of crack growth rate and finally a ductile static mode in the region of high growth rates.

The most significant findings in the fractographic study of drawn AISI 304 stainless steel wires was the difference in the fatigue fracture mode caused by the phase transformation that occurs during the fatigue process. Figures 4.89. and 4.90. show the typical fatigue fracture surface observed in the low and high drawn wire samples. The deleterious influence of the martensite phase formed during the fatigue process in the highly drawn AISI 304 stainless steel wires was observed in the samples having more than 20% of prior induced martensite, promoting brittle behaviour.

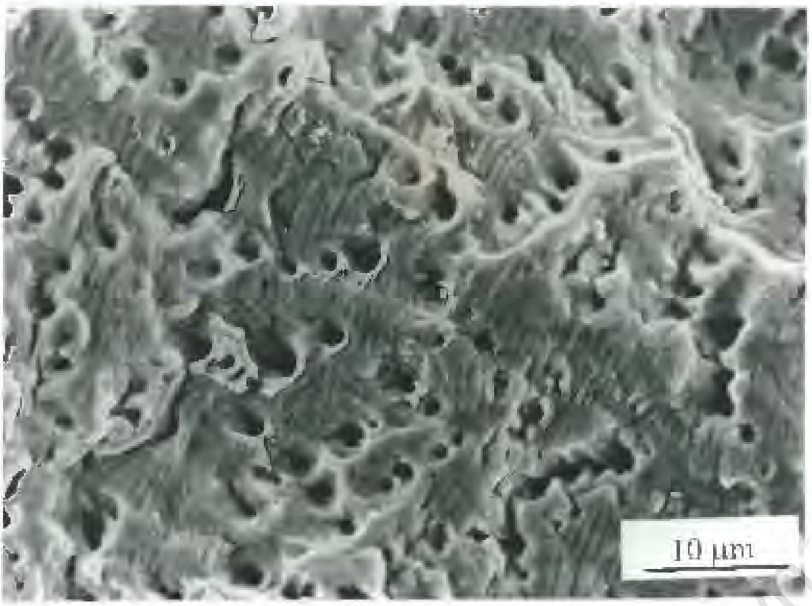

Fig.4.89. *Scanning electron micrograph taken at the fracture surface of AISI 304 stainless steel wire drawn to 0.37 strain, having approximately 20% of strain-induced martensite, showing a ductile mechanism of the fatigue crack growth*

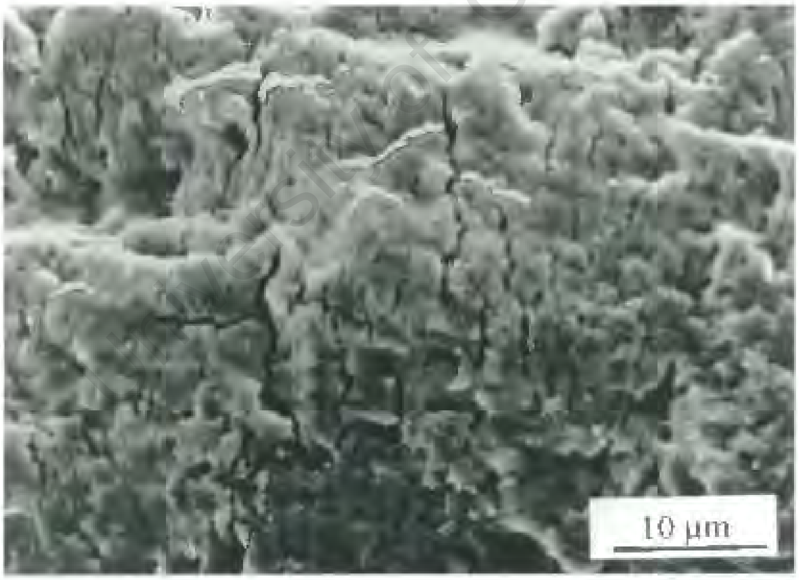

Fig.4.90. *Fracture surface of the AISI 304 stainless steel wire drawn to 0.585 strain having approximately 36% of strain-induced martensite, showing a 'brittle' appearance*

Summary:

The research performed on the AISI 304 stainless steel wire showed that the martensite phase transformation that occurs in both the drawing and fatigue processes, plays a very important role, and strongly influences the fatigue behaviour.

The overall role of martensite transformation on the mechanical properties, microstructural characterisation and fatigue properties has already been presented and has been partially discussed in the previous sections. The most important findings are as follows:

1. It was established that the extent of martensite transformation depends on both the maximum strain applied during the drawing process and also on the fatigue conditions such as cyclic amplitude, maximum stress, and duration of fatigue process.

2. Surface defects such as notches, their size, shape and manufacturing procedure also significantly influence the phase transformation.

3. However, the most important conclusion obtained from this research is that the extent of phase transformation and work hardening, and thus the fatigue response of AISI 304 stainless steel wire, is determined by the amount of the martensite phase developed during the drawing process which took place.

4. It was observed that a change in the fracture mode, from ductile to brittle, also depends of the amount of deformation-induced phase transformation in these steels.

4.3. 3CR12-Ferritic Steel Wire

4.3.1. Mechanical Properties of 3CR12 Steel Wire

The mechanical properties achieved in the ferritic steel 3CR12 by drawing to different strains between 0.09 to 0.68 are presented in Fig.4.91. Table 4.13. lists each of the properties that were calculated from the tensile data, together with the result of hardness measurements.

Figure 4.91. shows that the ultimate tensile strength, yield strength and hardness are increased by increasing drawing strain. The ultimate tensile strength increased approximately 60% from 442 MPa to 738 MPa whilst the yield strength increased approximately 35%. The hardness also increased from 150 HV to 246 HV as the strain increased from zero to 0.68. It is also noted from Table 4.13. that the total and plastic elongation to failure decreased as the yield and tensile strengths increased.

It can be seen in Fig.4.91. and Table 4.13. that a very small amount of drawing strain (0.09) lowers the total elongation value considerably, from 35% to 12.3% which indicates that the material work hardens extremely rapidly. Further straining to a level of 0.37 only reduces the total elongation to failure by a further 4%. Further straining to 0.68 reduces the total elongation to failure to approximately 8%.

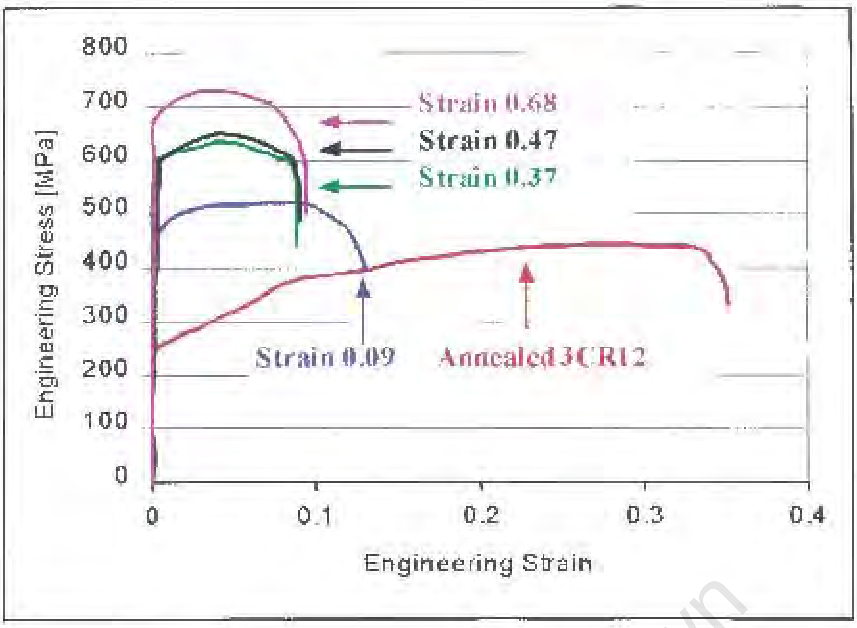

Fig.4.91. Tensile tests results of 3CR12 steel wires drawn to strains in the range between 0.09 and 0.68

Table 4.13. Tensile Properties and Hardness of 3CR12 Ferritic Steel Wire

Drawing Strain ε	Yield Strength [MPa]	Ultimate Tensile Strength [MPa]	Total Elongation to Failure [%]	Hardness (Vickers) HV 25
Annealed	250	442	35	150
0.09	469	516	12.3	183
0.37	603	635	8.96	220
0.47	607	647	8.2	234
0.68	687	738	8	246

True Stress-True Strain Tensile Behaviour

The true stress-strain curves of the drawn 3CR12 steel wires are shown in Fig.4.92.(a-b). In addition, the work hardening rate for each of these curves has also been plotted as a function of the drawing strain.

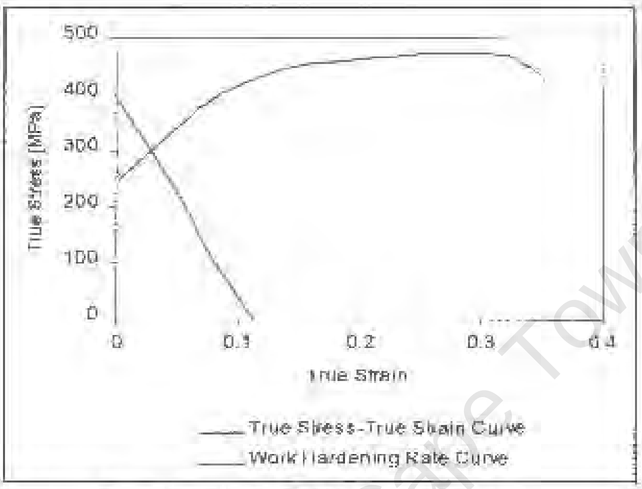

a) *Annealed 3CR12 steel wire*

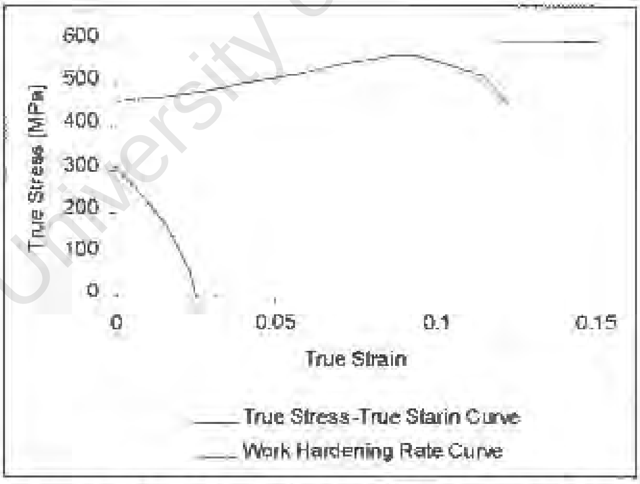

b) *Drawn 3CR12 steel wire (drawing strain 0.09)*

Fig.4.92.(a-b) *Tensile and Work Hardening Rate Graphs for annealed and drawn 3CR12 steel wires*

A negative work hardening rate was observed in both the annealed and drawn wire samples.
The high necking point indicates the ability of material to withstand plastic deformation without local yielding and the onset of necking during deformation can be predicted from the intersection point of the flow curves and work hardening rate curves.

Necking occurs at 3 percent strain in the annealed wires, Fig.4.92.(a). Further drawing drastically reduces the strain at which necking occurs and the results obtained for wires drawn between 0.09 and 0.68 strain showed only a minor amount of uniform elongation. Fig.4.92.(b) shows that necking occurs almost at the yield point for wires drawn to 0.09 strain.

In conclusion, the mechanical properties of 3CR12 ferritic steel are characterised by a high yield to tensile strength ratio compared to lower ratios for the AISI 304 stainless and pearlitic steels, indicating the restricted ability of 3CR12 steel to be plastically deformed.
It was also observed that small amounts of plastic straining increases the strength properties rapidly. Further straining does not increase the strength significantly and the plastic elongation to failure decreases drastically.

4.3.2. Microscopy of 3CR12 Steel Wire

3CR12 ferritic steel wires in the annealed and drawn condition were cut and prepared for both macrostructural and microstructural investigations. Macrostructural examination was performed in order to determine any possible surface damage caused by the drawing process. The microscopical investigation involved the polishing and etching of samples. The respective microstructures of annealed and drawn 3CR12 steel wires are shown in Figs.4.93.-4.98.

4.3.2.1. Surface Examination

Following the machining of reinforcing bars of 18mm diameter down to 6mm diameter, the samples were drawn to a final size of 3.5 mm diameter. The drawing process was performed at room temperature and without intermediate annealing. A careful examination was afterwards carried out on the surface of wire using an optical stereo microscope. No significant mechanical defects were observed in lightly drawn wires and the surface roughness of the drawn wire was measured between R_a=0.5-0.6 μm. Highly drawn wires, particularly those drawn to 0.68 strain, were found to have many surface defects and generally had a very poor surface quality with a surface roughness between R_a=0.8 and 1 μm. Due to the poor surface quality of the highly drawn wires, no fatigue studies were carried out on these specimens.

4.3.2.2. Metallography

The microstructure of the steel was investigated in the as received condition (hot rolled reinforcing bar) and after being annealed and then drawn to different strains. Figure 4.93. shows the microstructure of the reinforcing bar in its initial condition.

The microstructure consists of ferrite with a small amount of low carbon martensite islands, having an overall hardness of 290 HV50, Fig.4.93. The formation of a duplex microstructure is related to both the alloy composition and the thermal history of the steel.

The chemical etch solution gave rise to a tint contrast between the ferrite and martensite phases which resulted in the respective phases being easily identifiable. To make samples suitable for drawing, they were annealed at 760°C for 30 min. and air-cooled. The microstructure in the annealed condition is fully ferritic, as seen in Fig.4.94.

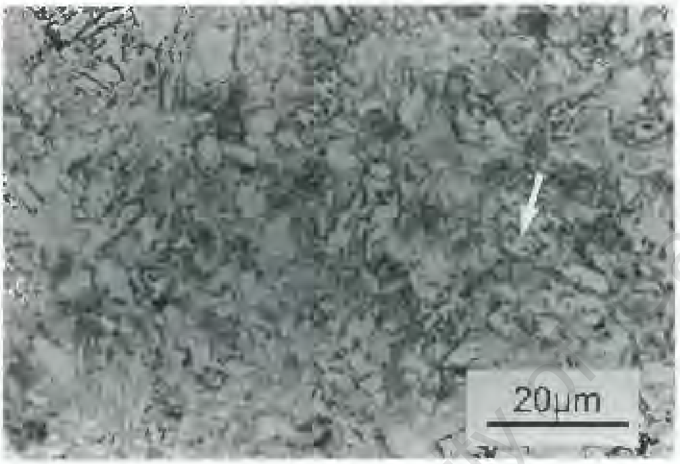

Fig.4.93. *Optical micrograph of hot rolled reinforcing bar, the microstructure consists of ferrite matrix with the martensite islands. Arrow indicates the martensite islands of 3-5 micron size Etchant: ($HCl+NH_4F.HF+K_2S_2O_5$)*

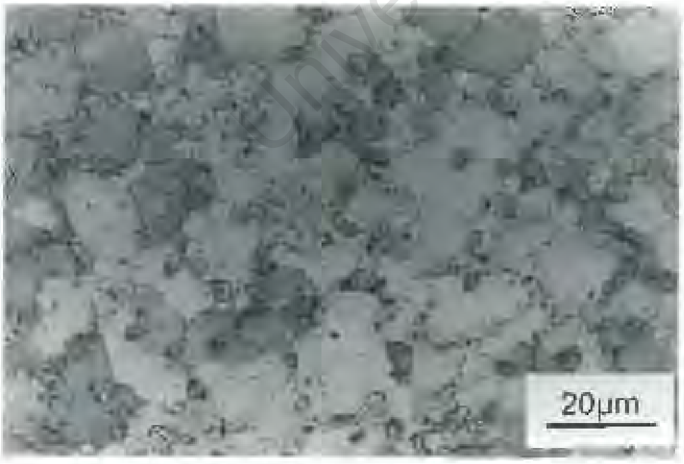

Fig.4.94. *Optical micrograph of annealed 3CR12 steel wire, taken in the cross-section. The microstructure consists of ferrite grains and subgrains. Etchant: ($HCl+NH_4F.HF+K_2S_2O_5$)*

Optical micrographs show that the grains are small with an average size of 15 microns determined using the standard linear intercept method.

The changes in microstructure caused by the drawing process are shown in Figs.4.95.-4.96. The microstructure of wire specimens drawn to a strain of 0.09 consists of deformed ferrite grains, but are very similar to the annealed microstructure. The application of a higher drawing strain of 0.47 creates changes in grain shape and size.

Fig.4.95. *The microstructure of drawn 3CR12 steel consists of ferrite grains and subgrains. <u>Conditions:</u> optical micrograph taken in cross sectional direction, drawing strain* $\varepsilon = 0.09$ *Etchant:* $(HCl + NH_4F.HF + K_2S_2O_5)$

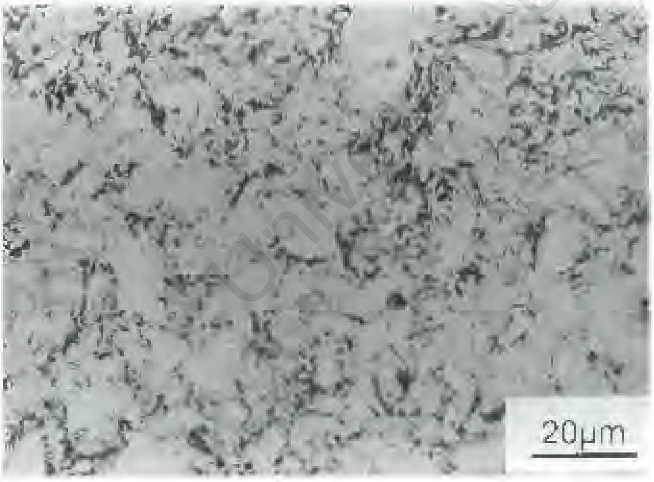

Fig.4.96. *Cross-section of the 3CR12 stainless steel wire drawn to 0.47 strain. The microstructure consists of deformed ferrite grains. Etchant:* $(HCl + NH_4F.HF + K_2S_2O_5)$

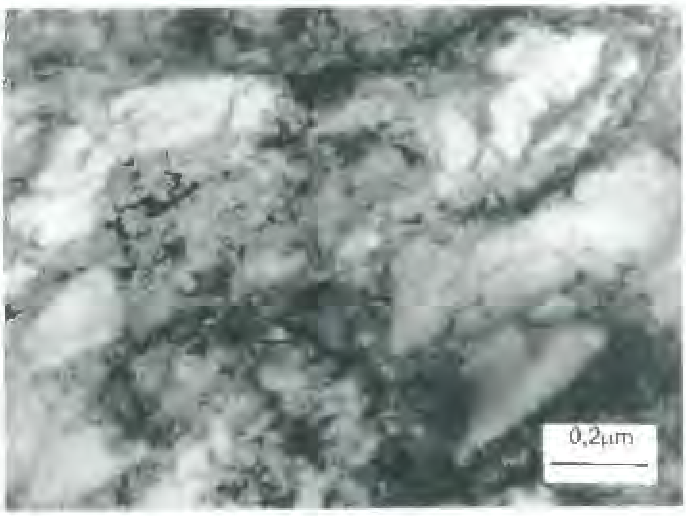

Fig.4.97. *Transmission electron micrograph of the dislocation structure developed at a strain of 0.47. The interior of ferrite grains are relativelly free of dislocations.*

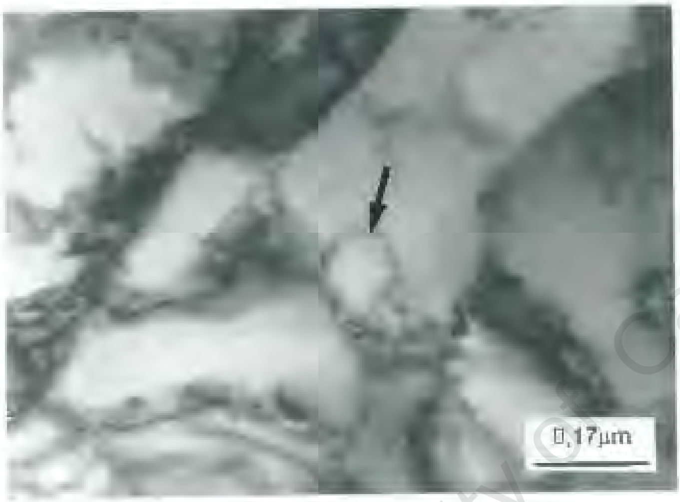

Fig.4.98. *Transmission electron micrograph image of the cell structure developed at strain of ε = 0.47. Arrow indicates a cell.*

An investigation of the microstructure using a transmission electron microscope, Figs.4.97.-4.98., revealed the dislocation structure caused by the drawing process. The microstructure even in the highly drawn 3CR12 steel wires consists of ferrite grains, together with dislocation cells. The regions inside the cells are relatively free of dislocations. One of the most obvious characteristics of the plastically deformed ferrite matrix of 3CR12 ferritic steel observed by transmission electron microscope is the high dislocation density in the cell boundaries.

Heat Treatment of 3CR12 Steel

Samples of wire were also heat treated to produce a dual phase microstructure of ferrite and low carbon martensite.

Reheating of the fully ferritic microstructure to a temperature of 950° C resulted in the formation of some austenite which subsequently transformed to martensite when cooled (oil quenched) to room temperature. The microstructure for 3CR12 specimens held at 950° C, for 0.5 hour, is shown in Figs.4.99.-4.100.

It is evident from these micrographs that areas of martensite are present. This is also reflected in the increase in bulk hardness. Although reaustenitisation has occurred, directionality is maintained with respect to the ferrite content. The ferrite banding, indicated by the darker etched bands, is illustrated in Fig.4.99.-4.100.

Fig.4.99. *Optical micrograph of 3CR12 steel reheated into $\alpha+\gamma$ phase region and quenched from 950° C after 30 minutes;*
microstructure consists of ferrite and martensite

Etchant:
$HCl + NH_4F.HF + K_2S_2O_5$

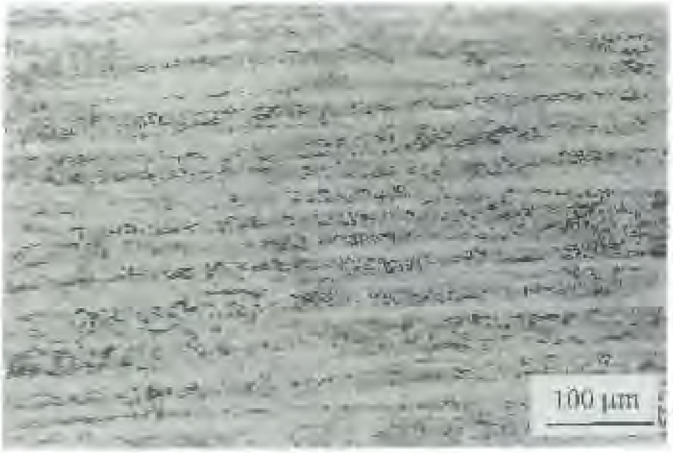

Fig.4.100. *Longitudinal direction of annealed and afterwards quenched 3CR12 steel wire*

Etchant:
$HCl+NH_4F.HF+K_2S_2O_5$

Hardness measurements showed that the quenching treatment increased the hardness from 150 HV25 to 246 HV25.

Compositional analysis of the banded features distinguishable in the annealed and quenched structures was carried out using energy dispersive X-ray spectroscopy (EDS). Analysis of the ferrite and martensite bands visible in the annealed and quenched structure, Figs.4.99.-4.100., shows the average Cr, Ni, and Mn concentrations in Table 4.14.

Table 4.14. Microanalysis of Banded Structures in 3CR12 Steel

Phase	Cr [%]	Ni [%]	Mn [%]
Martensite	11.87 ± 0.1	0.6 ± 0.1	1.4 ± 0.1
Ferrite	12.79 ± 0.2	0.4 ± 0.1	1.2 ± 0.1

4.3.3. Fatigue Behaviour of 3CR12 Steel Wire

An investigation of fatigue behaviour has been studied using both notched and smooth specimens. The effects of drawing strain and the resulting microstructures have been related to fatigue behaviour. These results have also been related to the changes in the mechanical properties as a consequence of the fatigue process.

4.3.3.1. Fatigue Limit of Notched Samples

The fatigue limit was determined on pre-notched wire samples at 10^6 cycles under stress controlled conditions. The investigation of fatigue limit was studied in the annealed wires and wires drawn to different strains between 0.09 and 0.47. The wire samples which were drawn to the highest strain (0.68), have not been included due to the presence of many flaws on the wire surface. The effect of drawing strain and heat treatment (quenched condition) on the fatigue limit are shown in Fig.4.101. and Table 4.15.

The relationship between the fatigue limit and the drawing strain shows a trend of increasing fatigue limit with drawing strain. Tests performed on annealed wires show a fatigue limit of 130 MPa, whilst the fatigue limit of wire drawn to a low strain of 0.09 is improved by almost 130% to 240 MPa. This improvement in fatigue strength is greatly enhanced due to the work hardening of the ferritic matrix. Further straining to 0.37 improves the fatigue limit further to 300 MPa. The fatigue limit of the wires drawn to the highest strain of 0.47 increased very little, from 300 MPa to 310 MPa.

However, it was observed that the fatigue limit of the smooth and heat-treated (quenched) wire sample is significantly higher than those in the drawn condition. The fatigue limit was increased by quenching to 480 MPa which is an improvement of more than 360% over the annealed fully ferritic steel.

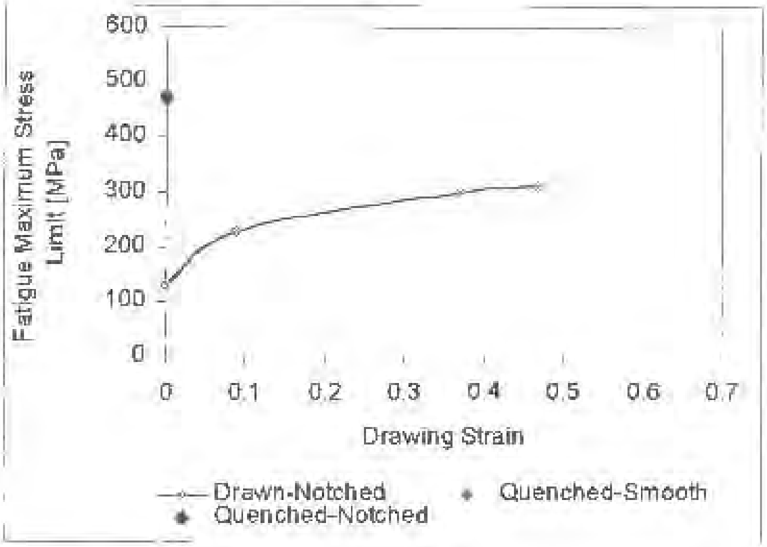

Fig.4.101. *Fatigue limit of drawn and quenched 3 CR12 wires*

Table 4.15. Fatigue Limit of Drawn and Quenched-Notched 3CR12 Steel-Wire

	Annealed	Strain 0.09	Strain 0.37	Strain 0.47	Quenched
Fatigue Maximum Stress Limit σ_{max} [MPa]	130	230	300	310	470

Fatigue tests were also performed on pre-notched dual-phase 3CR12 steel wires. The experimental results indicate that the fatigue limit of notched dual phase steel wire was not significantly reduced from that obtained on the un-notched specimen. It is apparent that the dual-phase microstructure acts beneficially by improving the fatigue strength.

In summary, the fatigue limit of 3CR12 steel is improved by a small amount of drawing strain. Drawing to higher strain values does not significantly improve the fatigue limit further. However, it was found that heat treatment which produces a dual phase ferritic structure containing martensite is more powerful than drawing in improving the fatigue limit.

4.3.4. Changes in 3CR12 Steel Wire

The changes in mechanical properties and microstructure of 3CR12 steel wire caused by the cyclic strain are described in this section.

4.3.4.1. Mechanical Properties

The changes in mechanical properties were assessed in the annealed and drawn 3CR12 steel wire subjected to various fatigue conditions. Table 4.16. and Fig.4.102. show the changes in the static mechanical properties of 3CR12 steel wire, while Fig.4.103.(a-d) shows the true-stress-true strain and the work hardening rate curves for annealed and lightly drawn wires subjected to cyclic strain at different load ratios and number of cycles.

The influence of fatigue on the cyclic tensile properties is seen in Fig.4.102. and Table 4.16. Results show that the monotonic properties, such as the ultimate tensile strength and yield strength were increased as a consequence of fatigue.
The ultimate tensile strength was increased from 442 MPa in the annealed condition to 465 MPa, or approximately 5%, after being subjected to fatigue at a load ratio of R=0.22 and a number of cycles N=120,000. The same fatigue conditions increased the yield strength from 250 MPa to 306 MPa, by approximately 22%.
An increase of the ultimate tensile strength of approximately 7%, was observed in wires drawn to a low strain of 0.09, after being subjected to fatigue at a load ratio of R=0.048 and a number of cycles N=300,000. The same fatigue conditions increased the yield strength from 469 MPa to 522 MPa, i.e. approximately 11%. The total elongation to failure was found to decrease in all cases.
Thus, an improvement in the mechanical properties caused by fatigue is more significant in annealed than slightly drawn conditions and the yield strength is more significantly affected than the ultimate tensile strength.

Table 4.16. Changes in Mechanical Properties caused by the Fatigue Process

Conditions: 3CR12-Ferritic Steel Wire	Yield Strength [MPa]	Ultimate Tensile Strength [MPa]	Total Elongation to Failure [%]
Annealed	250	442	35
Annealed + Fatigued	306	465	27.27
R=0.22 N=120,000	+22%	+5%	↓
Drawn to 0.09 strain	469	516	12.3
Drawn to 0.09 +Fatigued	522	551	5
R=0.048 N=300,000	+11%	+7%	↓

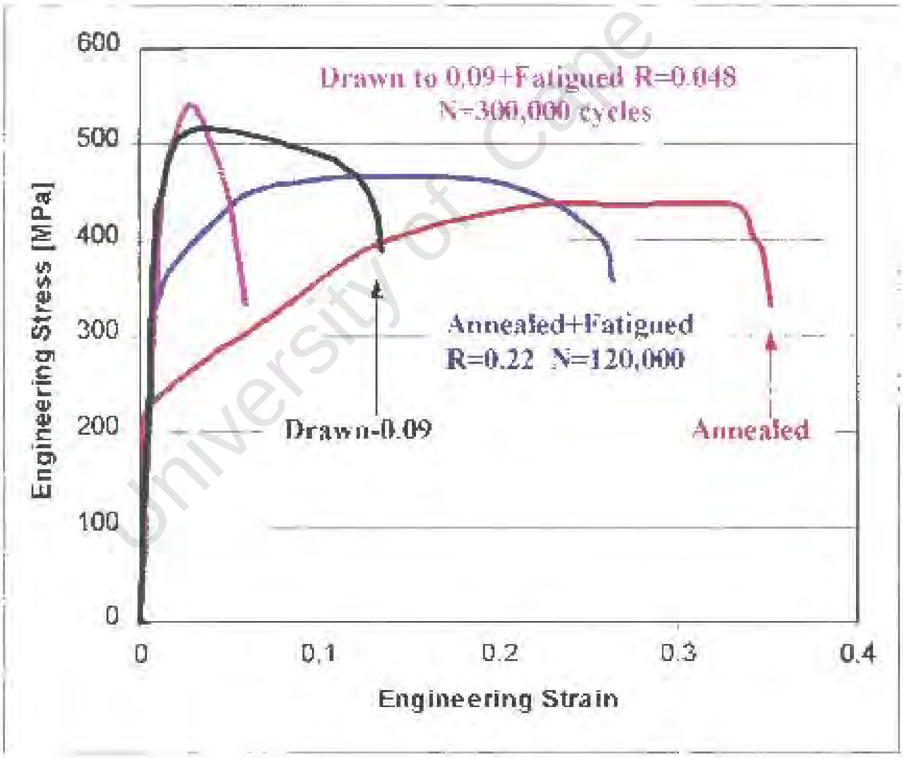

Fig.4.102. Tensile test results of annealed and wire drawn to 0.09 strain, subjected to different fatigue conditions

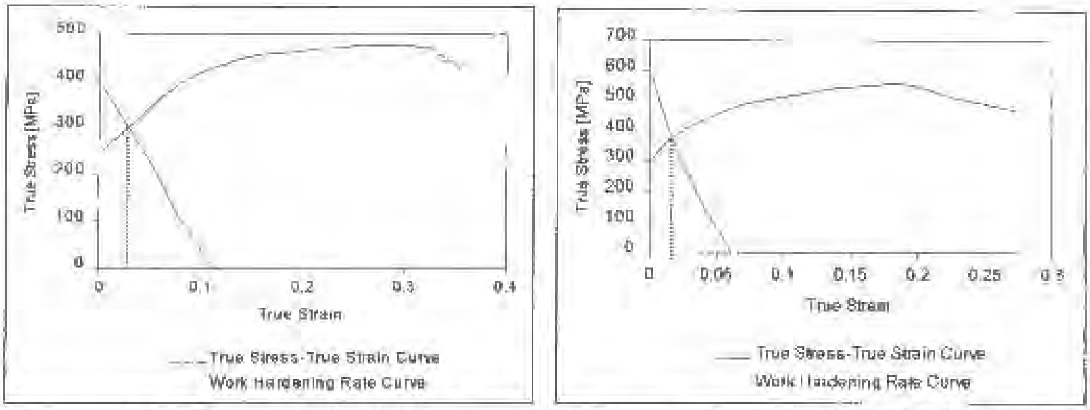

a) *Annealed 3CR12 steel wire*

b) *Annealed and Fatigued 3CR12 wire (Load ratio R=0.22 N=120,000 cycles)*

Fig.4.103.(a,b) *True stress-true strain and work hardening rate curves for annealed and fatigued 3CR12 steel wire*

The tensile /work hardening rate graphs for the annealed 3CR12 steel wires obtained for the fatigue conditions (R=0.22, N=120,000 cycles), Fig.4.103.(b), show a negative work hardening rate. Necking occurs at approximately 2 percent of strain showing that the work hardening caused by fatigue does not affect the strain at which necking occurs significantly.

The work hardening rate graphs for the wires drawn between 0.09 and 0.47 strain in the fatigue condition also show a negative work hardening rate immediately after the yield point has been reached.

Cyclic straining thus results in necking at the yield point and uniform elongation to failure to be significantly reduced.

4.3.4.2. Hardness Measurements

Hardness is also influenced by cyclic strain. Figure 4.104. and Table 4.17. show the changes in hardness caused by subsequent fatigue. The hardness was measured on annealed samples and on wire drawn to different strains (ten samples of each) before and after the fatigue process. The hardness changes caused by cyclic strain are also presented for heat-treated (quenched) 3CR12 steel wire.

Table 4.17. Hardness measurements of drawn and quenched 3CR12 steel wire

	Hardness 25 HV Drawn/Quenched	Fatigue Conditions	Hardness 25 HV After Fatigue
Annealed	150	R=0.22 N=120,000	180
Strain 0.09	183	R=0.048 N=300,000	205
Strain 0.37	220	R=0.048 N=300,000	230
Strain 0.47	234	R=0.048 N=300,000	No changes
Strain 0.68	246	Not tested	Not tested
Quenched	246	R=0.048 N=700,000	250

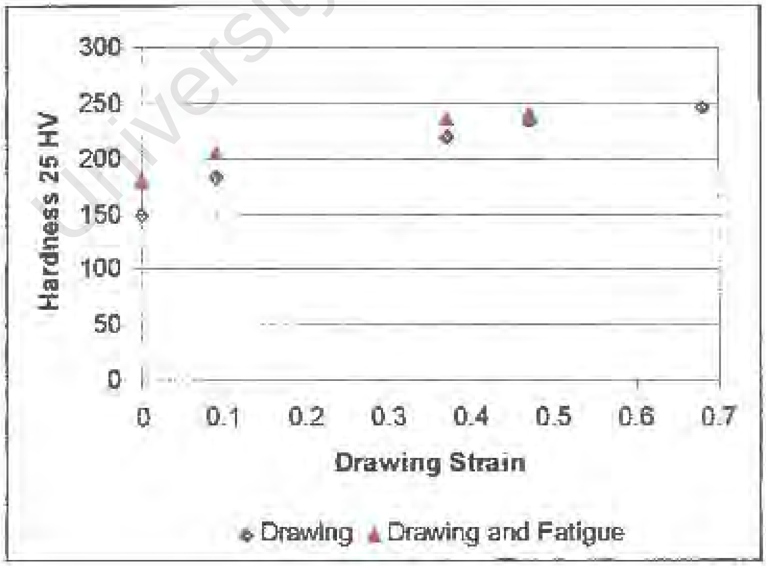

Fig.4.104. Hardness measurements of 3CR12 steel wire

The annealed and lightly drawn wire samples were hardened by fatigue cycling. The biggest increase was observed in annealed wires where the hardness increased from 150 HV25 to 180 HV25. Cyclic hardening is attributed to the work hardening of the ferrite matrix.

The measurements also show that the hardness of the ferrite/martensite microstructure obtained by quenching in oil was not changed by cyclic strain, Table 4.17.

4.3.5. Fractography of 3CR12 Steel Wire

4.3.5.1. Static Tensile Fractography

Static fracture surfaces were investigated in the pre-notched wire samples drawn to different strains, ranging from 0.09 to 0.47. A transgranular ductile mode is a common mode of failure for 3CR12 wires drawn to all strains which are shown in Figs 4.105.-4.106.

Fig.4.105. *Scanning electron micrograph displays the general view of highly drawn 3CR12 steel wire subjected to the tensile test.*
Conditions:
3CR12 wire drawn to 0.47 strain, pre-notched and subjected to the tensile test at strain rate of 0.001 s^{-1}
Note: Arrow indicates splitting

Examination of the fracture surfaces of drawn 3CR12 steel wire show that longitudinal splitting was partially present only on the highly drawn wires, at 0.47 strain.

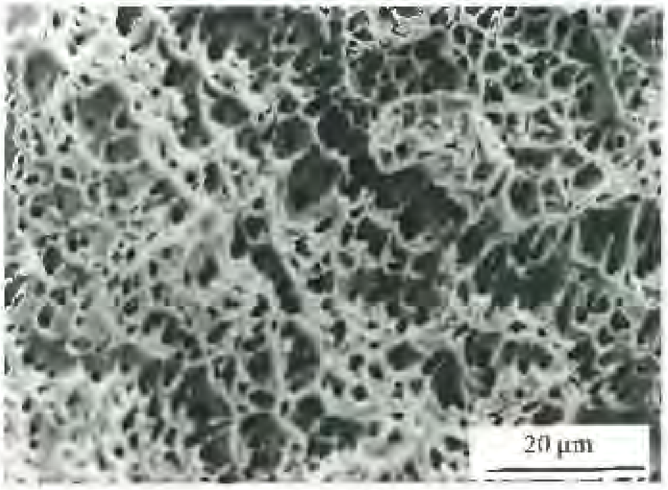

Fig.4.106. *SEM image observed at higher magnification shows the dimples, resulting from microvoid formation and coalescence.*

Fracture mode:
Transgranular ductile mode

4.3.5.2. Fatigue Fractography of 3CR12 Steel Wire

The fatigue crack growth characteristics and the fracture mode of 3CR12 corrosion resistant steel have been examined in terms of the influence of drawing strain between 0.09 and 0.47 subjected to fatigue at two different load ratios of R=0.048 and R=0.22.

Several different fracture modes, such as a fine 'feathery' transgranular appearance - mode A, quasi cleavages mode - B, and mode C - striations were observed.

Figures 4.107.-4.108. show the typical fatigue modes observed in wires drawn to 0.09 strain.

A transgranular ductile mode was observed in both low and high crack growth rate regions. Also, the proportion of intergranular facets is large in the region close to the threshold stress value and they represent slow fatigue propagation.

Fatigue striations have been noticed in the low crack growth region in the lightly drawn 3CR12 steel wires, which is very unusual for this region of the fatigue crack growth. They are usually restricted to small areas, with an approximate size of 15 microns, which corresponds to the size of a grain and very often they are observable in the neighbourhood of the cleavages, Fig.4.108.(a).

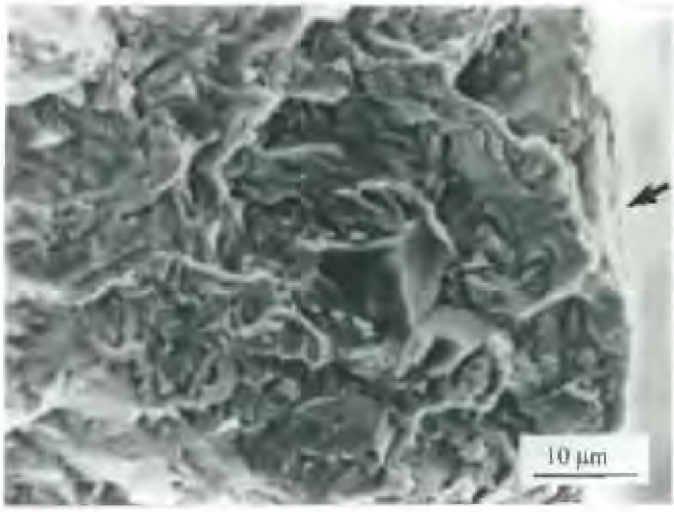

Fig.4.107. *Fracture mode of 3CR12 ferritic steel wire drawn to a low strain of 0.09. SEM micrograph shows the image close to the near-threshold region.* Arrow indicates the notch position.

Load Ratio: R=0.22

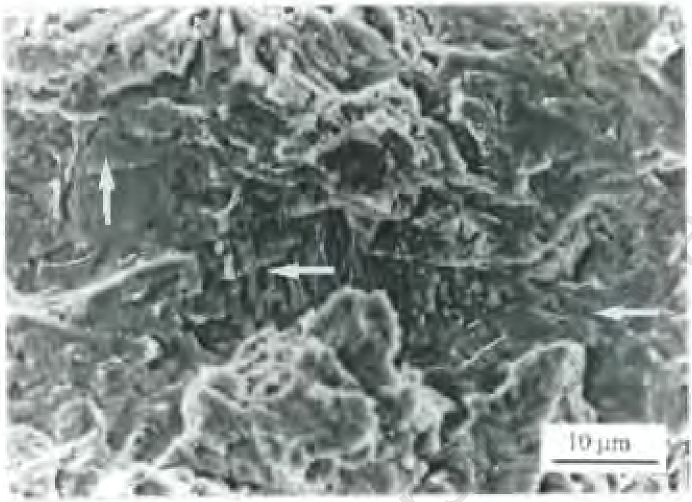

Fig.4.108.(a).*SEM micrograph of 3CR12 drawn wire, taken at* $\Delta K=10$ *[MPa m*$^{1/2}$*]* *-strain=0.09-*

Load Ratio: R=0.048

Fracture modes:
Transgranular ductile-mode A ←
cleavages-mode B ↑
striations-mode C ←

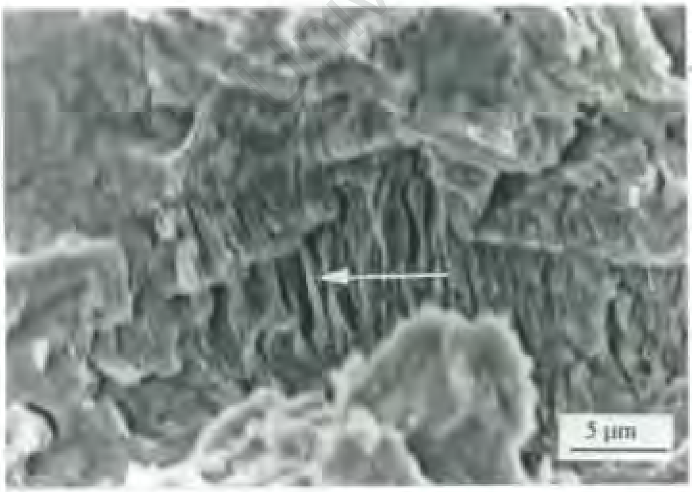

Fig.4.108.(b). *SEM micrograph, at high magnification, showing the 'striation area' developed during fatigue of 3CR12 steel*

Fatigue conditions:
Load Ratio R=0.048
Number of cycles:
N=10,000

Wire specimens drawn to higher strains showed different fatigue fracture modes. The presence of 'cleavages' was also observed in the highly drawn wire samples which were subjected to high cyclic stress (at a load ratio of $R=0.048$) and near-threshold fracture regions are very rough and consist of cleavages and coarse ridges. A transgranular ductile mode was observed in the near-threshold region, when the samples were subjected to a low stress level; for example, at a load ratio of $R=0.22$ and the presence of cleavages was not observed.

The fracture surface of wire tested at a load ratio of $R=0.22$, shows a much smoother appearance particularly in the near-threshold region, where the fatigue crack grows in a ductile manner.

Figures 4.109.-4.110. show the typical fracture surface of wire samples drawn to 0.47 strain, tested at a load ratio of $R=0.048$.

Fig.4.109. *Fractograph taken at position close to threshold*
Fatigue conditions:
Load Ratio $R=0.048$
$\Delta K = 10$ [MPa $m^{1/2}$]
3CR12 steel wire drawn to 0.47 strain
Arrow indicates the direction of the crack propagation
Fracture mode:
Mode A-ductile transgranular
Mode B-cleavages

Two different fracture modes were observed in the near-threshold region of highly drawn wire samples (strain of 0.47): namely, transgranular ductile mode and cleavage. Similar fracture modes were observed in the linear regime of the fatigue crack propagation. Striations were not observed in highly drawn wires in the mid-range of the fatigue crack growth.

Fig.4.110. *SEM micrograph at $\Delta K = 20$ [MPa $m^{1/2}$]*
Load ratio $R = 0.048$
(drawing strain $\varepsilon = 0.47$)

SEM micrograph shows very coarse ridges and cleavages, in the linear regime of the fatigue crack growth rate of 3CR12 steel drawn wire

Figures 4.111.-4.112. show fracture surface of 3CR12 steel wire, at a load ratio of R=0.22. Scanning electron micrographs taken at a position close to the notch shows a smoother fracture surface with transgranular ductile mode, and no cleavages, as shown in Fig.4.111.

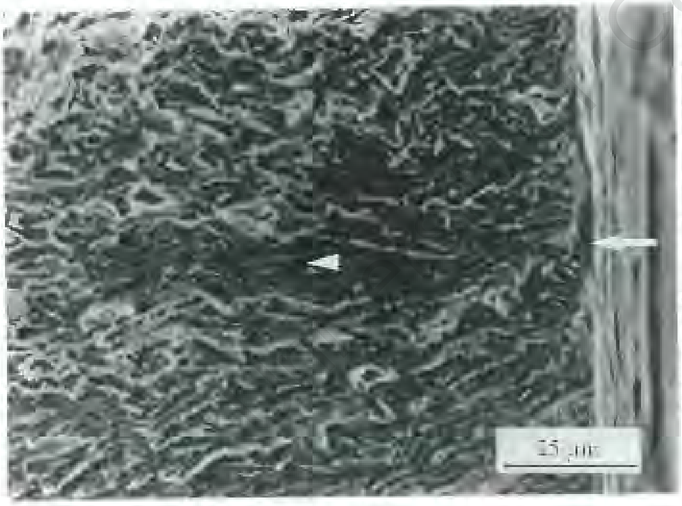

Fig.4.111. *SEM taken at the fracture surface of 3CR12 steel wire drawn to a strain of $\varepsilon = 0.47$*
Load ratio $R = 0.22$
$\Delta K = 10$ [MPa $m^{1/2}$]

Arrow indicates the notch position
mode-A, transgranular ductile mode

Figure 4.112. shows the typical fatigue fracture surface of the drawn 3CR12 steel wire (strain 0.47) in the linear regime of the crack growth rate. Coarse ridges and the presence of the cleavages are characteristics for this region of the fatigue crack propagation. A great similarity was observed between the fracture

appearance of light and hard drawn wires, in the Paris region of the fatigue crack propagation.

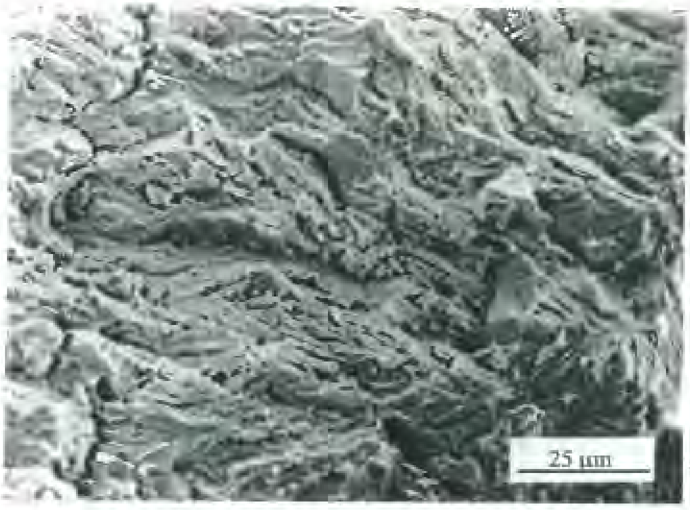

Fig.4.112. *Fracture surface at $\Delta K = 25$ [MPa $m^{1/2}$]*
Load ratio $R = 0.2$
strain 0.47
Arrow indicates the direction of the crack propagation

Fracture mode in the mid-range of the fatigue crack propagation:
coarse ridges and cleavages, similar as load ratio $R = 0.2$-

The fracture surfaces observed on unnotched dual phase 3CR12 steel wire subjected to cyclic strain is shown in Figs.4.113.-4.115.

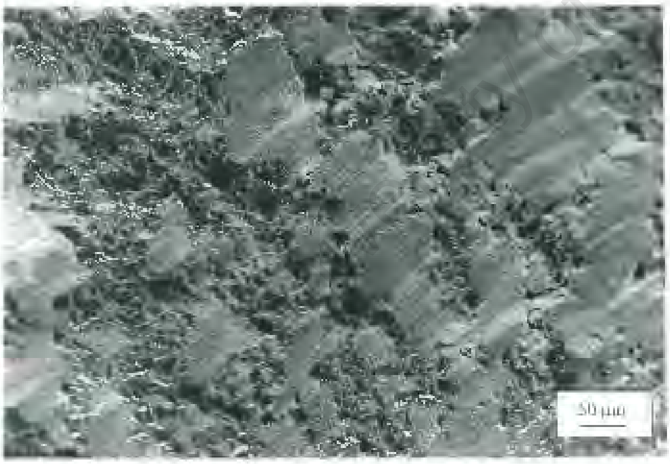

Fig.4.113. *SEM micrograph taken of dual-phase 3CR12 steel wire subjected to cyclic strain*

Conditions:
Smooth 3CR12 steel wire (annealed and quenched at 950^0 C) and fatigued

Region close to fatigue crack initiation shows a large amount of 'tyre tracks'

These micrographs show fracture modes which are very different compared to the modes observed in cold drawn 3CR12 steel wires. Both transgranular ductile fracture together with areas of 'tire tracks' are observed. These 'tyre tracks' have been described in high strength metastable austenitic steels as rubbing marks or striations by other workers [42]. Due to the fact that these features are present to a greater extent in the quenched than the in the drawn condition and that the quenched fatigue strength is significantly higher, it is reasonable to assume that the 'tire tracks' are characteristic of slow crack propagation.

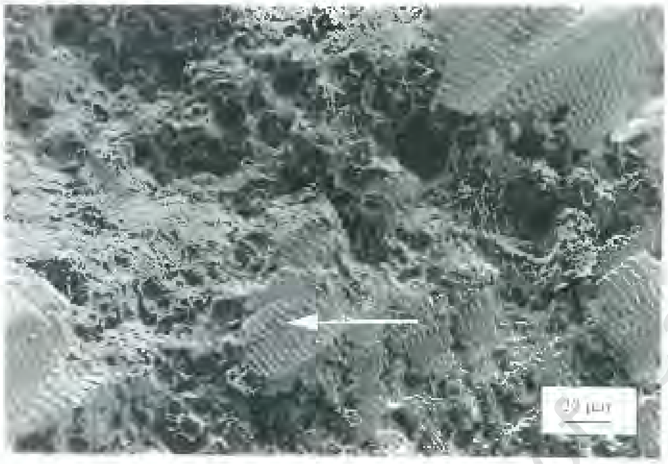

Fig.4.114. *A higher magnification of dual-phase 3CR12 steel wire fractured at the load ratio R = 0.05.*
<u>Fracture modes:</u>
-Typical 'tyre tracks'
-Transgranular ductile mode

Note: Arrow indicates the 'tire tracks' feature

Fig.4.115. *SEM fractograph taken in the higher stress intensity region, showing a very rough appearance.*

<u>Conditions:</u>
Load ratio R = 0.05
N = 160,000 cycles

Fracture mode: mixed (coarse ridges and dimples)

Summary:

It is evident that 3CR12 steel does work-harden during drawing although the high yield to tensile strength ratio indicates the restricted ability of this type of steel to be plastically deformed. Furthermore, the fatigue limit is also enhanced by increased drawing strain, although a certain limitation exists; thus further increase in strain did not influence the fatigue limit significantly, since surface cracking outweighted strength development.

Whilst annealed and drawn 3CR12 steel wire shows a very limited range of fatigue limit values, heat treatment to produce a dual phase microstructure results in much improved fatigue properties.

CHAPTER 5

DISCUSSION

5. Introduction

High carbon pearlitic steel is commonly used in the manufacture of wire ropes. In many cases, the most severe conditions of design loading are cyclic and this fact has given impetus to the study of the fatigue behaviour of these steels. However, the deterioration of steel wire ropes has many different forms, including corrosion, and thus a study of the fatigue behaviour of corrosion resistant steel wires is also of great importance.

The purpose of this study was to evaluate and compare the fatigue performance of three different steels, namely an austenitic AISI 304 stainless steel, a corrosion resistant ferritic steel 3CR12 and a high carbon pearlitic steel, together with the effect of different drawing strains on this performance.

Fatigue testing was performed on individual wire samples, regardless of the more complicated relationship between wires twisted together in the form of rope, in an attempt to elucidate the mechanisms and controlling factors in the fatigue process. It was anticipated that the optimisation of fatigue performance through the control of microstructure in stainless steels would result from this study.

This discussion initially deals with the fatigue behaviour of the individual types of wire and afterwards compares and discusses the advantages of each.

5.1. AISI 304 Stainless Steel Wire

5.1.1. Introduction

Stainless steels based on the iron-chromium-nickel ternary system are extremely important commercial alloys and there is a growing demand for the production of stainless steel wires. Due to its high corrosion resistant properties, high strength, good ductility and toughness, the AISI 304 stainless steel is admirably suited for use in the development of such wires.

The material used in this study was commercially available grade AISI 304 stainless steel in the form of rods, having approximately 18.65% chromium, 8.15% nickel and less than 0.02% carbon. This steel is mechanically metastable and undergoes a partial phase transformation when subjected to sufficient stress or strain.

While there have been many research studies on the influence of the mechanically induced martensite transformation on tensile properties, there is relatively little work that addresses its' effect on fatigue behaviour. Thus, the present study was undertaken to clarify the effect of drawing strain on the fatigue performance of AISI 304 stainless steel wire.

5.1.2. Mechanical Properties

In the present work, as received material was in the form of bars which were annealed at 1050° C for 15 minutes and water cooled afterwards in order to eliminate their previous rolling history and to obtain a fully austenitic structure which had a grain size of 30 μm. The stainless steel rods were repeatedly drawn, without intermediate annealing, to the fixed diameter of 3.5mm at a strain rate of 0.001 s^{-1} at room temperature.

In austenitic steels, there are two interrelated factors, which influence the extent of work hardening and the development of superior mechanical properties:

1. the stacking fault energy of the matrix which is determined by the composition, and
2. the stability of the matrix.

However, the largest effect on work hardening rates is undoubtedly the partial transformation of austenite to martensite. The amount of strain-induced martensite was found to vary from 8% in the wire specimens drawn to 0.09 strain to 36% in the heavily drawn samples to 0.585 strain. This relationship between the drawing strain, the amount of strain-induced martensite and its influence on the mechanical properties is shown in Fig.4.26., p.117.

It is concluded that the yield strength is increased by the drawing process by more than 400%, i.e. from 267 MPa in the annealed condition to 1137 MPa after drawing at 0.585 strain, as a consequence of the increased amount of the α'-martensite phase, up to 36%.

The beneficial effect of the martensite transformation on uniform elongation is due to the inhibition of necking by strain-hardening. It should be noted that wire samples having a high amount of strain-induced martensite showed a substantial decrease in ductility.

It is clear that the strain-induced transformation and amount of the α'-martensite phase has a crucial role in determining the tensile behaviour of metastable AISI 304 stainless steels; improving the tensile properties and decreasing the ductility. Although the strengthening effect of strain-induced martensite is well known, the effect of the martensite phase on the ability of metastable stainless steel to be plastically deformed (uniform elongation, the beginning of necking and total plastic elongation to failure) has to be taken into consideration during forming operations. Thus, the high work hardening rates and large total elongation to failure of austenitic stainless steels are of great importance for wire drawing operations which allow high strength wires to be produced.

5.1.3. Fatigue Behaviour

The influence of the martensite phase transformation on fatigue behaviour has previously been reported in TRIP steels and metastable AISI 304 stainless steels [41-42, 99-103]. The chemical stability of the austenite, the effect of heat treatment on the grain size, the temperature and environmental conditions, all affect the fatigue performance of these steels [39,40, 94-97].

However, the main objective of this study was to explore the potential benefit of deformation-induced martensitic transformation on the fatigue behaviour, and to establish the relationship between the amount of previously developed martensite phase on the fatigue performance of AISI 304 stainless steel wire.

Thus, the present research involved an investigation of both annealed and drawn wires to five different strains, ranging from 0.09 to 0.585. The effect of deformation-induced martensite transformation on the cyclic behaviour is analysed with regard to both the fatigue limit and the fatigue crack growth rate, on pre-notched and smooth wire samples.

Fatigue Limit

Experimental results obtained for both pre-notched and smooth samples show a general trend of increasing fatigue limit with increased strain.

Figure 4.40.,p.132, shows the relationship between the fatigue limit and the drawing strain, for the pre-notched samples, where it can be seen that drawing strain improves the fatigue limit over the entire life range examined. Tests performed on annealed wires show a fatigue limit of 215 MPa, while the fatigue limit of wire drawn to a low strain of 0.09 is improved almost 150% whilst a strain of 0.585 resulted in a fatigue limit of 630 MPa; a total improvement of some 450% over the original fatigue limit of the annealed steel. Thus, the

beneficial effect of drawing strain on the fatigue limit in AISI 304 stainless steel is significant.

Interestingly, the results obtained using the smooth samples (Fig.4.42., p.138) show a higher fatigue limit for all drawn conditions with the exception of annealed wire. The fatigue limit increased from 140 MPa for the annealed condition to 650 MPa as the drawing strain increased to 0.585 strain giving a total improvement of some 465%. It was also observed that the fatigue limit of wires drawn to low strain (0.09) was not influenced by a notch so significantly, and as a consequence the fatigue limits of smooth and pre-notched samples were similar, at 320 MPa.

The higher fatigue limit of the notched samples observed in annealed AISI 304 stainless steel wire is attributed to a number of different factors that are involved during the total process. Notching induces compressive stresses into a region of material around the notch root and also results in small amounts of martensite transformation at the notch tip.

During fatigue a greater percentage of martensite is formed in this region than in the unnotched bulk material and the work hardening rate as a consequence, is different from that in unnotched material. The increased amount of martensite which forms at the notch during fatigue results in rapid work hardening, an increase in strength and a higher fatigue limit than unnotched material.

Consequently, methods used to predict the behaviour of metastable austenitic stainless steels material under cyclic conditions for unnotched specimens have limited applicability.

Although, there has been no systematic investigation of the influence of notches on the fatigue strength of austenitic stainless steels, the data available show that it is less notch sensitive than almost any other metal, although the notch sensitivity is increased if the material is initially cold-worked [114].

The influence of notch geometry, the surface roughness of the notch and the load ratio have also been shown, during this investigation, to play an important role on fatigue life.

It was found that the amount of the α'-martensite phase depends on the notch size, its shape and production method. X-ray diffraction measurements, Figs.4.45.-4.46., showed that a V-shape notch induced a larger amount of α'-martensite phase of approximately 36% while approximately 28% of deformation-induced martensite was found in samples having U-shape notch following the fatigue process outlined in section 4.2.3.3. Also, a greater amount of martensite was found in samples having a bigger notch, as shown in Figs.4.47.-4.48. Further, larger amounts of the martensite phase was found in samples having a notch induced by filing, approximately 28%, whilst only 15% of martensite formed in samples having the same shape and size with notch induced by a cutting wheel. The reason for this is believed to be the higher stress concentration localised at the sharp notch induced by a file, as shown in Figs.4.46.-4.47.

In order to clarify further the material response to the presence of notch, the effect of load force ratios was also investigated. This showed that at the same mean stress, the higher peak stress or higher amplitude induces more martensite phase. Fatigue test results showed that the amplitude of $\sigma_a = 108$ MPa induces approximately 11% of martensite phase while the smaller amplitude of 80 MPa induces only 4% of α'-martensite phase, Fig.4.50., p.147.

Further, the fatigue tests performed at the same minimum stress also indicate that the higher maximum stress (160 MPa) induce the greater amount of martensite phase (28% vs 17%) compared to maximum stress of 100 MPa, Fig.4.55., p.150.

In conclusion, the investigation performed on annealed and drawn AISI 304 stainless steel wire show that is very important to be aware of the effects of stress raisers such as notches. In the case of annealed and low drawn wire, the notch effect is beneficial and increases the fatigue limit. Conversely, the presence of notches reduces the fatigue limit for wires drawn to higher strain, from 0.238 to 0.585 and the fatigue limit reduction factor depends on the amount of deformation-induced martensite formed during the drawing procedure.

Fatigue Crack Propagation Behaviour

The fatigue crack growth behaviour of annealed and drawn wires were also investigated at two load ratios, $R=0.048$ and $R=0.22$.

The experimental results obtained showed that the variation of threshold stress intensity has a direct relationship with the yield strengths of wires drawn to different strains. Figure 4.60. shows that the threshold stress intensity factor increases with increased yield strength. Accordingly, it can be concluded that the direct relationship between the threshold stress intensity factor and the yield strength is attributed to the quantity of the transformation-induced martensite phase. The presence of the martensite inhibits the process for fatigue crack initiation and as a consequence, the threshold stress intensity factor increases.

In the annealed samples, without any prior martensite phase, the fatigue crack initiates easier and the threshold stress intensity value is lower compared to the samples, which contain prior induced martensite. The threshold stress intensity is approximately $\Delta K_{th}=1.0$ MPa $m^{1/2}$ in the annealed samples and $\Delta K_{th}=1.17$ MPa $m^{1/2}$ in the lightly drawn samples (0.09 strain) having 8% of prior induced martensite, both tested at a load ratio of $R=0.22$, Fig.4.60., p.157.

The threshold stress intensity factor showed an increasing trend up to approximately $\Delta K_{th}=15.1$ MPa $m^{1/2}$, corresponding to approximately 32% of the (α') martensite phase. It is significant that the threshold stress intensity for the highly drawn wire (strain 0.585) was much lower ($\Delta K_{th}=9$ MPa $m^{1/2}$), showing that a large amount of strain induced α′-martensite phase (36%), acted deleteriously on the fatigue behaviour promoting rapid crack propagation and brittle behaviour. The deleterious effect of large amounts of α′-martensite phase formation on the fatigue performance is in agreement with the conclusions of Chanani et al and Olson et al for TRIP steel [40,64].

It is apparent from tests at different cyclic load levels that the amount of strain-induced martensite and consequently the level of monotonic yield strength also exerts a strong influence on the threshold stress intensity values and on the near-threshold crack growth rates.

Accordingly, as cyclic strength is increased, either because of high initial monotonic strength or by cyclic hardening, the threshold for fatigue-crack propagation is increased. This phenomenon can be explained by the role of deformation-induced martensite. In drawn wires, the previously developed martensite acts as a barrier for the crack initiation. Further cyclic strain induces more martensite and together with the increased work hardening rate of the dual phase microstructure (austenite and martensite), crack development is more difficult. Thus, the cumulative effect of previously developed martensite together with an increased work hardening rate increases the threshold stress for the fatigue crack initiation. However, in the annealed samples having a fully austenitic microstructure, cracks initiate much easier.

An interesting aspect of the strength effect in the metastable AISI 304 stainless steel is the fact that the threshold ΔK_{th} for fatigue crack initiation and the fatigue limit are increased with increasing strength. Both parameters represent limits for fatigue damage, but the threshold must be regarded as the minimum stress intensity below which long macrocracks do not grow, whereas the fatigue limit is generally the minimum stress below which short macrocracks do not initiate.

Thus, in making recommendations for the selection and suitability of AISI 304 stainless steel drawn wires to withstand low or high-amplitude cyclic loading, the influence of deformation-induced martensite transformation has been clearly established.

Thus, the austenite to martensite transformation in metastable AISI 304 stainless steel has been shown to play a beneficial role on the tensile monotonic properties and the high cycle fatigue limit. However, the results also show that the transformation does not always play a beneficial role in the fatigue process. It was observed that the martensite formed during the fatigue process acts beneficially in the case of lightly drawn AISI 304 stainless steel wires having less than 20% of prior-induced martensite phase (formed during the drawing process). The martensite delays crack initiation and additionally blunts and retards fatigue crack propagation. More than 20% of the strain-induced martensite phase promotes very rapid crack propagation, although the rate of fatigue crack propagation depends on the amount of the previously developed martensite. Consequently, the influence of the martensite transformation during the fatigue process depends on the amount of previously developed martensite during the drawing process.

Fatigue crack propagation is the result of the cumulative damage caused by cyclic strain of the material at the crack tip. The material at some point ahead of the crack tip experiences increasing strain amplitudes as the crack propagates toward that point and the cumulative strain is very high. The high cyclic plastic strain causes martensite to form in the austenite matrix, which surrounds the propagating crack and increases the effective strain-hardening rate.

In the high strength AISI 304 stainless steel wires, having more than 20% of α'-martensite phase, the number of cycles to cause fatigue failure is drastically decreased. A large amount of martensite changes the properties of the steel by promoting more brittle behaviour, and it is also possible that the deformation-induced martensite gave rise to more crack initiation sites.

It was also observed that the austenite to martensite transformation has a saturation character which is approximately 40%. It appears that for both cases, in the smooth and pre-notched specimens, the martensite phase saturation point can be reached either by a large amount of deformation-induced martensite (higher drawing strain induces a larger amount of martensite) with additional martensite formed by cyclic strain, or alternatively having a smaller amount of prior-induced martensite and a larger amount of martensite as a consequence of the cyclic strain.

5.1.4. Fatigue Fractography

A comparison between static and fatigue fracture surfaces showed that they are very different. Under quasi-static loading of the tensile test, considerable plastic flow of the metal precedes fracture and the fracture surface has a characteristic fibrous appearance. A fatigue crack, however, appears entirely different. The crack begins at a surface, often at the point of high stress concentration. Once the crack begins, the crack itself forms an area of even high stress concentration and it proceeds to propagate progressively with each application of load until the remaining stressed area finally becomes so small that it cannot support the load statically and fast fracture results.

Fractographic studies also showed that the sigmoidal variation of crack growth rate (da/dN) with stress intensity factor ΔK can be characterised in terms of different primary fracture mechanisms.

In the slow crack growth region (near-threshold region), the crack growth is sensitive to microstructure and load ratio and the formation of crystallographic facets are observed. The fracture morphology of near-threshold failure of annealed samples and samples drawn to low strains, consists of a flat, ductile transgranular mode with isolated segments of integranular separation, Figs.4.77.-4.79. Close to the threshold, the proportion of intergranular facets is small, increasing to a maximum and then gradually diminishing at high stress intensities. Significant numbers of intergranular facets were observed in the annealed samples and the samples having low strength. The high strength samples fractured in a completely ductile mode without intergranular separation, Fig.4.80., p.177.

The development of the facets was associated with a change from 'microstructure insensitive' to 'microstructure sensitive' crack growth and a transition from mode A to mode B.

For the mid-range of growth rate (regime B), failure is generally characterised by little influence of the microstructure and load ratio R on crack growth. In this regime of crack growth rate, failure occurs by a transgranular ductile striation mechanism, Fig.4.82, p.178. Striations are particularly well defined in the hard drawn stainless steel wire.

At higher growth rates (regime C), when K_{max} approaches K_{IC}, growth rates become extremely sensitive to both microstructure and the mean stress due to a departure from striation growth to a static fracture mode, such as a ductile fracture mode. Areas of microvoid coalescence were present in all structures.

In summary, the fatigue fractographic results of drawn AISI 304 stainless steel wires show that the low and high strength wires fractured by different modes; the low strength wires fractured in a ductile manner, while the high strength wires, having approximately 36% martensite, formed during drawing, fractured in a predominantly brittle manner.

5.1.5. Changes caused by Cyclic Strain

It was found that the annealed samples and lightly drawn wire samples were significantly hardened by any subsequent cyclic strain. For example, the hardness of the annealed samples is increased from 180 HV25 to 295 HV 25 following fatigue (load ratio R=0.048 and N=120,00 cycles), whilst in the highly drawn wire samples the hardness increases are very small or negligible, Fig.4.65. Accordingly, the monotonic mechanical properties were increased and this improvement depends on the duration of the fatigue process and maximum stress level, σ_{max}.

Cyclic hardening is attributed to the austenite to martensite transformation and to work hardening of both phases caused by subsequent fatigue. An investigation of the martensite phase transformation induced by fatigue was performed using X-ray diffraction techniques and the results showed that the fatigue process induced approximately 11% of α'-martensite phase in annealed AISI 304 stainless steel wires subjected to fatigue at a load ratio R=0.048 and 120,000 cycles. However, the X-ray diffraction technique was not sensitive enough to determine the amount of martensite formed during the fatigue process in highly drawn wire samples containing larger amounts of martensite.

The changes in microstructure were observed using the light optical microscopy and transmission electron microscopy. Optical micrographs show a higher rate of slip line formation; more slip lines and bands are distinct and present in numerous grains, Fig.4.67.(a). The dislocation structure in the immediate vicinity of the fracture, Fig.4.70., shows a high dislocation density and the tendency to develop a rough cell structure.

Nevertheless, the changes in the stress-strain response of a material due to cyclic deformation are of importance, especially in relation to the response of a crack tip. Cyclic hardening of a material will modify the opening/closing behaviour of a crack tip and consequently its crack growth rate. It can be considered that in the lightly drawn wire samples the formation of martensite at the crack blunts the crack tip and retards the growth process, although in the hard drawn wires, the martensite transformation promotes very rapid crack propagation; the crack propagation rate depends on the amount of previously developed martensite.

These results are particularly significant for the design of metastable austenitic stainless steels with improved resistance to high cycle fatigue damage, since the optimum microstructures will depend upon whether the structural design is to be based on the initiation or propagation of a 'fatal flaw'. For example, if the high strength properties are important for a particular structure, the designer should take into consideration the amount of prior martensite since the additional martensite that forms as a consequence of cyclic strain might lead to catastrophic failure in a very short period of time. Further, if the crack initiation is critical from design point of view, the presence of the martensite phase is more than desirable, since martensite delays crack initiation in cyclic conditions.

5.2. 3CR12-Ferritic Corrosion Resistant Steel

5.2.1. Introduction

3CR12 is a corrosion resistant alloy containing approximately 11% chromium and less than 0.1% carbon by weight. In the as received or normalised state the alloy has a duplex phase structure containing islands of low carbon martensite in a ferritic matrix whilst in the annealed state if has a fully ferritic structure.

It was originally developed as a direct replacement for mild steel structural applications for conditions which were mildly corrosive. Whilst much is known about the mechanical, chemical and other characteristics of 3CR12, little has been established on its fatigue behaviour or indeed on its drawability for use as wires. This work is an attempt to redress this balance.

5.2.2. Mechanical Behaviour

In the present work, the as received material was in the form of reinforcing bar which was annealed at 760^0 C for 30 minutes to produce a fully ferritic structure with a grain size of 15 μm. It was found that this structure exhibited a very high work hardening rate and that small amounts of strain reduced the ability of the material to be plastically deformed quite dramatically. A strain of 0.09, for example, reduced the tensile plastic elongation to failure from 27 to 4%; a decrease of some 85%. Whilst deformation increases the tensile strength of 3CR12 significantly from approximately 400 MPa to 700 MPa for a strain of 0.47, it also results in a high ratio of yield strength to tensile strength in excess of 0.9. Further, the onset of necking was found to occur at very low strain values, as shown in Fig.4.92., p.187, which additionally indicates the reduced ability of the material to be plastically deformed. Such behaviour contrasts strongly with that of the austenitic AISI 304 stainless steel, which exhibited good plasticity at all levels of prior strain and high strength levels.

It is no surprise therefore to find that 3CR12 is an extremely difficult material to draw into wires whilst maintaining enhanced strength levels. This inability to be drawn to high values of strain also lead to the development of significant surface flaws, which in turn are expected to lower any fatigue performance.

5.2.3. Fatigue Behaviour

As noted earlier, the fatigue behaviour of 3CR12 steel has not yet been established. Thus, one of the main foci of this study was to evaluate the relationship between the drawing strain and fatigue performance of 3CR12 drawn steel wires. The effect of drawing strain on the cyclic behaviour was analysed with regard to the fatigue limit using both pre-notched and smooth wire samples. The influence of heat treatment was also investigated.

Fatigue Limit

It was found that the fatigue limit of 3CR12 steel improves with increased drawing strain and that small amounts of strain increased the fatigue limit significantly, Fig.4.101., p.196. The fatigue limit of annealed 3CR12 of 130 MPa (maximum fatigue cyclic stress), was nearly doubled with 0.09 prior strain to 230 MPa. However, further straining had only a small further influence on the fatigue limit. For example, a fatigue limit of 300 MPa was obtained by drawing to 0.37 strain, and only 310 MPa by further drawing to 0.47 strain. The small increase of the fatigue limit in the highly drawn 3CR12 wires is clearly due to the limited ability of these wires to work-harden further.

It also was found that cyclic hardening, attributed to the rapid work hardening of the ferrite matrix, was more significant in the annealed and low strength 3CR12 steel wires.

In order to investigate the possibility of improving the fatigue strength of 3CR12 steel wires, the specimens were heat treated (quenched from 950^0 C in oil). The investigation showed that the presence of small islands of martensite in the microstructure acts beneficially and the fatigue limit was improved by approximately 400% compared to the annealed condition. The ferrite/martensite matrix also showed a better resistance to fatigue crack initiation started from a notch. As a consequence the fatigue limit of notched specimens was not reduced significantly; the fatigue limit is slightly lower (470 MPa) compared to the fatigue strength of un-notched specimens. This fact is a very important and the combination of heat treatment and drawing needs to be further investigated.

5.2.4. Fatigue Fractography

It was observed that the fatigue fracture surfaces show different characteristics in the near-threshold compared to the linear regime of crack growth. Further, the fatigue fracture surfaces are different in the low and high strength 3CR12 steel wires and a number of different fracture modes were identified, namely: ductile transgranular cracking, striation formation and quasi-cleavage.

In the near-threshold regime, the crack growth is strongly influenced by microstructure and load ratio which is directly related to a change in fracture mode.

The fatigue fracture morphology of the low strength 3CR12 wires, observed at the load ratio of $R=0.048$, is complex and consists of ductile transgranular cracking (feathery appearance), quasi-cleavage and striation formation.

Cleavage-like growth of fatigue cracks along grain boundaries and through grains has been observed in the low strength 3CR12 steel wires and they exhibit slow progressive failure rather than a brittle separation. In Fig.4.108.b), quasicleavage areas can be observed along with a region resembling fatigue striations. Similar observations have been reported in fatigued TRIP steel, by Chanani [42].

They suggested that these 'fatigue striations' are apparently rubbing marks similar to the 'tire tracks' observed on low cycle fatigue fracture surfaces.

Conversely, more detailed studies of striations in 3CR12 steel revealed that well-resolved striations exist in a few isolated grains, with randomly orientated deformation marks in surrounding grains. The appearance of 'tire tracks' become very significant in quenched and fatigued 3CR12 steel wire. The proportion of these features is dominant in the threshold region resulting in slow crack propagation in this region.

However, the appearance of the fatigue fracture surfaces of highly drawn wires investigated in the near-threshold regime, is strongly influenced by the load ratio. At the load ratio $R=0.048$ the fatigue fracture surface consists of a ductile transgranular mode with very coarse ridges consisting of a very rough topography, Fig.4.110. Conversely, the mode of the fatigue fracture at a load force ratio of $R=0.22$ is ductile transgranular and shows a very smooth appearance, Fig.4.111.

These results are in agreement with general facts that the microstructure and load ratio has only a minor influence on the fracture mode in the linear regime of crack growth. For both the low and high strength wires, investigated at the load ratios of $R=0.048$ and $R=0.22$ the fatigue fracture surfaces consists of a mixed mode of ductile transgranular and coarse ridges.

It is well known that the microstructure of an alloy influences the growth rates of large fatigue cracks to the maximum extent in the near-threshold region. Cyclic plastic deformation of the material during this period increases the densities of dislocations. When the densities of dislocations reach critical values, the crack will start to propagate. This transition from the near-threshold regime to the intermediate stage of fatigue crack growth is accompanied by a noticeable change from a 'microstructure-sensitive' to 'microstructure-insensitive' behaviour.

A characteristic of fatigue cracks is the sequence with which they open as the load is increased from a minimum. For large fatigue cracks under constant amplitude loading, the ratio of the crack tip opening to maximum load depends on the stress intensity factor [18]. The crack closure effect is different, depending on factors such as crack size, cycling loading conditions and environment. These differences are important, since the level of closure strongly affects the materials ability to translate the macroscopic application of load to the local stress driving the crack.

The mechanism by which the microstructure breaks down at a fatigue crack tip, resulting in a crack advance, is the key element connecting damage of the material with fatigue failure modes. The phase transformation of austenite to martensite and the work hardening mechanism are involved in the fatigue cracking of AISI 304 stainless steel whilst in a pearlitic steel and 3CR12 steel only the work hardening mechanism is involved to different extents.

A comparison between the fracture modes observed on the static tensile and fatigue fracture surfaces shows that their static tensile fractures are always ductile for 3CR12 steel wires, regardless of their mechanical properties. Fatigue conditions change the topography of the fracture surfaces and a ductile transgranular mode, quasi-cleavage and striations formations are modes of fatigue failure in the low strength 3CR12 steel wires. High strength 3CR12 wires fractures in a ductile mode together with very rough coarse ridges. The heat treated (quenched) 3CR12 wires also show ductile fatigue fracture surfaces with the presence of characteristic 'tire tracks' features.

5.2.5. Changes caused by cyclic strain

A cyclic hardening effect was observed in the 3CR12 steel, particularly in the annealed and lightly drawn condition. The influence of fatigue on the cyclic tensile properties is seen in Fig.4.102. and Table 4.16. The yield strength was increased from 250 MPa in the annealed condition to 306 MPa, or approximately 25%, after being subjected to fatigue at a load ratio of R=0.22 and a number of cycles N=120,000. The same fatigue conditions increase the ultimate tensile strength by approximately 5% and the work-hardening effect influences the strain at which the necking point occurs.

Further evidence of the strong work hardening effect that occurs in 3CR12 steel is the change in hardness. The hardness of the annealed samples is increased from 150 HV25 to 180 HV25 during fatigue performed at a load ratio of R=0.22 and N=120,000 cycles. The hardening affects the beginning of necking (at the yield point) and as a consequence, the elongation to failure was reduced. Hardness changes were not detected in the highly drawn wire samples, for example in the samples drawn to 0.47 strain.

Microstructure changes were not detected either by optical microscopy or by X-ray diffraction. Further, no significant changes were observed in the dislocation structure of 3CR12 steel subjected to fatigue. This can be explained by the restriction to further dislocation movement which is imposed by high density dislocations.

In conclusion, the corrosion resistance of 3CR12 steel is an undoubted advantage in comparison to mild steel, although the low fracture toughness and limited drawing ability are of the main concern. Further, results obtained from the fatigue study of 3CR12 steel suggest that the use of this steel in the form of wire is restricted to lower strength applications.

However, the experimental results also show that the application of heat treatment significantly improves the fatigue strength of 3CR12 steel, and thus further investigations need to be carried out.

5.3. High Carbon Steel Wire

5.3.1. Introduction

High carbon pearlitic steel is an alloy containing approximately 0.8 % carbon by weight, which in the as received or drawn condition has a fully pearlitic microstructure. The high strength of pearlitic steel wire results from a combination of the inherent 'as patented' strength of the steel and further strengthening due to the work hardening. The main parameters affecting the tensile strength of the pearlitic steel wire are the carbon content, the transformation temperature and most importantly, the amount of cold deformation. The initial ultimate tensile strength of 1300 MPa, obtained after patenting, is increased to more than 2000 MPa by subsequent drawing.

High carbon pearlitic steel in the form of wire has been widely investigated, thus the influence of factors affecting the microstructure evolution, the static mechanical and fatigue behaviour are very well known. This study performed on high carbon pearlitic steel has been undertaken for comparative purposes, namely to compare the results obtained on the commercial wire with the results obtained by other authors and also to compare the fatigue behaviour of pearlitic steel with AISI 304 stainless steel and 3CR12 corrosion resistant steel wires.

5.3.2. Fatigue Behaviour

This study has confirmed that among the many factors influencing the cyclic deformation, the surface finish, the stress levels, cyclic amplitude and load ratio R, the microstructure and the yield strength are of major importance influencing the fatigue behaviour of high carbon steel wire.

It was observed that the drawn pearlitic steel wire investigated had a very poor surface quality. Surface defects, such as longitudinal scratches, pits and non-metallic inclusions were present which have a detrimental effect, leading to early crack initiation and reduced fatigue performance. The experimental results show that the fatigue limit of approximately 250 MPa (stress amplitude) at mean stress of 550 MPa, is very low compared to the extremely high monotonic properties of pearlitic steel.

These results do, however, illustrate the structure sensitivity of fatigue properties, compared with tensile properties, and that the fatigue behaviour is closely related to notch sensitivity. This can be explained by the fact that by notching, fatigue is characterised by early crack initiation and that the fatigue strength of this steel is dominated by crack propagation. Higher strength materials do not have advantages in reducing the rate of crack propagation and thus they usually have a higher notch sensitivity [37].

The high notch sensitivity of this steel was confirmed during the notched fatigue testing of the wire. The fatigue limit of pre-notched wire samples showed a fatigue limit of only 80 MPa (stress amplitude), at the same mean stress of 550 MPa as the unnotched sample. The reason for such behaviour is explained by the sensitivity of the pearlitic microstructure to a notch effect. It has been found that the pearlitic microstructure and especially the cementite lamellae are very sensitive to the notch effect, making the high mechanical properties of this steel less valuable during fatigue conditions [37]. Sensitivity to the notch effect is attributed to the extremely hard and brittle cementite lamellae.

This illustrates that the microstructure does not control the crack initiation but rather that the notch itself is a controlling factor in the fatigue process. Such data shows the inadequacy of using notched specimens to study microstructural effects on crack initiation.

In order to improve the fatigue limit of pearlitic steel wire in this study both shot peening and polishing of the surface were employed. It was found that both methods increased the fatigue limit properties, although the reasons for the improvement are different. The increase in fatigue limit caused by shot peening is associated with the introduction of residual compressive stresses and increased hardness in the surface layer, whilst the beneficial effect of polishing is due to better surface quality.

During shot peening, the steel balls impact the surface with a very high kinetic energy, which is then converted to a highly localised force on impact. The material on the surface is stressed above its yield strength during each impact so that plastic deformation occurs, leading to the formation of a rough topography. On the microscale, shot peening, like any other cold working process, greatly increases the dislocation density, and at the same time produces various forms of barriers, such as forest dislocations, jogs and pile-ups. To attain further plastic deformation, the dislocations must move across these barriers and against the i) the internal elastic stresses from the forest dislocations, ii) the long range stresses from groups of dislocations piled-up behind barriers, and iii) the frictional resistance of jogs; thus, a higher stress is required [124]. This is the basic theory for work hardening in metals and alloys.

The development of compressive residual stresses in a shot peened surface depends upon the plastic deformation of the surface, which tends to expand and seek to occupy more space. However it is restrained by the adjacent undeformed material and as a result, compressive residual stresses are produced in the surface layer. The level of compressive residual stresses induced by shot peening were experimentally determined and calculated according to the procedure presented in Chapter 3.

It was found that shot peening results in compressive residual stresses to a depth of 50 μm with a magnitude up to –780 MPa (at 25 μm below the surface), Fig.4.11, p.101 and produces a remarkable increase in the fatigue limit of the pearlitic steel. The total stress amplitude fatigue limit at 10^6 cycle is increased from 500 MPa to 700 MPa, i.e. approximately by 40% (Fig.4.9b), despite an increase in surface roughness from $R_a = 1.6$ to $R_a = 1.9$ microns. It is normally expected that as the surface roughness increases the fatigue performance will decline since crack initiation is expected to be easier.

Surface polishing was found to result in a large decrease in surface roughness, from $R_a = 1.6$ to $R_a = 0.3$ microns and this improved the fatigue limit by approximately 24%, i.e. the fatigue limit was increased from 500 MPa to 620 MPa (total amplitude), at a mean stress of 550 MPa. The beneficial influence of polishing is attributed to the better surface quality obtained by eliminating the surface defects or stress concentrators.

5.3.3. Fatigue Fractography

Fractographic studies performed on the pearlitic steel wire revealed the following observations. The crack always initiates from a surface flaw and following this initial period, which is under shear stress control, the cracks changed orientation to become perpendicular to the load axis, Fig.4.15., p.106. Normally, only one crack was associated with fatigue failure. The size of the crack initiation region was comparable to the size of the austenite grain, approximately 20 μm.

A detailed examination of the main crack shows that the cracks tend to propagate through the pearlite colonies at approximately right angles, whilst less commonly the cracks propagate parallel to the cementite lamelle.

The transition from shear stress to normal stress-controlled crack propagation resulted in an increase in fracture roughness. The fatigue fracture surfaces suggest that crack propagation occurs by interlamellar cracking ahead of the main crack followed by tearing across the damaged region.

5.3.4. Changes caused by the Fatigue Process

Cyclic deformation behaviour in high carbon pearlitic steels is known to depend strongly on the interlamellar spacing. Steels with fine interlamellar spacing show only cyclic softening. With medium interlamellar carbide spacing, cyclic softening at low strain amplitudes and hardening at high strain amplitudes were observed. Coarse pearlite exhibited only cyclic hardening throughout the entire range of strain amplitudes investigated [37,36].

In this study the high carbon steel showed a very stable microstructure and only slight softening was observed under the load controlled fatigue process. The steel had a interlamellar spacing of approximately 45nm and the small interlamellar spacing requires a higher stress for the dislocation generation.

Cyclic deformation appears to increase further the mobile dislocation density relative to monotonic deformation and results in softening. It is suggested that the small interlamellar spacing also limits the number of operating slip systems, reducing hardening due to dislocation-dislocation interactions, and thus limits the driving force to form cell boundaries. The results of this study confirm the findings of other authors' [37,36].

5.4. Comparative Discussion

This part of the discussion attempts to compare the differences and similarities in behaviour of the three steels investigated in this study, AISI 304 austenitic stainless steel, 3CR12 corrosion resistant steel and a high carbon pearlitic steel.
All of them have their own characteristics, advantages and disadvantages and the differences in their fatigue performance with respect to the different drawing strains were especially investigated in this study.
The critical characteristics and differences, which have been identified during performing of this study, are as follows:

1. *Mechanical properties and work-hardening rate*
2. *Microstructure*
3. *Fatigue properties*
4. *Fatigue mechanisms*
5. *Changes caused by fatigue, and*
6. *Fractography.*

There are discussed in turn from a comparative viewpoint in this section 5.4.

Mechanical Properties and Work-Hardening

It is known that the metals having an fcc cubic structure show a greater work hardening rate than metals having a bcc structure. Thus, it is apparent that annealed AISI 304 austenitic stainless steel has a greater work-hardening potential and consequently the ability to be plastically deformed. In addition, austenitic stainless steel is metastable and undergo a phase transformation during plastic deformation. Consequently, the total work-hardening of this steel is attributed to the work hardening of the austenite phase, the austenite to martensite transformation together with the work-hardening of the mixed microstructure. This work hardening ability of metastable austenitic stainless steel was utilized in the drawing process in order to obtain high mechanical properties; the maximum ultimate tensile strength achieved in laboratory drawn wires at a strain of 0.585, was 1346 MPa.

High carbon steel, having a bcc cubic structure, also shows a high work hardening rate due to the combination of plastic deformation and heat treatment. This eutectoid steel has a fully pearlitic microstructure consisting of ferrite and cementite lamellae. When these steels are subjected to drawing to increase the yield and ultimate tensile strength, the work hardening mechanism activates. The static properties, particularly the yield strength, are proportional to the interlamellar spacing [37]. Thus, wire obtained by patenting and cold drawing (1.86 strain) achieves an ultimate tensile strength of 1982 MPa.

The mechanical properties of 3CR12 steel are characterised by a high yield strength to tensile strength ratio compared to lower ratios in AISI 304 stainless steel and pearlitic steels, and thus indicate the restricted ability of 3CR12 steel to be plastically deformed. The maximum ultimate tensile strength achieved at the highest strain applied in laboratory conditions of 0.68 strain is 738 MPa.

Generally, the bcc metals work harden to a lesser extent than fcc metals. However, whilst high carbon steel with a pearlitic lamellar structure and fully ferritic 3CR12 steel, have the same bcc crystal structure, there is a great difference in the strain hardening rate of these steels. The distance between carbide lamellae determines the dislocation multiplication in pearlitic steel.

It is known that strain hardening is caused by dislocations interacting with each other and with barriers which impede their motion through the crystal lattice [57]. The high preponderance of barriers results in high work hardening rates in pearlitic steels. The absence of a large number of barriers to pile-up of dislocations in 3CR12 steel results in a lower strain hardening rate compared to that in the pearlitic steel.

Microstructure

It is apparent that steels used in this investigation have different microstructures. The microstructure of AISI 304 stainless steel wire consists of an austenite matrix and different amounts of the martensite phase induced by plastic deformation; a higher drawing strain induces a higher amount of the α'-martensite phase. The formation of martensite as a consequence of cyclic strain is dependent on the amount of previously developed martensite, which in turn affects fatigue behaviour. Namely, the formation of α'-martensite by cyclic straining acts beneficially in low strength wires (having a small amount of α'-martensite phase), by delaying and retarding crack initiation, while in the highly drawn steel wires (containing a higher amount of original martensite phase) the martensite acts deleteriously by promoting rapid crack propagation.

Eutectoid pearlitic microstructure is a composite mictostructure consisting of a very fine cementite lamellae and ferrite matrix. Experimental results show that the fine pearlitic microstructure acts beneficially on the fatigue limit; the high fatigue strength is attributed to the fine pearlitic microstructure, i.e. to a small interlamellar spacing.

The microstructure of cold drawn 3CR12 steel is fully ferritic and it does not undergo a phase transformation during the drawing process. The change in microstructure from fully ferritic to dual-phase microstructure (martensite and ferrite) by heat treatment (quenching from 950^0 C in oil) improves the fatigue strength significantly. Also, notches do not reduce the fatigue strength significantly of the dual-phase microstructure as they do in the fully ferritic matrix. The presence of martensite islands in the ferritic matrix acts in a similar manner to the carbide lamellae in the pearlitic steel or austenite/martensite microstructure in AISI 304 stainless steel. The martensite phase is an effective barrier to dislocation movement and thus crack initiation.

Fatigue Properties

Table 5.1. summarises the experimental data obtained for wire samples of AISI 304 stainless steel, 3CR12 steel both drawn to different strains ranging from 0.09 to 0.6, together with the results of a high carbon steel investigated in as received condition (drawn to 1.86 strain by Haggie-Rand).

The results show that the highest fatigue limit was observed in the high carbon steel wire in spite of the low fatigue ratio (0.4) between the fatigue limit and yield strength. This value indicates that the fatigue limit of high carbon steel wire is low compared to its exceptional high monotonic strength properties. The presence of the non-metallic inclusions in the steel and a very poor surface containing deep grooves, corrosion pits and deposits remaining from the wire coating are considered to be the main reasons for such behaviour since they act as stress raisers and encourage crack initiation.

The table also indicates that increasing drawing strain to 0.585 also improves the fatigue limit of both notched and smooth AISI 304 stainless steel wires to approximately 650 MPa. The experimental results also show that the fatigue limit of notched (annealed) samples is a higher compared to the unnotched fatigue limit. This phenomenon is explained by the influence of notches on the extent of martensite transformation. Martensite forms preferentially at stress sites, such as notches, raising strength levels, work hardening rates and improving fatigue behaviour. Sharper and deeper notches induce a higher amount of the martensite phase.

It should be mentioned that another important parameter that influences the fatigue performance of AISI 304 stainless steel is the load force ratio. It was established that more martensite was induced by mean peak stresses associated with a load ratio of $R=0.048$ than to lower peak stresses associated with a load ratio of $R=0.22$.

Table 5.1. *Static and Fatigue Properties of AISI 304 Stainless Steel, High Carbon and 3CR12 Steel Wires*

Steel Wire	**Drawing Strain**	**Static Mechanical Properties**				**Smooth Fatigue Limit**	**Notched Fatigue Limit**	**Changes after Fatigue**
	ε	**UTS** [MPa]	**Yield** [MPa]	**Hardness** HV 25	**Microstructure**	σ_{max} [MPa]	σ_{max} [MPa]	
High Carbon Steel Drawn	1.82	1982	1546	465	Pearlite	800	630	Slight Softening
AISI 304 Steel								
Annealed	0	642	267	180	Austenite	140	215	Hardened
Drawn	0.09	752	480	192	$\gamma+\alpha'$-8%	320	320	Hardened
Drawn	0.238	941	810	310	$\gamma+\alpha'$-16%	471	420	Hardened
Drawn	0.37	1060	995	360	$\gamma+\alpha'$-20%	498	460	Hardened
Drawn	0.52	1247	1100	410	$\gamma+\alpha'$-32%	610	503	Hardened
Drawn	0.585	1346	1137	465	$\gamma+\alpha'$-36%	650	630	Hardened
Drawn	Comm.	1550	1260	465	$\gamma+\alpha'$-10%	660	650	None
3CR12 Steel								
Annealed	0	442	250	150	Ferrite		130	Hardened
Drawn	0.09	516	469	183	Ferrite		230	Hardened
Drawn	0.37	635	603	220	Ferrite		300	Hardened
Drawn	0.47	647	607	234	Ferrite		310	Hardened
Drawn	0.68	738	687	246	Ferrite		-	
Quenched	0			246	Mart.+Ferrite	480	470	None

The results also show that the maximum stress during each cycle is the factor which most significantly influences the extent of martensite transformation, higher mean stresses induces more martensite which retards crack initiation and improves fatigue lives.

In 3CR12 steel wire, the fatigue limit is improved with increased drawing strain and small amounts of strain increase the fatigue limit significantly. However, further drawing above 0.47 strain has no significant influence on the mechanical properties and fatigue limit.

The heat treatment (quenching) of 3CR12 steel changes the initial (ferritic) to dual-phase microstructure (martensite and ferrite) which results in increased fatigue strength of 480 MPa. The fatigue strength improvement is attributed to the higher strength properties which delay crack initiation.

The mechanisms involved in fatigue crack initiation and propagation

The mechanisms involved in fatigue crack initiation and propagation in a pearlitic steel as a composite material, AISI 304 austenitic stainless steel and 3CR12 ferritic steel are discussed in this section.

Experimental data show that the work hardening mechanisms and martensite phase transformation play a crucial role in determining fatigue behaviour. The work hardening effect is significant in high carbon steel, while the work hardening, together with martensite phase transformation, determine the fatigue behaviour of the AISI 304 stainless steel. 3CR12 steel does not undergo a phase transformation under plastic deformation and furthermore the work hardening rate is relatively low.

In the discussion to follow, the mechanisms involved are discussed separately for each material, followed by an hypothesis proposed in order to explain the specific role of martensite transformation on the fatigue behaviour of metastable austenitic steels.

High Carbon Steel

It is generally agreed that the strength of fully pearlitic eutectoid steel is controlled microstructurally by the pearlite interlamellar spacing [38]. The high strength is attributed to the small interlamellar spacing, thus the fatigue properties are also influenced by this microstructural parameter.

The large number of cycles necessary before a crack was observed on the surface is consistent with current theories of accumulated dislocation damage leading to cracks. The manner by which microstructural refinement, especially decreasing the interlamellar spacing, increases the fatigue limit is believed to be linked to the role of dislocations in crack initiation.

The mechanism of sufficient dislocations piling up at an obstacle to activate a dislocation avalanche, causing slip-band formation, inclusion cracking, or decohesion at a second phase-matrix interface essentially depends on the slip length. Smaller mean free paths, with corresponding reductions in the magnitude of local plastic strain, reduce the ease of crack initiation and result in increased fatigue strength. Refining the interlamellar spacing should reduce the pile-up stress, thereby reducing the stress which could cause a cementite plate to fail. This explanation is consistent with the demonstration of Rosenfield et al, as stated by Gray [37], which showed that carbide lamellae are effective barriers to dislocation motion. This argument is additionally consistent with several theories of crack initiation in pearlite which require the stress build-up at the ferrite-carbide interface to be large enough to cleave the carbide lamellae [37].

Research performed on the characterisation of the effect of microstructure on the fatigue crack initiation in high carbon steel has shown a direct correlation between fatigue resistance and yield strength or interlamellar distance. The high fatigue strength of this steel is attributed to the high work hardening rate as a consequence of the combined heat treatment and high drawing strain lowering the interlamellar spacing at the pearlite.

However, the work hardening mechanism has little influence on the fatigue crack propagation stage since slight softening was caused by cyclic strain.

AISI 304 Stainless Steel

Deformation twinning, martensite phase transformation and work hardening of the dual-phase matrix control the strength properties of metastable austenitic stainless steels and accordingly, these mechanisms play a critical role determining the fatigue performance.

The fatigue behaviour of AISI 304 stainless steel wires, investigated in this study, has shown interesting differences between the behaviour of high strength wires and that of low strength wires. Fatigue crack propagation studies showed that the deformation-induced martensite transformation retards crack propagation in lower strength austenites and fatigue life is greatly enhanced by the martensite transformation. The influence of the martensite transformation in the high strength austenitic wires could be beneficial or detrimental depending on the amount of previously developed martensite phase. These findings are consistent with study performed on TRIP steels by Olson et al [64].

A number of mechanisms have been proposed that may contribute to the influence of the martensite transformation on crack initiation and propagation mechanisms. These include the incremental strain added by the transformation at the crack tip, the influence of the transformation and the resulting dual-phase microstructure on the crack path, the influence of the transformation on the aggregate mechanical properties of the material at the crack tip and the influence of the transformation on the fracture mode.

The most obvious mechanism that influences crack growth in metastable austenitic steels is the perturbation of the crack tip stress field by the strain associated with the transformation. Mangonon found that the austenite to martensite transformation in AISI 304-type steels involves both an ≈2% volume expansion and an ≈ 10% shear strain, as stated by [125].

However, this present study has shown that the amount of previously developed α'-martensite phase is most important since it is responsible for a transition in the fatigue behaviour and influences the mechanisms involved in fatigue crack initiation and propagation.

This hypothesis considers that the dual-phase microstructure changes the inherent crack growth resistance of the material ahead of the crack tip and that the introduction of a harder martensite phase and the local disturbance of the microstructure increases the strain-hardening rate.

It has been established that approximately 20% of deformation-induced martensite is a critical amount which results in a drastic change in the fatigue performance and fracture mode.

It is proposed that the deformation-induced martertensite phase in metastable austenitic stainless steels has a similar role to carbide lamellae in pearlitic steel. The high strength of martensite implies that there are many strong barriers to dislocation motion in this structure. The martensite structure contains a high dislocation density, thus the high strength of martensite arises from the effective barriers to slip provided by the fine twin structure or the high dislocation density. Thus, the formation of a dual-phase (austenite and martensite) prolongs the crack initiation period because the martensite plates act as barriers to dislocation movement. As a result, the fatigue crack initiates easier in the single phase microstructure (annealed condition of AISI 304), whilst in the drawn wires having a dual-phase structure, fatigue crack initiation is hindered.

However, the presence of more than 20% of martensite in the microstructure results in a lowering of the fatigue performance since crack propagation becomes easier. Furthermore, any phase transformation that occurs at the crack tip will also influence fatigue through cumulative action with the martensite already present.

The critical amount of martensite in the structure is reached at a drawing strain of 0.37 when blocky deformation twins form. Thus, work hardening, deformation twinning and deformation-induced phase transformation are mechanisms relevant to the crack initiation and propagation in AISI 304 stainless steel wires.
It is clearly advantageous to be able to predict the behaviour of cold drawn AISI 304 stainless steel wire during cyclic conditions. Therefore, an attempt has been made to model the behaviour of this steel by incorporating all relevant factors obtained through this study.

A model for predicting the fatigue behaviour of cold drawn AISI 304 Stainless Steel Wire

The experimental results obtained in this study, indicate that the volume of martensite transformation that occurs in metastable AISI 304 austenitic stainless steels is most important in determining it's fatigue behaviour.

In annealed AISI 304 stainless steel wire, subjected to cyclic conditions in the stress range below the fatigue limit, the austenite to martensite transformation can occur due to the ability of the steel to be plastically deformed even at stresses well below the fatigue limit. The amount of martensite in the bulk material increases, during stress cycling, up to a maximum value close to 40% without crack initiation. 35% of martensite, for example, was measured in a fractured surface which had been fatigued at a mean value of 120 MPa, which is just below the fatigue limit for the annealed steel, for 10^8 cycles without fracturing.

In the case where the annealed steel is subjected to fatigue at stresses above the fatigue limit, it was observed that there is a variable initiation period, depending on the mean stress level, prior to crack initiation. During this crack incubation period, some transformation of the austenite to martensite takes place, until the total value of the martensite in the crack initiation region reaches a saturation level. Transmission electron microscopy studies of the fracture surface region suggest this level is at approximately 40% martensite. The newly formed crack extends through this small volume of dual phase material, and further local transformation of the austenite to martensite occurs at the crack tip until the saturation level is reached, and the process is repeated continuously until final or fast fracture occurs.

It is also well established that the AISI 304 austenic steel undergoes a similar phase transformation of austenite to martensite during general plastic deformation, such as drawing. Experimental results show that the amount of deformation-induced martensite is related to the drawing strain and it varies from 8 to 36% in samples drawn from 0.09 to 0.585 strain respectively. This amount of austenite to martensite phase transformation subsequently influences the ease with which slip and deformation can occur in dual phase microstructure and delays crack initiation and propagation by strengthening the material. As a consequence, the fatigue limit is improved at all cyclic stress levels compared to the annealed material.

However, in the region of high stress/low cycle fatigue, i.e. above the fatigue limit, this work has also established that approximately 20% of deformation-induced martensite is a critical amount which determines the subsequent fatigue response of this steel. If the amount of previously developed martensite is less than the critical amount of 20%, the martensite formed during the fatigue process will act beneficially by retarding fatigue failure and result in a ductile fatigue fracture surface. Conversely, in the presence of a greater amount of martensite, more than 20%, any martensite induced by cyclic strain will encourage more rapid crack propagation compared to a material containing 20% martensite, which leads to more brittle fracture surface characteristics.

The experimental results from this work demonstrate that whilst the presence of increasing quantities of martensite in the austenite structure will strengthen the material, by making slip and deformation more difficult, it also leads to a reduction in the ductility of the material. Furthermore, the work hardening rate of the material changes from being positive to negative, as the amount of martensite increases above 20%, resulting in early necking and low uniform elongation. It has also been shown that crack propagation rates increase dramatically in material containing more than 20% martensite. Such results suggest, therefore, in steel subjected to cyclic stresses above the fatigue limit, that whilst crack initiation will become easier with increasing amounts of martensite above 20%, crack propagation rates will increase due to decreasing ductility and that the fatigue life of the material will also decrease as shown in this work.

The effect of introducing a notch is to raise the nominal applied stress locally but additionally it also encourages the formation of martensite in the austenitic structure during cyclic straining which strengthens the material and makes deformation more difficult. Clearly the severity of the notch influences the rate of this martensite formation. Consequently, in annealed or lightly drawn steel containing low quantities of martensite, the introduction of a notch does not lead to a deterioration of the fatigue properties but rather the reverse as has been demonstrated in this work. Thus, annealed or lightly drawn AISI 304 stainless steel containing martensite contents up to approximately 20% are not notch sensitive whilst those with higher quantities have been shown in this work to be notch sensitive. Such a result is important in practical situations where surface flaws are likely to be induced.

This study has shown that the amount of martensite in the steel is critical and that for high stress/low cycle fatigue conditions, the drawing or straining operation needs to controlled to give less than 20% of martensite in the structure if superior fatigue performance is to be achieved in practice. At this level of strain the tensile strength is close to 1000 MPa which is considered to be adequate for many applications.

The influence of martensite on fatigue behaviour is shown schematically in Fig.5.1. by the so-called Martensite Transformation (MT) model.

- Martensite Transformation Model -

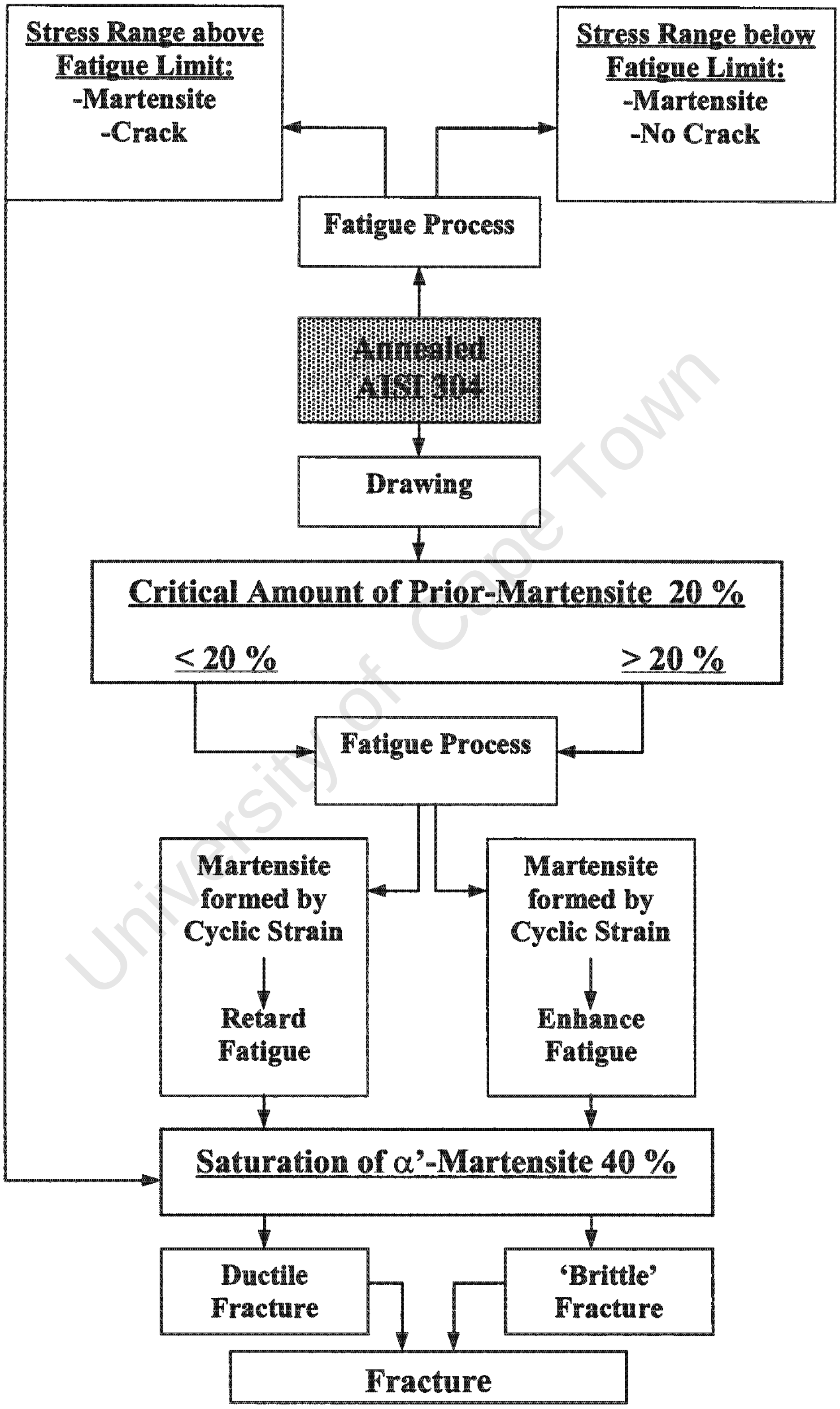

Fig.5.1. *MT model for predicting the fatigue behaviour of AISI 304 stainless steel wire*

3CR12 Corrosion-Resistant Steel

The mechanical properties and the fatigue performance of the ferritic 3CR12 steel wire were influenced only by work hardening mechanisms involved during the drawing and fatigue processes. The relatively small effect of work hardening on the fatigue behaviour of this steel restricts the applicability of 3CR12 steel wire in cyclic conditions. However, it was confirmed that the effect of a double-phase microstructure containing martensite has a beneficial effect on the fatigue performance.

In summary, three types of steel and three different mechanisms that influence the fatigue behaviour have been investigated and demonstrated in this research.

It has been concluded that generally, the work hardening, deformation twinning and phase transformation can influence mechanical properties. These factors compete in different steels but undoubtedly have a significant influence on the fatigue properties. The beneficial effect of the work hardening mechanism is restricted in all steels. However, the influence of the martensite transformation should be carefully considered due to the influence of α'-phase on the fatigue behaviour in metastable austenitic steels which is strongly dependent on the amount of this phase developed during the drawing process.

The dual-phase microstructure observed in quenched 3CR12 steel is considered as beneficial in terms of fatigue crack initiation and propagation processes.

Changes caused by fatigue

This comparative study shows that the steels investigated respond differently to cyclic strain.

Transmission electron microscopy shows no significant changes in the dislocation structure of high carbon steel samples subjected to cyclic strain. The microstructure remained very stable in cyclic conditions, although a slight softening (decrease in the yield strength) was observed.

However, the cyclic strain causes enormous changes in the AISI 304 stainless steel wire samples. Both annealed and drawn wire samples were cyclically hardened. The cyclic hardening is attributed to formation of the martensite phase and to work hardening of the dual-phase microstructure. A larger amount of martensite lower the strain at which necking occurs and consequently reduces the plastic elongation. The cyclic strain also influences the changes on the microscopic level, namely the dislocations formed the dislocation cells which increase considerably.

3CR12 steel samples, after being fatigued, show hardening but to a far less extent compared to the hardening effect observed in fatigued AISI 304 stainless steels. However, the work hardening significantly affects the strain at which necking starts and thus dramatically reduces the total elongation to failure.

Fractography

During the fractographic examination of fatigued carbon steel wires, a number of fracture modes were identified, namely: ductile transgranular mode, intergranular separation and so called 'tearing' topography.

In AISI 304 stainless steel wires, the fracture modes vary with variation of fatigue crack propagation. The intergranular separations were observed in the near-threshold region of the fatigue crack initiation, while the middle region of crack propagation was characterized by the appearance of striations.

The isolated facets are present in the near-threshold region; they are transgranular in AISI 304 stainless steels and intergranular in ferritic 3CR12 steel. Furthermore, the fractography of 3CR12 steel shows features, which are commonly referred to as 'tire tracks' and they are more significant in quenched than in annealed and drawn 3CR12 steel. These marks are believed to result from the relative motion between two closely-mating fracture surfaces in metastable austenitic stainless steel under the action of high cyclic stresses [42].

Changes in fracture mode are related to changes in crack growth from 'microstructurally sensitive' to 'microstructurally insensitive' in the intermediate growth rates.

Short Comparison between 3CR12 and AISI 304 Stainless Steel Wires

A different behaviour between the light and hard drawn 3CR12 stainless steel wires has been observed during this fatigue investigation. Besides the differences in the fracture modes and general response to fatigue, interesting differences were found between 3CR12 steel and AISI 304 austenitic stainless steel wire, with similar yield strengths.

3CR12 steel wires with a yield strength of 469 MPa and AISI 304 stainless steel having a yield strength of 480 MPa, both drawn to 0.09 strain, were subjected to fatigue, as the same stress level (load ratio R=0.2, mean stress 120 MPa and amplitude 80 MPa).

In both cases, the diameter of the wires was 4mm and the stress level was approximately 40% of the yield strength, as shown in Table 5.2.

Table 5.2. shows the comparison between the mechanical properties, drawing strain and fatigue response for both, the AISI 304-austenitic and 3CR12 ferritic corrosion resistant steels.

The data shows that 3CR12 wires drawn to 0.09 strain, exhibit significant plastic yielding during the subsequent fatigue process. This yielding occurred on the surface directly opposite the notch. At approximately 16,700 cycles, the plastic deformation of the wire is visible to the naked eye during the test, as shown schematically in Fig.5.2. and Figs.5.3,-5.7. In the case of AISI 304 stainless steel wire, the fatigue crack grows with increasing number of cycles without the yielding observed in the 3CR12 steel wires.

Table 5.2. AISI 304-Austenitic Stainless Steel vs 3CR12-Ferritic Steel

Steel	Dia. mm	ε	UTS [MP]	Yield Strength [MPa]	Load Ratio R	σ_y/R	Fatigue Response
AISI-304	4	0.09	752	480	120/80	0.42	FCG*
3CR12	4	0.09	516	469	120/80	0.43	FCG+ Yielding

* FCG - Fatigue Crack Growth

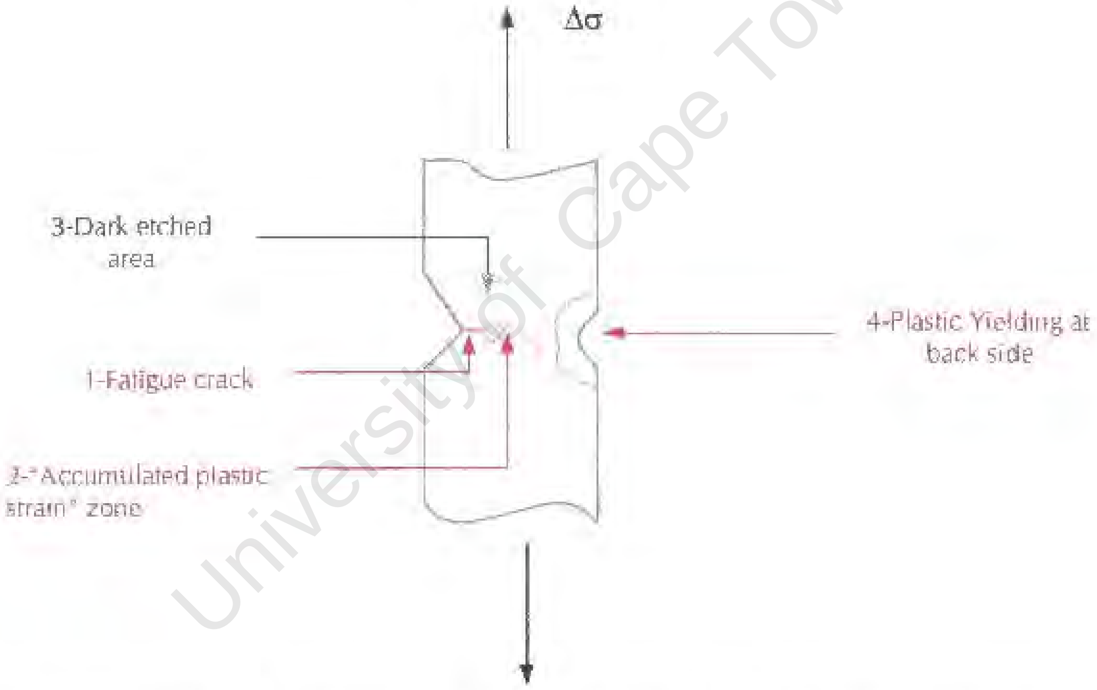

Fig.5.2. *Schematic of accumulated strain distribution and plastically deformed zone at the crack tip, in low strength 3CR12 –ferritic steel wire*

Figure 5.3. shows the fracture surface of low strength 3CR12 steel wire which consists of three distinctive regions: a) region 1-fatigue crack growth, b) region 2-plastic tearing area, and c) region 3-final ductile fracture.

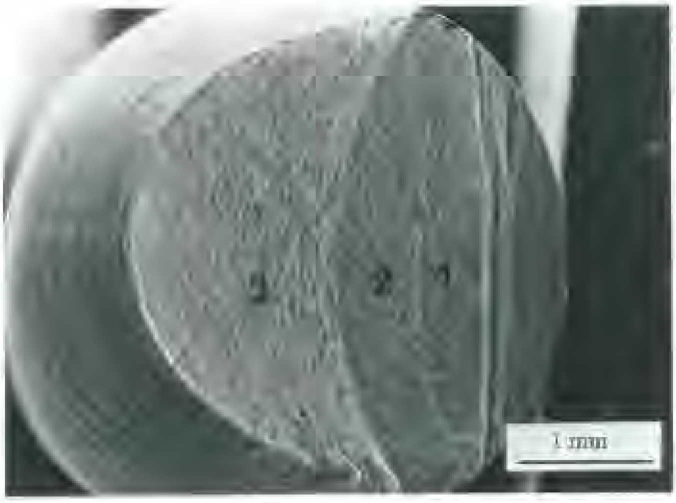

Fig.5.3. *SEM micrograph of fractured surface in lightly drawn 3CR12 steel wire (drawing strain 0.09)*
Fatigue conditions:
Mean stress:120 MPa
Amplitude:80 MPa
Arrow shows the different regions.

A explanation for this phenomenon is based upon the formation of a large plastic strain zone at the crack tip. The material work hardens very rapidly in a large plastic zone ahead of the crack, which reaches the tensile strength of the material quickly and yielding then occurs ahead of this zone i.e. on the back surface.

The reduction of cross sectional area of the wire sample and consequently a higher level of applied stress is the reason for the plastic deformation of the material on the side opposite the notch. A schematic drawing, Fig.5.2., shows the plastic zones revealed by etching, which is a typical example of the overloading in low toughness materials.

The high concentration of plastic strain in front of the fatigue crack revealed by etching is shown in Figs.5.4.-5.5. The application of a different etchant also shows that as a fatigue crack starts to grow the plastic zone increases in size and overloads occur, Figs.5.6.-5.7.

The hardness was measured in the plastically deformed crack tip region as HV25 = 230, compared to the hardness of the base material, HV25 = 180.

An increase in hardness was also observed in the deformed zone formed at the backside, opposite to the notch, (labelled 4) to HV25 = 210.

Fig.5.4. *Optical micrograph of low strength 3CR12 steel wire subjected to fatigue shows high strain concentration in front of the crack (Arrow indicates position of notch)*

Etchant: $CuSO_4$ + methanol

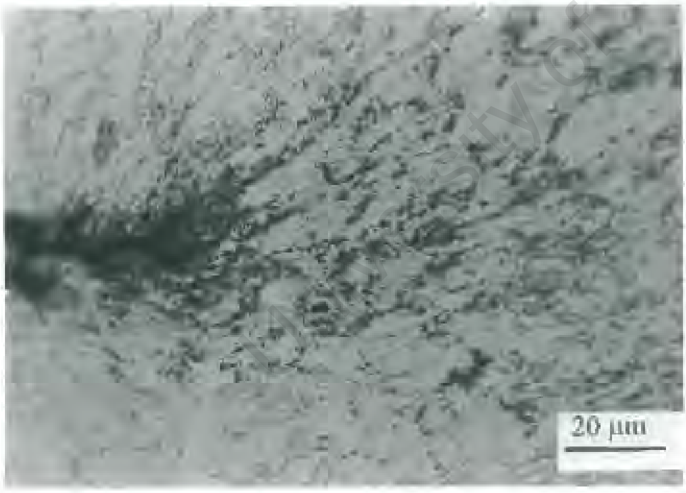

Fig.5.5. *Strain concentration in front of fatigue crack tip (higher magnification) Etchant: $CuSO_4$ + methanol*

Conditions:

3CR12 steel wire drawn to 0.09 strain

Fatigue condition:

$\sigma_m = 120$ MPa, $\sigma_a = 80$ MPa

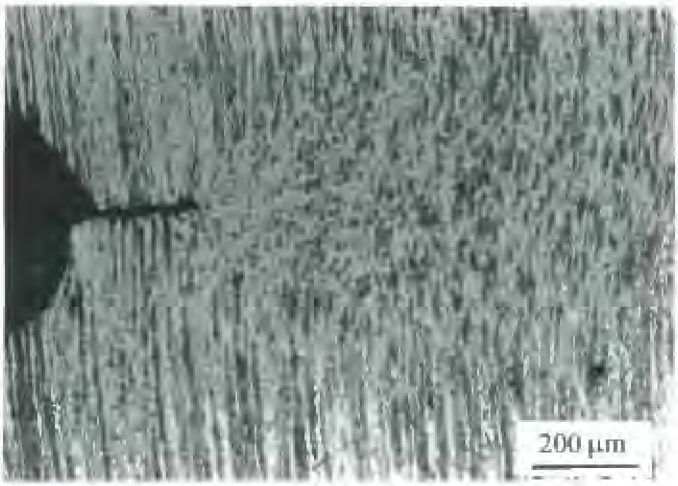

Fig.5.6. *Plastically deformed zone formed ahead of crack (labelled 2 in Fig.5.2.)*

etchant:
($HCl + NH_4F.HF + K_2S_2O_8$)

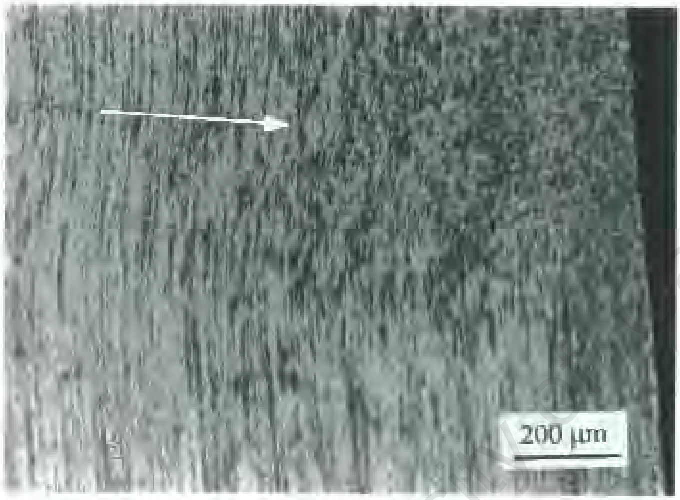

Fig.5.7. *Deformed zone at the side opposite of notch. (labelled 4 in Fig.5.2.)*

These fracture modes in 3CR12 differ to these in the AISI 304 stainless steel. It was found, for example, that fatigue striations appear in low strength 3CR12 wire samples, in the near-threshold region, whilst striations appear only in the linear regime of crack growth of AISI 304 stainless steel. It was also found that the cleavage mode is involved in high strength 3CR12 steel in the near-threshold region only at high cyclic stress levels. Both fatigue fracture modes suggest low fatigue resistance of annealed and drawn 3CR12 steel.

This also shows the effect of microstructure of different materials on the failure mode. However, the cleavage mode of fatigue fracture was not observed in high strength AISI 304 stainless steels.

The fatigue fracture modes shown in different steels are attributed to their crystal structure (fcc/bcc), the presence of a single or dual-phase microstructure and load ratio.

The low strength properties and fracture toughness of lightly drawn 3CR12 has been recognised as a major concem [126]. In order to improve the fracture toughness of this material, the chemical composition and thermo-mechanical processing should be taken in consideration. One of the potential ways of overcoming this problem is to develop steels composition having mixed structures in which separate constituents are responsible for the different property requirements. Modified heat treatments, which utilise the beneficial properties of a mixed structure, has shown that the strength and fatigue properties of the 3CR12 steel were significantly improved.

CHAPTER 6

CONCLUSIONS AND FUTURE WORK

6.1. Conclusions

AISI 304 AUSTENITIC STAINLESS STEEL WIRE

1. The mechanical properties are strongly influenced by the work-hardening process. The monotonic tensile properties increase with drawing strain, the ultimate tensile strength approximately doubled from 642 MPa to 1346 MPa, whilst the yield strength increased from 267 MPa to 1137 MPa as the strain increased from 0 to 0.585.

2. The amount of strain-induced martensite is related to the drawing strain. As the drawing strain increases from 0.09 to 0.585, the amount of strain-induced martensite is increased from 8% to 36%.

3. Prior induced martensite (formed during the drawing process) has a significant influence on the fatigue behaviour in the near-threshold region. The threshold stress intensity increases with increased amounts of the strain-induced martensite; the further crack increment depends on the amount of the previously developed martensite phase.

4. The fatigue limit increases with drawing strain. As the strain increased from 0 to 0.585, the smooth fatigue limit is increased from 140 MPa to 650 MPa.

5. The fatigue limit of annealed and notched samples is higher (215 MPa) compared to the fatigue limit of smooth specimens (140 MPa).

6. The threshold stress intensity is directly related to the drawing strain and to the yield strength of metastable AISI 304-stainless steels. The presence of the martensite phase inhibits crack initiation and prolongs the period for fatigue crack initiation. As the cyclic strength is increased, either because of a high initial monotonic strength or by cyclic hardening, the threshold for fatigue-crack propagation is increased.

7. Martensite formed during the fatigue process is beneficial for lightly drawn stainless steel wires. The martensite phase blunts the crack tip and retards the crack propagation.

8. In the hard drawn wires, the martensite transformation promotes brittle behaviour and very rapid crack propagation, but the crack propagation depends on the amount of previously developed martensite. More than 20% of martensite acts deleteriously.

9. Fatigue cyclic strain induces a hardening effect. The hardening effect is a time dependent process and the influence of this effect is more pronounced in the annealed and low strength austenites.

10. Low strength austenitic steel wires fracture in a ductile manner, whilst a brittle mode is dominant in a high strength wires.

3CR12 FERRITIC STEEL WIRE

1. The mechanical properties increase with increased drawing strain. The ultimate tensile strength increases approximately 60%, from 442 MPa to 738 MPa whilst the yield strength increases approximately 35%.

2. 3CR12 steel is extremely difficult material to draw into wires. The limited ability of 3CR12 steel to be plastically deformed is attributed to the high ratio of yield strength to tensile strength. The application of extensive plastic deformation during the drawing process creates a rough surface with many flaws. These flaws are undesirable due to their negative effect on the further drawing process; the flaws are potential sites for fatigue crack nucleation.

3. Drawing strain increases the fatigue limit. The fatigue limit of annealed 3CR12 steel (130 MPa) was greatly improved to 240 MPa by a strain of 0.09 (approximately 100%). Drawing to higher strain values does not significantly improve the fatigue limit further.

4. Fatigue cyclic strain induces a hardening effect. An improvement of the mechanical properties by cyclic strain is more significant in annealed than slightly drawn conditions. The yield strength is more affected by the hardening process that the ultimate tensile strength.

5. An application of heat treatment such as quenching significantly improves the fatigue limit. Quenching at 900^0 C for 30 minutes and oil cooling induce the dual-phase microstructure and consequently improves the fatigue strength to 480 MPa.

HIGH CARBON STEEL WIRE

1. Fatigue fractures observed in the high carbon steel wire always initiate at a surface flaw (cavity) with depths between 20 and 50 microns. Such flaws are often produced during cold drawing.

2. The fatigue limit increases with drawing strain, according to data presented by authors' [70] and experimental results obtained in this study. Note: authors' [70] investigated a range of drawing strain up to 1.2, whilst the steel wire investigated in this study was drawn to 1.8 strain.

3. Carbon steel wire shows a very high notch sensitivity reducing the fatigue limit by more than 30%. This phenomenon is explained by the extremely high notch sensitivity of the fine pearlite microstructure, in particular, of the hard and brittle carbide lamellae.

4. The fatigue limit shows a very strong dependence on the surface condition of the wire. Surface defects such as scratches, cavities and other discontinuities resulting from the drawing process, reduce the fatigue strength of carbon steel wire significantly.

5. Surface treatments, such as shot peening and polishing increase the fatigue limit significantly. Shot peening increases the fatigue strength by 40%, while reducing surface roughness from $R_a=1.6$ to $R_a=0.3$ microns by polishing gives 24% improvement in the fatigue limit.

6. The microstructure of high carbon steel is stable and the monotonic properties were only slightly changed by cyclic strain (softening).

GENERAL CONCLUSIONS

From the fatigue study performed on the three types of steel, AISI 304 stainless steel and 3CR12 steel, pearlitic high carbon, the following general conclusions may be drawn:

1. Pearlitic high carbon steel wire has superior fatigue behaviour compared to both the AISI 304 stainless steel and 3CR12 steel wire.
2. The biggest disadvantage of the pearlitic steel wire is it's poor surface quality and notch sensitivity. This problem can be partially solved by improving the surface finish following the drawing process.
3. In AISI 304 stainless steel wire, the transformation-induced martensite phase should be carefully controlled in order to optimise fatigue resistance. It was established that the more than approximately 20% of the strain-induced martensite acts deleteriously, i.e. promotes rapid crack propagation and more brittle behaviour.
4. The application of cold drawn annealed 3CR12 steel wires is limited to low stress fatigue conditions.
5. The fatigue performance of 3CR12 steel is significantly improved by heat treatment to produce a dual-phase ferrite/martensite microstructure.
6. A dual-phase microstructure has a significant benefit in terms of fatigue behaviour; dual-phase acts beneficially in terms of delaying crack initiation and retarding the fatigue crack propagation.

7. Finally, in the design of material for wire application it is very important to optimise microstructure, since the optimum microstructures desired will depend upon whether structural design is to be based on the initiation or propagation of a 'fatal flaw'.

6.2. Suggestions to Future Work

The work has shown that the monotonic and fatigue properties are improved by drawing strain. Surface treatments act beneficially on the fatigue performance. To explore the potential for further enhancing fatigue properties, and further understanding the factors dominating fatigue performance of steel investigated in the present study, the following work are suggested:

1. Further investigation concerning the influence of the chemical composition of AISI 304 stainless steel. In tests performed in this work, the commercially supplied AISI 304 stainless steel wire, having a higher amount of nickel, showed better fatigue properties.

2. In order to establish the conditions and role of the initiation of deformation twinning under fatigue conditions, it is necessary to extend investigations to include a number of other parameters which have not been done in the present work.

3. Further investigation concerning the influence of the load ratio on the austenite to martensite transformation of AISI 304 stainless steel, in particular the effect of minimal cyclic stress.

4. The experimental results obtained using quenched 3CR12 having a martensite-ferrite microstructure show a positive improvement of fatigue strength. It is worth investigating the effect of drawing strain on the fatigue performance of such material.

5. Further investigations are required on the fretting fatigue of stainless steels. Fretting conditions exist in wire rope applications which can lower fatigue lives substantially.

REFERENCES

1. F B Pickering, *The Metallurgical Evolution of Stainless Steels,* The Metals Society, London, England 1979
2. S Suresh, *Fatigue of Materials*, Cambridge University Press, 1991
3. K J Miller, *Materials Science and Technology*, June, Vol.9, p. 453, 1993
4. W A Wood, *Philosophical Magazine 3*, p.692, 1958
5. P J E Forsyth, A Stubbington, *Journal of the Institute of Metals* 84, p.173, 1955
6. A H Cottrell, D Hull, *Proceeding Royal Society*, A 242, p.211, 1957
7. P J E Forsyth, *Acta Metallurgica*, Vol.11, July, p.703, 1963
8. W A Wood, *Treatise of Materials Science and Technology*, Vol.5, p.129,1974
9. P Neumann, *Acta Metallurgica*, Vol.17, September, p.1219,1969
10. M Klesnil, P Lukas, *Materials Science Monographs*, Vol. 17, Elsevier, Amsterdam, 1992
11. A S Cheng, C Laird, *Materials Science and Engineering*, 60, p.177, 1983
12. C J Beevers, *Metal Science*, 14, p.418, 1980
13. C Laird, G C Smith, *Philosophical Magazine*, Vol.17, p.847, 1963
14. C Laird, ASTM STP 415, *American Society for Testing and Materials*, , p.131, 1967
15. C Laird, R De La Veaux, *Metallurgical Transactions A*, Vol.8A, April, p.657, 1977
16. W J Plumbridge, *Journal of Materials Science*, Vol.7, p.939, 1972
17. R M N Pelloux, *Transactions ASM*, 62, p.281, 1969
18. D L Davidson, J Lankford, *International Materials Reviews*, Vol.37, No.2, p.42, 1992
19. G A Miller, *Transactions ASM*, 62, p.651, 1969
20. P J E Forsyth, C A Stubington, D Clark, J. *Institute of Metals*, Vol.90, p.238, 1961
21. W J Plumbridge, D A Ryder, *Metallurgical Review of Metals and Materials*, Vol.3, p.119, 1969
22. R O Richie, *Metal Science*, 11, p.368, 1977

23. J F Knott, *Fundamentals of Fracture Mechanics*, Butterworths, London, 1973
24. H H Johnson, P C Paris, *Engineering Fracture Mechanics*, 1, p.3, 1968
25. P Paris, F Erdogan, *Journal of Basic Engineering Transactions, ASME*, Vol. 85, December, p.459, 1963
26. G Forman, V E Kearney, R M Engle, *Journal of Basic Engineering Transactions, ASME*, September, p.459, 1967
27. S T Rolfe, J M Barsom, *Fracture and Fatigue Control in Structures*, Prentice Hall, 1977
28. C E Richards, T Lindley, *Engineering Fracture Mechanics*, 4, p.951, 1972
29. R O Ritchie, J F Knott, *Acta Metallurgica*, 21, p.639, 1973
30. R O Ritchie, J F Knott, *Materials Science Engineering*, 14, p.7, 1974
31. R O Ritchie, *Journal of Engineering Materials Technology*, 99, 1977
32. M Klesnil, P Lukas, *Material Science Engineering*, 9, p.231. 1972
33. J K Tien, AIME, p.301, 1976
34. G Baundry, A Pineau, *Materials and Science Engineering*, 28, p.229,1977
35. G T Gray III, J C Williams, A W Thomson, *Metallurgical Transactions A*, Vol.14A, p.421, 1985
36. J M Hyzak, I M Bernstein, *Metallurgical Transactions A*, Vol.7A, p.1217, 1976
37. G T Gray III, A W Thompson, J S Williams, *Metallurgical Transactions A*, Vol.16A, May, p.753, 1983
38. H Sunwoo, M E Fine, M Meshii, D H Stone, *Metallurgical Transactions A*, Vol.13A, November, p.2035, 1982
39. V F Zackay, E R Parker, D Fahr, R Busch, *Transactions ASM*, Vol.60, p.252, 1967
40. G R Chanani, V F Zackay, E R Parker, *Metallurgical Transactions*, Vol.2, p.133, 1971
41. S D Antolovich, B Singh, *Metallurgical Transactions*, Vol.1, p.2135, 1970
42. G R Chanani, S D Antolovich, W W Gerberich, *Metallurgical Transactions*, Vol.3, p.2661, 1972
43. M F Carlson, R O Ritchie, *Scripta Metallurgica*, 11, p.1113, 1977
44. R O Ritchie, *International Metals Reviews*, Nos. 5 and 6, p.205, 1979

45. J L Robinson, C J Beevers, *Metal Science Journal*, 7, p.153, 1973
46. A W Thompson, R J Bucci, *Metallurgical Transactions*, 4, p.1173, 1973
47. S Ganesh, S Raman, K A Padmanbhan, *Materials Science and Technology*, July, Vol.10, p.614, 1994
48. A G Pineau, R M Pelloux, *Metallurgical Transactions*, 5, p.1103, 1974
49. D Hennessey, G Stickel, C Altstetter, *Metallurgical Transactions*, Vol.7A, p.415, 1976
50. S D Antolovich, B Singh, *Metallurgical Transactions*, 2, p.2135, 1971
51. V Shrinivas, S K Varma, L E Murr, *Metallurgical Transactions*, Vol.26A, p.661,1995
52. C Bathias, R M Pelloux, *Metallurgical Transactions*, 4, p.1265, 1973
53. E Hornbogen, *Acta Metallurgica*, 26, p.147, 1978
54. M Bayerlein, H J Christ, H Mughrabi, *Materials and Science Engineering*, A114, L11, 1989
55. G R Chanani, S D Antolovich, *Metallurgical Transactions*, Vol.5, 5, p.217, 1974
56. N J Ho, S C Tjong, *Materials and Science Engineering*, 94, p.195, 1987
57. G E Dieter, *Mechanical Metallurgy*, Mc Graw-Hill Book Company, 1986
58. T C Lindley, C E Richards, R O Ritchie, *Metallurgical Metal Forming*, 43, p.268, 1976
59. O Visikovsky, *Engineering Fracture Mechanics*, 11, p.595, 1979
60. M F Carlson, R O Ritchie, *Scripta Metallurgica*, 11, p.1113, 1977
61. J P Benson, D V Edmonds, *Metal Science*, 12, p.223, 1978
62. R G Luther, T R G Williams, *Metal Science*, June, p.219, 1977
63. M Azrin, G B Olson, R A Gagne, *Materials Science and Engineering*, Vol.40, No.2, p.175, 1979
64. G B Olson, R Chait, M Azrin, R A Gagne, *Metallurgical Transactions A*, Vol.11A, June, p.1069, 1980
65. R A Cottis, Z Husain, *Metal Technology*, 9, p.104, 1982
66. R Kiesslimg, *The Metal Society*, 1988
67. T Y Shih, T Araki, *Transactions ISIJ* 13, p.11, 1973

68. G X Y Zhu, W J D Shaw, *Fatigue Fracture Engineering Materials Structure*, Vol.18, No.7/8, p.811, 1995
69. R J Cooke, C J Beevers, *Materials Science and Engineering*, 13, p.201, 1974
70. J Llorca, V Sanchez-Galvez, *Engineering Fracture Mechanics*, Vol.26, No.6, p.869, 1987
71. J Mausonave, J P Bailon, *Scripta Metallurgica*, 9, p.723, 1975
72. A J Mc Evily, *Metal Science*, Vol.11, p.274,1977
73. N Walker, C J Beevers, *Fatigue Engineering and Materials Structure*, Vol.1, p.135, 1979
74. M N James, E R de los Rios, *Fatigue and Fracture of Engineering Materials and Structure 19, N.4. p.413-426, 1996*
75. M N James, I Wentong, *Materials Science and Engineering* A 265, p.129-139, 1999
76. W Elber, *Damage Tolerance in Aircraft Structures, ASTM STP 486*, p.280, 1971
77. R O Ritchie, S Suresh, *Metallurgical Transactions 13 A*, p.937, 1981
78. M D Halliday, C J Beevers, *Journal of Testing and Evaluation 9*, p.195, 1981
79. Purushothaman, J K Tien, *Scripta Metallurgica 9*, p.923, 1975.
80. S Suresh, G F Zamski, R O Ritchie, *Metallurgical Transactions A*, Vol.12A, p.1435, 1981
81. R O Ritchie, *Fatigue Thresholds*, Emas Publications, p.503, 1981
82. M Minakawa, A J Mc Evily, *Scripta Metallurgica*, 16, p.618, 1981
83. M Minakawa, A J Mc Evily, *Scripta Metallurgica*, Vol.15, p.633, 1982
84. G T Gray III, J C Williams, A W Thompson, *Metallurgical Transactions A*, Vol.14A, March, p.421, 1983
85. J D Embury, R M Fisher, *Acta Metallurgica*, 14, p.147, 1966
86. P G Maxwell, A Goldberg, J C Shyne, *Metallurgical Transactions*, Vol.5, p.1305, 1974
87. Langford, *Metallurgical Transactions A*, Vol.8A, June, p.861, 1977
88. J G Sevillano, *Materials Science and Engineering*, Vol.21, p.221, 1975
89. F Lecroisey, A Pineau, *Metallurgical Transactions*, Vol.3, p.387, 1972

90. J W Brooks, M H Loretto, R E Smallman, *Acta Metallurgica*, Vol.27, p.1829, 1979
91. H Otte, *Acta Metallurgica*, Vol.5, p.614, 1957
92. Languillaume, G Kapelski, B Baudelet, *Acta Metallurgica*, 45, p.1201, 1997
93. J F Breedis, W D Robertson, *Acta Metallurgica*, Vol.11, p.547, 1963
94. W O Binder, *Metal Progress*, Vol.58, p.201, 1950
95. B A Bilby, J W Christian, *Journal of Iron and Steel Institute*, Vol.197, p.122, 1961
96. A Venables, *Philosophical Magazine*, Vol.7, p.35, 1962
97. P G Bastien, J M B Dedieu, *Journal of Iron and Steel Institute*, Vol.183, p.254, 1956
98. R Lagneborg, *Acta Metallurgica*, Vol.12, p.823, 1964
99. G B Olson, M Cohen, *Metallurgical Transactions A*, Vol.6A, p.791, 1975
100. G B Olson, M Azrin, *Metallurgical Transactions A*, Vol.9A, p.713, 1978
101. G B Olson, M Cohen, *Metallurgical Transactions A*, Vol.7A, p.1897, 1976
102. G B Olson, M Cohen, *Metallurgical Transactions A*, Vol.7A, p.1905, 1976
103. G B Olson, M Cohen, *Metallurgical Transactions A*, Vol.7A, p.1915, 1976
104. S S Hecker, M G Stout, K P Staudhammer, *Metallurgical Transactions A*, Vol.13A, p.619, 1982
105. L E Murr, K P Staudhammer, S S Hecker, *Metallurgical Transactions A*, Vol.13A, p.627, 1982
106. S K Varma, J Kalyanam, L E Murr, V Shrinivas, *Journal of Materials and Science Letters*, Vol.13, p.107, 1994
107. G B Olson, R Chait, M Azrin, R A Gagne, *Metallurgical Transactions 11A*, p.1069, 1980
108. N Ridley, *Wire Industry*, September, p. 829, 1976
109. K Katagiri, T Sato, H S Shin, L Takahashi, H Mori, H Tashiro, S Sasaki, *Fatigue Fract. Engng. Mater. Struct.* Vol.20, N.12, p.1677, 1997

110. D Y Holliday, R Resnick, *Fundamentals of Physics*, John Wiley and Sons, New York, p.764, 1981

111. C F Jatczak, S W Shin, *Society of Automotive Engineers Inc.*, Warrendale, p. 9, 1980

112. ASTM Standards E 647-78T, *American Society for Testing and Materials*, Philadelphia, p.749, 1980

113. R E Peterson, *Stress Concentration Design Factors*, J Wiley and sons, inc., Chapman and Hall, Ltd. Publishers, London

114. P G Forrest, *Fatigue of Metals*, Pergamon Press, London, 1970

115. ASTM Standards E 112-63, *ASTM Standards, Philadelphia*, p.204, 1974

116. G F Vander Voort, *Metallography*,17, 00, 1984

117. K Katagiri, T Sato, K Kasaba, S Sassaki, H Tashiro, *Fatigue Fracture and Engineering Structures*, 22, p.753, 1999

118. J R Franklin, C Allen, *Wire Industry*, November 1980, p.958

119. W F Hosford, *The Mechanics of Crystals and Textured Polycrystals*, Oxford Engineering Series-32, Oxford Science Publications, 1993

120. M A Daeubler, A W Thompson, I M Bernstein, *Metallurgical Transactions A*, Vol21A, April, p.925, 1990

121. X F Fang, W Dahl, *Materials Science and Engineering*, A 141, p. 189, 1991

122. F Knap, J Pilarczyk, *Wire Industry*, August, p.583, 1994

123. L Remy, A Pineau, *Materials Science and Engineering*, 26, p. 123, 1976

124. R Smallman, *Modern Physical Metallurgy*, Butterworth and Co (publishers) Ltd, London, 1985

125. P L Manganon, G Thomas, *Metallurgical Transactions*, Vol.1, p.1577, 1974

126. *Proceedings of the Inaugural International 3CR12 Conference*, Johannesburg, March, 1984

127. C P Livitsanos et al, *Journal of Materials Science* 12, p.2209, 1977